Fingerprints and Drivers of Recent Changes in Oceanic Oxygen: From Regional to Global Scales

A thesis submitted to the School of Environmental Sciences of the University of East Anglia in partial fulfilment of the requirements for the degree of Doctor of Philosophy

By Oliver David Andrews

September 2014

In loving memory of my mother, Sylvia, my inspiration and a ray of sunshine for all time.

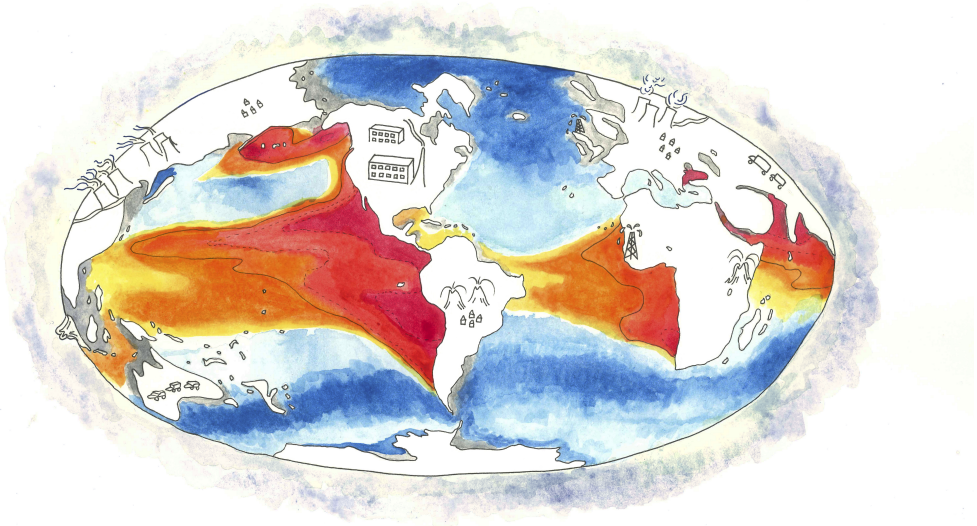

Abstract

Observations and Earth System Model (ESM) projections indicate that a reduction in the oxygen inventory of the global ocean, termed ocean deoxygenation, is a likely consequence of on-going anthropogenic warming. The contribution of external forcing factors to observed changes in dissolved oxygen concentration ($[O_2]$) relative to natural internal variability is examined using statistical methods which synthesise historical measurements and ocean biogeochemistry model output. Using a formal optimal fingerprinting method, an externally forced signal, derived from ESM response patterns, is detected within the observational record of $[O_2]$ between ~ 1970 and ~ 1992 at the $90\,\%$ confidence level. Positive detection results in response to external forcing are robust for depth-averaged (100–3000 m) and depth-resolving zonal mean patterns globally and for the Pacific basin, however $[O_2]$ changes in the Atlantic basin are indistinguishable from internal variability as characterised by unforced ESM integrations. Current ESMs are also shown, using optimal detection techniques, to consistently underestimate the magnitude of observed $[O_2]$ change by a factor of $\sim 2 - 4$. Accordingly, targeted hindcast experiments are conducted using the PlankTOM10-NEMO3.1 model, quantifying the impact of physical and biogeochemical processes on the spatiotemporal distribution of O_2. The largest magnitude of uncertainty is shown to be entrained into $[O_2]$ response patterns due to model parameterisation of pCO_2-sensitive C:N ratios in carbon fixation and imposed atmospheric forcing data. Historical trends and variability in Bottom Mixed Layer (BML) $[O_2]$ for the North Sea region are also investigated. Observed ($-0.62\,\mu\mathrm{mol\,L^{-1}}$) and regional model simulated ($-0.35\,\mu\mathrm{mol\,L^{-1}}$ [GETM-ERSEM]) area mean linear trends in summer BML $[O_2]$ (1959–2006) are shown to exceed global estimates, suggesting that stratified shelf seas could be especially sensitive to warming-driven deoxygenation. However, the detectability of secular changes is reduced by model error and internal variability associated with historical transitions between hydrodynamic regimes.

Acknowledgements

I am eternally indebted to my primary supervisor, Corinne Le Quéré, whose patient and unwavering support has been invaluable in bringing this work to fruition. I would also like to thank Andrew Manning for providing much-needed perspective and counsel throughout this project as a member of my supervisory team. I am immensely grateful to Erik Buitenhuis and Clare Enright for providing scientific and technical assistance throughout this project on occasions too numerous to recount. I would also like to thank Nathan Bindoff for introducing me to the "D&A" game, and generously hosting me for an enjoyable and productive Spring at the University of Tasmania in Hobart.

Most of all, I consider myself blessed to have had a wonderful Mum, to whom this work is dedicated, expertly guiding me through this, at times isolating, endeavour in ways I am only now beginning to fully understand. She instilled in me the strength and self confidence to follow my passions, and has taught me the true meaning of fortitude. Also, my Dad and brother, Ed, have provided a rock-solid support network throughout.

Aside from this I am lucky to have had great, silly, inspiring friends for days off (Tom D, Monk, Lax, Tom P, Matthew, Merkin, Jono, Ben, Ed, Peter), days on (Jeppe, Martin, Phil, Ben, Henry, Powly, Delphine), and everything in between (Iain, Will, Phil, Edwin). Finally, I owe a terrific debt to my wonderful girlfriend, Holly, for, well, everything.

Contents

List of tables

List of figures

Chapter 1

Introduction

Section 1.4 of Chapter 1 was written by ODA as a contribution to Chapter 6 (Section 6.4.5) of Working Group I of the Intergovernmental Panel on Climate Change's Fifth Assessment Report (Ciais et al. 2013), where it is incorporated in a condensed form.

Citation: Andrews, O. D., Contributing Author in: Ciais, P., Sabine, C., Bala, G., Bopp, L., Brovkin, V., Canadell, J., Chhabra, A., DeFries, R., Galloway, J., Heimann, M., Jones, C., Le Quéré, C., Myneni, R. B., Piao, S., and Thornton, P.: Carbon and Other Biogeochemical Cycles, in: *Climate Change 2013: The Physical Science Basis. Contribution of Working Group I to the Fifth Assessment Report of the Intergovernmental Panel on Climate Change*, edited by: T. F. Stocker, Qin, D., Plattner, G.-K., Tignor, M., Allen, S. K., Boschung, J., Nauels, A., Xia, Y., Bex, V., and Midgley, P. M., Cambridge University Press, Cambridge, United Kingdom and New York, NY, USA, 2013.

1.1 The Anthropocene ocean

1.1.1 Overview

The ocean is the largest ecosystem on Earth, occupying more than 70 % of the planet's surface and containing 97 % of all water. As a major part of the *hydrosphere*, the ocean communicates with other *spheres* of the Earth System via physical fluxes of energy, momentum, and matter (Fig. 1.1). Biogeochemical exchanges also occur between the ocean and *atmosphere* across the air-sea interface, providing a principal vector for transfer of carbon and other biologically active elements. The ocean also acts as a globally important store of thermal energy and carbon within the Earth System by virtue of its large mass and volume ($\sim 1.33 \times 10^9$ km^3 based on satellite altimetry data [Charette and Smith, 2010]), high heat capacity, and many points of contact with other spheres. These properties are central to understanding the role of the ocean in regulating climate on various timescales.

Increased human population and economic development has brought about a profound alteration to many physical and biogeochemical aspects of the "natural" Earth System, a change which has been conceptualised by some as indicative of transition into a new geological epoch – the Anthropocene (*cf.* Crutzen and Stoermer, 2000; Crutzen, 2002). Particularly, since the start of the industrial revolution ($\sim$ 1750) human activities including fossil fuel burning, land use change and, to a lesser extent, cement production have led to an increase in the atmospheric abundance of greenhouse gases such that current concentrations of carbon dioxide (CO_2), methane (CH_4) and nitrous oxide (N_2O) are unprecedented over the last 800 ka (based on polar ice core records [Masson-Delmotte et al., 2013]). These anthropogenic changes to atmospheric composition have brought about a radiative imbalance since at least $\sim$ 1970 (Church et al., 2011), whereby more incident solar radiation is retained in the Earth System than exits at the top of the atmosphere due to the increased absorption and re-emission of outgoing long-wave infrared radiation by greenhouse gases. Perturbation of Earth's energy balance via a net positive radiative forcing has caused the climate system to warm, driving an increase in global mean surface temperature for the combined land and ocean of 0.85°C over the period 1880-2012 (Hartmann et al., 2013). Ocean warming accounts for most ($\sim$ 93 %) of excess heat energy that has accumulated in the Earth System between 1971 and 2010, two thirds of which is confined to the upper 700 m (Fig. 1.2; Rhein et al., 2013).

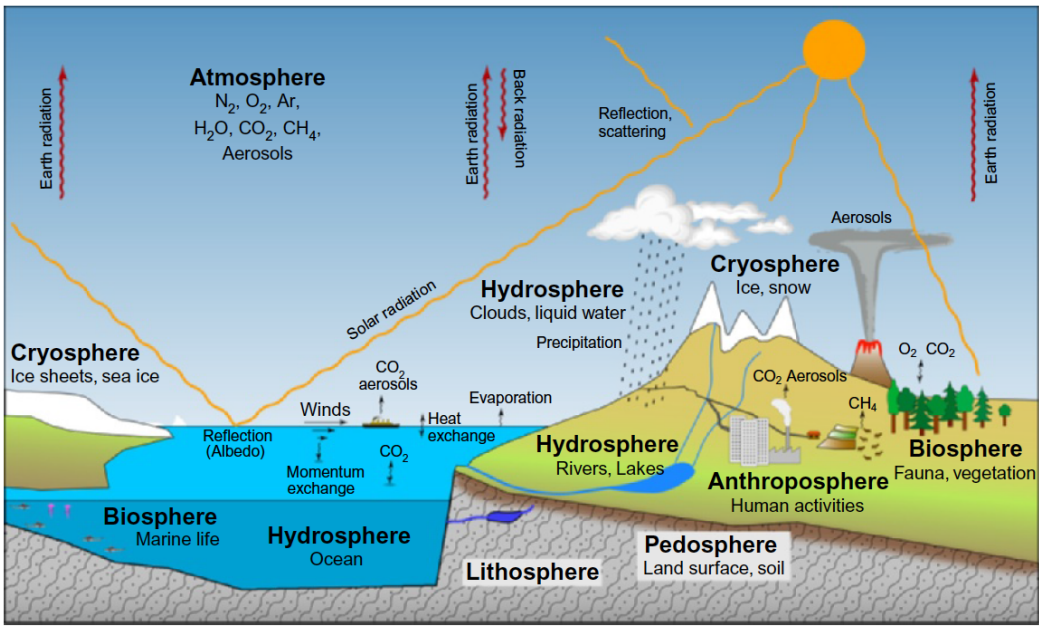

Figure 1.1: Schematic summarising the major physical and biogeochemical connections between spheres of the Earth System. Reproduced with permission from Stocker (2013).

1.1.2 Oceanic climate change

Figure 1.3 summarises recent changes in major physical and biogeochemical properties of the ocean system in response to climate warming, centered around 50-year temperature and salinity trends reported by Durack and Wijffels (2010), expressed as zonal averages. Observed ocean warming is largest in near surface waters, with global mean temperature increases of 0.11°C per decade for the upper 75 m compared to 0.015°C per decade at 700 m depth (Rhein et al., 2013). Intensified near surface ocean warming and decreases in density relative to the subsurface have been associated with a 4 % increase in thermal stratification (0-200 m depth) over the same time period (Levitus et al., 2009) with significant implications for ventilation processes (See Sect. 1.2.2). Temperature changes are also observed within the ocean interior as the signal of surface heating is transported downward via mixing and water mass subduction. However temperature anomalies in the ocean interior are more heterogeneous, smaller in magnitude and based on more spatiotemporally limited data from repeat transects. As shown in Figure 1.3, coherent zonal mean temperature increases are generally observed down to $\sim$ 2000 m depth and in deep and abyssal waters (from 3000 m depth to the ocean floor), particularly in the recently ventilated Antarctic Bottom Water (AABW) in the Southern Ocean (e.g. Purkey and Johnson, 2010). Some other

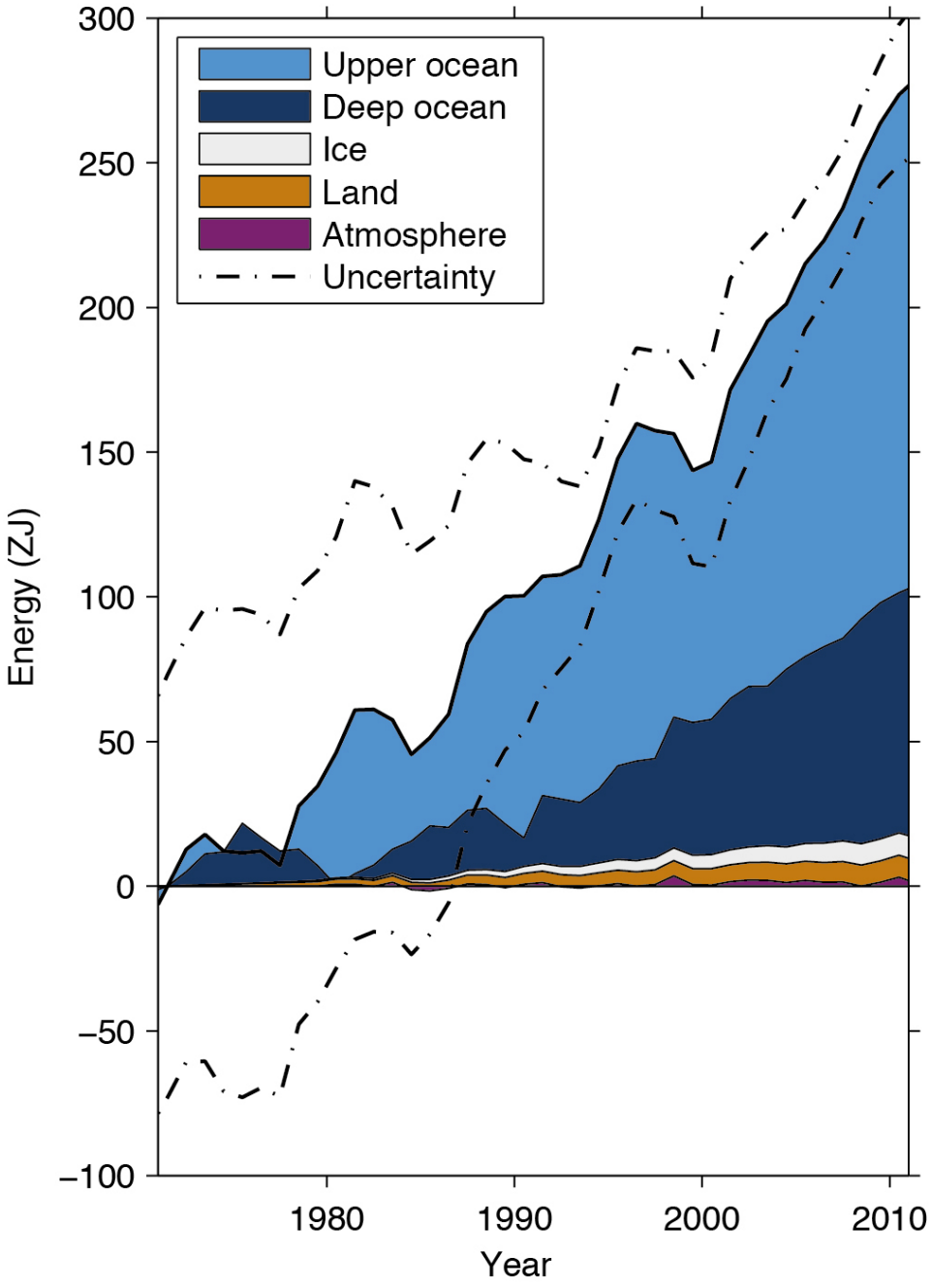

Figure 1.2: Time-series of the energy accumulated within each component of the Earth System between 1971 and 2010 (in ZJ; 1 ZJ = 1021 J). Upper ocean warming (light blue; < 700 m depth); deep ocean warming (dark blue; > 700 m depth); ice melt (grey; Greenland and Antarctic ice sheet estimates start from 1992, Arctic sea ice estimate 1979-2008); land warming (orange); and atmospheric warming (pink). Errors (dot-dashed line) are provided at the 90 % confidence level. Reproduced from Rhein et al. (2013).

volumetrically important water masses have, however, cooled over the historical period, particularly the Antarctic Intermediate Water (AAIW) north of 30°S and the Lower North Atlantic Deep Water (LNADW, for which a net heat loss of $-4.3 \pm 0.5 \times 10^{21}$ J is reported by Mauritzen et al [2012] for the period 1955–2005). However, the detection of long-term changes in NADW properties is complicated by strong decadal scale internal variability associated predominantly with the North Atlantic Oscillation (NAO; See Sect. 1.1.3).

Distinct regional changes in ocean salinity have been reported over the historical period. Consistent with a climate-driven intensification of the hydrological cycle ($\sim 8 \pm 3$ % per degree of surface warming [Durack et al., 2012]), observations indicate an enhancement of existing patterns of surface water fluxes (evaporation-minus-precipitation [$E - P$]) such that subtropical ($E > P$) regimes are becoming more saline, whereas water masses formed in tropical and polar regions ($E < P$) are becoming fresher. Observed freshening within the subpolar domain has also been associated with enhanced ice melt and riverine freshwater input, along with changes in ocean circulation (Bindoff et al., 2007; Helm et al., 2010). Rhein et al. (2013) report that, as a result of this regional divergence in hydrologic forcing, the global mean contrast between high and low salinity regimes has increased by 0.12-0.13 PSS78 between 1950 and 2008, based on the Sea Surface Salinity (SSS) data of Boyer et al. (2009) and Durack and Wijffels (2010).

Marked changes in ocean biogeochemistry have also been observed in response to rising greenhouse gas concentrations and climate warming. The ocean is an important store of anthropogenic carbon (C_{ANT}), having absorbed 155 $\pm$ 30 Pg C of atmospheric CO_2 for the period 1750-2010 (Rhein et al., 2013; Khatiwala et al., 2013), equivalent to ~ 25 % of total anthropogenic carbon emissions since the onset of the industrial era (Le Quéré et al., 2014b). The oceanic sink of carbon therefore plays an important role in buffering rising atmospheric CO_2, with recent accumulation of C_{ANT} in the subsurface associated with interior transport along major ventilation pathways (C_{ANT} inferred indirectly using observational or model-based methods [Khatiwala et al., 2013]). However, increased carbon uptake and surface ocean pCO_2 via enhanced air-sea fluxes down a partial pressure gradient has significantly reduced the pH and calcium carbonate ($CaCO_3$) saturation state (Ω) of seawater (called "ocean acidification" [*cf.* Doney et al., 2009]). Specifically, the dissolution of CO_2 gas in seawater drives an increase in hydrogen ion concentration [H+],

which has caused a global decrease in surface pH of 0.1 units and associated reductions in $[CO_3^{2-}]$ of up to 10 %, relative to pre-industrial values (Orr et al., 2005). A decrease in subsurface dissolved oxygen concentration (hereafter $[O_2]$) has also been observed across nearly all ocean basins over the last 50 years. Understanding the processes controlling the climate response of ocean $[O_2]$ on regional and global scales is a central objective of this research (Sect. 1.5.1), such that a thorough appraisal of the oceanic oxygen cycle (Sect. 1.2) along with observed (Sect. 1.3) and projected (Sect. 1.4) changes is provided subsequently.

1.1.3 Detection and attribution of oceanic climate change

The ocean responds gradually to imposed climate forcing owing to its large heat capacity and slow circulation driven by wind and density contrasts. This thermal inertia within the ocean system acts to damp large magnitude temperature changes, and causes a lag in the forced response of near-surface temperatures to rising greenhouse gas concentrations (e.g. Pierce et al., 2011; Hansen et al., 1985). The long (multi-decadal) timescales over which ocean processes occur also integrate short-term climate noise (or "internal variability") such that secular changes within the climate system can be more readily identified in ocean properties (e.g. Hegerl et al., 2006; Bindoff et al., 2013). Observed changes in a climate-sensitive variable result from a combination of processes that are both *internal* and *external* to the climate system. *External* factors (or "forcings") that alter the radiative balance or other aspect of the climate system can be natural (e.g. changes in solar output or stratospheric volcanic aerosols) or anthropogenic (e.g. changes in well-mixed greenhouse gas concentrations) in origin. Variability is also *internal* to the climate system, generated by non-linear dynamical (and thermodynamical) processes within the atmosphere, ocean or coupled ocean-atmosphere system (e.g. Deser et al., 2012). This variability is generally characterised as a series of preferred spatial patterns that comprise the dominant climate modes (e.g. the North Atlantic Oscillation [NAO; Hurrell et al., 2003]), often identified through inter-regional spatial teleconnections. Internal variability occurs on all timescales (Hasselmann, 1976), complicating the separation (or "detection") of externally forced changes from these chaotic, unforced variations within the climate system. *Detection* is defined by the IPCC Good Practise Guidance Paper on Detection and Attribution (Hegerl

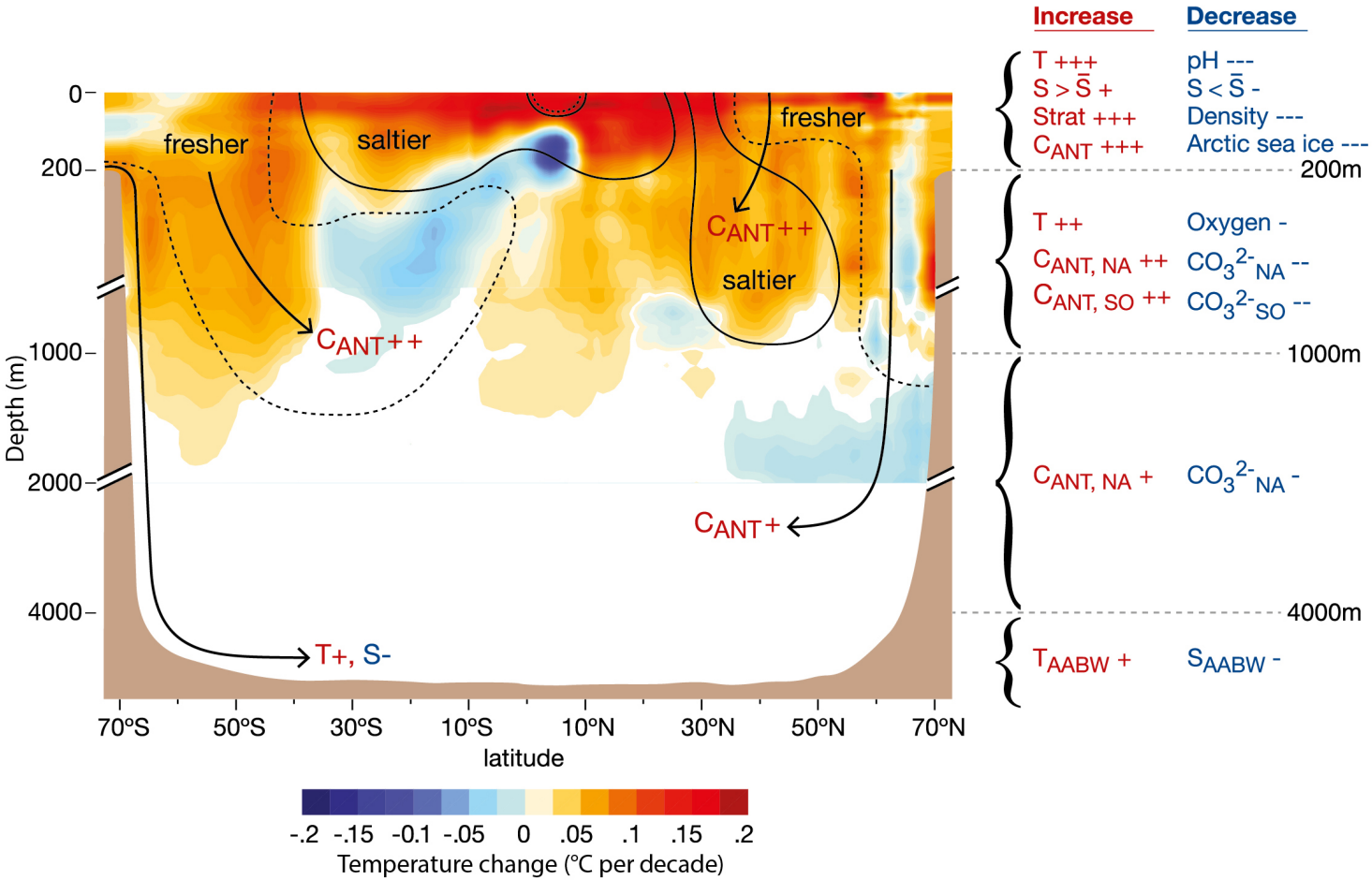

Figure 1.3: Summary of observed zonal mean changes in ocean variables. Temperature (°C per decade) and salinity (dotted line = freshening; solid line = salinification) changes are based on the 50-year trends of Durack and Wifjjels (2010) from 0-2000 m depth. Dominant ventilation pathways are overlain as solid arrows. Confidence levels (+++ = high confidence, ++ = medium confidence, + = low confidence) are assigned to observed increases (red, plus sign) or decreases (blue, minus sign). T = temperature, S = salinity, NA = North Atlantic, SO = Southern Ocean, AABW = Antarctic Bottom Water. Reproduced from Rhein et al. (2013).

et al., 2010) as the process of demonstrating that the climate, or a system affected by climate, has changed in a statistical sense, and that the likelihood of this observed change being caused by natural internal variability is low. *Attribution*, however, requires that an assignment of confidence can be given to the various forcing factors that cause a detected change.

Atmosphere-Ocean General Circulation Model (AOGCM) simulations can be used to separate the contributions of different external forcing factors and internal variability to observed climate change (e.g. Hegerl and Zwiers, 2011). The standard "optimal fingerprinting" approach (Hegerl et al., 1996; Hasselmann, 1997; Allen and Tett, 1999) involves the use of linear regression methods to compare observed changes in a climate variable against a series of model simulated spatial, temporal (or space-time) response patterns to different external forcings (or "fingerprints"). These so-called detection and attribution studies seek to express an observed change as the linear sum of various spatiotemporally unique responses to external forcings, such as changes in greenhouse gas concentration or solar output, and natural internal variability. A reliable estimate of observed internal variability is a necessary pre-requisite for detection and attribution assessment (e.g. Imbers et al., 2014). However, in lieu of centennial-scale climate records which are uncontaminated by external forcing this is generally provided by sampling long, unforced AOGCM simulations (or in some cases by using the intra-ensemble variability from a suite of transient simulations [e.g. Stott et al., 2003b]). A number of enhancements to the original Ordinary Least Squares (OLS; Hegerl et al., 1996) regression model used in detection studies have been made in recent years (*cf.* Stone et al., 2009; Hegerl and Zwiers, 2011). Particular focus has been given to accounting for sampling (Total Least Squares [TLS] regression; Allen and Stott, 2003) and structural (Error-In-Variables [EIV] regression; Huntingford et al., 2006) errors in model fingerprints. Large uncertainties remain, however, particularly with regard to quantifying the contribution of external forcing to climate change at regional scales and extreme events (Hegerl and Stott, 2014).

Detection and attribution studies conducted over the past ~ 20 years have been instrumental in quantifying the anthropogenic contribution to observed changes in Global Mean Surface Temperature (GMST). Based partly on the results of these analyses, Working Group 1 (WG1) of the Intergovernmental Panel on Climate Change (IPCC) states in its

Fifth Assessment Report (AR5) that "It is *extremely likely* that human activities caused more than half of the observed increase in GMST from 1951 to 2010" (Bindoff et al., 2013). A number of formal, fingerprint-based detection studies have also been conducted in order to detect external influences on observed changes in ocean properties (e.g. Hegerl et al., 2007; Bindoff et al., 2013). These studies have focused mainly on changes in ocean temperature (e.g. Barnett et al, 2005; Pierce et al., 2006; Palmer et al., 2009), with the most recent analysis of Pierce et al. (2012) identifying a detectable change in observed upper ocean (0–700 m) temperature for the period 1955–2004 based on combined space-time model fingerprints derived from 12 models participating in Phase 5 of the Coupled Model Intercomparison Project (CMIP5). Observed temperature changes are shown to be inconsistent with internal variability or natural external factors (volcanic and solar forcings) and consistent with anthropogenic external forcing at the 95 % confidence level, with Gleckler et al. (2012) demonstrating similar positive detection results to be robust across a range of different bias-corrected ocean temperature datasets.

External forcings have also been detected in observed 33-year trends of SSS for the global ocean and Pacific basin at the 90 % confidence level using model fingerprints which include natural and anthropogenic forcings, however for the Atlantic ocean observed changes are indistinguishable from model estimates of internal variability (Terray et al., 2012). This work has been extended by Pierce et al. (2012) who isolate a detectable anthropogenic signal in observed interior salinity changes down to 250 m depth at the 5 % significance level for the period 1955–2004. Interestingly, the authors also find that by combining physically linked temperature and salinity changes into a multi-tracer fingerprint the model-predicted anthropogenic signal strength increases, such that detection results are more robust than for each variable in isolation. This highlights the potential utility of multivariate signal vectors as a means of improving the detectability of externally forced changes in ocean properties relative to internal climate variability (Santer et al., 1995).

The detectability of external influences on recent changes in biogeochemical variables is less well constrained. As highlighted by Beaulieu et al. (2013) and Henson et al. (2010) in statistical analyses of ocean colour satellite records, confidence in detection is restricted by the lack of observations of sufficient duration to separate secular trends from long period internal variability within the ocean system. However, recently published synthesis

datasets of dissolved oxygen concentration ($[O_2]$; Sect. 1.3.2) and carbon (e.g. Surface Ocean CO_2 Atlas [SOCAT; Bakker et al., 2014b]) provide multi-decadal records of ocean biogeochemistry change, and could form the basis of formal detection and attribution studies (Sect. 1.5). Moreover, the most recent generation of Earth System Models (ESMs) output biogeochemical variables as standard practice for simulations co-ordinated through CMIP5 (Taylor et al., 2012), providing a suite of targeted historical experiments for analysis under a detection and attribution framework.

1.2 The oceanic oxygen cycle

1.2.1 Overview

The atmospheric and oceanic inventories of oxygen (O_2) are coupled via air-sea gas transfer (Q_F) down a partial pressure gradient, a relationship that can be expressed as:

$$Q_F = k_w \alpha (pO_2^{atm} - pO_2^{ocean}) \tag{1.1}$$

where k_w is the gas transfer velocity, α is the solubility of O_2 in seawater (e.g. Weiss et al., 1970) and pO_2^{atm} and pO_2^{ocean} are the partial pressures of oxygen in the atmosphere and surface ocean, respectively. This rapid exchange maintains surface ocean mixed layer ($<$ 100 m) dissolved oxygen concentration ($[O_2]_{surface}$) close to its saturation value ($[O_2]_{sat}$) for a given potential temperature and salinity (Garcia and Gordon, 1992). Equilibration of surface O_2 with the overlying atmosphere is, however, never perfect (Ito et al., 2004), with the largest near-surface oxygen disequilibria having been identified in high-latitude regions of water mass renewal (e.g. Gordon and Huber, 1990; Duteil et al., 2013).

In the oceanic interior, $[O_2]$ is chiefly set by the balance between the physical supply of this O_2-rich water into the subsurface via transport and mixing processes (hereafter, "ventilation"), biological supply from photosynthesis in the euphotic zone, and subsequent consumption of oxygen in the remineralisation of organic material. Accordingly, in ocean biogeochemistry models the conservation equation that describes the temporal evolution of passive tracers like oxygen can be written as (Eq. 1.2; after Enright et al., [2014] and Matear [2004]):

$$\frac{dO_2}{dt} = \nabla \cdot (\vec{u}O_2) + \nabla \cdot (\vec{K}\nabla O_2) + Q_F + Q_R \tag{1.2}$$

where $\vec{u}$ is fluid velocity (representing advection), $\vec{K}$ is the diffusion co-efficient, and Q_R represents oxygen production (via photosynthesis in the euphotic zone) and consumption (via remineralisation of organic material, with a contribution from the growth of nitrogen fixers on N_2 [Le Quéré et al., 2014a; Enright et al., 2014]).

Deviation over time in the observed [O_2] of a recently ventilated water parcel from [O_2]$_{sat}$ is termed the Apparent Oxygen Utilisation (AOU; Equation 1.3). AOU increases with ventilation age according to the rate at which organic material is oxidised by bacteria (Oxygen Utilisation Rate; $OUR = \frac{dAOU}{dt}$), and thus is used as a classical measure of respiration in the ocean interior (assuming that [O_2]$_{sat}$ = [O_2]$_{surface}$).

$$AOU = [O_2]_{sat} - [O_2] \tag{1.3}$$

High OUR and weakening ventilation allow for the development of a natural O_2 minimum near the base of the permanent thermocline (Wyrtki, 1962). These [O_2] minima are most pronounced within the so-called Oxygen Minimum Zones (OMZs; Fig. 1.4) of the eastern tropical oceans (e.g. Karstensen et al., 2008; Paulmier and Ruiz-Pino, 2009). In these regions, sluggish cyclonic circulation (within poorly ventilated "shadow zones" [Luyten et al., 1983]) and elevated export production maintain low-O_2 conditions at intermediate depths. As a result, open ocean OMZs contribute significantly to the global inventory of hypoxic ([O_2] $< 60\,\mu$mol kg^{-1}; $\sim 5\,\%$ of ocean volume [Deutsch et al., 2011]) and suboxic ([O_2] $< 5\,\mu$mol kg^{-1}; $\sim 0.05\,\%$ of ocean volume [Karstensen et al., 2008]) waters. Comparatively, as shown in Figure 1.4, upper ocean [O_2] is generally much higher across much of the well-ventilated mid- to high-latitude ocean where colder (more soluble) nutrient rich waters can be supersaturated with respect to atmospheric O_2 (e.g. $140\,\%$ saturation in surface waters west of the Antarctic peninsula [Carrillo et al., 2004]).

Exposure to low-O_2 conditions (or "dead zones" [Diaz and Rosenberg, 2008]) can cause negative physiological effects and increased mortality in aerobic marine biota if ambient [O_2] falls below a taxon-specific hypoxic threshold (e.g. Vaquer-Sunyer and Duarte, 2008; Gray et al., 2002). O_2 depletion can also impact significantly upon marine biogeochemical

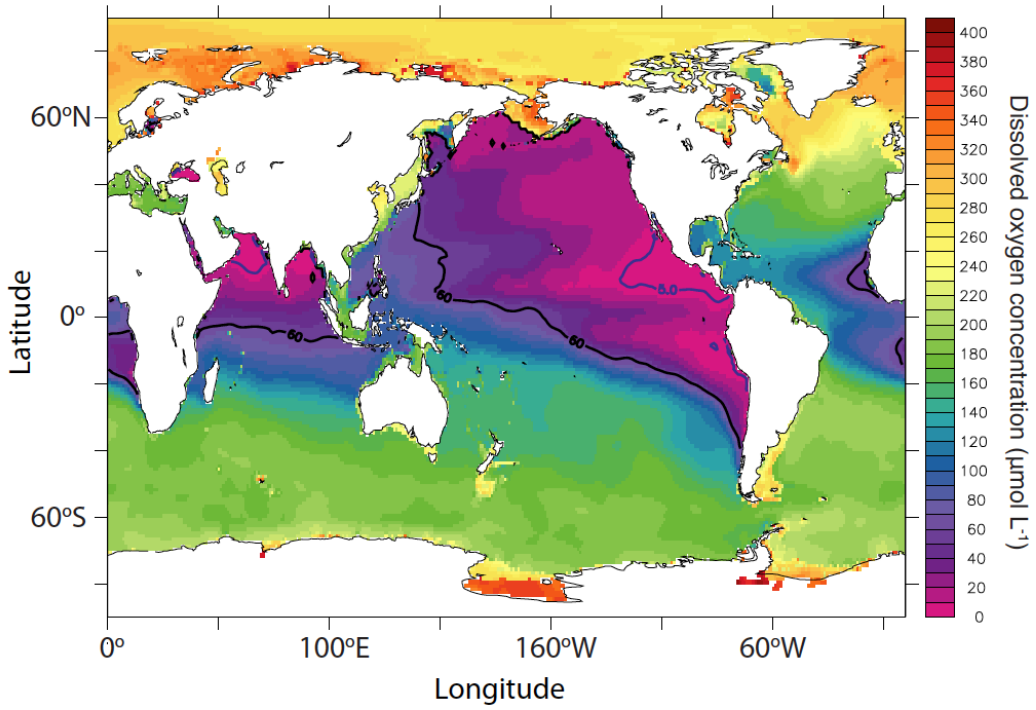

Figure 1.4: Distribution of $[O_2]$ minima (μmol L^{-1}) for the global ocean. Data obtained from Bianchi et al. (2012), who apply a linear correction to World Ocean Atlas (2005) $[O_2]$ based on *in situ* measurements, which reduces the underestimation of OMZ extent in gridded WOA fields. Hypoxic (60 μmol L^{-1}; black) and suboxic (5 μmol L^{-1}; purple) contours are overlain.

cycles, particularly nitrogen, with implications for nutrient availability and greenhouse gas emissions. Particularly, under suboxic conditions a shift occurs towards the use of nitrate (NO_3^-) as an oxidant in the microbial decomposition of organic material via denitrification – a dominant pathway for the removal of fixed inorganic nitrogen from the ocean (e.g. Gruber, 2008). In addition, despite occupying less than 10 % of the ocean by volume, hypoxic and suboxic waters account for $\sim$25–50 % of open ocean N_2O production (Codispoti, 2010; Suntharalingam et al., 2000) as a consequence of both enhanced denitrification (e.g. Naqvi et al., 2010a) and improved N_2O yields from nitrification (e.g. Frame and Casciotti, 2010; Bakker et al., 2014a) under low-O_2 conditions. Enhanced oceanic production of nitrous oxide has important implications for climate mitigation: since 2011, N_2O has the third largest radiative forcing of all anthropogenic greenhouse gases (0.17 ± 0.03 W m^{-2} [Myhre et al., 2013]). Uncertainties are large, however, particularly regarding the interaction between projected future oxygen changes and marine N_2O production (e.g. Bianchi et al., 2012; Freing et al., 2012).

1.2.2 Drivers of change in oceanic oxygen

Observations (Sect. 1.3) and prognostic model experiments (Sect. 1.4) indicate that a reduction in the oxygen inventory of the global ocean, termed "ocean deoxygenation" (Keeling et al., 2010; Falkowski et al., 2011), is a likely consequence of global climate change and ocean heat uptake. [O_2] responds to climate forcing both directly, via the reduced solubility of [O_2] at higher temperatures (ΔO_2^{sol}), and indirectly as a result of perturbation to the physical and biological processes which control [O_2] within the ocean interior (see Figure 1.5; Equation 1.4). Specifically, warming-induced stratification of the upper ocean (Rhein et al., 2013; Capotondi et al., 2012) reduces exchange between surface waters and the ocean interior, increasing ventilation age and allowing for more oxygen utilisation to occur. Importantly, ventilation is taken here to mean all processes which transport oxygen to the ocean interior ($sensu$ Keeling et al., 2010), since increases in thermal stratification will impede both: (1) ΔO_2^{mld} : the immediate re-supply of O_2 from near-surface to thermocline (i.e. mixed layer detrainment [e.g. Deutsch et al., 2006; Kwon et al., 2014]) and (2) ΔO_2^{circ} : water mass renewal and circulation pathways within the ocean interior (e.g. Helm et al., 2011; Brennan et al., 2008).

Linked to these physical controls, biological processes (ΔO_2^{bio}) such as changes in export production (Bopp et al., 2001) and the fraction of particulate organic material (POM) which is remineralised at a given depth (e.g. Hofmann and Schellnhuber, 2009) will also impact upon ΔO_2^{tot}. For example, increased thermal stratification at mid- to low latitudes has also been shown to drive a reduction in upwelling of nutrient-rich waters into the photic zone (Bopp et al., 2001) yielding a decrease in biological export production and thus OUR, such that thermocline [O_2] increases (e.g. Bopp et al., 2002). The relative contribution of this process, which reduces deoxygenation associated with increases in ventilation age, will be related in part to the disproportionate contributions of organic (Particular Organic Carbon [POC]) versus inorganic (preformed) pathways of nutrient export in a more stratified ocean (Keeling et al., 2010).

These competing processes can be combined simply as follows to provide an estimate of the overall change in subsurface [O_2] (ΔO_2^{tot}) in response to external perturbation (with an additional term, ΔO_2^{diseq}, representing changes in the atmosphere-ocean disequilibrium of $[O_2]_{surface}$, as noted in Section 1.2.1).

$$\Delta O_2^{tot} = \Delta O_2^{sol} + \Delta O_2^{mld} + \Delta O_2^{circ} + \Delta O_2^{bio} + \Delta O_2^{diseq} \tag{1.4}$$

1.3 Observed changes in oceanic oxygen

1.3.1 Regional perspective

Dissolved oxygen has been a staple oceanographic measurement for more than a century, used alongside temperature and salinity as a tool for understanding ocean circulation (e.g. Körtzinger et al., 2005). As a result, the spatiotemporal record of [O_2] is more complete than for any other biogeochemical parameter, the reliability of which owes a debt to the early development of an elegant chemical titration method which remains in use today (Winkler titration; Winkler [1888]). These data, therefore, have the potential to provide unique insights into the state of the ocean system over the historical period, particularly with regard to the influence of anthropogenic warming on coupled physical-biogeochemical processes (Joos et al., 2003).

It must, however, be acknowledged that early titration measurements contain some inaccuracies (e.g. Wong and Li, 2009; Bindoff et al., 2007), owing, for instance, to the use of visual rather than automated methods in the identification of titration end points (Naqvi et al., 2010b). Particularly, a systematic [O_2] overestimation of up to 5 μmol L^{-1} has been identified in early measurements of low-O_2 (OMZ) waters (Naqvi et al., 2010b; Codispoti and Christensen, 1985). Bianchi et al. (2012) demonstrate that this positive observational bias within OMZs is also entrained into gridded, climatological [O_2] data products (e.g. World Ocean Atlas 2005 [Garcia et al., 2006]; See Figure 1.4), due to a combination of measurement error, interpolation artifacts, and natural internal variability in oceanic oxygen (as also noted by Garcia et al. [2005]). However, Gilbert et al. (2010) show in a meta-analysis of [O_2] data that measurement inconsistences associated with refinements to analytical methods (e.g. Jones et al., 1992; Morrison et al., 1999) have a negligible impact on the calculation of large-scale historical trends. Moreover, recent data compilations (see Section 1.3.2) synthesise quality-controlled *in-situ* datasets (e.g. Hydrobase-2 [Curry, 2008]) and state-of-the-art optode O_2 measurements from profiling floats (e.g. Gruber et al., 2010; Johnson et al., 2009; Körtzinger et al., 2005) to generate

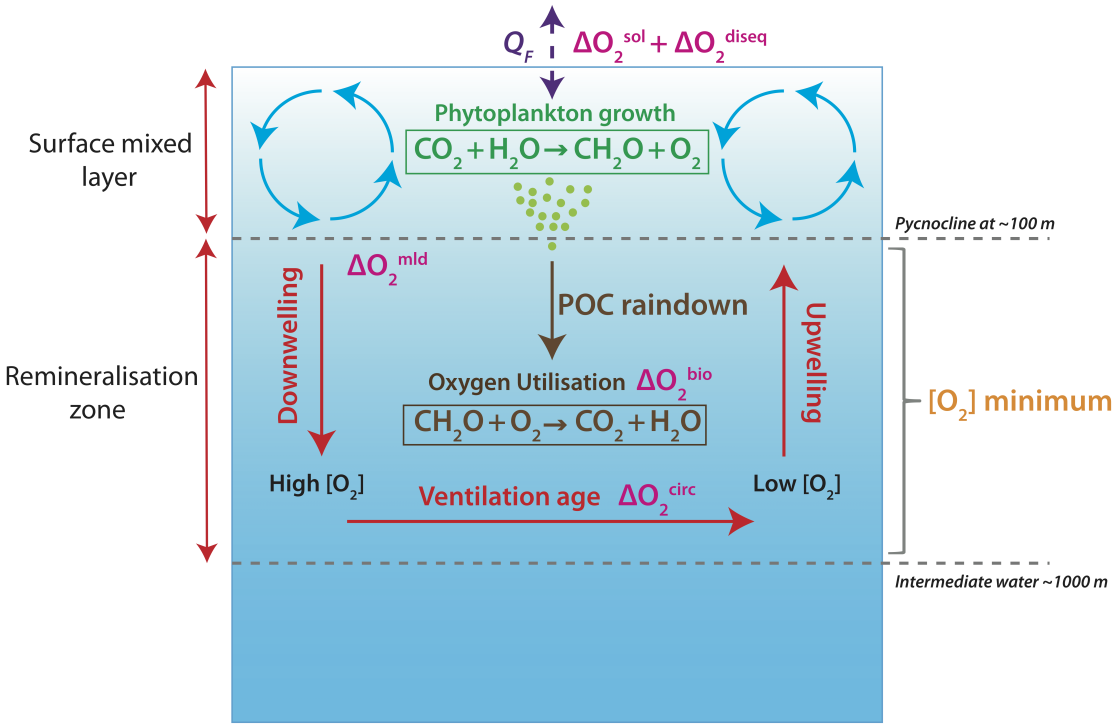

Figure 1.5: Diagram summarising the changing oceanic oxygen cycle. The oceanic reservoir of oxygen communicates with the atmosphere via air-sea gas exchange (Q_R). In the ocean interior a change in [O_2] over time can be driven by changes in: (1) surface ocean O_2 solubility (ΔO_2^{sol}) and atmosphere-ocean disequilibrium (ΔO_2^{diseq}) (2) ventilation (ΔO_2^{mld} + ΔO_2^{circ}) and (3) biological utilisation of oxygen in the remineralisation of POC (ΔO_2^{bio}).

reliable [O_2] trend estimates, whilst also objectively mapping data to reduce sampling biases associated with changing observational coverage (e.g. Stramma et al., 2012a; Helm et al., 2011).

Continuous time series measurements in the subarctic North Pacific (Whitney et al., 2007; Ono et al., 2001) provide the longest record of open ocean [O_2] change, allowing historical trends and variability to be interrogated. These data reveal compelling evidence of secular subsurface [O_2] decreases over the last $\sim$ 50 years, with linear [O_2] declines of $\sim 0.7\ \mu\text{mol}\,\text{kg}^{-1}\,\text{yr}^{-1}$ at both Ocean Station Papa in the Eastern North Pacific (Whitney et al., 2007) and within the Oyashio Current region of the Western North Pacific (Ono et al., 2001) on isopycnal surfaces within the 100-450 m depth range (Fig. 1.6). Major [O_2] decreases across much of the subarctic North Pacific are also evident in ocean "snapshots" obtained from World Ocean Circulation Experiment (WOCE) repeat sections between the 1980s and 1990s (Emerson et al., 2004), and have been associated with a long-term reduction in outcropping of lower ventilated thermocline waters (σ = $\sim$ 26.6) in response

to elevated stratification using model hindcasts (Deutsch et al., 2005; Deutsch et al., 2006). However, as shown in Figure 1.6, North Pacific [O_2] time series measurements also exhibit significant variability on quasi-decadal timescales, which complicates the interpretation of secular changes and potential detection of climate signals. Such patterns are characteristic of basin scale variability in upper ocean [O_2] and AOU, whereby small linear trends are often superimposed upon significant interannual to decadal fluctuations (Garcia et al., 2005). In the case of the subarctic North Pacific, the mechanism driving observed (natural) variability in mid-depth [O_2] remains uncertain (Keeling et al., 2010; Cummins and Masson, 2012; Ito and Deutsch, 2010). However, Andreev and Baturina (2006) suggest that these low frequency ($\sim$ 17 year period [Ito and Deutsch, 2010]) oscillations can be explained by a combination of large-scale climate variability associated with the intensity of the Aleutian low-pressure system (North Pacific Index [Trenberth and Hurrell, 1994]), tidal forcing and wind stress.

Observations from the North Atlantic provide a complementary perspective, with substantial decreases in upper-ocean [O_2] reported in subpolar mode waters between 1988 and 2003 by Johnson and Gruber (2007). The authors attribute these changes to cooling driven by a shift from high to low NAO (Hurrell et al., 2003) state, however the short ($\sim$ 15 year) time period and limited spatial coverage confound a full attribution. Since then, Stendardo and Gruber (2012) have compiled a high quality [O_2] dataset for the entire North Atlantic Ocean that provides an unprecedented assessment of long-term [O_2] changes along isopycnal surfaces for the period 1960-2009. Similarly, these data show decreases of $\sim -4.8 \pm 2.2\,\mu\text{mol}\,\text{kg}^{-1}$ across mode and upper intermediate waters of the North Atlantic. This decline is, however, unrelated to NAO shifts and attributable mainly to ventilation and circulation changes (ΔO_2^{mld} + ΔO_2^{circ}), based on water mass O_2 to heat change ratios which exceed those expected in response to solubility changes (ΔO_2^{sol}) alone. Interestingly, deeper layers of the North Atlantic (Lower Intermediate and Labrador Sea Water) exhibit coeval increases in [O_2] which can be associated mainly with NAO factors – a consequence of increased oxygen solubility driven by strong water mass cooling under an increasingly positive NAO. The recent shift in NAO towards a more negative state, as noted by Stendardo and Gruber (2012), could have important implications for future oxygenation of lower North Atlantic intermediate waters with the potential for exacerbation of any [O_2] changes

driven by ocean warming. Moreover, the differing interpretations of oxygen changes in the North Atlantic offered by Johnson and Gruber (2007) and Stendardo and Gruber (2012) highlight the importance of spatiotemporal coverage to process level understanding.

At lower latitudes, Stramma et al. (2008) also report long-term negative trends in $[O_2]$ (-0.13 to $-0.34\,\mu\text{mol}\,\text{kg}^{-1}\,\text{yr}^{-1}$) over the last 50 years at intermediate depths within the established OMZs of the eastern tropical Atlantic and equatorial Pacific Ocean (Fig. 1.6). It has been suggested that these changes may be related to a weakening of the zonal jets that supply oxygenated water into OMZs along isopycnal surfaces (e.g. the tropical North Atlantic [Brandt et al., 2010]). Observed $[O_2]$ decreases have been accompanied with a marked vertical expansion of OMZ waters and shoaling of the mid-depth hypoxic boundary – a phenomenon with wide-ranging implications for pelagic ecosystems and fisheries (*cf.* Gilly et al., 2013). For example, OMZ shoaling of $\leq 1\,\text{m}\,\text{yr}^{-1}$ has been associated with a 15 % habitat loss in the upper 200 m of the tropical northeast Atlantic OMZ between 1960 and 2010 (Stramma et al., 2012b). However, as with historical changes in the subpolar North Pacific and North Atlantic $[O_2]$, the role of multidecadal variability driven by the dominant climate modes remains important to OMZ dynamics. For example, Deutsch et al. (2011) show, using a forced ocean biogeochemistry model, that thermocline depths in the tropical Pacific OMZ are highly correlated with the Pacific Decadal Oscillation (an index of North Pacific Sea Surface Temperature variability), which can be invoked to explain 24 % of simulated historical variability in suboxic volume.

A recent meta-analysis of $[O_2]$ time series data carried out by Gilbert et al. (2010) suggests the coastal zone may also be an import locus of historical deoxygenation – with an order of magnitude larger median rate of coastal $[O_2]$ decrease (0–30 km from coast) relative to the open ocean between 1976 and 2000. In addition, a significantly greater proportion of negative $[O_2]$ trends are found in available time series data for the coastal zone (64 %) compared to the open ocean (49 %). As such, an understanding of coastal hypoxia is necessary to fully quantify changes to the global ocean oxygen inventory. Various coastal and shelf sea regimes have experienced $[O_2]$ decreases and increasing hypoxia over the historical period (*cf.* Rabalais et al., 2010; Zhang et al., 2010). Particularly, oxygen depletion has been reported in eastern boundary current systems, where upwelling and advective processes can transfer O_2-poor water from offshore onto the inner shelf (e.g.

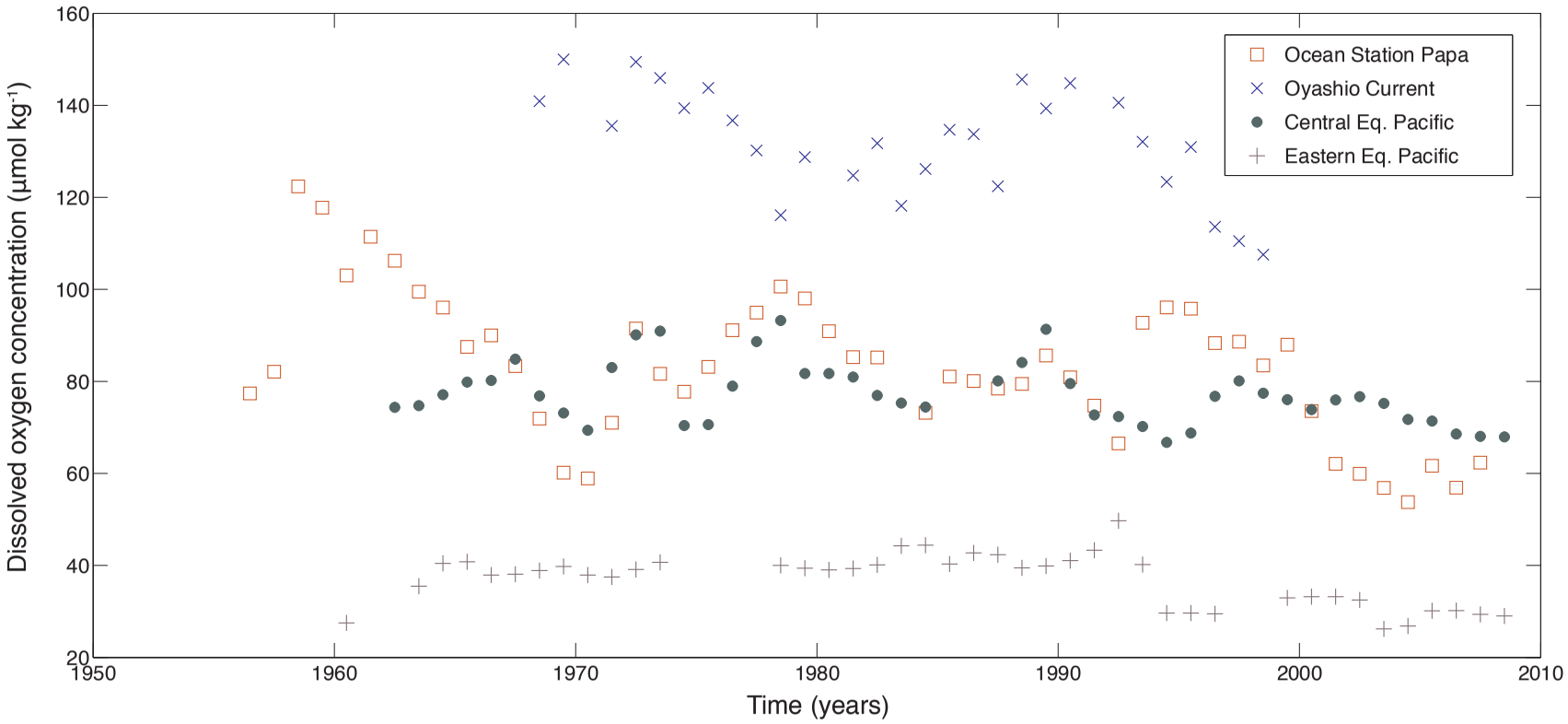

Figure 1.6: Summary of [O_2] time series measurements (μmol kg^{-1}) for the Pacific Ocean. Data are from Ocean Station Papa in the Eastern North Pacific (50°N, 145°W; σ = 26.9 $\sim$ 250–350 m [Whitney, F. Pers. Comm.; Whitney et al., 2007; Whitney et al., 2013]), the Oyashio Current region in the Western North Pacific (39–42°N, 143–145°E, σ = 26.9 $\sim$ 400–450 m [Ono, T., Pers. Comm.; Keeling, R., Pers. Comm.; Ono et al., 2001]), and the central (5°S–5°N, 165–175°W) and eastern (5°S–5°N, 105–115°W) equatorial Pacific (300–700 m [Stramma, L., Pers. Comm.; Stramma et al., 2008]).

Chan et al., 2008; Bograd et al., 2008; Grantham et al., 2004), providing a mechanism by which open ocean oxygen dynamics can influence the coastal zone. Summer stratified regimes, such as the semi-enclosed shelf seas, have also experienced secular oxygen decreases in bottom waters over the historical period (e.g. the North Sea; Queste et al., 2012), however the detectability of these changes relative to internal variability remains uncertain (e.g. Greenwood et al., 2010; Weston et al., 2008; see Section 1.5).

There has also been a global increase in the number of low-[O_2] coastal "dead zones", with hypoxic systems now occupying an area of more than 245,000 km^2 (Diaz and Rosenberg, 2008). Hypoxic development in the coastal ocean is predominantly driven by anthropogenic perturbation to the riverine flux of nutrients and organic material, which stimulates localised eutrophic conditions and elevated AOU in the coastal ocean (e.g. Rabalais et al., 2010). However physical alteration to the coastal zone by climate change may also influence [O_2] dynamics, for example via changes in stratification and regional wind patterns, which impose a significant control on mixing processes (see Figure 1.7; Rabalais et al., 2010; Rabalais et al., 2009). Notably, Gilbert et al. (2010) find that the most acute coastal [O_2] declines are detected both at the surface and beneath the mixed layer ($>$ 100 m), which is inconsistent with the expected [O_2] signature of enhanced eutrophication ($\sim$ 20-50 m depth), suggesting a link to solubility and ventilation changes. This [O_2] fingerprint indicates that increased hypoxia in the coastal zone may be modulated by historical warming, warranting further investigation (Sect. 1.5).

1.3.2 Global perspective

Observations and model hindcasts across ocean basins provide a consistent view of recent changes in oceanic oxygen whereby secular (mainly) decreasing trends in subsurface [O_2] driven by physical processes (ΔO_2^{mld} + ΔO_2^{circ}) are overlain by significant interannual to decadal variability. This interaction between forced and unforced variability, associated mainly with the dominant climate modes (e.g. NAO [Stendardo and Gruber, 2012]; PDO [Deutsch et al., 2011]), complicates the interpretation of trends, particularly on relatively short ($<$ 20 year) timescales (Gruber, 2009). Unforced AOGCM simulations also highlight the importance of natural climate modes in modulating [O_2] changes, with the NAO and PDO explaining more than 50 % of simulated internal variability in [O_2] of the North

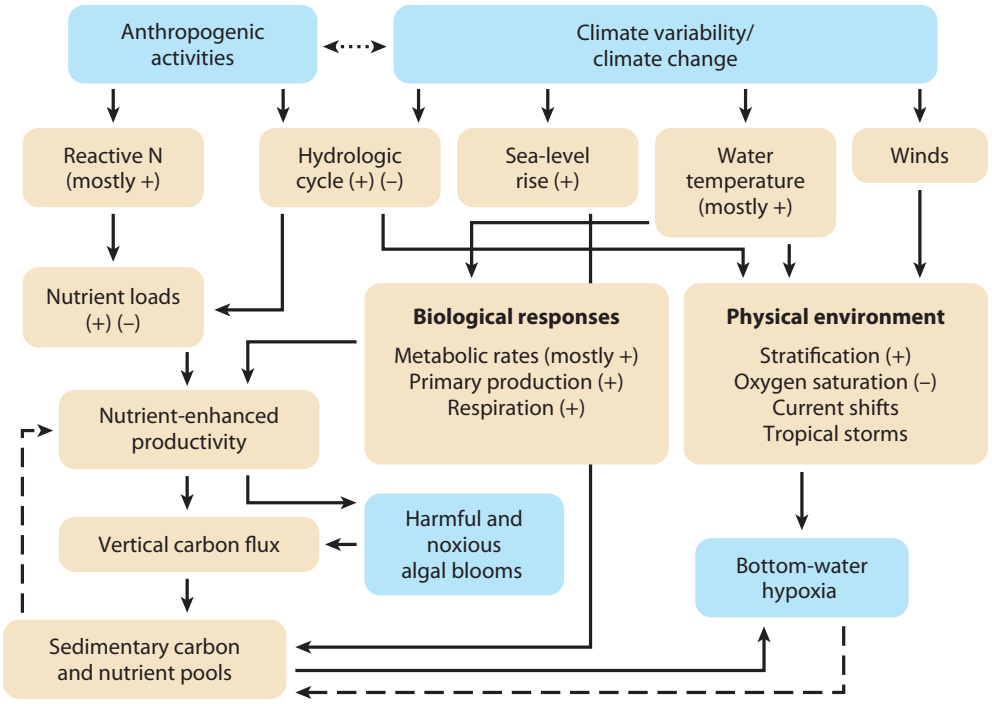

Figure 1.7: Summary of physical and biological responses to climate change and anthropogenic activities, and their influence on coastal hypoxia and algal bloom formation. Positive (+) interactions indicate a worsening of hypoxia and vice versa. Dashed lines indicate negative feedbacks within the system. Reproduced with permission from Doney et al. (2012).

Atlantic and North Pacific, respectively (Frölicher et al., 2009). This climate variability has been associated with large-scale propagating [O_2] anomalies (e.g. Deutsch et al., 2006), which, along with incomplete data coverage, preclude unequivocal detection of anthropogenic climate trends. Particularly, the potential exists for aliasing of a secular forced response with climate noise where temporal resolution is limited and internal variability is large, for instance, in the analysis of repeat hydrographic sections in the North Atlantic (Johnson and Gruber, 2007). In this case, decadal scale fluctuations in [O_2] associated with natural patterns of variability may be projected onto long-term trends, yielding erroneous attribution to an external forcing. Gilbert et al. (2010) demonstrate this point using multiple synthetic time series of different lengths (10, 25, and 50 year), assuming random white (climate) noise with a realistic interannual variability ($\sigma = 23\,\mu\text{mol}\,\text{L}^{-1}$), finding that the likelihood of large amplitude trends in [O_2] increases as time series become shorter, and vice versa. Thus, in order to constrain the anthropogenic component of observed [O_2] changes there is a requirement for internally consistent data (e.g. Stendardo and Gruber, 2012) on large spatiotemporal scales so as to improve the signal to noise ratio.

A more holistic perspective is provided by recent global compilations of $[O_2]$ data, which reveal coherent subsurface $[O_2]$ decreases across nearly all ocean basins, particularly at mid- to high latitudes and within established OMZs (as reviewed in Section 1.3.1). Area mean trends derived from historical data converge on a global thermocline $[O_2]$ decrease of $\sim 0.05\,\mu\text{mol kg}^{-1}\,\text{yr}^{-1}$, however trend estimates range from $-0.042\,\mu\text{mol kg}^{-1}\,\text{yr}^{-1}$ (1970s–1990s [Helm et al., 2011]) to $-0.066\,\mu\text{mol kg}^{-1}\,\text{yr}^{-1}$ (1960–2010 [Stramma et al., 2012a]), primarily due to differences in the sampled time period and data used. These trends are allied with a $\sim 0.55 \pm 0.13 \times 10^{14}$ mol yr^{-1} depletion to the global oceanic oxygen inventory (Helm et al., 2011), consistent with, but slightly larger than, observational estimates of oceanic O_2 outgassing since $\sim$ 1990 (0.44×10^{14} mol O_2 yr^{-1}) derived from air-sea heat fluxes (Keeling and Manning, 2014; Keeling and Garcia, 2002). Based on these results, the IPCC, in WG1 of AR5, states that there is *medium confidence* (high agreement based on limited evidence) that observed thermocline $[O_2]$ has declined in many regions of the ocean since the 1960s, and that this decrease is consistent with the expected response of oxygen to climate-driven ventilation changes and thermal effects (Rhein et al., 2013).

1.4 Future ocean oxygen depletion

Future changes in oceanic oxygen have been investigated using a range of Intermediate Complexity Earth System Models (EMICs; Plattner et al., 2001; Schmittner et al., 2008; Oschlies et al., 2008; Shaffer et al., 2009) and AOGCMs (Sarmiento et al., 1998; Matear et al., 2000; Bopp et al., 2002; Matear and Hirst, 2003; Frölicher et al., 2009; Cocco et al., 2013; Bopp et al., 2013; Gnanadesikan et al., 2012). There is broad consensus that future climate warming will exacerbate observed ocean oxygen depletion and increase the role of the ocean as a net source of oxygen to the atmosphere. As shown in Table 1.1, model simulated decreases in global mean $[O_2]$ range from 3 to 12 $\mu\text{mol kg}^{-1}$ for the end of the century (equivalent to a 1–7 % total inventory loss) under a range of future climate forcings. The lower bound placed on this multi-model estimate is provided by Frölicher al. (2009) who attribute their more muted global $[O_2]$ decrease (3–4 $\mu\text{mol kg}^{-1}$) in part to the lower climate sensitivity of CSM1.4-CCCM. These changes are generally consistent with the most recent suite of Earth System Model (ESM) experiments conducted under

CMIP5 (Taylor et al., 2012), which project global [O_2] decreases of 1.5–4 % between 1990–1999 and 2090–2099 for all Representative Concentration Pathways (RCPs; Fig. 1.8A). AOGCMs also simulate significant increases in net sea-air oxygen flux over the 21st century in response to protracted ocean warming, with outgassing of 0.23–0.40 mol O_2 m^{-2} y^{-1} for the year 2100 (relative to a modern baseline of $\sim$ 0–0.1 O_2 m^{-2} y^{-1} [Bopp et al., 2002; Frölicher et al., 2009]). However, there is considerable natural internal variability in sea-air O_2 fluxes on interannual ($\pm$ 0.12 mol O_2 m^{-2} y^{-1}) to decadal ($\pm$ 0.04 mol O_2 m^{-2} y^{-1}) timescales (Bopp et al., 2002), which is generally poorly constrained by the current generation of ocean biogeochemistry models (Rödenbeck et al., 2008).

Nearly all models project future declines in subsurface [O_2] to be mainly driven by warming-induced increases in density stratification, reducing the resupply of oxygen to the ocean interior via circulation (ΔO_2^{circ}) and mixing (ΔO_2^{mld}) processes (Plattner et al., 2001; Bopp et al., 2002; Matear and Hirst, 2003). Comparatively, solubility changes (ΔO_2^{sol}) are projected to explain between 18–50 % of simulated total ocean deoxygenation by 2100 (Table 1.1). This prediction is consistent with observed patterns of [O_2] change, with Helm et al. (2011) attributing up to 85 % of recent deoxygenation of the ocean interior to weakening ventilation, and the remainder to reduced solubility (ΔO_2^{sol}).

Prognostic ocean biogeochemistry models consistently project ventilation driven deoxygenation across much of the mid- to high-latitude ocean by the end of the century, with CMIP5 ESMs simulating the largest subsurface [O_2] decreases (up to 50 mmol m^{-3}) in the North Atlantic, North Pacific and Southern Ocean for both RCP2.6 and RCP8.5 (Fig. 1.8C–1.8D). There is good agreement between models that persistent [O_2] decreases are expected in mode and intermediate waters of the North Pacific by 2100, driven predominantly by shoaling of the mixed layer, but with a significant contribution from solubility effects (Frölicher et al., 2009; Matear and Hirst, 2003; Bopp et al., 2013).

A number of model studies also indicate that changes in overturning circulation and rates of water mass renewal will contribute significantly to future ocean deoxygenation, particularly in the North Atlantic and Southern Ocean (Plattner et al., 2001; Frölicher et al., 2009). For example, Plattner et al. (2001) simulate decreases in North Atlantic Deep Water (NADW) formation of 40–60 % associated with considerable ($> 100\,\mu$mol kg^{-1}) [O_2] depletion of the intermediate and deep North Atlantic by the end of the century.

Table 1.1: Summary of projected future global ocean deoxygenation by 2100 for a range of AOGCMs and EMICs (adapted from Keeling et al. [2010]).

Study	Model	Forcing	Mean $[O_2]$ Decrease (μmol kg^{-1}) [1, 2]	Solubility Contribution (%)	Net Sea-Air O_2 Flux at 2100 (mol m^{-2} y^{-1}) [2]
Sarmiento et al., 1998	GFDL		7 [3]		
Matear et al., 2000	CSIRO	IS92a		18	0.40
Plattner et al., 2001, 2002	Bern 2D	SRES A1	12	35	
Bopp et al., 2002	OPAICE-LMD5	SRES A2 [4]	4	25	0.35
Matear and Hirst, 2003	CSIRO	IS92a	9	26	
Schmittner et al., 2008	UVic	SRES A2	9		
Oschlies et al., 2008	UVic	SRES A2	9		
	UVic-variable C:N	SRES A2	12		
Frölicher et al., 2009	NCAR CSM1.4-CCCM	SRES A2	4	50	0.23 ± 0.1
		SRES B1	3		
Shaffer et al., 2009	DCESS	SRES A2	10 [5]		

[1] Assuming a total ocean mass of 1.48×10^{21} kg.
[2] Relative to pre-industrial baseline in 1750.
[3] Model simulation ends at 2065.
[4] Radiative forcing of non-CO_2 GHGs is excluded from this simulation.
[5] For simulations with reduced ocean exchange (Shaffer, G., Pers. Comm.).

CCCM = Coupled-Climate-Carbon Model; CSIRO = Commonwealth Scientific and Industrial Research Organisation; DCESS = Danish Center for Earth System Science; GFDL = Geophysical Fluid Dynamics Laboratory; IPSL = Institute Pierre Simon Laplace; NCAR = National Center for Atmospheric Research; IS92 = IPCC scenarios for 1992; SRES = Special Report on Emission Scenarios; UVic = University of Victoria.

Similarly, Frölicher et al. (2009) found decreases in Atlantic Meridional Overturning Circulation (AMOC) of 27 % by 2100 under a SRES A2 emissions scenario, attributing $[O_2]$ decreases of $\sim 30\,\mu\text{mol}\,\text{kg}^{-1}$ in deep (> 2000 m) water masses of the North Atlantic to coeval increases in ventilation age and OUR. However, as noted by Bopp et al. (2013) in their analysis of 10 CMIP5 ESMs, projected deoxygenation and warming trends in North Atlantic water masses vary considerably between models due to considerable differences in simulated AMOC weakening (Cheng et al., 2013). For instance, Bopp et al. (2002) report much smaller reductions in NADW and Antarctic Bottom Water (AABW) formation (10 % and 13 %, respectively, for 2100) which yield more muted $[O_2]$ decreases (15–20 $\mu\text{mol}\,\text{kg}^{-1}$) at high latitudes when compared to other physical models in which overturning responds strongly to imposed climate forcing (e.g. Plattner et al., 2001; Matear and Hirst, 2003).

The Southern Ocean (south of 60°S) is also predicted to experience considerable subsurface deoxygenation in response to future reductions in high-latitude convection and ventilation processes. Projected $[O_2]$ decreases at intermediate depths ($\sim$ 200–400 m) range from 50–70 $\mu\text{mol}\,\text{kg}^{-1}$ for model simulations integrated to 2100 (Matear et al., 2000; Matear and Hirst, 2003; Frölicher et al., 2009). However, major uncertainties remain regarding the impact of climate change on ocean ventilation processes (particularly as to the roles of stratification and wind forcing [e.g., Le Quéré et al., 2007; Böning et al., 2008]) such that model projections of large magnitude mid- to high-latitude deoxygenation remain tentative.

Uncertainties are even larger regarding the impact of climate change on $[O_2]$ within the tropical oceans. Central to this uncertainty is the inability of current ESMs to reproduce observed (climatological) volumes of observed hypoxic and suboxic water (Cocco et al., 2013; Bopp et al., 2013; Fig. 1.8B) and the recent vertical expansion and intensification of eastern tropical OMZs (e.g. Stramma et al., 2012a; Sect. 1.3.1). Particularly, models generally simulate anomalously large suboxic volumes at low latitudes (Cocco et al., 2013; Duteil and Oschlies, 2011) along with historical $[O_2]$ increases in the tropical thermocline, counter to observed deoxygenation (Stramma et al., 2012a). These model uncertainties are also evident in future projections of hypoxia (defined in their study as $< 50\,\mu\text{mol}\,\text{kg}^{-1}$) provided by CMIP5 ESMs, which variously simulate both increases and decreases in

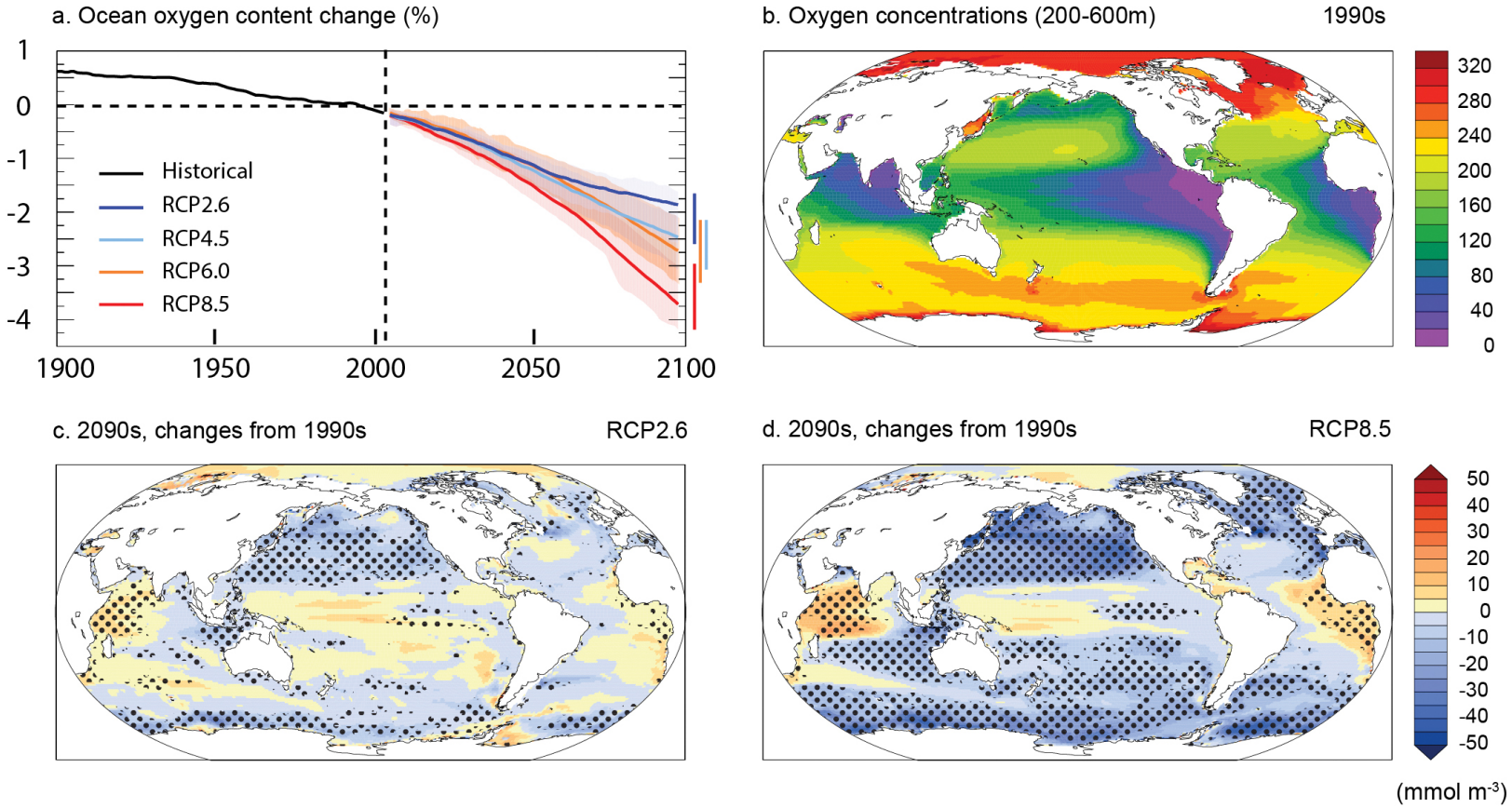

Figure 1.8: (**A**) Summary of CMIP5 model simulated projections for future ocean oxygen content change under a range of RCPs. Presented as a multi-model mean anomaly relative to the 1990s (%), with shading representing inter-model range. (**B**) CMIP5 model [O_2] (μmol L^{-1}) distribution for the thermocline (200–600 m). (**C**) and (**D**) show changes in simulated thermocline [O_2] for the 2090s relative to the 1990s for RCP2.6 and RCP8.5, respectively. Stippling indicates agreement in the sign of change for at least 80 % of CMIP5 models. Reproduced from Ciais et al. (2013).

hypoxic volume by 2100 under RCP8.5 (Bopp et al., 2013). Cocco et al. (2013) find more model-model agreement for simulated changes in suboxia ($< 5\,\mu\text{mol}\,\text{kg}^{-1}$), however the majority of ESMs project a contraction in suboxic volume (up to $-10\,\%$) between the 1870s and 2090s following a SRES A2 emissions pathway. These projections are contrary to recent quasi-continuous time series measurements, which indicate an expansion of low-O_2 waters in the tropical oceans over the last 50 years (Stramma et al., 2008; Sect. 1.3.1).

Over oxygenation of the tropical thermocline in hindcast and prognostic model simulations has been attributed to a range of physical and biogeochemical model deficiencies. A widely posited driver for poor performance in coarse resolution ocean-climate models is the absence of mesoscale eddies and tropical zonal currents which exert a major control on ventilation processes within the eastern tropical OMZs (Brandt et al., 2010; Keeling et al., 2010). Duteil et al. (2014) address this point using 2 configurations of the NEMO physical ocean model with differing horizontal resolutions, and find that representation of the eastern tropical Atlantic OMZ improves significantly when using a high resolution (eddying) physical model, owing to a more intense equatorial current system supplying oxygen into the OMZ. Other physical processes have also been shown to be important in controlling tropical [O_2] dynamics and the propagation of low-O_2 waters, particularly model parameterisation of isopycnal (Gnanadesikan et al., 2012) and diapycnal (Duteil and Oschlies, 2011) mixing, and the impact of upper ocean stratification on ventilation ages in the tropical thermocline (Gnanadesikan et al., 2007).

A number of poorly constrained ocean carbon cycle feedbacks not included in most ESMs could also impact upon model representation of tropical [O_2]. For example, EMIC experiments which include a pCO_2-sensitive C:N drawdown ratio in primary production, as suggested by some mesocosm experiments (Riebesell et al., 2007), project future increases of up to 50 % in the volume of the suboxic waters by 2100 associated with enhanced remineralisation of POC (Oschlies et al., 2008; Tagliabue et al., 2011). Additionally, Hofmann and Schellnhuber (2009) suggest, using targeted ocean carbon cycle model experiments, that future hypoxic extent could be amplified by changes in the POC - $CaCO_3$ export ratio in response to rising pCO_2. Ocean acidification under simulated high-CO_2 conditions reduces biogenic calcification and the rain rate of $CaCO_3$ from the surface

ocean, weakening the effect of $CaCO_3$ mineral ballasting on POC export fluxes. As a result, POC is remineralised at shallower depths (200 – 800 m) as mineral ballast fluxes weaken, exacerbating the projected expansion of established shallow hypoxic waters (Hofmann and Schellnhuber, 2009). These studies suggest that the interactive effects of climate change and ocean acidification on the biological pump could be significant in driving future propagation of low-O_2 and OMZ waters.

Overall, there is significant qualitative agreement between prognostic ocean-climate models that future anthropogenic warming will exacerbate observed [O_2] decreases, however regional heterogeneities and differences in the magnitude of projected [O_2] change are evident. Inconsistencies between model platforms can be attributed to differences in parameterisation of key processes which control oceanic oxygen, and uncertainties as to the response of ocean biogeochemistry and circulation to future climate change. However, most models agree that future ocean deoxygenation will be driven chiefly by changes in ventilation of the ocean interior in response to enhanced stratification, with pronounced [O_2] depletion projected for subsurface waters of the North Pacific, North Atlantic and Southern Ocean by the end of the century. EMICs integrated over longer (millennial) timescales also suggest that on-going anthropogenic ocean warming amplified by positive feedbacks within the Earth System could yield severe, long-term ocean deoxygenation, with global mean [O_2] decreases of up to 56 μmol kg^{-1} below pre-industrial levels in idealised experiments using an A2 emissions scenario and high climate sensitivity (Shaffer et al., 2009). However, as noted by Keeling et al. (2010), a necessary prerequisite for credible projections are models that can adequately reproduce observed trends and variability in oceanic oxygen.

1.5 Thesis structure

1.5.1 Objectives

The overarching aim of this research is to investigate the detectability of secular changes in [O_2] relative to natural variability at regional and global scales, using both statistical methods and targeted model experiments. Particularly, this work aims to advance the current understanding of the role of external factors in driving observed changes in oceanic

oxygen by synthesising observations and output from a range of ocean biogeochemistry models.

Specific objectives are to:

1. Evaluate the performance of recent ESM simulations in reproducing observed historical changes and variability in oceanic oxygen

2. Quantify the detectability of observed changes in open ocean [O_2] at global and ocean basin scales relative to natural internal variability

3. Investigate the impact of imposed atmospheric forcing on the spatiotemporal distribution of oceanic oxygen over the last $\sim$ 50 years in a hindcast ocean biogeochemistry model

4. Investigate the impact of biogeochemical parameterisations of ocean carbon cycle feedbacks on the spatiotemporal distribution of oceanic oxygen in a hindcast ocean biogeochemistry model

5. Examine fingerprints of secular ocean deoxygenation in the coastal ocean, with a focus on summer stratified shelf sea regimes

1.5.2 Chapter outine

In order to achieve the objectives outlined in Section 1.5.1 this thesis is arranged as follows. Chapter 2 describes the application of optimal fingerprinting methods (Sect. 1.1.3) in order to determine the contribution of external forcing and natural internal variability to observed changes in oceanic oxygen at global and ocean basin scales. This study makes use of a suite of recently available historical and unforced ESM experiments (CMIP5 [Taylor et al., 2012]) along with a multi-decadal global [O_2] dataset (Helm et al., 2011) in order to quantify, for the first time, the detectability of secular changes in oceanic oxygen using formal detection and attribution techniques. Optimal fingerprinting methods also provide an effective and rigorous strategy for evaluating ocean-climate model simulations against observations (*cf.* Hegerl and Zwiers, 2011), such that this study also implicitly provides an assessment of ESM performance with respect to historical changes and variability in ocean [O_2]. Chapter 2 is presented as published in *Biogeosciences* (Andrews et al., 2013).

Chapter 3 presents an analysis of ocean-only hindcasts conducted as part of this thesis using a forced global ocean biogeochemistry model (PlankTOM10-NEMO3.1; Le Quéré et al., 2014a; Enright et al., 2014). The simulated spatiotemporal distribution of passive tracers in ocean-only models has been shown to be sensitive to imposed atmospheric forcing, as demonstrated in modelling studies which investigate trends and variability in the ocean carbon cycle (e.g. Le Quéré et al., 2010; Ishi et al., 2014; Swart et al., 2014). As a result, a series of model experiments are initialised in this study using different atmospheric forcing products in order to investigate the sensitivity of "exogenous" variability and historical changes in oceanic oxygen over the last $\sim$ 50 years to the meteorological data provided to calculate turbulent fluxes of heat, freshwater and momentum in hindcast models (*cf.* Brodeau et al., 2010; Large and Yeager, 2004). The impact of ocean carbon cycle and acidification feedbacks on the historical distribution of $[O_2]$ in ocean biogeochemistry models also remains poorly understood (*cf.* Stramma et al., 2012a; Keeling et al., 2010). To address this uncertainty, a number of hindcast model experiments are initialised which include newly developed biogeochemical parameterisations accounting for the *interactive* (*cf.* Matear and Lenton, 2014) effects of ocean acidification on mineral ballasting (e.g. Heinze, 2004; Hofmann and Schellnhuber, 2009; Armstrong et al., 2002) and C:N ratios in primary production (e.g. Oschlies et al., 2008; Tagliabue et al., 2011; Stramma et al., 2012a).

In Chapter 4, a synthesis of observed and model simulated historical $[O_2]$ changes within the shelf and coastal ocean is carried out, focusing on the summer stratified Greater North Sea, part of the NW European continental shelf regime. This work makes use of a recent hindcast experiment carried out with a state-of-the-art regional ecosystem model configured for the North Sea domain (GETM-ERSEM; van Leeuwen et al., 2013) along with a recent compilation of historical North Sea $[O_2]$, temperature and salinity data (Queste et al., 2012) in order to quantify the signal of secular changes in ocean properties relative to internal climate noise. Chapter 4 is presented as a "scoping report" which has contributed to a collaborative research project between the Tyndall Centre for Climate Change Research and the Centre for Environment, Fisheries and Aquaculture Science (CEFAS): *Fingerprints of Ocean Deoxygenation in the North Sea* (FODINS).

Finally, Chapter 5 provides a précis of key results along with limitations and possible

ways to extend this work in the future. Perspectives are also provided on the implications of the research, focusing on the notion of optimal metrics for detecting climate change in the ocean and the role of model skill in informing policy-relevant detection and attribution results.

Chapter 2

Detecting an External Influence on Recent Changes in Oceanic Oxygen using an Optimal Fingerprinting Method

Detecting an External Influence on Recent Changes in Oceanic Oxygen Using an Optimal Fingerprinting Method

O. D. Andrews[1], N. L. Bindoff[2,3,4], P. R. Halloran[5], T. Ilyina[6], Corinne Le Quéré[1]

[1] Tyndall Centre for Climate Change Research, School of Environmental Sciences, University of East Anglia, Norwich, UK

[2] IMAS, University of Tasmania, Hobart, Australia

[3] CSIRO Marine and Atmospheric Research, Hobart, Australia

[4] ACE CRC, University of Tasmania, Hobart, Australia

[5] Met Office Hadley Centre, FitzRoy Road, Exeter, UK

[6] Max Planck Institute for Meteorology, Hamburg 20146, Germany

Citation: Andrews, O. D., Bindoff, N. L., Halloran, P. R., Ilyina, T., and Le Quéré, C.: Detecting an external influence on recent changes in oceanic oxygen using an optimal fingerprinting method, Biogeosciences, 10, 1799-1813, doi:10.5194/bg-10-1799-2013, 2013.

This chapter is presented as published in Biogeosciences. All writing and analysis was undertaken by O.D.A. N.L.B. provided access to oxygen data. T.I. and P.R.H. gave details of CMIP5 experiments and provided additional model output. C.L.Q. and N.L.B. contributed to both the design of this study and the interpretation of results.

2.1 Abstract

Ocean deoxygenation has been observed in all major ocean basins over the past 50 yr. Although this signal is largely consistent with oxygen changes expected from anthropogenic climate change, the contribution of external forcing to recent deoxygenation trends relative to natural internal variability is yet to be established. Here we conduct a formal optimal fingerprinting analysis to investigate if external forcing has had a detectable influence on observed dissolved oxygen concentration ($[O_2]$) changes between $\sim$1970 and $\sim$1992 using simulations from two Earth System Models (MPI-ESM-LR and HadGEM2-ES). We detect a response to external forcing at a 90 % confidence level and find that observed $[O_2]$ changes are inconsistent with internal variability as simulated by models. This result is robust in the global ocean for depth-averaged (1-D) zonal mean patterns of $[O_2]$ change in both models. Further analysis with the MPI-ESM-LR model shows similar positive detection results for depth-resolved (2-D) zonal mean $[O_2]$ changes globally and for the Pacific Ocean individually. Observed oxygen changes in the Atlantic Ocean are indistinguishable from natural internal variability. Simulations from both models consistently underestimate the amplitude of historical $[O_2]$ changes in response to external forcing, suggesting that model projections for future ocean deoxygenation may also be underestimated.

2.2 Introduction

The oceanic oxygen inventory is coupled to the climate system via a number of physical and biogeochemical processes making oxygen a useful tracer for detecting changes in the state of the earth system (Joos et al., 2003; Brennan et al., 2008). In particular, changes in temperature, ocean circulation, biological production and respiration, expected in response to global climate change, all exert a major control on dissolved oxygen concentration ($[O_2]$). Open ocean deoxygenation has been recorded in nearly all ocean basins during the second half of the 20th century (Helm et al., 2011) with more acute $[O_2]$ decreases in the coastal ocean (Gilbert et al., 2010). Oxygen time series measurements also show historical expansion and intensification of established oxygen minimum zones (OMZs) in the eastern tropical Atlantic and equatorial Pacific since 1960 (Stramma et al., 2008) along with long-term $[O_2]$ decreases in the subarctic North Pacific between 1956 and 2006 (Whitney et al., 2007).

Historical deoxygenation has been associated with global climate change, chiefly due to enhanced ocean stratification in a warming climate which increases the ventilation age of downwelling water masses, and augmented by the reduced solubility of dissolved oxygen at higher temperatures (Keeling et al., 2010). These findings are supported by prognostic simulations from a suite of Atmosphere-Ocean General Circulation Models (AOGCMs), which show ventilation-driven reductions in global mean $[O_2]$ between 3 and 12 μmol kg^{-1} by 2100 (Sarmiento et al., 1998; Bopp et al., 2002; Matear and Hirst, 2003; Frölicher et al., 2009). Global $[O_2]$ decreases have also been simulated over longer timescales in response to protracted ocean warming. For example, model simulations using Intermediate Complexity Earth System Models (EMICs) produce a tripling in the volume of suboxic ($[O_2] < 5$ μmol kg^{-1}) waters by 2500 (Schmittner et al., 2008). Ocean deoxygenation and expansion of the OMZs has also been projected to persist on millennial timescales for EMIC simulations with high greenhouse gas emissions or high climate sensitivity (Shaffer et al., 2009).

All global models simulate that the most significant $[O_2]$ decreases occur at mid- to high latitudes, consistent with observations and caused by decreasing ventilation of the oceanic interior in response to enhanced upper ocean stratification. However, models generally do not reproduce the deoxygenation observed at low latitudes, which leads to

considerable uncertainties for future projections. The predictive skill of coarse resolution ocean models at low latitudes is limited by the need to resolve zonal currents thought to be important in supplying oxygen into the tropical OMZs (Keeling et al., 2010; Brandt et al., 2010; Stramma et al., 2010). Climate change integrations of coupled AOGCMs often simulate [O_2] increases in the tropical thermocline associated with reductions in the volume of O_2-depleted waters at low latitudes, contrary to recent trends (Matear and Hirst, 2003; Gnanadesikan et al., 2012). Gnanadesikan et al. (2007) propose that this oxygenation is driven by reduced exchange between poorly ventilated deep water and the tropical thermocline in a more stratified ocean. However, this process has been posited to be a numerical artifact tied to unrealistically high rates of diapycnal mixing in coarse resolution ocean models (Keeling et al., 2010). A recent sensitivity study by Duteil and Oschlies (2011) confirms the importance of vertical diffusivity and its parameterisation on the evolution of suboxic areas in global models. Simulated oxygenation of suboxic zones has also been attributed to an elevated supply of oxygen from isopycnal diffusion in one study using the GFDL ESM2.1 (Gnanadesikan et al., 2012). Up to now, biogeochemical models can reproduce observed low-latitude deoxygenation and expansion of hypoxic and suboxic waters in the tropical OMZs only when they take into account poorly constrained pCO_2-driven changes to the C:N ratio in primary production (Oschlies et al., 2008; Tagliabue et al., 2011) or the alteration to $CaCO_3$ mineral ballasting in response to ocean acidification (Hofmann and Schellnhuber, 2009).

The implications of a climate change signal in [O_2] changes are profound, owing to the deleterious impact of reduced oxygen concentrations and expanding hypoxic zones on marine ecosystems and fisheries (e.g., Doney et al., 2012; Stramma et al., 2012b), and the sensitivity of biolimiting marine nutrient cycles such as nitrogen and phosphorous to oceanic redox conditions (Keeling et al., 2010). However, attribution of secular [O_2] changes to global climate change is confounded by natural interannual to decadal variability driven by the leading climate modes which act to mask any climate-driven signal (e.g., the North Atlantic Oscillation, Frölicher et al., 2009). To this end, modelling studies have demonstrated that internal variability associated with the major climate modes in the North Pacific drive propagating O_2 anomalies that are large enough to frequently preclude unequivocal detection of anthropogenic trends in dissolved oxygen on decadal timescales

and regional scales (Deutsch et al., 2006; Ito and Deutsch, 2010). However, Deutsch et al. (2005, 2006) highlight that in the North Pacific strong historical [O_2] decreases within the lower ventilated thermocline are reproduced by models and are likely to be driven by long-term changes in ocean ventilation and circulation, but a formal detection study is required to separate external causes from internal variability.

We use an optimal fingerprinting methodology to objectively quantify the detectability of externally forced changes in oceanic [O_2] relative to natural internal periodicity. Numerous detection studies have been conducted investigating the impact of external forcing on oceanic variables such as ocean temperature (e.g., Barnett et al., 2005; Pierce et al., 2006; Gleckler et al., 2012) and salinity (Stott et al., 2008; Terray et al., 2012), but these techniques have not yet been used for biogeochemical tracers like oxygen. [O_2] changes, therefore, provide a novel means for detecting and attributing anthropogenic climate change in the oceans and for the evaluation of model performance (Hegerl et al., 2006). As such, this study aims to conduct a formal optimal fingerprinting analysis to investigate the "signal in noise" problem of historical changes in oceanic oxygen using [O_2] data and simulations from two Earth System Models (ESMs) participating in Phase 5 of the Coupled Model Intercomparison Project (CMIP5).

2.3 Methods

2.3.1 Observations and CMIP5 models

We use a recent collation of global World Ocean Circulation Experiment (WOCE) O_2 data compared with earlier ocean oxygen profiles (Helm et al., 2011) to investigate the cause of the observed historical changes in global marine oxygen distribution. This compilation maps all historical [O_2] data (1940–1988; mean year $\sim$ 1970) onto the locations of WOCE profiles to facilitate comparison with WOCE measurements ($\sim$ 1989–2000; mean year $\sim$ 1992) using an optimal-interpolation technique that adapts the length scales to suit the density and distribution of oxygen data (Helm et al., 2010). The [O_2] data is binned into regular $1^\circ \times 1^\circ$ grid cells with 101 fixed pressure levels, excluding shallow (< 1000 m) profiles and observations above 100 m where seasonal variability dominates the oxygen signal (Garcia et al., 2005). Noise variance calculated using the difference between

neighbouring data points is used to provide an a priori estimate of natural variability in $[O_2]$ data (Helm et al., 2010, 2011; Bindoff and Wunsch, 1992). This technique accounts for mesoscale processes and to some extent longer period internal variability such as the dominant climate modes.

This dataset is used in an optimal detection analysis along with the biogeochemical output from two state-of-the-art ESMs (MPI-ESM-LR and HadGEM2-ES) participating in the CMIP5 experiments (Taylor et al., 2009, 2012). $[O_2]$ fields from MPI-ESM-LR and HadGEM2-ES have been selected here because they display a higher level of realism in simulating both climatological $[O_2]$ distribution and historical oxygen changes compared to the other available CMIP5 ESMs. Sufficient qualitative agreement between modelled and observed $[O_2]$ distribution allows for direct quantitative comparison using an optimal fingerprinting algorithm without any requirement for a prior transformation of the model's variables (e.g., Banks and Bindoff, 2003).

The Max Plank Institute for Meteorology Earth System Model used here (MPI-ESM-LR; Giorgetta et al., 2012) is a low resolution model version that includes the ECHAM6 atmospheric GCM with T63 horizontal resolution (1.875°) and 47 vertical layers (Stevens et al., 2013; developed from ECHAM5 (Roeckner et al., 2006) with modifications in the shortwave radiative transfer and representation of the middle atmosphere). It is coupled to the MPIOM physical ocean model (Jungclaus et al., 2013; Marsland et al., 2003) which includes a thermodynamic-dynamic sea ice component (Notz et al., 2013) and ocean biogeochemistry model (HAMOCC5; Ilyina et al., 2013; Maier-Reimer, 1993; Maier-Reimer et al., 2005) implemented on a curvilinear bipolar orthogonal grid with a nominal horizontal resolution of 1.5° and 40 z-levels which increase in thickness with depth. The HAMOCC5 ocean biogeochemistry component includes an extended Nutrient-Phytoplankton-Zooplankton-Detritus (NPZD) type ecosystem model (Six and Maier-Reimer, 1996) along with over 30 prognostic variables in the water column and the upper sediments including co-limiting nutrients nitrate, phosphate and iron, as well as DIC and oxygen. The ocean and atmosphere components are coupled daily without flux corrections.

The Hadley Centre Global Environment Model Version 2 Earth System Model (HadGEM2-ES, Collins et al., 2011; HadGEM2 Development Team, 2011) is also a coupled AOGCM

and has an atmospheric resolution of N96 ($1.875^\circ \times 1.25^\circ$) with 38 vertical levels. The ocean model has a $1^\circ \times 1^\circ$ horizontal resolution (increasing smoothly to $1/3^\circ$ at the equator) with 40 unevenly spaced depth levels. The ocean biogeochemistry component of this model is Diat-HadOCC, which is an NPZD model with two phytoplankton functional types (developed from the HadOCC model; Palmer and Totterdell, 2001), and includes the nutrient cycles of nitrogen, silica and iron along with prognostic tracers such as dissolved oxygen.

We use output from the ~ 1000 yr control (piControl) experiments of MPI-ESM-LR and HadGEM2-ES, which prescribe non-evolving pre-industrial forcings, and an ensemble of historical experiments for the period ~ 1850 to 2005 (Table 2.1). The piControl runs were initialised from a pre-industrial spin-up to pseudo-equilibrium. Boundary conditions for the historical experiments are prescribed from observations as an evolving record of climate forcing factors. These include external forcings from: historical greenhouse gas concentrations, tropospheric and stratospheric ozone changes, surface emissions of tropospheric aerosols and land use changes as well as the natural forcings from changes in solar irradiance and volcanic aerosols. Each member of the model ensemble is initialised from a different point in the control simulation in order to create a spectrum of equally plausible historical simulations each starting at a different phase of internal variability. The MPI-ESM-LR and HadGEM2-ES CMIP5 experimental design and spin-up are described in Mauritsen et al. (2012) and Jones et al. (2011), respectively. A persistent climate drift in HadGEM2-ES oxygen fields has been isolated from a 20 yr low-pass filtered version of the control run and subtracted at each grid point of the historical [O_2] data using the corresponding segment of the piControl integration. Since residual drift can also bias noise estimates required for the optimal fingerprinting procedure (as estimated from long control experiments) an equivalent point-by-point drift is also removed from the HadGEM2-ES piControl integration. In this case removal of a linear trend diagnosed from a low pass filter provides an adequate representation of climate drift behaviour, as distinct from natural internal periodicity.

Model	Experiment (name)	Forcing	Ensemble size (n)	Control length (years)
MPI-ESM-LR	Historical (r1:ni1p1)	ALL	3	
	piControl (r1i1p1)		1	1000
HadGEM2-ES	Historical (r1:ni1p1)	ALL	4	
	piControl (r1i1p1)		1	965*

Table 2.1: Summary of CMIP5 model output used in the optimal detection, comprising MPI-ESM-LR and HadGEM2-ES historical and piControl integrations. ALL = natural + anthropogenic external forcing. * control length after drift removal.

2.3.2 Optimal fingerprinting method

We test the null hypothesis that historical changes in [O_2] are indistinguishable from natural internal variability ($\beta = 0$) using an optimal detection algorithm (Hasselmann, 1997; Allen and Tett, 1999). This statistical technique is widely used in the detection and attribution of climate change (e.g., IDAG, 2005; Hegerl et al., 2010) and also provides a powerful test of ESM performance which includes the effect of natural internal variability. We use this technique to regress model simulated patterns of [O_2] change (x_i) against corresponding observed patterns (y) using a Total Least Squares (TLS) method (Allen and Stott, 2003) which estimates the scaling factors (β_i) required to match simulated and observed changes following Eq. (2.1):

$$y = \sum_{i=1}^{1} \beta_i (x_i - v_i) + v_0 \tag{2.1}$$

where in the single signal case, for the i-th forcing, v_i is the error in the model response x_i and v_0 is the climate noise in the observations. If the confidence interval that contains β exceeds zero a signal is detected in response to an imposed forcing i. If this scaling factor is consistent with one the simulated and observed responses are said to be similar in magnitude. In this study, the simulation consists of the ESM, all of its parameters and all of the temporal and spatial variations of the external forcing i transformed through the physical and chemical processes represented in the model. Thus, a value of β consistent with one demonstrates that forcing i and the theory are consistent with the observations, and a β estimate which is significantly greater than 0 demonstrates that the null hypothesis of no contribution from forcing i can be rejected. TLS is likely to yield a more robust β estimate than an Ordinary Least Squares (OLS) approach because it also includes a signal error

term (v_i) arising from averaging across a finite model ensemble to obtain the simulated response pattern. Signal error (v_i) is inversely proportional to the model ensemble size (n) and can negatively bias scaling factors (Allen and Tett, 1999), particularly for variables where the forced response is small relative to internal variability. Thus, TLS is widely used in optimal detection studies as a more conservative approach which explicitly accounts for the effect of noise in simulated response patterns relative to that which is found in the observations (e.g., Stott et al., 2003a; Stott et al., 2008; Terray et al., 2012).

We focus our single fingerprint analysis on the "all forcings" historical scenario of MPI-ESM-LR and HadGEM2-ES, with model output being bi-linearly interpolated onto a $1^\circ \times 1^\circ$ grid and masked to emulate the pattern of missing values found in the observations of Helm et al. (2011) (Fig. 2.1). [O_2] changes between $\sim$1970 and $\sim$1992 are then calculated for these experiments and provided as model response patterns (x_{HIST}) in the TLS regression against corresponding observed [O_2] changes (y) in order to estimate scaling factors (β). The instrumental record of dissolved O_2 measurements is not sufficiently long to get a reliable approximation of internal climate variability (v_0), and also includes perturbations driven by external forcing. In order to characterise unforced climate variability in [O_2] on a global scale, we estimate v_0 by sampling non-overlapping 22 yr slabs of [O_2] fields taken from the long ($\sim$1000 yr) control integrations of MPI-ESM-LR and HadGEM2-ES. The non-overlapping model [O_2] fields are also masked and re-gridded as "pseudo-observations". Subsampled model piControl output is then used to (1) estimate internal variability in [O_2] data and (2) place 5–95 % uncertainty limits on calculated scaling factors.

The TLS regression is carried out in a reduced dimension space where model and observed data are projected onto k leading Empirical Orthogonal Functions (EOFs) of simulated internal variability. Signal-to-noise ratios are optimised in a standard way via normalisation of observations and model response patterns by internal climate variability (e.g., IDAG, 2005), a transformation which down-weights patterns of [O_2] change with high internal variability and vice versa. Dimensionality of the detection space in this study is further reduced by averaging across multiple ensemble members in each historical CMIP5 experiment (see Table 2.1), and by calculating zonal means for observed and modelled [O_2] changes. The analysis of Helm et al. (2011) shows pronounced global

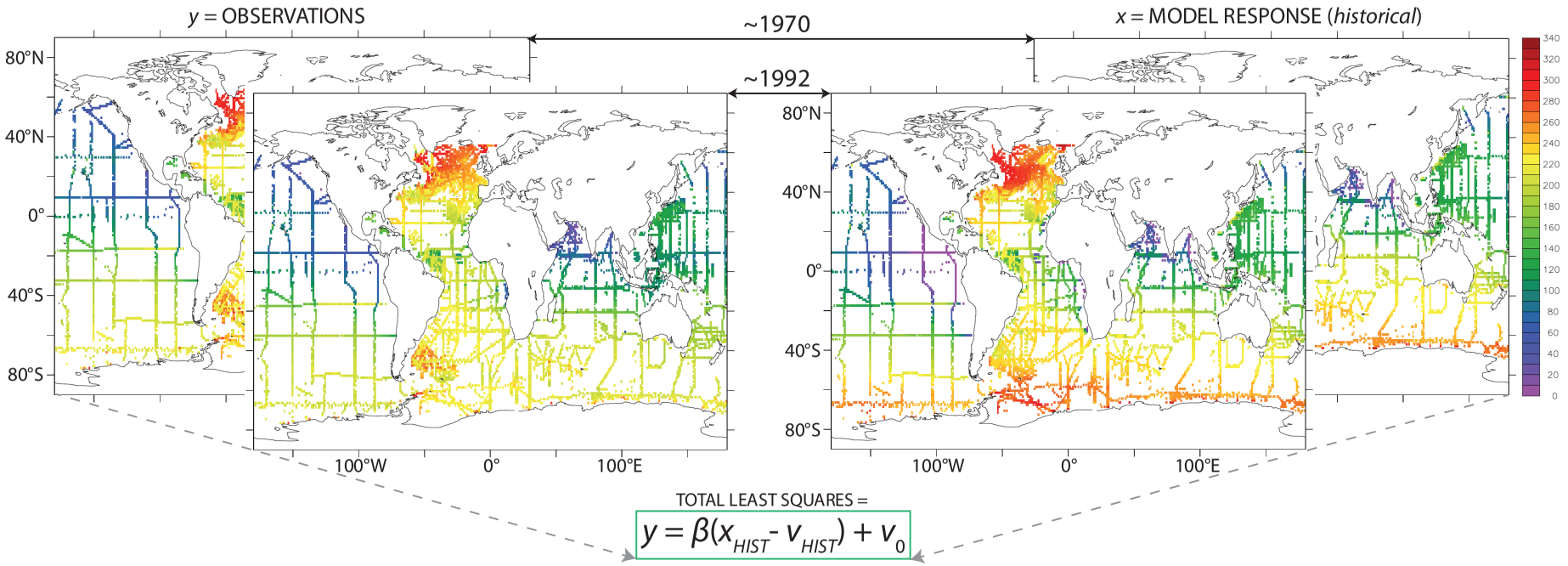

Figure 2.1: Schematic summary of the optimal detection method used here. The left panels show the observed distribution of dissolved oxygen data (y; μmol kg^{-1}) for $\sim$ 1970 and $\sim$ 1992, averaged between 100–3000 m. The right panels show the masked and re-mapped ensemble mean model output (x_{HIST}) from historical simulations of ESMs (MPI-ESM-LR or HadGEM2-ES) averaged between 100–3000 m. y and x_{HIST} are then provided to the Total Least Squares regression as zonal mean [O_2] differences between the two time periods, where v_{HIST} and v_0 are estimates of the noise in the model response and observations, respectively.

$[O_2]$ decreases between $\sim$ 1970 and $\sim$ 1992 in all ocean basins, accommodating a zonally averaged spatial domain. This removes small-scale variability in $[O_2]$ and allows the detection analysis to focus on global and basin-scale patterns of oxygen change. Gridded dissolved oxygen data are also smoothed vertically and horizontally. Modelled $[O_2]$ changes are calculated as temporal averages of annual data between 1960–1980 and 1990–2000 in order to be consistent with the historical spread of observations, with sensitivity tests demonstrating simulated $[O_2]$ changes to be relatively invariant across a range of small changes in averaging period.

We prepare model fingerprints and observations for the optimal detection analysis using two different zonal averaging schemes: (1) 1-D analysis: zonal mean of depth-averaged $[O_2]$ changes between 100 and 3000 m; (2) 2-D analysis: zonal mean $[O_2]$ changes explicitly resolve depth (between 100–3000 m) globally and separately for the Atlantic and Pacific basins. Both MPI-ESM-LR and HadGEM2-ES models are used in the 1-D analysis. The MPI-ESM-LR model only is used to extend the work and provide a more detailed 2-D analysis. For the 2-D optimal detection, masked MPI-ESM-LR output and observations are remapped onto a $\sim 5^\circ$ latitude by $\sim 10^\circ$ longitude grid with 40 unevenly spaced z-levels to mediate the effects of internal noise on the signal whilst still retaining the depth structure of meridional $[O_2]$ change between $\sim$ 1970 and $\sim$ 1992. The use of several models and several spatial averaging schemes provides multiple model fingerprints that are used to quantify possible errors in model response patterns ("structural uncertainty") driven by inadequate representation of physical and biogeochemical process in ESMs (e.g., Hegerl and Zwiers, 2011).

In order to avoid spurious detection it is a necessary prerequisite that the internal variability estimated from control simulations (v_0) provides a realistic estimate of observed climate noise in $[O_2]$. As such, the number of EOFs retained in the optimal detection analysis is guided by checking the fidelity of model simulated internal variability against the residual observed variance at k truncations using a standard residual consistency F test (Allen and Tett, 1999). This check is used to test the null hypothesis that internal variability as simulated by models is consistent with observed variability on the scales retained in the analysis. Failure of the residual consistency test could also indicate that the timing or pattern of ESM response is incorrect. We choose to truncate the 1-D MPI-ESM-LR

analysis at 40 EOFs ($k = 40$) since this is the first truncation for which the residual test passes the consistency check, reducing the likelihood of keeping poorly sampled higher order EOFs in the optimal detection. Fewer truncations ($k = 31$) are needed to pass the residual consistency check in the 1-D HadGEM2-ES analysis, however, scaling factors are not substantially different at higher k values (see Sect. 2.4.2). The 2-D analysis both globally and between ocean basins required the maximum number of EOFs ($k = 49$) to be retained in the regression to pass the residual consistency check (apart from for the Atlantic basin where the F test p value falls marginally outside the 5–95 % range). A higher number of retained EOFs is consistent with the greater amount of information needed to describe spatial patterns of both depth and latitude variations, with more modes being necessary to explain variability in the depth-resolved signal.

In addition to the residual consistency test, we assess the reliability of model simulated climate variability by comparing piControl output with detrended subsurface [O_2] measurements from two long-term time series: Ocean Station Papa (1956–2007, Whitney et al., 2007) and the Oyashio Current region (1968–1998, Ono et al., 2001). Observed decadal standard deviations calculated for both time series fall within the 10–90 % ranges of MPI-ESM-LR control simulation estimates, demonstrating that this model provides a robust estimate of internal variability in [O_2] on decadal timescales (Table 2.2). The HadGEM2-ES control simulation significantly underestimates decadal variability in [O_2] when compared to time series data and is, thus, less reliable than simulations from MPI-ESM-LR in the context of our analysis.

	Observations	MPI-ESM-LR	HadGEM2-ES
Ocean Station Papa	11.1	9.1 (6.2–12.0)	5.3 (3.9–6.7)
Oyashio Current region	8.1	9.9 (4.9–15.1)	1.4 (0.4–2.4)

Table 2.2: Comparison of decadal standard deviations of [O_2] (μmol kg^{-1}) between observations and CMIP5 piControl experiments at Ocean Station Papa in the Eastern North Pacific (50° N, 145° W, $\sigma = 26.9$, $\sim$250–350 m) and the Oyashio Current region in the Western North Pacific (39–42° N, 143–145° E, $\sigma = 26.9$, $\sim$400–450 m). piControl output from MPI-ESM-LR and HadGEM2-ES is sampled to calculate multiple estimates of decadal standard deviations for each time series. The mean and (10th–90th) percentile ranges of piControl estimates are shown. Observations are detrended using a linear fit to extract variability. Drift has been removed from the control integration of HadGEM2-ES as described in Sect. 2.3.1

2.4 Results

2.4.1 Model-data comparison

We evaluate model performance by comparing simulated and observed zonally averaged [O_2] distributions for the $\sim$ 1992 time period. Historical integrations of MPI-ESM-LR and HadGEM2-ES are able to capture the general latitude-depth pattern of [O_2] distribution present in the observations (Fig. 2.2). The [O_2] minimum between 20° S and 20° N is reproduced at mid-depths by both models, with increasing [O_2] towards higher latitudes in both hemispheres. However, HadGEM2-ES simulates higher than observed oxygen concentrations in the [O_2] minimum. MPI-ESM-LR overestimates the spatial extent of low-latitude [O_2] minimum waters and produces erroneously high [O_2] south of 60° S. Ilyina et al. (2013) present a detailed comparison between biogeochemical tracers in MPI-ESM-LR CMIP5 historical simulations and observations using a range of statistical metrics to assess model capability.

A marked meridional structure also exists in observed depth-averaged zonal mean [O_2] changes, with deoxygenation increasing with latitude poleward of 40° (up to 12 μmol kg^{-1}) in both hemispheres (Fig. 2.3). Pronounced deoxygenation in the mid- to high-latitude ocean is opposed by no change or a small zonal mean [O_2] increase of $\sim$ 1–2 μmol kg^{-1} between 20° S and 20° N. Both MPI-ESM-LR and HadGEM2-ES historical integrations show predominant global decreases in [O_2] at high latitudes consistent with but smaller (< 5 μmol kg^{-1}) than the observations, with no net oxygen change at low latitudes. Observed and modelled global mean [O_2] decreases both reach their maxima at $\sim$ 60° N. In some regions MPI-ESM-LR and HadGEM2-ES historical experiments show a much reduced or inverse [O_2] change signal, particularly in areas of the Southern Ocean (65° S) and at $\sim$ 50° N where significant observed zonal mean [O_2] decreases (3–6 μmol kg^{-1}) contrast with small oxygen increases in both models.

The consistency between models and observations is further examined in zonal mean sections as a function of depth (Fig. 2.4). [O_2] data show acute deoxygenation of the ventilated thermocline (100–1000 m depth) at all latitudes, with large oxygen decreases (> 10 μmol kg^{-1}) extending throughout the water column poleward of 40° in both hemispheres (Fig. 2.4a). These regions of deoxygenation are countered by areas of increasing [O_2] (5–10 μmol kg^{-1}) located between 30° S and 30° N below 1000 m depth and within

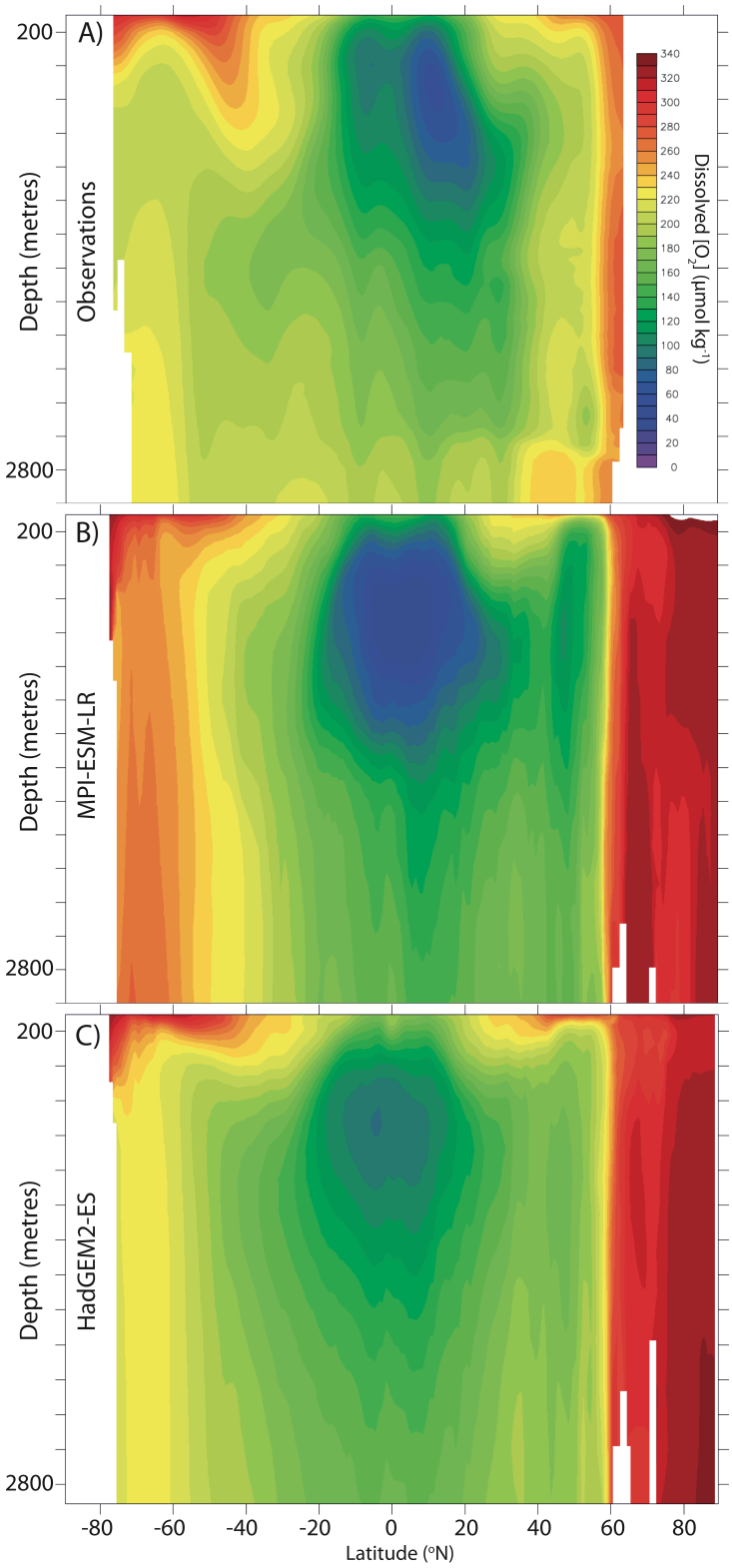

Figure 2.2: Zonal mean $[O_2]$ distribution (μmol kg^{-1}) for $\sim$ 1992 as a function of latitude and depth from **(A)** observations (Helm et al., 2011), and historical integrations of **(B)** MPI-ESM-LR and **(C)** HadGEM2-ES.

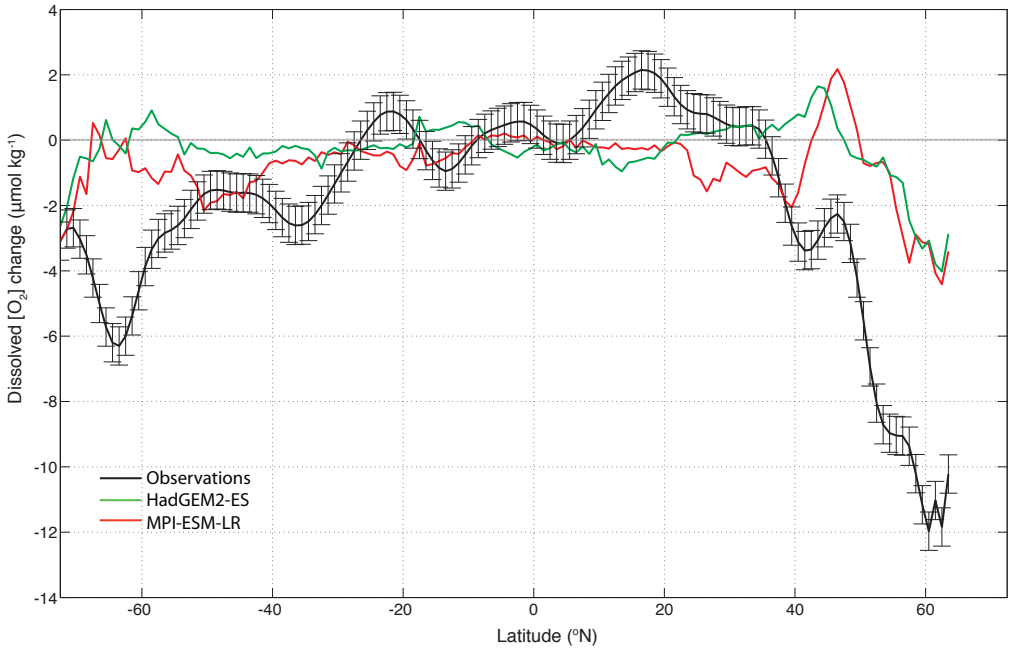

Figure 2.3: Zonal mean change ($\sim$ 1992 minus $\sim$ 1970) in [O_2] (μmol kg^{-1}) as a function of latitude averaged between 100–3000 m depth for observations (black; Helm et al., 2011), and HadGEM2-ES (green) and MPI-ESM-LR (red) historical integrations. Error bars in observed [O_2] are given at the 95 % confidence level and are associated with instrumental uncertainty, un-resolved ocean processes and methodological uncertainty in forming the zonal averages (derived from an a priori estimate of noise using the method of Bindoff and Wunsch, 1992).

the shallow subtropical gyres (15–30°). Both models generally reproduce the key zonal mean features of observed [O_2] change, simulating [O_2] decreases at high latitudes and within the thermocline, with an area of increasing [O_2] beneath $\sim$ 1500 m depth at mid- to low latitudes. In agreement with data, MPI-ESM-LR simulates strong [O_2] depletion extending throughout the water column north of 40° N and shows a distinct region of increased [O_2] beneath $\sim$ 1500 m between 30° S and 30° N (Fig. 2.4b). MPI-ESM-LR also displays significant deoxygenation between 40° S and 60° S, but this is opposed by a limb of [O_2] increase within the interior of the Southern Ocean (a feature which is entrained into the depth-averaged trend of Fig. 2.3). HadGEM2-ES exhibits deoxygenation in the upper ocean at mid- to high latitudes in both hemispheres, with [O_2] depletion extending down to $\sim$ 3000 m depth south of 65° S and at $\sim$ 60° N (Fig. 2.4c). Near ubiquitous [O_2] decreases are also simulated in the ventilated thermocline, apart from within the subtropical gyres (15–30°) where HadGEM2-ES reproduces, in part, the observed [O_2] increases. However, the oceanic interior between 60° S and 40° N becomes increasingly oxygenated over the modelled analysis period, with an anomalous region of positive [O_2] change below

~ 1500 m in the polar north and protruding into the upper ocean at $\sim 65°$ S. Both models fail to emulate the pattern of $[O_2]$ loss recorded by observations in the low-latitude OMZs (< 1000 m), displaying small $[O_2]$ increases within the tropical thermocline between 20° S and 20° N. This failure of the models to replicate the low-latitude OMZs is discussed in Sect. 2.2 and is well known. Overall, simulated $[O_2]$ changes for both models tend to be similar but smaller in magnitude than recorded by observations, with MPI-ESM-LR exhibiting generally more skill at reproducing patterns of observed $[O_2]$ change as a function of depth.

On a basin scale (Fig. 2.5) there is a higher level of agreement between modelled and observed water mass changes over the analysis period in the Pacific compared to the Atlantic. MPI-ESM-LR reproduces observed deoxygenation of the high-latitude North Pacific down to ~ 3000 m depth, and shows a general trend towards decreasing $[O_2]$ levels within the ventilated thermocline. In comparison, the structure of modelled oxygen changes within the Atlantic Ocean is largely inconsistent with observations. MPI-ESM-LR simulates extensive deoxygenation (up to 4 μmol kg^{-1}) throughout much of the Atlantic between 1000 and 3000 m depth, and does not resolve major regions of observed $[O_2]$ increase in the interior of the Atlantic between 30° S and 30° N. In both the Atlantic and Pacific basins, following the global trend, MPI-ESM-LR does not reproduce the pronounced deoxygenation signal recorded within the low-latitude OMZs. This model-data mismatch is most apparent in the thermocline of the tropical Atlantic where MPI-ESM-LR shows strong $[O_2]$ increases of > 5 μmol kg^{-1} in opposition to observed $[O_2]$ depletion.

Changes in upper ocean stratification are associated with changes in the ventilation (and oxygenation) of subsurface water masses. Figure 2.6 shows historical changes in zonal mean upper ocean density stratification as a function of latitude (between 200 m and 1000 m) from observations and for MPI-ESM-LR and HadGEM2-ES models. Observed and model derived zonal mean density stratification generally increases at mid- to high latitudes between ~ 1970 and ~ 1992, with decreases in global stratification within the subtropical and equatorial ocean. However, at high latitudes in the Southern Ocean both MPI-ESM-LR and HadGEM2-ES underestimate the observed stratification change signal, with major increases in stratification between 50° S and 60° S not reproduced by either model. Analysis of the density structure of these models show that in this region the density

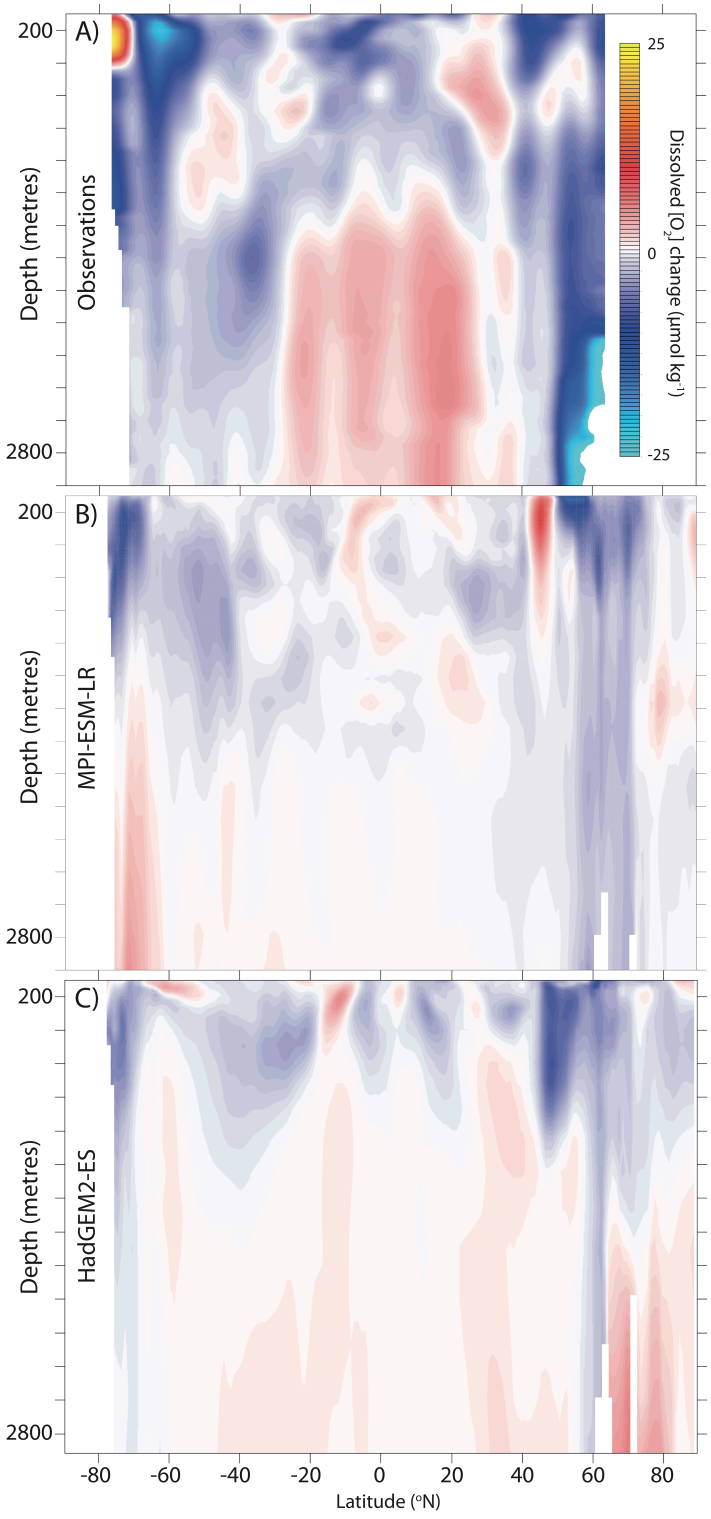

Figure 2.4: Zonal mean change ($\sim$ 1992 minus $\sim$ 1970) in [O_2] (μmol kg^{-1}) as a function of latitude and depth from **(A)** observations (Helm et al., 2011), and historical integrations of **(B)** MPI-ESM-LR and **(C)** HadGEM2-ES.

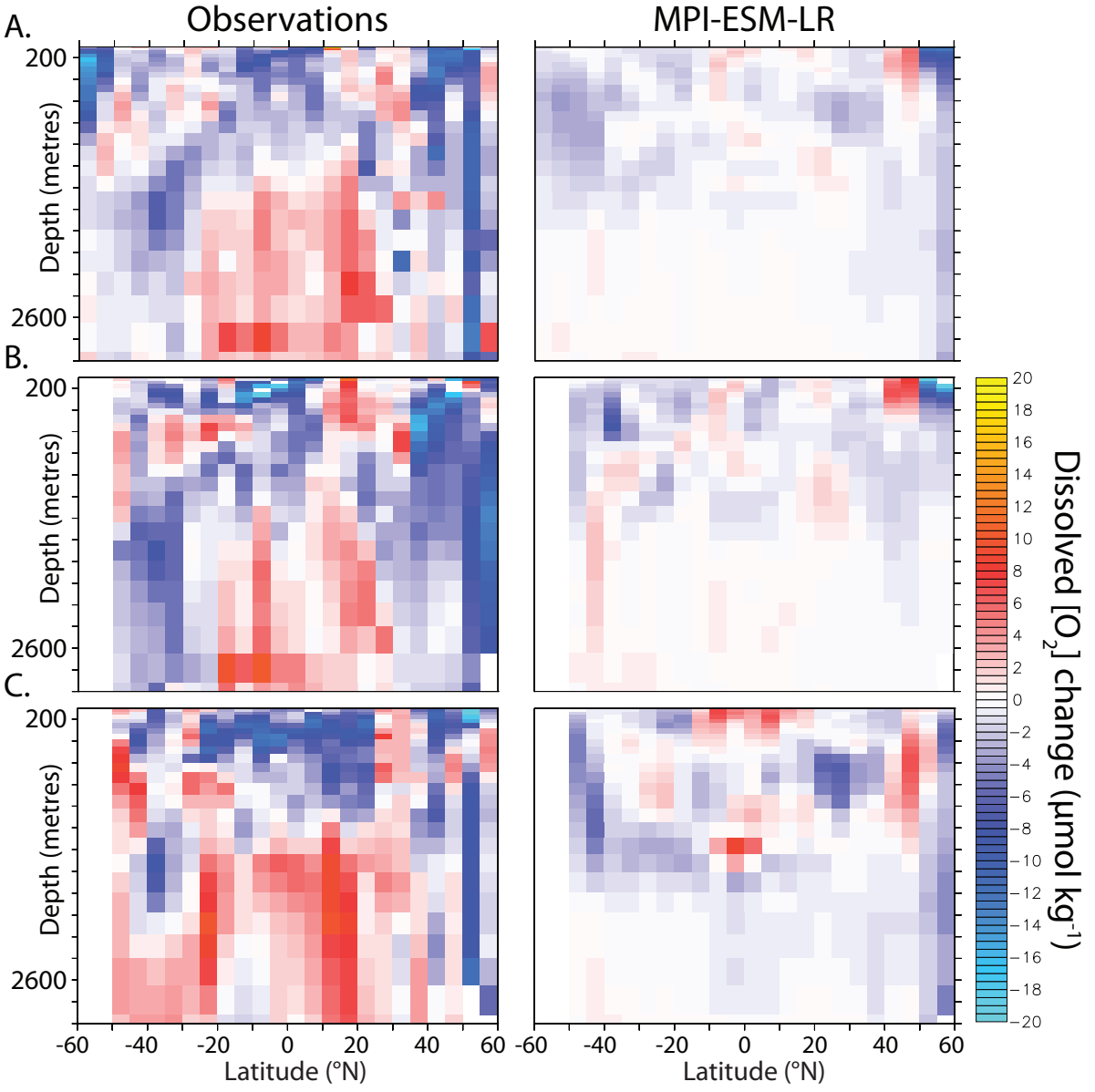

Figure 2.5: Observed (left) and simulated (right) patterns provided to the 2-D optimal detection as zonal mean $[O_2]$ changes (μmol kg^{-1}) as a function of latitude and depth for the global ocean (60° S–60° N; **A**), and for the Pacific **(B)** and Atlantic **(C)** ocean basins. Masked MPI-ESM-LR $[O_2]$ fields and observations are interpolated onto a $\sim 5°$ latitude by $\sim 10°$ longitude grid with 40 unevenly spaced depth levels and zonally averaged.

profile is more homogeneous than observed with more vigorous vertical mixing.

2.4.2 Optimal detection analysis

We apply the optimal detection approach outlined in Sect. 2.3.2 to quantitatively investigate the consistency of modelled and observed changes in $[O_2]$, and to assess the detectability of observed changes in response to external forcing. Figure 2.7 shows observations and model response patterns provided to the 1-D TLS regression using MPI-ESM-LR and HadGEM2-ES oxygen fields, plotted against the model-estimated range of internal variability. The envelope of estimated internal variability in $[O_2]$ scales with latitude in both models such that sub-polar and polar regions where a strong zonal mean deoxygenation signal is observed coincide with areas of largest internal variability ($\pm$2–4 μmol kg^{-1}). Nevertheless, the magnitude of observed zonal mean $[O_2]$ change exceeds the spread of simulated internal variability in the mid- to high-latitude ocean, with a deoxygenation signal emerging above natural internal variability poleward of 30–40° in both hemispheres. Simulated internal variability is smaller in the HadGEM2-ES piControl experiment such that observed $[O_2]$ decreases become distinct from internal variability across more of the mid-latitude ocean. Both MPI-ESM-LR and HadGEM2-ES historical integrations simulate more muted deoxygenation signals compared to the observations which are largely within the range of internal variability at all latitudes. Structural errors in the pattern of $[O_2]$ change simulated by both models also generally fall within the spread of internal variability. Observations and model response patterns have also been provided to the TLS regression from depth-resolved 2-D $[O_2]$ changes globally and for the Pacific and Atlantic basins between 100–3000 m depth (Fig. 2.5).

Scaling factors (β) resulting from the single fingerprint analysis confirm that a statistically significant change in observed $[O_2]$ in response to external forcing is detected and inconsistent with simulated internal variability at a 90 % confidence level (Fig. 2.8). Projection of observations onto the simulated "all forcings" response of MPI-ESM-LR and HadGEM2-ES shows a detectable change in depth-averaged zonal mean $[O_2]$ between $\sim$ 1970 and $\sim$ 1992, since the best estimates of the scaling factors and their confidence intervals at the global scale are significantly different from 0. Scaling factors calculated for the MPI-ESM-LR and HadGEM2-ES 1-D analyses are 2.82 and 3.59, respectively,

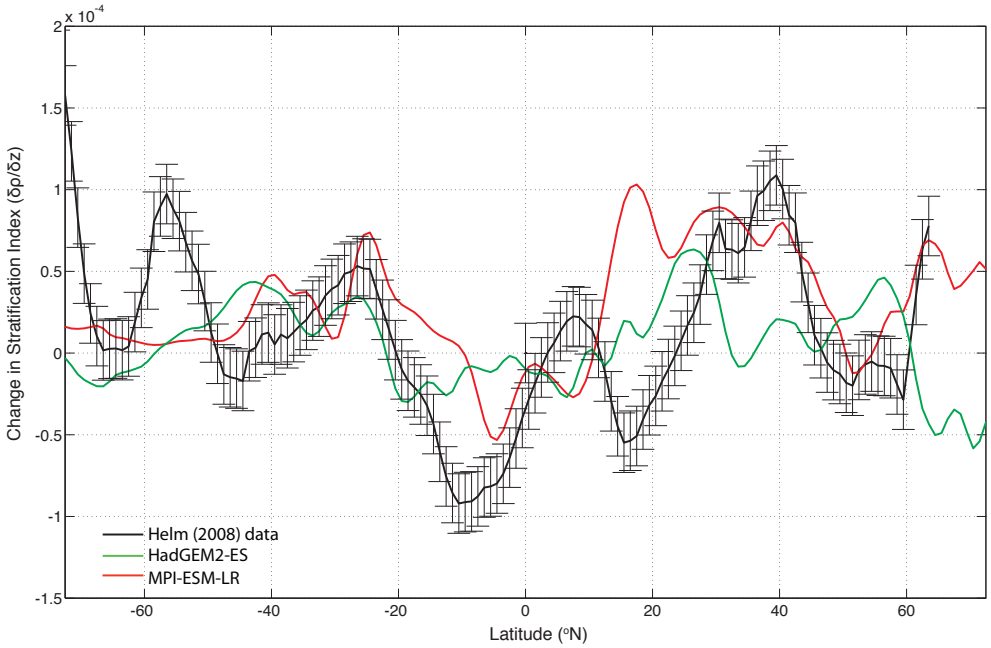

Figure 2.6: Zonal mean change ($\sim$ 1992 minus $\sim$ 1970) in upper ocean stratification as a function of latitude from observations (black; Helm, 2008), and HadGEM2-ES (green) and MPI-ESM-LR (red) historical integrations. The Stratification Index is calculated as the vertical density gradient ($\delta\rho/\delta z$) between 200–1000 m depth. Model stratification is estimated by calculating density (kg m^{-3}) from CMIP5 historical temperature and salinity fields at 200 m and 1000 m depth levels. Positive values indicate an increase in upper ocean stratification over time. These stratification changes differ from those presented by Helm et al. (2011) because we exclude surface data ($<$ 100 m) from the Hadley SST climatology. Error bars for observed stratification changes are given at the 95 % confidence level as in Fig. 2.3

indicating that the effect of external forcing is detectable and that the models and observations have significant correlations in the latitudinal pattern of variation. However, since these β values are greater than one we can infer that the ESM simulated [O_2] responses to external forcing are significantly underestimated and need to be amplified (by a factor of between ~ 2 and ~ 4) to be consistent with observed changes. The residual consistency test passes for both model experiments indicating no inconsistency between residual observed variance and model simulated internal variability, and suggesting that both ESMs simulate the externally forced signal adequately to explain observed [O_2] changes. For both MPI-ESM-LR and HadGEM2-ES β estimates for the 1-D analysis are robust across a range of truncations proximal to the chosen values of k, adding confidence to the presented optimal detection results (Fig. 2.9).

In agreement with the 1-D result, the 2-D detection analysis using MPI-ESM-LR yields a best estimate scaling factor of greater than 1 ($\beta = 2.26$) for the global ocean, although in

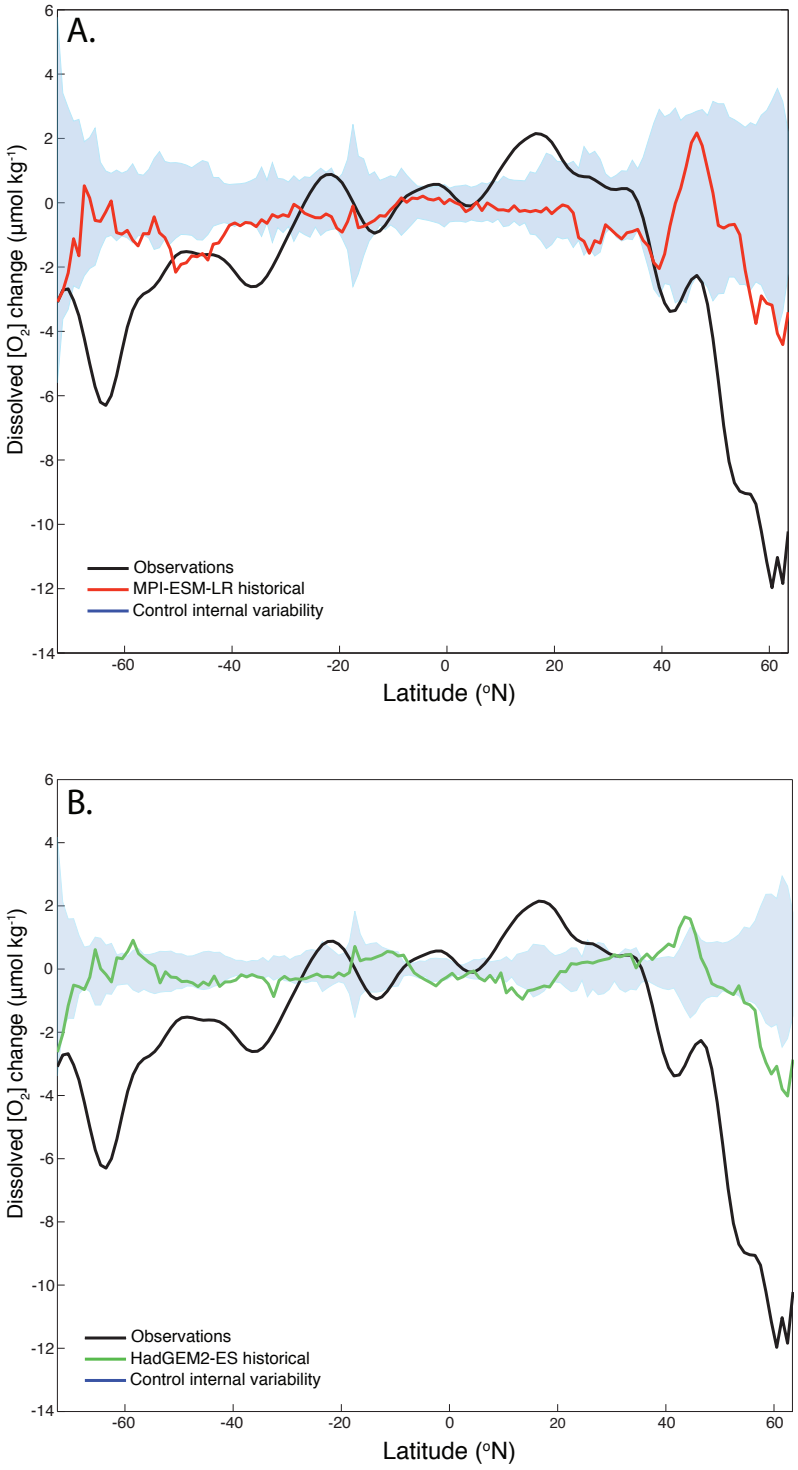

Figure 2.7: Observed (black) and simulated (red or green) patterns provided to the 1-D optimal detection as zonal mean $[O_2]$ changes (μmol kg^{-1}) averaged between 100–3000 m depth using MPI-ESM-LR **(A)** and HadGEM2-ES **(B)** historical experiments. The spread of internal variability (shown by the shaded area) is estimated by sampling model piControl simulations, as described in Sect. 2.3.2

this case the 5–95 % uncertainty bounds on this value are consistent with 1. This range of estimated β values demonstrates that the simulated response of the MPI-ESM-LR model provides a good fit to observed zonal mean [O_2] changes between $\sim$ 1970 and $\sim$ 1992 in response to external forcing. A positive detection result ($\beta = 5.30$) is also found for observed [O_2] changes in the Pacific Ocean using a 2-D pattern with MPI-ESM-LR. However, this scaling factor is much larger than 1 indicating poor model-data agreement in amplitude. In contrast, the null hypothesis that observed changes in marine oxygen are caused by natural internal variability cannot be rejected for the Atlantic Ocean, where the 5–95 % range of β estimates are indistinguishable from zero, with a best estimate scaling factor of less than 1 ($\beta = 0.89$). The residual consistency test fails for this region only, suggesting that there are elements of the observed [O_2] variability which are not well captured by the model in the Atlantic Ocean. Overall, an external influence on historical changes in observed [O_2] is detected for the zonally averaged global ocean and Pacific basin, although the observed response is larger than that simulated by ESMs at all scales.

2.5 Discussion

This study presents, for the first time, an optimal fingerprinting analysis detecting statistically significant global decreases in observed oceanic [O_2] in response to external forcing, as distinct from internal variability driven by the leading climate modes. The primary natural external forcing imposed on [O_2] is explosive volcanism, a perturbation on the climate system that is generally limited to the ocean's upper $\sim$ 500 m on interannual timescales (Frölicher et al., 2009). Because the observed and modelled deoxygenation occurs throughout the water column and on interdecadal timescales, we can infer that rising greenhouse gas concentration is the main driver of a detectable external forcing on historical [O_2] changes between $\sim$ 1970 and $\sim$ 1992. In the 1-D analysis we find the most detectable [O_2] change signal relative to internal variability at mid- to high latitudes in regions of water mass renewal where the observed subsurface zonal mean oxygen decreases are largest. Helm et al. (2011) attribute $\sim$ 85 % of global ocean deoxygenation in polar regions to elevated upper ocean stratification which increases the ventilation age of downwelling water parcels allowing for more biological oxygen consumption to occur, consistent with a range of prognostic modelling studies (Sarmiento et al., 1998; Bopp et al.,

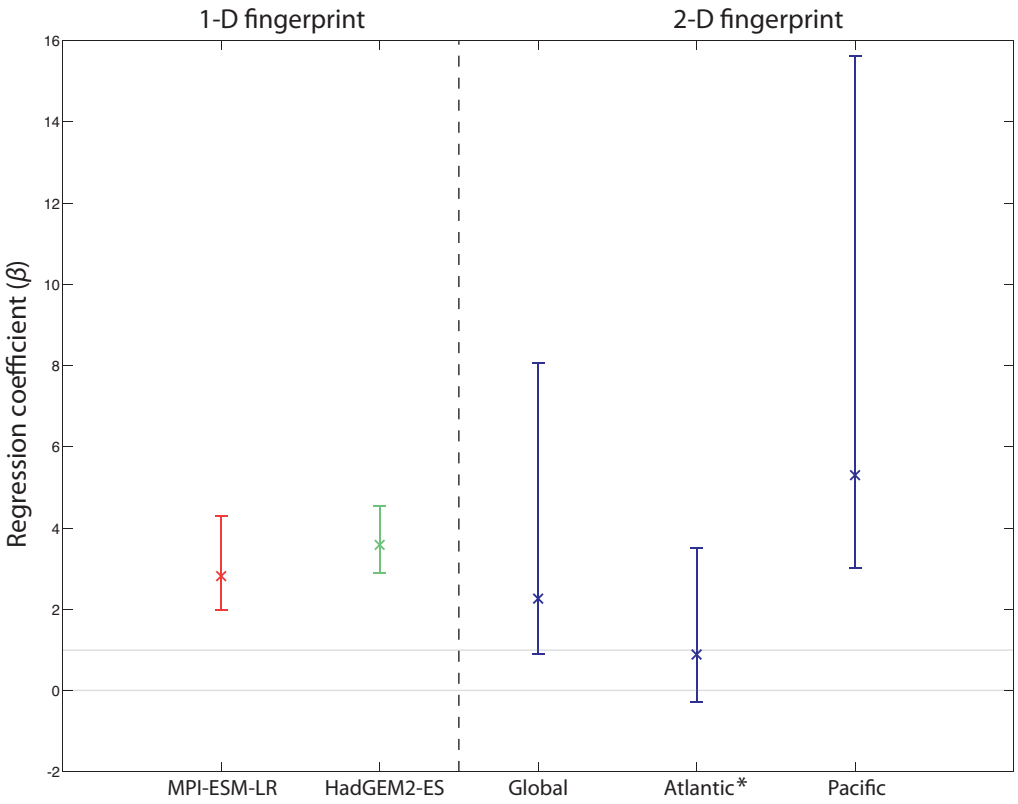

Figure 2.8: Best estimates and 5–95 % uncertainty ranges of regression coefficients (β) from single fingerprint optimal detection analysis. Two types of model response pattern are projected onto dissolved oxygen observations. Left: a 1-D global depth-averaged (100–3000 m) zonal mean [O_2] change using MPI-ESM-LR ($k = 40$) and HadGEM2-ES ($k = 31$). Right: a 2-D depth-resolving zonal mean [O_2] change globally and for the Atlantic and Pacific Ocean basins ($k = 49$) using MPI-ESM-LR only (* indicates a failed residual consistency test at all EOF truncations).

2002; Matear and Hirst, 2003). We also find significant increases in upper ocean stratification between $\sim$ 1970 and $\sim$ 1992 at high latitudes for MPI-ESM-LR and HadGEM2-ES historical integrations concurrent with enhanced subsurface deoxygenation. Moreover, the inability of either model to reproduce observed increases in zonal mean stratification in the Southern Ocean could provide a mechanistic explanation for why modelled [O_2] decreases are considerably smaller than observed in this region. Jungclaus et al. (2013) also show that the ocean model within MPI-ESM-LR overestimates ventilation in the Antarctic Circumpolar Current system, producing enhanced oxygenation of the oceanic interior in this region. Large uncertainties are entrained into model estimates of physical circulation changes owing to incomplete assessments of the competing roles of stratification and wind forcing (e.g., Le Quéré et al., 2007; Böning et al., 2008; Downes et al., 2011) in controlling ventilation processes in a warmer world.

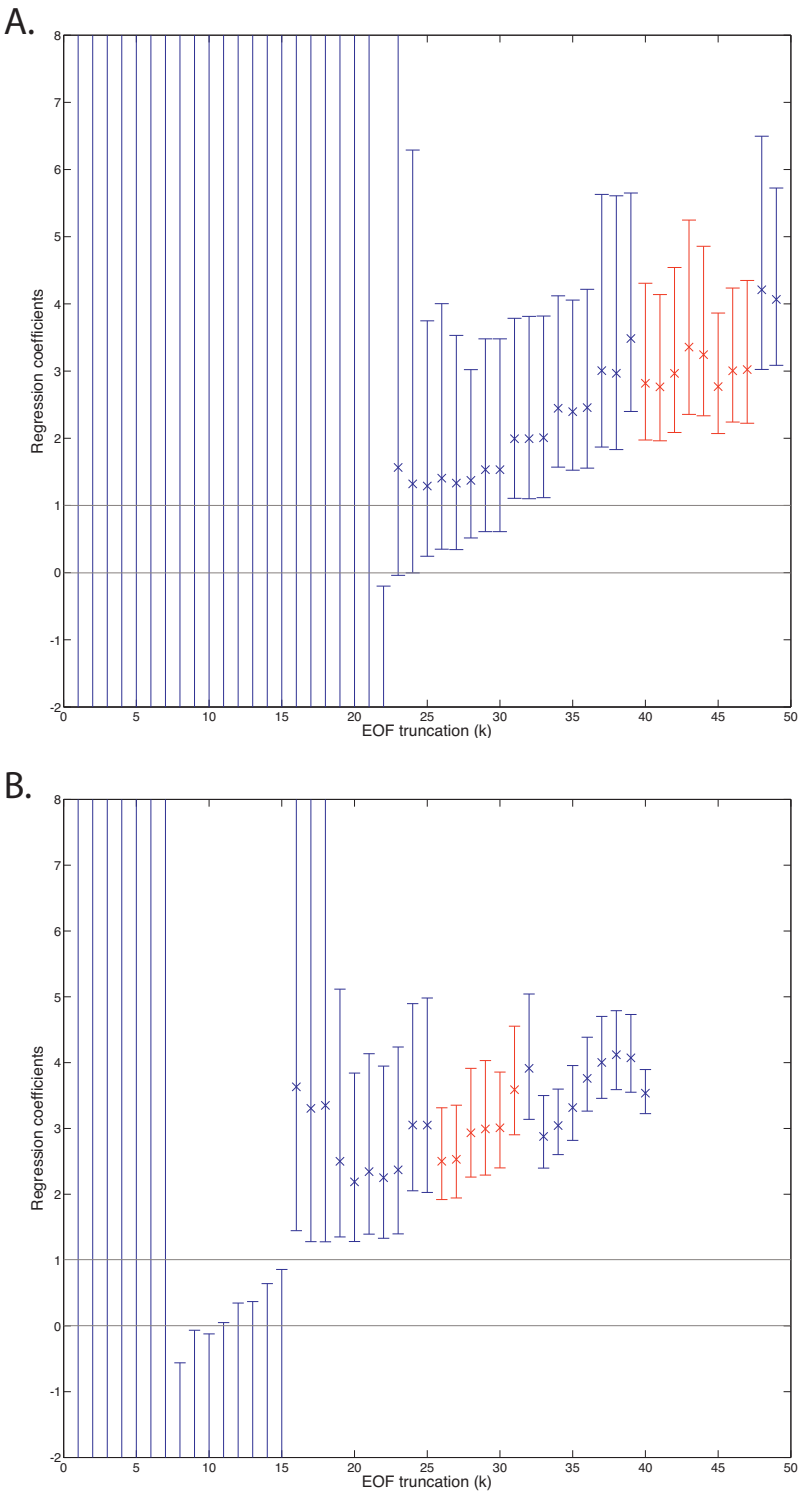

Figure 2.9: Regression coefficients (β) and their 90 % confidence intervals plotted as a function of EOF truncation (k) for 1-D MPI-ESM-LR **(A)** and HadGEM2-ES **(B)** optimal detection analyses. β estimates are relatively invariant where the residual consistency check passes (at k values shown in red).

Although we find a clearly identifiable influence of external forcing on recorded patterns of $[O_2]$ change, best estimates of β for both 1-D and 2-D global analyses are consistently greater than one suggesting that model responses need to be scaled up to match the observations. There are a number of potential explanations for this result. One possibility, endemic to climate sensitive variables that are locally heterogeneous and difficult to simulate (Masson and Knutti, 2011), is that $[O_2]$ data could exhibit too much small-scale variability to be directly comparable with smoother model fields. This potential discrepancy could yield observed change signals with artificially inflated amplitudes relative to model response patterns, although we try to account for this effect by spatially smoothing the data prior to model evaluation. Detection results are robust across a range of EOF truncations and temporal averaging schemes with no evidence of under or over fitting within the TLS regression, such that methodological choices about data processing are unlikely to have significantly biased scaling factors. Model errors could also contribute to elevated β values if imposed forcings in CMIP5 historical experiments are too weak or ESMs are less responsive to external forcing than in reality. Since CMIP5 historical forcings are prescribed from observations (Taylor et al., 2009, 2012) the former seems unlikely; however, there is evidence to support the proposition that the current generation of ESMs systematically underestimate observed variability in $[O_2]$. For example, in good agreement with our 1-D scaling factors, hindcast simulations initialised globally (Rödenbeck et al., 2008) and for the North Pacific (Deutsch et al., 2005, 2006) underestimate observed interannual to decadal variability in ocean oxygen by a factor of between ~ 2 and ~ 3. It has been suggested that coarse resolution models might underestimate variability in simulated passive tracers since they do not resolve mesoscale ocean dynamics (Hirst et al., 2000; Jochum et al., 2007). Moreover, coupling frequency between the ocean and atmosphere (once a day in MPI-ESM-LR and HadGEM2-ES simulations) might also be insufficient to fully capture climate variability in state-of-the-art ESMs. This could support the assertion that the response of models to secular climate change may also be underestimated, since a more naturally variable ocean-climate system will likely be more sensitive to imposed external forcings (von Storch and Zwiers, 1999; Swanson et al., 2009). However, the piControl derived estimates of natural internal variability used in this analysis are shown to be consistent with observed variance using a standard residual consistency

test and comparison of simulated noise with two observational estimates (Sect. 2.3.2 and Table 2.2).

Qualitative model-data comparison (Sect. 2.4.1) suggests that regional differences between modelled and observed patterns of $[O_2]$ change could also contribute to the weaker simulated zonal mean signal. However, consistent with the assumption of the TLS detection model that "structural uncertainty" has the same structure as internal variability (e.g., Terray et al., 2012), model errors generally fall within the range of internal variability (Fig. 2.7). Regional differences probably result from the omission of key biogeochemical and physical processes that control marine oxygen distribution at a local scale. Particularly, 2-D model response patterns are unable to reproduce a net deoxygenation signal in the tropical thermocline, consistent with deficiencies in modelling studies (Bopp et al., 2002; Matear and Hirst, 2003; Stramma et al., 2012a). Stramma et al. (2012a) report that the spurious tropical $[O_2]$ increases at 300 dbar in the UVic ESM may be primarily related to the inability of coarse resolution ocean models to resolve the fine scale equatorial currents which control the oxygen budget of the OMZs (Brandt et al., 2010; Stramma et al., 2010). Their sensitivity study suggests that alternative proposed model deficiencies such as artificially high rates of diapycnal mixing within the tropical thermocline (Gnanadesikan et al., 2007) and the omission of a pCO_2 sensitive C:N stoichiometry in primary production (Oschlies et al., 2008; Tagliabue et al., 2011) do not resolve the erroneous tropical $[O_2]$ increases in their model. In the case of MPI-ESM, a comparison between the low resolution (analysed in this study) and eddy-permitting model configurations (MPI-ESM-MR with a nominal resolution of $\sim 0.4^{\circ}$) shows only a slight improvement in the representation of $[O_2]$ in the thermocline (Ilyina et al., 2013). This indicates that eddy-permitting spatial resolution of the ocean model alone is insufficient to solve the coupled models deficiencies with respect to $[O_2]$ dynamics. Other model-data discrepancies, particularly simulated oxygen increases within the ocean interior at high latitudes, are likely to be related to persistent errors in model physical mixing and deep ocean ventilation, as reported for historical CMIP5 experiments of IPSL-CM5A and CNRM-CM5.1 (Séférian et al., 2013). In addition, the inability of models to capture $[O_2]$ dynamics in ice-covered high-latitude areas can be attributed to uncertainties in the underlying sea-ice models related to the growth and melting of seasonal ice (e.g., Notz et al., 2013).

Counter to the global and Pacific Ocean detection results, our analysis finds observed patterns of $[O_2]$ change in the Atlantic basin to be indistinguishable from natural internal variability. The high internal variability of Atlantic oxygen has been reported by others (e.g., Johnson and Gruber, 2007) and in an analysis of the essential ocean indices the Atlantic scored poorly from the perspective of the strength of signal-to-noise ratio (Banks and Wood, 2002). These findings are supported by modelling studies which show secular increases in Apparent Oxygen Utilisation (AOU) of the subsurface North Atlantic to be rendered statistically insignificant by internal variability associated with the North Atlantic Oscillation (Frölicher et al., 2009). Thus, in the Atlantic, high levels of internal variability coupled to a smaller observed mid- to high-latitude deoxygenation trend (relative to the Pacific and Southern Oceans; Helm et al., 2011) reduce the signal-to-noise ratio, contributing to the null detection result for this basin. The same conclusion was reached for sea surface salinity where the single fingerprint analysis of Terray et al. (2012) shows robust detection of observed salinity changes in response to anthropogenic forcing for the Pacific basin but with scaling factors consistent with 0 for the Atlantic Ocean.

2.6 Summary and conclusions

Our analysis shows that the global consistency and pronounced meridional structure of $[O_2]$ changes between $\sim$ 1970 and $\sim$ 1992 recorded by Helm et al. (2011) provide a distinct fingerprint of climate change in the oceans, which is robustly detected against internal variability as simulated by models. The unprecedented spatiotemporal coverage of data and sensitivity of $[O_2]$ to climate perturbation provides a unique opportunity to validate the response of ESMs to conditions of global change on multidecadal timescales. Rigorous assessment of ESMs against observations using detection and attribution methods supports the need to improve model physics and biogeochemistry, but also reveals that these models already have significant capacity to simulate many aspects of the ocean system, particularly the deoxygenation at mid- to high latitudes. However, both MPI-ESM-LR and HadGEM2-ES underestimate the observed $[O_2]$ response to external forcing, suggesting that model projections for future ocean deoxygenation in response to climate change may be too conservative. Furthermore, both models perform poorly at low latitudes, indicating that model projections in that region may not be reliable.

Detectable anthropogenic contributions to recent trends in ocean temperature (Barnett et al., 2005; Pierce et al., 2006; Gleckler et al., 2012) and salinity (Stott et al., 2008; Terray et al., 2012) have already been identified. Taken together, these marked changes to global heat and freshwater fluxes implicitly support our finding that stratification-driven global deoxygenation has started to emerge from the envelope of internal variability. We find the most detectable changes in $[O_2]$ relative to internal variability to occur at high latitudes where the independent and synergistic effects of secular ocean warming, acidification and deoxygenation could have a major impact on polar ecosystems and biogeochemical cycles (Gruber, 2011). Subsurface $[O_2]$ changes at high latitudes (particularly in the Pacific and Southern Oceans) should, therefore, be monitored closely alongside more widely documented $[O_2]$ decreases within the OMZs (e.g., Stramma et al., 2008) to better constrain the anthropogenic fingerprint of climate change in the oceans. Models predict that ocean deoxygenation at mid- to high latitudes will continue to intensify under global warming conditions, such that climate-driven perturbation to oceanic oxygen will become more distinct with time. Therefore, on-going observational efforts from time-series, repeat hydrographic sections and global in-situ profiling floats (e.g., Argo; Gruber et al., 2010) are crucial to better understanding natural variability in marine O_2 on multidecadal timescales and improving the detectability of emergent anthropogenic trends.

2.7 Acknowledgements

We thank K. Helm for making oxygen data and MATLAB code available, D. Stone for provision of IDL Optimal Detection routines and helpful comments, T. Ono and F. Whitney for providing time series data, and C. Enright for programming support. We also acknowledge the World Climate Research Programme's Working Group on Coupled Modelling, which is responsible for CMIP, and we thank the climate modelling groups for producing and making available their model output. For CMIP the US Department of Energy's Programme for Climate Model Diagnosis and Intercomparison provides coordinating support and led development of software infrastructure in partnership with the Global Organisation for Earth System Science Portals. The optimal detection calculations and data processing presented in this paper were carried out on the High Performance Computing Cluster supported by the Research Computing Service at the University of East

Anglia. PH's contribution to this work was supported by the Joint DECC/Defra Met Office Hadley Centre Climate Programme (GA01101). NLB acknowledges the support from the ARC Centre of Excellence for Climate System Science. This study is a contribution to EU FP7 project CARBOCHANGE (grant no. 264879).

Chapter 3

Physical and Biogeochemical Controls on Historical Dissolved Oxygen Concentration in a Forced Ocean Biogeochemistry Model

3.1 Introduction

The implementation of realistic oxygen cycling remains an important and active area of ocean–climate model development (e.g. the Fast Met Office UK Universities Simulator [FAMOUS]; Williams et al., 2014) owing to the ecological importance of [O_2] and its sensitivity to climatic perturbation on interannual to millennial timescales (Keeling et al., 2010). A pervasive feature of recent ESM projections is a reduction in the oxygen content of the global ocean in response to future anthropogenic climate change (e.g. Sect. 1.4; Ciais et al., 2013; Doney et al., 2014). Despite widespread model agreement in terms of the sign of change in a globally integrated sense, there is significant uncertainty as to the spatial pattern (or "fingerprint") and magnitude of future ocean deoxygenation (Bopp et al., 2013; Cocco et al., 2013). The ability of current models to reproduce the observed dynamics and distribution of ocean [O_2] therefore forms a central line of enquiry towards isolating uncertainties entrained into prognostic experiments (e.g. Sect. 2.4.1; Stramma et al., 2012a).

A number of persistent model biases have been identified in the [O_2] fields of both Ocean General Circulation Models (OGCMs; Chapter 2; Duteil et al., 2014) and EMICs (Stramma et al., 2012a) initialised for the historical period (see Section 1.4 for a comprehensive review). Most evident is the inability of current ocean–climate biogeochemistry models to reproduce the observed distribution and variability of [O_2] at low latitudes, particularly within the eastern tropical OMZs (e.g. Keeling et al., 2010; Stramma et al., 2012a). For example, coupled AOGCMs generally simulate [O_2] increases within the tropical thermocline (e.g. Bopp et al., 2002; Matear and Hirst, 2003) and a contraction of suboxic waters (Cocco et al., 2013) in response to ocean warming. This ubiquitous model response is contrary to time series data constructed by Stramma et al. (2008) for the eastern tropical OMZs, which show marked deoxygenation trends and expansion of low-O_2 waters over the last ~ 50 years. Gnanadesikan et al. (2013) also highlight the limited capacity of recent CMIP5 ESMs to reproduce the observed climatological distribution of [O_2] at intermediate depths. This systematic model bias is entrained into the biogeochemically significant (*cf.* Bianchi et al., 2012) volume censuses of low-O_2 waters, with models variously both underestimating (e.g. HadGEM2-ES [Jones et al., 2011]) and overestimating (e.g. MPI-ESM-LR [Ilyina et al., 2013]; GFDL-ESM2.1 [Dunne et al., 2013])

hypoxic and suboxic extent within the ocean interior (see also Section 2.4.1; Figure 2.2). A range of dynamical and biogeochemical model deficiencies have been invoked to explain the divergence between observed and simulated [O_2] at low latitudes (e.g. Keeling et al., 2010). Chief among them is the inability of coarse resolution global ocean–climate models to explicitly simulate the mesoscale structures which resupply O_2 into the eastern tropical OMZs (e.g. Brandt et al., 2010). To this end, eddy-resolving spatial resolution has been shown to improve representation of [O_2] in the Arabian Sea (Resplandy et al., 2012) and eastern tropical Atlantic (Duteil et al., 2014) OMZs via more realistic transport processes in the physical model. Uncertainties surrounding the parameterisation of lateral (Gnanadesikan et al., 2012; Gnanadesikan et al., 2013) and vertical (Duteil and Oschlies, 2011) diffusion have also been shown to place important constraints on the extent and evolution of low-O_2 waters in ESMs.

The simplistic representation of biological processes in ecosystem models and their response to physical and geochemical forcing has also been suggested as an important limitation on O_2 dynamics in ocean models (e.g. McKinley et al., 2003; Rödenbeck et al., 2008). For example, Matear and Lenton (2014) show using an ensemble of coupled carbon-climate ESM experiments that the *interactive* effects of climate change and ocean acidification could drive significant alteration to biogeochemical cycles, suggesting that ocean warming should not be considered in isolation when considering future ocean deoxygenation. Of most importance to model representation of oxygen cycling are the potential impacts of ocean acidification on primary production and the biological pump. Particularly, mesocosm experiments carried out using natural plankton communities (Riebesell et al., 2007; Bellerby et al., 2008) suggest that the C:N uptake ratio in photosynthetic carbon fixation increases under elevated pCO_2 due to DIC over-consumption, causing the composition of exported organic material to deviate from classical Redfield stoichiometry (e.g. C:N = 6.6 [Redfield, 1963]). Specifically, Riebesell et al. (2007) report higher C:N drawdown ratios in diatom and coccolithophore-dominated mesocosm enclosures exposed to increased partial pressures of CO_2 (pCO_2 = 700 μatm, C:N = 7.1; pCO_2 = 1050 μatm, C:N = 8.0), whilst N:P ratios remain unchanged from Redfield proportions. The effects of stoichiometric plasticity in marine ecosystems remain largely unaccounted for in current ocean biogeochemistry models (*cf.* Flynn, 2010), which generally rely on fixed elemental

ratios in the formation of organic material (e.g. Aumont and Bopp, 2006). However, recent studies using configurations of the UVic EMIC (Oschlies et al., 2008) and PISCES Ocean Biogeochemistry General Circulation Model (OBGCM; Tagliabue et al., 2011) which implement a pCO_2 sensitive C:N ratio in primary production suggest that stoichiometric effects in response to ocean acidification could have a major impact on biogeochemical cycles. Particularly, model experiments with variable C:N stoichiometry simulate increases in cumulative carbon export of between 70 and 100 Pg C by 2100 in response to future CO_2 forcing. Moreover, the export of (relatively) more carbonaceous organic material from the surface in response to acidification-driven DIC over-consumption also causes biological oxygen demand to increase. As a result, these model experiments project elevated deoxygenation of the tropical thermocline ($> 20\,\mu\text{mol}\,\text{L}^{-1}$) and 36 – 50 % increases in the volume of suboxic waters by 2100 (Tagliabue et al., 2011; Oschlies et al., 2008), compared to no change or a small $[O_2]$ increases as simulated by fixed stoichiometry ESMs (CMIP5; Bopp et al., 2013). Stramma et al. (2012a) investigate the impact of variable C:N ratios on historical $[O_2]$ trends using a low-resolution EMIC, and find that this effect reduces model-data disagreement in zonal mean depth averaged $[O_2]$ trends. However, the impact of accounting for variable stoichiometry on historical $[O_2]$ changes in more complex OBGCMs (e.g. Tagliabue et al., 2011) or Plankton Functional Type (PFT) ecosystem models (e.g. Buitenhuis et al., 2013; Le Quéré et al., 2014a) remains uncertain.

The dissolution of gaseous CO_2 in seawater causes a decrease in pH as weak carbonic acid (H_2CO_3) forms and dissociates into bicarbonate (HCO_3^-) and hydrogen (H^+) ions. However, the hydrolysis of CO_2 concomitantly consumes carbonate ions (CO_3^{2-}) following Equation 3.1, thereby reducing the saturation state of seawater with respect to calcium carbonate (both calcite [Ω_{cal}] and its less stable polymorph, aragonite [Ω_{arag}]).

$$CO_2 + H_2O + CO_3^{2-} \rightarrow 2HCO_3^- \tag{3.1}$$

A decrease in Ω under elevated pCO_2 has been shown by a number of laboratory and field studies to reduce biogenic calcification rates in some calcareous holoplankton (coccolithophores, foraminifera and pteropods) and warm-water corals (*cf.* Fabry et al., 2008; Doney et al., 2009). Extrapolating these results, Heinze (2004) projects a $\sim 50\,\%$ decline in global $CaCO_3$ export production by 2250 using an ocean biogeochemistry model

which accounts for reduced biocalcification rates in response to ocean acidification (SRES A1B emissions scenario). Beyond direct effects, it has been suggested by Armstrong et al. (2002) that changes in the "carbonate pump" may also impact upon the export of organic material, since fluxes of POC and PIC are highly correlated beneath ~ 1000 m depth (the so-called "PIC:POC rain ratio" [Archer et al., 2000; Klaas and Archer, 2002]). Specifically, it has been proposed that export fluxes of dense calcareous ($CaCO_3$) and siliceous (SiO_2) biominerals provide ballast which increases the sinking speed and transfer efficiency of POC into the ocean interior. Therefore, reduced export production of $CaCO_3$ in response to ocean acidification could impact upon the efficiency of the organic ("soft tissue") biological pump, such that POC remineralises at shallower depths as mineral ballast fluxes weaken. This effect has been reproduced by 3-D ocean biogeochemistry models which include simple ballasting sub-models (e.g. Heinze, 2004), with implications for other biogeochemical cycles including oxygen. For example, Hofmann and Schellenhuber (2009) have demonstrated, using idealised experiments of the POTSMOM-C low resolution ($3.75° \times 3.75°$) OGCM with a [$CO_3{}^{2-}$] dependency in calcification rates (R_{CAL}), that shallower POC remineralisation depths in response to weakened ballasting exacerbates O_2 depletion within established subsurface O_2 minima. In particular, reduced ballasting alone is shown in prognostic experiments under a SRES A1F1 emissions scenario until 2100 (with emissions declining to 0 at 2200) to reduce [O_2] by 20 – 40 μmol L^{-1} between ~ 200 – 800 m depth by the year 3000, with the largest decreases within tropical OMZs (e.g. > 50 μmol L^{-1} at 500 m depth in the Arabian Sea). As such, the interactive effects of ocean acidification on carbon export have been shown to have a major impact on O_2 distributions and forced responses in ocean-climate model projections. However, no studies have so far addressed the impact of accounting for these processes in reconciling the mismatch between observed [O_2] and that simulated by hindcast models.

Current ocean biogeochemistry models also underestimate temporal variability in O_2 on interannual to decadal timescales. For example, Deutsch et al. (2005, 2006) report decadal scale variability in Apparent Oxygen Utilisation (AOU) as simulated by an ensemble of ocean-only hindcast model experiments for the North Pacific region to be underestimated by a factor of ~ 3 relative to repeat hydrographic section data. Similarly, interannual variability in global Atmospheric Potential Oxygen (APO) fluxes have been shown to be

underestimated by a factor of $\sim 2 - 4$ in hindcast ocean biogeochemistry models relative to those estimated using global atmospheric transport inversions (Rödenbeck et al., 2008). These results are also consistent with the model-data comparison presented in Chapter 2, where optimal fingerprinting methods applied to recent CMIP5 ESMs show that model $[O_2]$ responses need to be scaled up by a factor of between ~ 2 and 4 to match observed changes (see Section 2.4.2, Figure 2.8). Recent work using hindcast configurations of the UVic EMIC (Swart et al., 2014) and PlankTOM5 OBGCM (Le Quéré et al., 2010; Ishi et al., 2014) demonstrate the sensitivity of simulated trends and variability in the ocean carbon cycle to imposed atmospheric forcing. For instance, Ishi et al. (2014) find significant differences in the interannual variability of CO_2 outgassing fluxes from the tropical Pacific using PlankTOM5.3 ocean-only experiments forced with the JPL CCMP Ocean Surface Wind Product (Atlas et al., 2011) compared to those derived from NCEP/NCAR reanalysis data (Kalnay et al., 1996). Additionally, model representation of large scale physical transport processes such as the Atlantic Meridional Overturning Circulation (AMOC) have been shown to be sensitive to the choice of imposed atmospheric forcing. For example, Stepanov and Haines (2013) show model simulated long period variability in AMOC transport at 26.5°N to be significantly different between hindcast experiments which employ ECMWF ERAInterim reanalysis data (Simmons et al., 2007) compared to those which calculate bulk fluxes using the Drakkar Forcing Set 3 (DFS3; Brodeau et al., 2010) hybrid (blended meteorological and satellite) forcing product. As a result, whilst it must be acknowledged that natural variability is also generated internally to the ocean system, ocean-only model configurations allow considerable "exogenous" variability to be directly related to the imposed atmospheric forcing (e.g. Stepanov and Haines, 2013). Therefore, the use of high frequency, high quality atmospheric data to calculate turbulent fluxes of heat, freshwater and momentum in hindcast models (*cf.* Large and Yeager, 2004; Brodeau et al., 2010) could provide a mechanism for improving interannual to decadal variability in simulated O_2.

In the present study a range of physical and biogeochemical perturbation experiments are conducted using a state-of-the-art global ocean biogeochemistry model (PlankTOM10; Le Quéré et al., 2014a) in order to better constrain the source of systematic biases in model representation of O_2 (e.g. Keeling et al., 2010). Specifically, this work aims to quantify

the impact of (1) imposed atmospheric forcing and (2) interactive ocean acidification effects (variable C:N stoichiometry and reduced mineral ballasting) on the spatiotemporal distribution of [O_2] over the last $\sim$ 50 years.

3.2 Model description

3.2.1 Ocean biogeochemistry model

The PlankTOM10 Dynamic Green Ocean Model (DGOM; Le Quéré et al., 2014a) is a global ocean biogeochemistry model which describes lower-trophic level ecosystem dynamics explicitly based on dominant PFTs, following the rationale of Le Quéré et al. (2005). PlankTOM10 builds on previous DGOMs (PlankTOM5.2 [Buitenhuis et al., 2010] and PlankTOM5.3 [Buitenhuis et al., 2013]) by including ten PFTs: picophytoplankton, N_2-fixers, coccolithophores, mixed phytoplankton, diatoms, colonial *Phaeocystis*, bacteria, protozooplankton, mesozooplankton and macrozooplankton. The present model version comprises 39 biogeochemical tracers, and simulates the full marine cycles of Carbon (C), Phosphorous (P), Oxygen (O_2), Silicon (Si), along with simplified cycles of Nitrogen (N) and Iron (Fe). Growth of PFTs is co-limited by temperature, light, macronutrients (N, P and Si) and Fe. PlankTOM10 includes 3 detrital pools (semi-labile dissolved organic material [DOM], and small and large POC), with a fixed Redfield stoichiometry (172O:122C: 16N:1P [Anderson and Sarmiento, 1994]) in the formation and remineralisation of organic material for the standard model configuration (see Section 3.3.1). However, Fe:C, Chl:C and Si:C (for diatoms) ratios are variable, as calculated by the model based on PFT and abiotic factors. N pools are also subject to denitrification and N_2-fixation processes.

As described in Buitenhuis et al. (2013), PlankTOM10 also includes a sophisticated parameterisation of mineral ballasting, whereby the sinking speed of large POC increases as a function of opal (SiO_2) and calcite ($CaCO_3$) content. This parameterisation applies the direct measurements of mineral ballasting by opal and calcite in copepod fecal pellets (Ploug et al., 2008) to the drag equations of Buitenhuis et al. (2001) in order to derive a relationship between particle density and gravitational sinking speed of large POC (v_{sink}) following Equation 3.2.

$$v_{sink} = a(\rho_{par} - \rho_{sw})^b \tag{3.2}$$

Where a = 0.0303, b = 0.6923, ρ_{sw} is the density of seawater and ρ_{par} is the density of the particle, calculated by:

$$\rho_{par} = \frac{(LPOC \times 240 + CAL \times 100 + SIL \times 60)}{max(\frac{LPOC \times 240}{\rho_{LPOC}} + \frac{CAL \times 100}{\rho_{CAL}} + \frac{SIL \times 60}{\rho_{SIL}}, 10^{-15})} \tag{3.3}$$

Where $LPOC$ is large particulate organic carbon, CAL is sinking calcite, SIL is sinking opal, 240 is wet weight/mol POC, 100 is the molar mass of calcite, 60 is the molar mass of opal, and ρ_{LPOC} = 1.08 kg L^{-1}, ρ_{CAL} = 1.34 kg L^{-1}, ρ_{SIL} = 1.2 kg L^{-1} (calculated based on the data of Ploug et al. [2008]). Small POC is set to sink at a constant rate of 3 m d^{-1}, whereas $LPOC$ has a maximum numerically stable sinking speed set to 150 m d^{-1}. For further details of the PlankTOM10 biogeochemistry model, Le Quéré et al. (2014a) and Enright et al. (2014) present a full description of parameter values and model equations.

In all model experiments described subsequently biogeochemical fields are initialised from Global Ocean Data Analysis Project (GLODAP; Key et al., 2004) data for Dissolved Inorganic Carbon (DIC) and alkalinity, and World Ocean Atlas 2005 observations for O_2 (Garcia et al., 2006a) and nutrients (phosphate, nitrate and silicate [Garcia et al., 2006b]). Biological variables are restarted from the output of a previous PlankTOM10 model run (e.g. Vogt et al., 2010). The model is forced with atmospheric CO_2 data at each timestep (Keeling and Whorf, 2005). Dust fluxes are interpolated to daily values from the monthly fields of Jickells et al. (2005) and provide Fe (0.035g Fe per g dust) and Si (0.308 g Si per g dust) inputs to the surface ocean.

3.2.2 Physical model

PlankTOM10 is embedded within the Nucleus for European Modelling of the Ocean version 3.1 (NEMOv3.1; `http://www.nemo-ocean.eu`) physical model, which comprises the primitive equation Océan Parallélisé version 9 (OPA9; Madec, 2008) OGCM

coupled to the Louvain-la-Neuve Ice version 2 (LIM2; Timmermann et al., 2005) dynamic-thermodynamic sea ice model. This study employs a global configuration (ORCA2; Madec and Imbard, 1996) of NEMOv3.1 where the model is discretised on a tripolar curvilinear grid with a zonal resolution of 2°, and a meridional resolution of $2^\circ \times cos$(latitude) increasing to $\sim 0.5^\circ$ at the equator and towards the poles. In the vertical, ORCA2 has 30 z-levels with a maximum resolution of 10 m for the upper 100 m, decreasing to ~ 500 m at 5 km depth. Vertical mixing is calculated using a turbulent kinetic energy model (Gaspar et al., 1990), with subgrid scale eddy-induced mixing processes accounted for using the parameterisation of Gent and McWilliams (1990). Active tracers are initialised from World Ocean Atlas 2005 temperature (Antonov et al., 2006) and salinity (Locarnini et al., 2006) observations in all model experiments. A range of atmospheric forcing data has been used to derive surface fluxes of momentum, heat and freshwater as boundary conditions to the hindcast NEMOv3.1 physical model, as described in Section 3.3.2.

3.3 Model set-up

As outlined in Table 3.1, sensitivity experiments are carried out using the PlankTOM10-NEMO3.1 model which examine the impact of ocean carbon cycle feedbacks and imposed physical forcing on the simulated spatiotemporal distribution of [O_2] over the historical period. Further details of ocean biogeochemistry (Sect. 3.3.1) and atmospheric forcing (Sect. 3.3.2) model runs are provided subsequently.

Model Experiment	Time Period	Atmospheric Forcing	pCO$_2$-sensitive C:N ratio	pCO$_2$-sensitive R_{CAL}
REF	1948 – 2013	NCEP/NCAR	No	No
STO10	1948 – 2013	NCEP/NCAR	Yes	No
BAL10	1948 – 2013	NCEP/NCAR	No	Yes
CORE2	1948 – 2007	COREv2-IAF	No	No
DFS4	1958 – 2006	DFS4.3	No	No
IPSL	1948 – 2005	IPSL-CM5A-LR	No	No

Table 3.1: Summary of the model configurations used in each ocean-only hindcast PlankTOM10-NEMO3.1 experiment.

3.3.1 Ocean biogeochemistry experiments

In order to investigate the impact of ocean acidification on the spatiotemporal distribution of $[O_2]$ for the historical period two biogeochemistry perturbation experiments are conducted, alongside a baseline (*REF*) experiment following the standard model configuration as described in Section 3.2. These comprise explicit representation within the PlankTOM10 biogeochemical model of (1) a pCO_2-sensitive C:N ratio in primary production (*STO10*) and (2) a pCO_2-sensitive calcification rate (R_{CAL}) and associated impacts on the PIC:POC rain ratio (*BAL10*). As discussed in Section 3.3.2 all ocean biogeochemistry experiments are conducted using a common NCEP/NCAR atmospheric forcing with the greatest temporal coverage (1948 – 2013; *REF*).

For the *STO10* experiment, following the prognostic modelling studies of Oschlies et al. (2008) and Tagliabue et al. (2011), a change in the C:N ratio of organic matter via increased photosynthetic carbon fixation in response to ocean acidification is parameterised using the results of mesocosm experiments carried out on natural plankton communities under elevated pCO_2 (Riebesell et al., 2007). Based on these experiments, a non-dimensional "CO_2 sensitivity" factor (see Figure 3.1) is derived to provide a relationship between observed pCO_2 model forcing and the C:N ratio in organic carbon production and remineralisation. In *STO10* this factor is multiplied by the rate of net organic carbon production (*prodt*) and used to calculate a variable (pCO_2-sensitive) O:C ratio in organic material.

A second experiment, *BAL10*, investigates the impact of a pCO_2-sensitive biogenic calcification rate (R_{CAL}) on marine biogeochemical cycles. The parameterisation used in this study is taken directly from laboratory manipulations carried out with the coccolithophore species *Emiliania huxleyi* and *Gephyrocapsa oceanica*, in which the PIC:POC rain ratio is measured to decrease under elevated $[CO_{2(aq)}]$ (Zondervan et al., 2001). PlankTOM10 includes explicit representation of coccolithophores as a calcifying PFT with growth rates based on observations (*cf.* Le Quéré et al., 2014a). Thus, when compared to other NPZD-type biogeochemistry models which have investigated an acidification response in calcification (e.g. Heinze, 2004; Hofmann and Schellnhuber, 2009), an experimentally-derived parameterisation based on coccolithophore responses to acidification can be more appropriately applied to PlankTOM10 model equations. Following Zondervan et al. (2001) and Heinze (2004), the $CaCO_3$:C_{org} production ratio ($R_{CaCO_3/C_{org}}$) is parameterised in

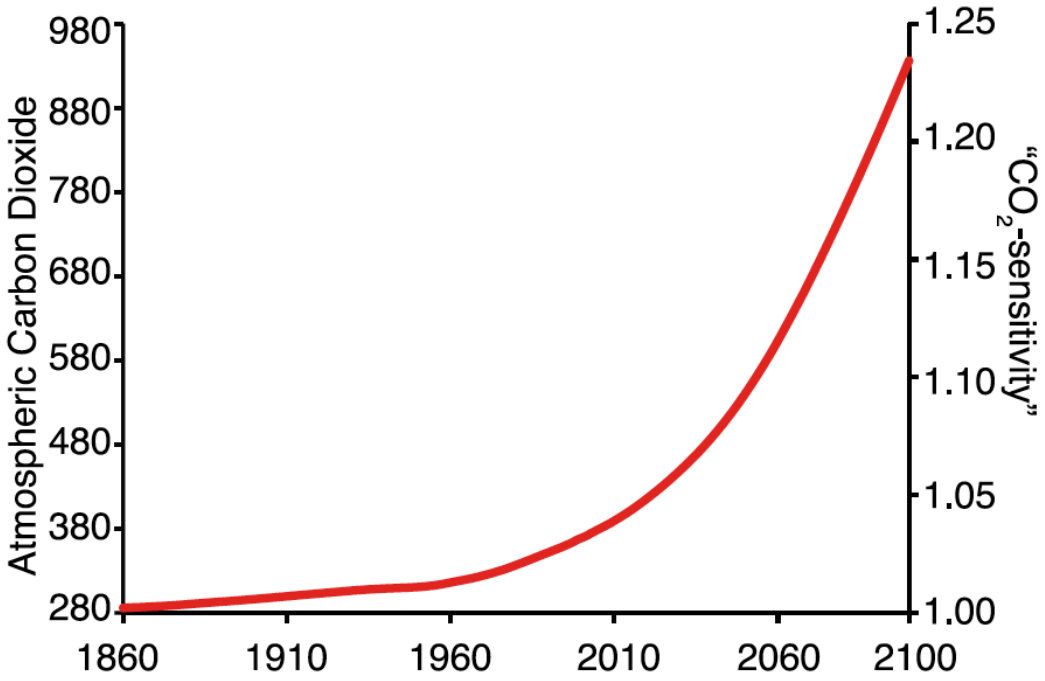

Figure 3.1: "CO_2 sensitivity" factor applied to the *STO10* PlankTOM10-NEMO3.1 model experiment based on prescribed atmospheric CO_2 following the results of mesocosm experiments conducted by Riebesell et al. (2007). Reproduced with permission from Tagliabue et al. (2011).

experiment *BAL10* as a function of the partial pressure of CO_2 (pCO_2):

$$R^{CaCO_3/C_{org}} = R^{CaCO_3/C_{org}}_{max}(1 - A(pCO_2^{obs} - pCO_2^{preindustrial})) \quad (3.4)$$

where $A = 4.4 \times 10^{-4}$ (based on Zondervan et al. [2001]), $pCO_2^{preindustrial}$ = 277.32 ppm and pCO_2^{obs} is prescribed to the biogeochemical model from observations (following Keeling and Whorf [2005]).

3.3.2 Atmospheric forcing experiments

Globally gridded atmospheric fields from interannual weather reanalyses provide a means of prescribing surface boundary conditions to drive multi-decadal hindcasts in OBGCMs. In this study, a series of PlankTOM10-NEMOv3.1 experiments are conducted using a range of atmospheric fields in order to investigate the sensitivity of historical changes and variability in simulated ocean [O_2] to imposed forcing. Model experiments are initialised using four different atmospheric forcing data products (see Table 3.2). As shown in Figure 3.2, these experiments also differ in terms of the bulk formulae used to provide turbulent fluxes of momentum, heat and freshwater to the NEMOv3.1 physical ocean

model.

The baseline experiment used in this study (*REF*) employs the CLIO bulk formulation of Goosse et al. (1999) to calculate surface boundary conditions, using NCEP/NCAR reanalysis data (Kalnay et al., 1996). This forcing approach is supported by the NEMO System Team as the reference configuration for NEMOv3.1 (Madec, 2008) and is consistent with other recent hindcast experiments conducted using the PlankTOM DGOM platform (e.g. Da Cunha et al., 2013; Buitenhuis et al., 2013). Moreover, NCEP/NCAR reanalysis data are updated annually (`http://www.esrl.noaa.gov/psd/data/gridded/data.ncep.reanalysis.html#temp`) such that the *REF* experiment has the longest temporal coverage, being forced with interannually varying NCEP/NCAR fields from 1948 to 2013. As summarised in Table 3.2, the *REF* experiment uses daily frequency NCEP/NCAR 10 m air temperature (θ_{10}), 10 m u and v wind components (U_{10}, V_{10}), total precipitation rate ($pptn$), 10 m specific humidity (q_{10}) and total cloud cover ($tcdc$). Wind speed is computed offline ($wspd = [u^2 + v^2]^{0.5}$) and used to calculate surface ocean stress (τ_x, τ_y) which is provided directly to the ocean model as a surface momentum flux. Sensible and latent heat fluxes are calculated using the CLIO bulk formulation based on the difference between imposed surface air temperature and model simulated SST, taking into account the specific humidity. Radiative fluxes are calculated from daily total cloud cover fields from NCEP/NCAR reanalysis.

Three other experiments (*CORE2*, *DFS4*, *IPSL*) are conducted using different imposed atmospheric forcings, all of which employ a more recent bulk formulation (CORE; Large and Yeager, 2004, 2009), which requires a slightly different set of meteorological surface variables (Table 2). The CORE bulk formulae use an inertial-dissipative method to calculate turbulent fluxes (momentum, sensible heat and evaporation) using 10 m wind speed components (U_{10}, V_{10}) along with specific humidity and air temperature, referenced at either 10 m (q_{10}, θ_{10}; *CORE2*) or 2 m (q_2, θ_2; *DFS4* and *IPSL*) dependent on input atmospheric data. Under a CORE bulk formulation shortwave and longwave components of the radiative heat flux are estimated directly based on downwelling shortwave (rad_{sw}) and longwave (rad_{lw}) radiation at the sea surface. Precipitation is provided as a total precipitation rate ($precip$) along with a solid fraction ($snow$). The details of each model experiment are given in Table 3.2, but are summarised here for clarity:

Table 3.2: Summary of atmospheric forcing datasets used in *REF*, *CORE2*, *DFS4*, and *IPSL* model experiments. The temporal frequency of meteorological surface variables is provided in parentheses (*di* = 6 hourly [diurnal]; *d* = daily, *m* = monthly).

EXP	Forcing dataset	Time period	Bulk formulae	U_{10}, V_{10}	θ, q	rad_{sw}, rad_{lw}	$precip$	$snow$
REF [1]	NCEP/NCAR	1948 – 2013	CLIO	NCEP/NCAR (*d*)	NCEP/NCAR (*d*)	N/A [2]	NCEP/NCAR (*d*)	N/A
CORE	COREv2-IAF	1948 – 2007	CORE	NCEP/NCAR [3] (*di*)	NCEP/NCAR [3] (*di*)	ISCCP-FD [3, 5] (*d*)	GCGCS [6] (*m*)	GCGCS (*m*)
DFS4	DFS4.3	1958 – 2006	CORE	ERA-40 [4] (*di*)	ERA40 [4] (*di*)	ISCCP-FD [4, 5] (*d*)	GCGCS [6] (*m*)	GCGCS (*m*)
IPSL	IPSL-CM5A-LR	1948 – 2005	CORE	CMIP5 (*d*)	CMIP5 (*d*)	CMIP5 (*d*)	CMIP5 (*m*)	CMIP5 (*m*)

[1] The baseline *REF* atmospheric forcing configuration is used for all ocean biogeochemistry experiments (*STO10*, *BAL10*; as described in Section 3.3.1)

[2] Radiative fluxes calculated from total cloud cover ($tcdc$) following Goosse et al. (1999)

[3] Bias corrections applied as described in Large and Yeager (2004, 2009)

[4] Bias corrections applied as described in Brodeau et al. (2010)

[5] Forcing provided as a climatological mean annual cycle for prior to 1984

[6] Forcing provided as a climatological mean annual cycle for prior to 1979

1. *CORE2*: Following Large and Yeager (2004, 2009) this model experiment is initialised with Version 2 of the Common Ocean-Ice Reference Experiments interannually Varying Forcing (COREv2-IAF) dataset for the period 1948 – 2007. COREv2-IAF is a blended (or "hybrid") atmospheric forcing data product, which applies corrections to known biases in NCEP/NCAR reanalysis state variables (U_{10}, V_{10}, θ_{10}, q_{10}) and utilises satellite derived radiative flux (ISCCP-FD [Zhang et al., 2004]) and precipitation (merged GCGCS product [Large and Yeager, 2009]) estimates so as to limit the imbalance in model heat and freshwater budgets. As such, COREv2-IAF comprises bias corrected 6 hourly 10 m NCEP/NCAR surface air temperature (θ_{10}), 10 m specific humidity (q_{10}), and 10 m wind components (U_{10}, V_{10}), daily frequency incoming shortwave (rad_{sw}) and longwave (rad_{lw}) radiation, and monthly total precipitation (precip) and solid precipitation ($snow$). Climatological mean annual cycles are provided for rad_{sw} and rad_{lw} prior to 1984 and for $precip$ and $snow$ prior to 1979.

2. *DFS4*: This experiment uses the DRAKKAR Atmospheric Forcing Set Version 4.3 (DFS4.3) for the period 1958 – 2006, as presented in Brodeau et al. (2010). Following the approach used to generate COREv2-IAF fields, DFS4.3 is a blended atmospheric forcing dataset which uses satellite radiation (ISCCP-FD) and precipitation (GCGCS) products. Surface atmospheric state variables are, however, provided from ERA-40 ECMWF reanalysis data (Uppala et al., 2005), with adjustments as described in Brodeau et al. (2010). ERA-40 is considered a "second generation" reanalysis product, with improvements in terms of resolution, data assimilation methods, and atmospheric models. Temporal frequency and input variables follow those described for *CORE2*, however surface air temperature and specific humidity are referenced at 2 m (θ_2, q_2) rather than 10 m in ERA-40.

3. *IPSL*: Forcing data for the *IPSL* experiment has been generated from the output of an ESM participating in Phase 5 of the Coupled Model Intercomparison Project (CMIP5). Historical integrations of the IPSL-CM5A-LR ESM (Séférian et al., 2013) were conducted under CMIP5 for the period 1850 – 2005 using climatic forcings which are prescribed from observations (Taylor et al., 2012). In this study, atmospheric fields from one ensemble member of the "historical" IPSL-CM5A-LR

experiment (*r1i1p1*) were processed in order to extract surface meteorological variables according to the approach of *DFS4* and *CORE2*, however temporal frequency was limited by the availability of model output. Thus, for this hindcast experiment, daily frequency U_{10}, V_{10}, θ_2, q_2, $radsw$ and $radlw$ were used along with monthly mean $precip$ and $snow$, with modifications made to the NEMOv3.1 physical model set-up to account for changes to the temporal frequency of imposed forcing. The IPSL-CM5A-LR ESM was selected in order to limit the physical inconsistency with the PlankTOM10-NEMOv3.1 model platform, since IPSL-CM5A-LR also utilises the NEMO physical modelling framework, whilst also reducing the impact of errors associated with spatial interpolation. Other studies have conducted prognostic ocean-only OBGCM experiments using CMIP5 atmospheric fields (e.g. MEDUSA-2.0; Yool et al., 2013), however the impact of an ESM-derived forcing in hindcast model configurations remains uncertain.

3.4 Results

Section 3.4.1 and Section 3.4.2 present results from a series of PlankTOM10-NEMOv3.1 ocean biogeochemistry (*STO10* and *BAL10*) and atmospheric forcing (*CORE2*, *DFS4*, *IPSL*) model experiments (*EXP*), respectively. In order to isolate the impact of these biogeochemical and physical perturbations, model fields are generally presented relative to baseline *REF* configurations ($EXP - REF$). This approach is consistent with other studies which evaluate the impact of incorporating new processes (Manizza et al., 2008) or anthropogenic impacts (Suntharalingam et al., 2012) into the PlankTOM biogeochemistry model via comparison with an unperturbed hindcast experiment. As a result, non-equilibrium artefacts and other dynamical processes are removed, such that this analysis focuses on understanding the impact of these imposed physical and biogeochemical assumptions on hindcast biogeochemical tracers. This work therefore presents a synthesis of "process level" sensitivity experiments, and differs from other modelling studies (e.g. Chapter 2; Stramma et al., 2012a) focusing on model-data comparison of absolute changes in [O_2] over the historical period.

In Section 3.4.1, output from ocean biogeochemistry experiments is analysed for the full 1948 – 2013 NCEP/NCAR reanalysis period (*REF* forcing). In Section 3.4.2 results

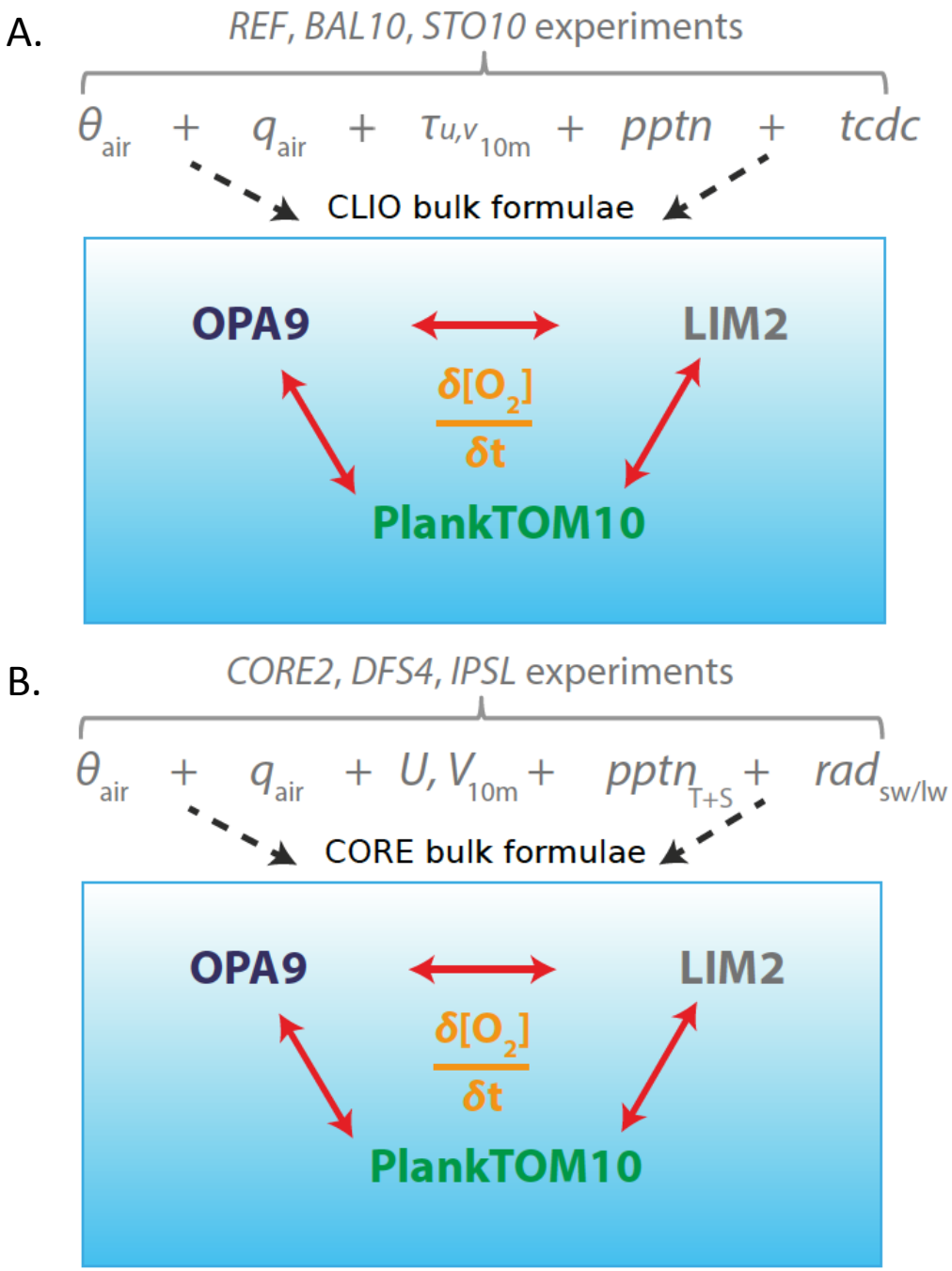

Figure 3.2: Schematic summary of meteorological variables used to provide surface fluxes of heat, freshwater and momentum as boundary conditions to PlankTOM10-NEMOv3.1 ocean-only model experiments using CLIO (**A**) and CORE (**B**) bulk formulations. "T+S" = Total and solid precipitation rate.

from the ensemble of atmospheric forcing experiments are analysed over a common time period (1958 – 2005) to avoid sampling biases associated with the differing temporal ranges of forcing products. All 3-D PlankTOM10-NEMO3.1 model fields are interpolated from the curvilinear ORCA2 grid onto a regular $1^\circ \times 1^\circ$ grid using weighted nearest neighbour interpolation, whilst retaining the native ORCA2 z-axis. Scalar and vectorial (U_{10} and V_{10}) 2-D surface forcing data are remapped from various native atmospheric grids onto the regular $1^\circ \times 1^\circ$ grid using bilinear and bicubic interpolation algorithms, respectively.

3.4.1 Ocean biogeochemistry experiments

3.4.1.1 Ocean carbon cycle

The interactive effects of ocean acidification included in *BAL10* and *STO10* model experiments impact upon ocean carbon cycle variables as simulated by PlankTOM10-NEMOv3.1. For *STO10*, the dominant carbon cycle effects of including a pCO_2-sensitive C:N ratio in organic carbon production are modification to simulated POC export from the euphotic zone (Fig. 3.3A) and changes to the spatial distribution of DIC within the ocean interior (Fig. 3.3B – 3.3D). Globally, POC export at 100 m increases in *STO10* by 0.22 mol C m^{-2} y^{-1} relative to the fixed C:N ratio *REF* experiment, for the period 1993 – 2013. This corresponds to 20 % increase in area mean POC export at 100 m associated with the inclusion of a pCO_2-sensitive carbon fixation rate. Increases in POC export in *STO10* are most pronounced (> 0.3 mol C m^{-2} y^{-1}) within established high-production regions of the global ocean, as shown in Figure 3.3A. Specifically, elevated POC export in *STO10* is simulated in the productive eastern boundary upwelling systems, such as the eastern equatorial Pacific. Comparable increases in export are also found at mid- to high latitudes (40 – 60°) within the subpolar North Pacific, North Atlantic and Southern Ocean, where existing high rates of annual primary production associated within the boreal (and austral) spring blooms are accentuated. A marked increase in POC export fluxes for *STO10* across many high-production open (and coastal) ocean regimes is opposed by no change or a smaller increase within the mid-latitude oligotrophic gyres. Coeval decreases in DIC at 100 m depth across much of the tropical and mid-latitude ocean (up to 3 μmol L^{-1} for 1993 – 2013) are consistent with carbon overconsumption within the euphotic zone in response to the CO_2 fertilisation as parameterised in *STO10* (Fig. 3.3B). Lower DIC concentrations

([DIC]) simulated in *STO10* within the euphotic zone are opposed by zonal mean [DIC] increases ([DIC] $> 5\,\mu\text{mol}\,\text{L}^{-1}$) between 500 – 3000 m, associated with a strengthened "soft tissue" pump as more exported POC is remineralised at depth (Fig. 3.3C). The temporal fingerprint of DIC changes associated with a $p\text{CO}_2$-sensitive C:N ratio in organic carbon fixation is shown in Figure 3.3D. Alteration to the depth profile of DIC as simulated in *STO10* becomes most apparent in the 2000s, with a signal of increased [DIC] within the ocean interior propagating surfacewards towards the base of the ventilated thermocline ($\sim$ 1000 m depth) over the course of the hindcast, consistent with rising atmospheric CO_2.

Similarly, Figure 3.4 presents major ocean carbon cycle changes associated with the *BAL10* perturbation experiment, which includes a $p\text{CO}_2$-sensitive calcification rate. The global mean ratio of CaCO_3 to POC export production ($\text{EXP}_{CaCO_3}/\text{EXP}_{POC}$) at 100 m decreases in *BAL10* by 4.9 % relative to *REF* for the period 2003 – 2013, consistent with a reduced rate of biogenic calcification in response to historical ocean acidification. As shown in Figure 3.4A, the largest decreases in $\text{EXP}_{CaCO_3}/\text{EXP}_{POC}$ occur within the tropical Indian Ocean and eastern tropical Atlantic Ocean, and in mid- to high-latitude regions of the North Atlantic and North Pacific. Reductions in $\text{EXP}_{CaCO_3}/\text{EXP}_{POC}$ of up to ~ 0.01 are similar in magnitude to those reported by Hofmann and Schellnhuber (2009) between control and $[\text{CO}_3^{2-}]$-sensitive R_{CAL} experiments for the period 2003 – 2013. Within the North Pacific, marked decreases in $\text{EXP}_{CaCO_3}/\text{EXP}_{POC}$ are centered on the North Pacific Current (NPC) region. The eastward flowing NPC is a major transverse surface current which bisects the subtropical and subarctic North Pacific and plays an important role in the resupply of nutrients and oxygen into the interior of the Alaskan gyre (Whitney et al., 2013), where secular $[\text{O}_2]$ decreases have been observed for the historical period (Whitney et al., 2007). Thus, $\text{EXP}_{CaCO_3}/\text{EXP}_{POC}$ reductions as simulated by *BAL10* for the NPC could have important downstream implications for biogeochemical cycles in the eastern subpolar North Pacific and California Current region (e.g. Sydeman et al., 2011).

Reduced export of CaCO_3 mineral ballast from the surface ocean causes a global mean reduction in model simulated gravitational sinking speeds for large POC (v_{sink}) between 0 – 2000 m depth of 0.2 m d^{-1} (0.4 %) between 2003 and 2013. The spatial pattern of v_{sink} reductions in *BAL10* is most pronounced ($>$ 0.5 m d^{-1}) where

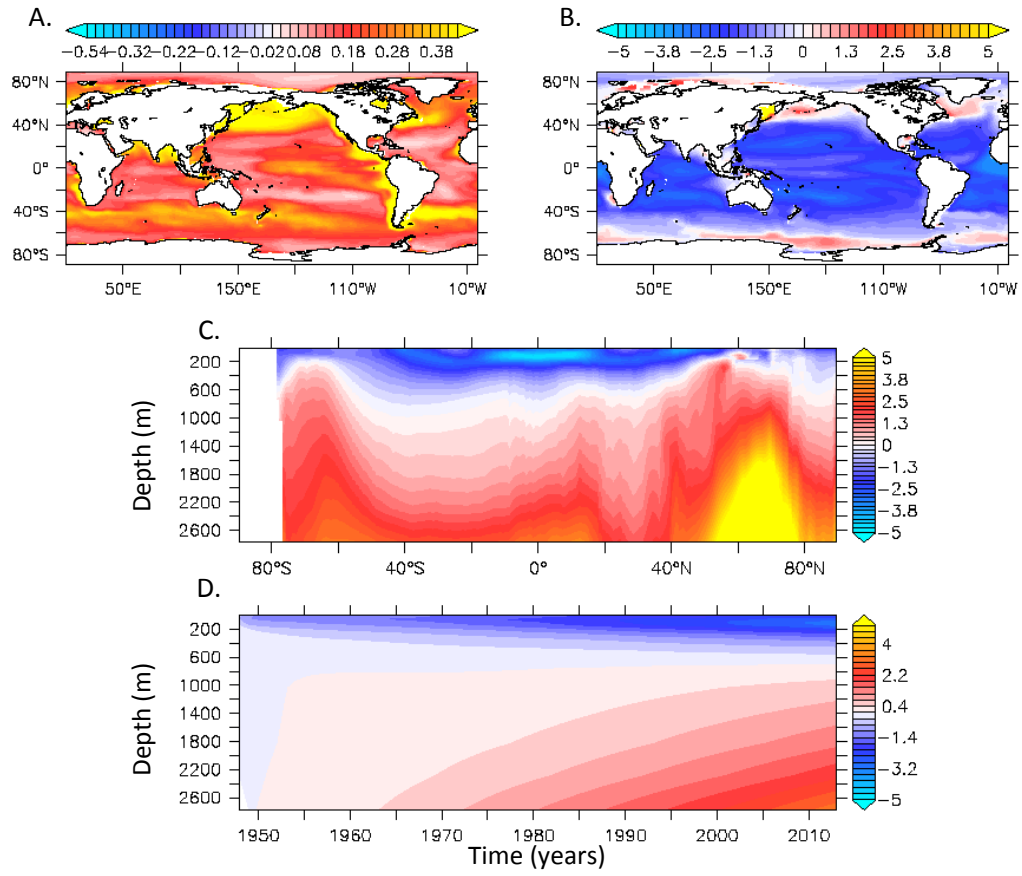

Figure 3.3: Summary of differences in simulated *STO10* ocean carbon cycle variables ($STO - REF$). (**A**) POC export (mol C m^{-2} y^{-1}) at 100 m depth, (**B**) Concentration of DIC (μmol L^{-1}) at 100 m depth, (**C**) zonal mean DIC concentration for the period 2003 – 2013. (**D**) Depth-time Hovmöller plot of global mean DIC concentration, for the period 1948 – 2013.

EXP_{CaCO_3}/EXP_{POC} decreases are largest (Fig. 3.4B). As such, consistent with other model studies (e.g. Heinze, 2004; Hofmann and Schellnhuber, 2009), perturbation to the PIC:POC "rain ratio" can be invoked to explain coeval changes in sinking speeds of large POC. Figure 3.4C and Figure 3.4D present depth-time Hovmöller plots showing the temporal changes in EXP_{CaCO_3}/EXP_{POC} and v_{sink}, respectively, as a function of depth. The most pronounced changes in EXP_{CaCO_3}/EXP_{POC} and v_{sink} occur at intermediate depths (within the upper 3000 m), and become more acute as the concentration of atmospheric CO_2 increases (particularly from 2000 onwards).

3.4.1.2 Oxygen

Carbon cycle changes as described in Section 3.4.1.1 impact upon the spatiotemporal distribution of [O_2] in *STO10* and *BAL10* experiments via changes to the rate of oxygen

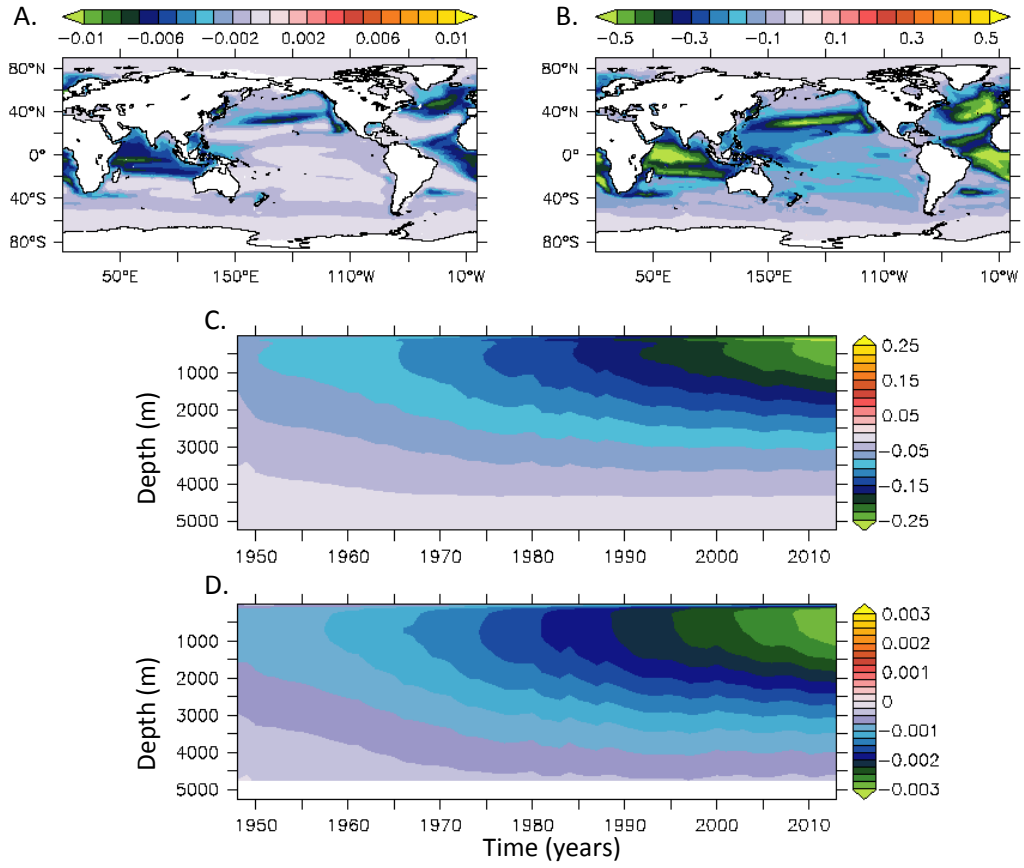

Figure 3.4: Summary of differences in simulated *BAL10* ocean carbon cycle variables (*BAL10*$-REF$). (**A**) EXP$_{CaCO_3}$/EXP$_{POC}$ at 100 m depth and (**B**) gravitational sinking speeds for large POC v_{sink} (m d^{-1}) between 0 – 2000 m for the period 2003 – 2013, relative to *REF*. (**C**) Depth-time Hovmöller plot of global mean EXP$_{CaCO_3}$/EXP$_{POC}$ and (**D**) v_{sink} for the period 1948 – 2013.

production and consumption. Figure 3.5 shows the difference in zonal mean (Fig. 3.5A – 3.5B) and depth-averaged zonal mean (Fig. 3.5C) [O_2] for the upper 3000 m, displayed as a temporal mean for the last 10 years of integration (2003 – 2013; $EXP - REF$). Mirroring the pattern of DIC concentration changes presented in Figure 3.3C, zonal mean [O_2] in *STO10* increases by up to 6 μmol L^{-1} within the more productive (sub)tropical euphotic zone. These near-surface [O_2] increases are opposed by marked deoxygenation throughout much of the ocean interior, particularly at mid- to high latitudes, where biological oxygen demand rises as more carbonaceous ($>$ C:N ratio) organic material is remineralised at depth. Subsurface [O_2] depletion for 2003 – 2013 reaches a zonal mean maximum of > 10 μmol L^{-1} within intermediate waters of the subpolar North Atlantic (~ 60°N). As shown in Figure 3.5C, the signature of depth-averaged zonal mean [O_2] change scales with latitude, such that the largest [O_2] decreases (≥ 2 μmol L^{-1}) occur poleward of 60° in

regions of deep water renewal.

Comparatively, carbon cycle feedbacks associated with *BAL10* cause almost no change in zonal mean [O_2] relative to *REF* for the period 2003 – 2013 (Fig. 3.5B). However, in agreement with the prognostic model results of Hofmann and Schellnhuber (2009), *BAL10* reproduces a small [O_2] decrease relative to *REF* within the ventilated thermocline (100 – 1000 m), which is likely to be exacerbated in response to future pCO_2 forcing. Aside from imposed pCO_2, the more muted magnitude of [O_2] change simulated by *BAL10* can also be attributed to the relatively small overall global export production which dampens the impact of any acidification driven reductions in EXP_{CaCO_3} on EXP_{CaCO_3}/EXP_{POC}. However, generally the results of *BAL10* suggest that the inclusion of a pCO_2-sensitive biocalcification rate in an ocean biogeochemistry model does not impact significantly upon simulated O_2 dynamics for the historical period, despite alteration to EXP_{CaCO_3}/EXP_{POC} and sinking speeds of large POC, as described in Section 3.4.1.1. Accordingly, Section 3.4.1.2 now focuses on hindcast O_2 changes associated with the *STO10* model experiment.

Inclusion of a variable C:N ratio in photosynthetic carbon production also impacts upon the characteristics of model simulated low-O_2 waters, with implications for the biogeochemical cycling of nitrogen (*cf.* Bianchi et al., 2012). As shown in Figure 3.6, near global decreases in the absolute values of [O_2] minima throughout the water column are simulated in *STO10* relative to *REF* for the period 2003 – 2013. Simulated decreases in the absolute value of [O_2] minimum values are most pronounced ($> 8\,\mu mol\,L^{-1}$) within the subpolar North Atlantic, and for the Indian Ocean and eastern equatorial Pacific OMZ waters. Associated with this intensification of low-O_2 conditions within the ocean interior, *STO10* also simulates a 2 % increase in the number of suboxic ([O_2] $\leq 5\,\mu mol\,L^{-1}$) grid cells along with a 13 % increase in the number of hypoxic grid cells ([O_2] $\leq 60\,\mu mol\,L^{-1}$) relative to *REF* by 2013. Expansion of low-O_2 waters within the *STO10* integration also has significant implications for nitrogen cycling, with the promotion of denitrification processes under low-O_2 (suboxic) conditions where nitrate (NO_3^-) is used as an oxidant in the remineralisation of organic material (e.g. Gruber, 2008). For the period 2003 – 2013, area mean *STO10* denitrification rates increase by $0.27\,\mu mol\,N\,m^{-3}\,y^{-1}$ (34 %) for the global ocean between 0 – 2000 m depth, associated with oxygen depletion in response to elevated POC export fluxes.

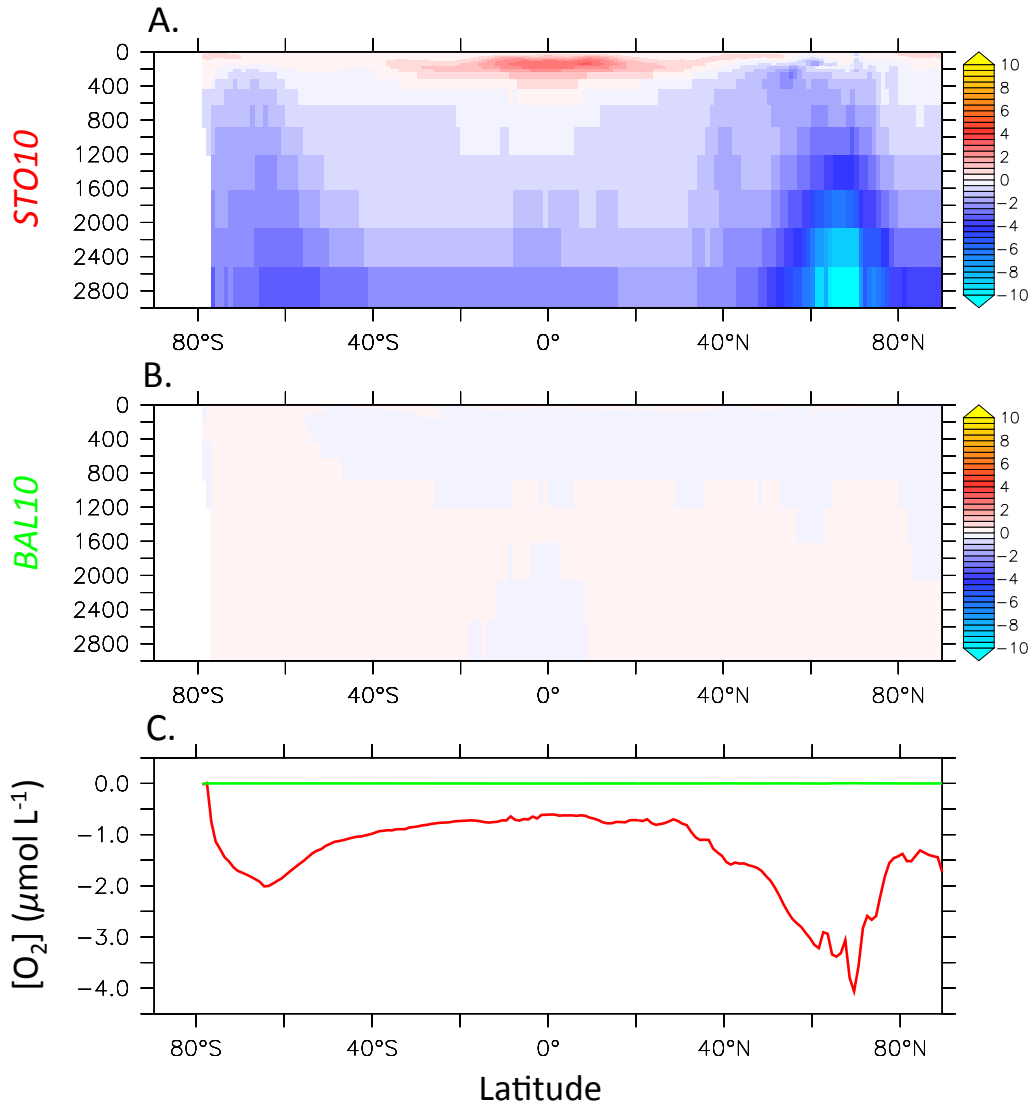

Figure 3.5: Difference ($EXP - REF$) in zonal mean [O_2] (μmol L^{-1}) for (**A**) *STO10*, (**B**) *BAL10* and (**C**) depth-averaged zonal mean [O_2] between 0 – 3000 m (*STO10* = red, *BAL10* = green). Results plotted for the temporal mean of 2003 – 2013.

Historical trends in [O_2] are also influenced by inclusion of a pCO_2-sensitive C:N ratio in *STO10*. Figure 3.7 shows 50-year changes in [O_2] as simulated by the *STO10* model experiment, expressed relative to baseline *REF* changes ($\Delta[O_2]_{STO10-REF}$). Consistent with the climatological fingerprints of $STO10-REF$ [O_2] depletion presented in Figure 3.5, the *STO10* CO_2 fertilisation effect produces an additional historical [O_2] increase within the low-latitude euphotic zone ($\sim$ 300 m depth; Fig. 3.5A) opposed by marked deoxygenation of up to 10 μmol L^{-1} throughout much of the ocean interior (Fig. 3.7B). Significantly, this pattern of elevated historical deoxygenation in *STO10*, which extends throughout the water

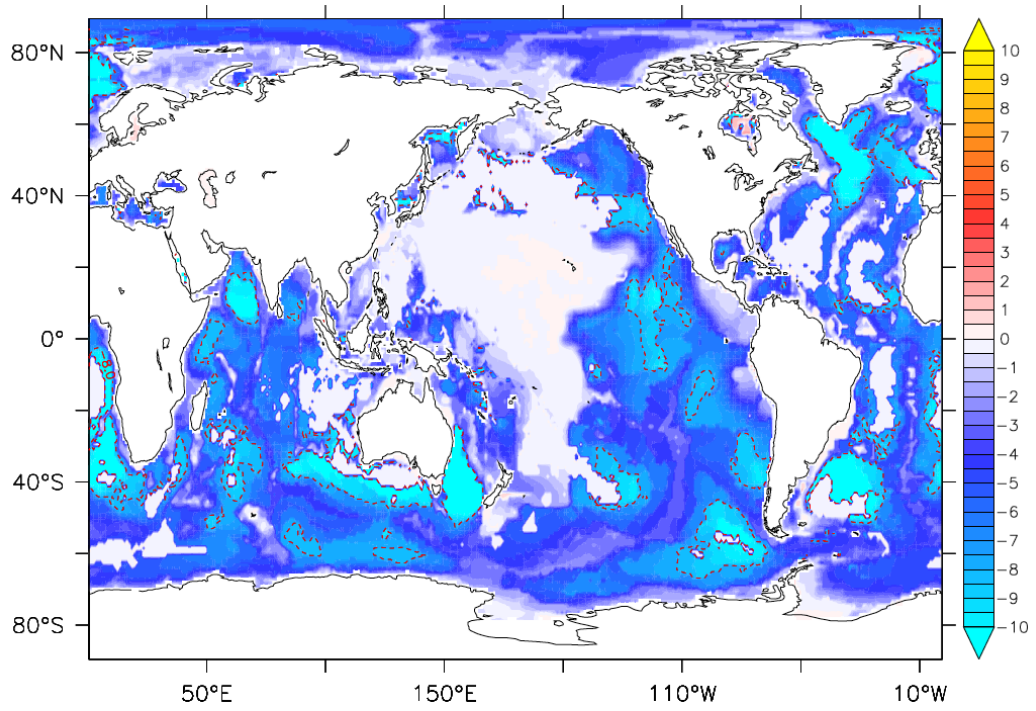

Figure 3.6: Difference ($STO10 - REF$) in the minimum [O_2] values throughout the water column at each grid point (μmol L^{-1}) for the period 2003 – 2013. Contours are overlain for $\Delta[O_2]$ = $-8\,\mu$mol L^{-1} (dotted red).

column poleward of 60° (Fig. 3.7C), is in good agreement with the global fingerprint of absolute [O_2] change as simulated by the most recent generation of ESMs over the last 50 years (see Chapter 2). As such, the inclusion of a variable C:N ratio in organic carbon production could act to augment the fingerprint of climate-driven ocean deoxygenation produced by fixed stoichiometry models for the historical period (e.g. Bopp et al., 2013). Stoichiometric diversity in OBGCMs should, therefore, be considered an important vector for reducing the discrepancy between observed and model simulated oxygen depletion, which are both primarily driven by changes in physical (mixing) processes (Helm et al., 2011). As shown in Figure 3.7D, the signal of enhanced [O_2] depletion associated with elevated POC export propagates towards the surface over the course of the *STO10* model hindcast in response to rising atmospheric CO_2. Further deoxygenation within established subsurface O_2-minima ($\sim$ 200 – 700 m) will act to exacerbate the climate-driven shoaling of OMZ waters (e.g. Stramma et al., 2008), leading to further habitat compression and associated impacts on tropical pelagic fish (e.g. within tropical Northeast Atlantic [Stramma et al., 2012b] and eastern tropical Pacific [Prince and Goodyear, 2006]).

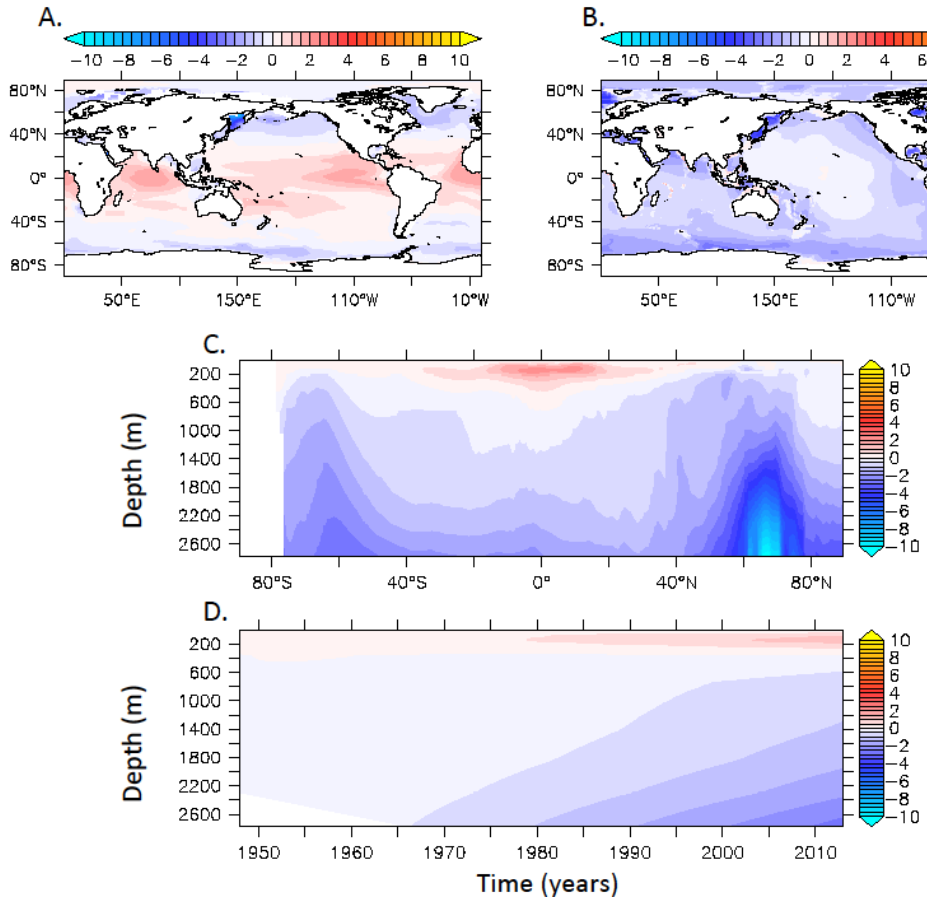

Figure 3.7: Historical change in *STO10* [O_2] (μmol L^{-1}) between 1953 – 1963 and 2003 – 2013 compared to *REF* ($\Delta[O_2]_{STO10} - \Delta[O_2]_{REF}$; blue colours indicate historical deoxygenation relative to *REF*). [O_2] changes presented at (**A**) 300 m depth, (**B**) 0 – 3000 m depth, and as zonal mean (**C**) and depth-time Hovmöller (**D**) plots for the period 1948 – 2013.

3.4.2 Atmospheric forcing experiments

The imposed time-varying meteorological data used to force the ocean-only models provides important constraints on temporal variability in [O_2]. As such, the sensitivity of hindcast PlankTOM10-NEMO3.1 [O_2] fields to atmospheric forcing is investigated here, both in terms of interannual variability (Sect. 3.4.2.1) and historical changes (Sect. 3.4.2.2).

3.4.2.1 Interannual variability

Interannual variability in model simulated thermocline [O_2] for a range of atmospheric forcing experiments (*REF*, *CORE2*, *DFS4*, *IPSL*) is presented in Figure 3.8 (A – D) as the temporal standard deviation (σ) of annual mean [O_2] fields at 300 m over the common hindcast forcing period (1958 – 2005). [O_2] fields are also taken from biogeochemical output of the IPSL-CM5A-LR CMIP5 "historical" experiment (*ESM*; Fig. 3.8E) used to

derive the atmospheric forcing for *IPSL*. As a result, direct comparison can be drawn between variability in the coupled IPSL-CM5A-LR ESM configuration and the ocean-only PlankTOM10-NEMOv3.1 experiment conducted using atmospheric fields from this integration. A boxcar (low-pass) filter is applied in order to diagnose secular trends in subsurface $[O_2]$, with the 10-year running mean being removed at each grid point in order to retain only an estimate of interannual (unforced) variability. This transformation is robust to changes in the width of the imposed boxcar window.

Simulated interannual variability in thermocline $[O_2]$ differs between hindcast PlankTOM10-NEMOv3.1 experiments, with *DFS4* exhibiting the largest area mean variability ($\sigma[O_2]$ = 2.4 μmol L^{-1}) when compared to *CORE* ($\sigma[O_2]$ = 1.9 μmol L^{-1}) and *IPSL* ($\sigma[O_2]$ = 1.8 μmol L^{-1}) model experiments. Elevated $\sigma[O_2]$ in the DFS4.3 hindcast suggests that ERA-40 derived forcing products generate more exogenous variability in passive tracer fields of ocean-only models when compared to NCEP/NCAR (*REF*, *CORE2*) or ESM (*IPSL*) based atmospheric data. However, a number of other differences between forcing products (see Table 3.2) could also contribute to the larger interannual variability in *DFS4*, for instance the alteration to surface fluxes caused by referencing of DFS4.3 surface air temperature and specific humidity at 2 m rather than 10 m.

Comparatively, the coupled IPSL-CM5A-LR model (*ESM*) simulates more variability in thermocline $[O_2]$ (area mean $\sigma[O_2]$ = 2.7 μmol L^{-1}) relative to the ensemble mean of all ocean-only atmospheric forcing experiments ($\sigma[O_2]$ = 2.1 μmol L^{-1}). Since *IPSL* and *ESM* experiments include identical atmospheric forcings along with similar physical and biogeochemical model components (*IPSL* = PlankTOM10-NEMOv3.1; *ESM* = PISCES-NEMOv3.2 [Séférian et al., 2013]) the residual interannual variability between experiments ($\sigma[O_2]^{ESM-IPSL}$ = $\sim$ 1 μmol L^{-1}) can plausibly be attributed to that which is generated internally to the ocean-atmosphere system under a coupled formulation.

As shown in Figure 3.8, simulated interannual variability scales with latitude for all model experiments, such that $\sigma[O_2]$ is most pronounced ($\sigma \geq 4$ μmol L^{-1}) poleward of 40° in both hemispheres. This result is consistent with data based reconstructions (e.g. Levine et al., 2008) which show interannual variability in subsurface biogeochemistry to be largest in regions of mid- to high-latitude water mass renewal. All model experiments exhibit an elevated $\sigma[O_2]$ signal of up to 10 μmol L^{-1} within the north-western subpolar

gyre of the North Atlantic and subpolar central and western North Pacific (Fig. 3.8A – 3.8E). These regional patterns have been identified in other O_2 modelling studies (e.g. Frölicher et al., 2009; McKinley et al., 2003) and are associated with the NAO and PDO, respectively, which provide the dominant source of Northern Hemisphere climate variability on interannual to decadal timescales. As such, all experiments converge on a maximum $\sigma[O_2]$ of $\sim 6\,\mu\text{mol}\,L^{-1}$ at $\sim 60°N$ consistent with variability associated with the dominant climate modes, whereas the signal of interannual variability in the Southern Ocean is less certain – with zonal mean $\sigma[O_2]$ ranging from $1 – 7\,\mu\text{mol}\,L^{-1}$ for different atmospheric forcings south of 60°S (Fig. 3.8F). Particularly, the *CORE2* and *IPSL* experiments simulate $\sigma[O_2] \leq 2\,\mu\text{mol}\,L^{-1}$ across much of the Southern Ocean (Fig. 3.8B, Fig. 3.8D) whereas zonal mean $\sigma[O_2]$ exceeds $4\,\mu\text{mol}\,L^{-1}$ for *REF*, *DFS4* and *ESM* (Fig. 3.8F).

As presented in Figure 3.9, interannual variability in windspeed (σ_{wspd}; Fig. 3.9A) and near-surface air temperature (σ_θ; Fig. 3.9B) also differ between imposed atmospheric forcing products. DFS4.3 exhibits the largest zonal mean variability in windspeed and near-surface air temperature, consistent with the largest simulated $\sigma[O_2]$ of all ocean-only experiments (Fig. 3.8C). However, DFS4.3 windspeed and near-surface air temperature data do not reproduce the meridional structure of σ_{wspd} and σ_θ exhibited by all other atmospheric forcing fields. Excluding DFS4.3, the largest inter-forcing divergence in σ_{wspd} occurs in the tropics (20°S – 20°N) where elevated interannual variability in COREv2-IAF tropical windspeeds ($\sim 0.5\,\text{m}\,s^{-1}$) relative to IPSL-CM5A-LR derived winds ($\sim 0.25\,\text{m}\,s^{-1}$) can be invoked to explain the more muted tropical variability in thermocline $[O_2]$ ($\sigma[O_2]$) of *IPSL* compared to *CORE2* (Fig. 3.8F). In contrast, larger interannual variability in σ_{wspd} does not generate a first-order response in $\sigma[O_2]$ at mid- to high latitudes, with, for example, elevated variance in the westerlies over the Southern Ocean for *IPSL* not being associated with a coeval increase in $\sigma[O_2]$ (Fig. 3.8D).

Comparatively, the largest deviation in zonal mean σ_θ between atmospheric datasets occurs poleward of 60°S, where COREv2-IAF exhibits lower interannual variability ($\sigma_\theta = \sim 0.4\,K$) when compared to IPSL-CM5A-LR ($\sigma_\theta = \sim 0.8\,K$) and NCEP/NCAR reanalysis ($\sigma_\theta = \sim 1.2\,K$) derived near-surface air temperatures. These σ_θ differences track the inter-experiment divergence in $\sigma[O_2]$ for the Southern Ocean, such that model biases in the simulation of thermocline $[O_2]$ variability agree with differences in the magnitude of

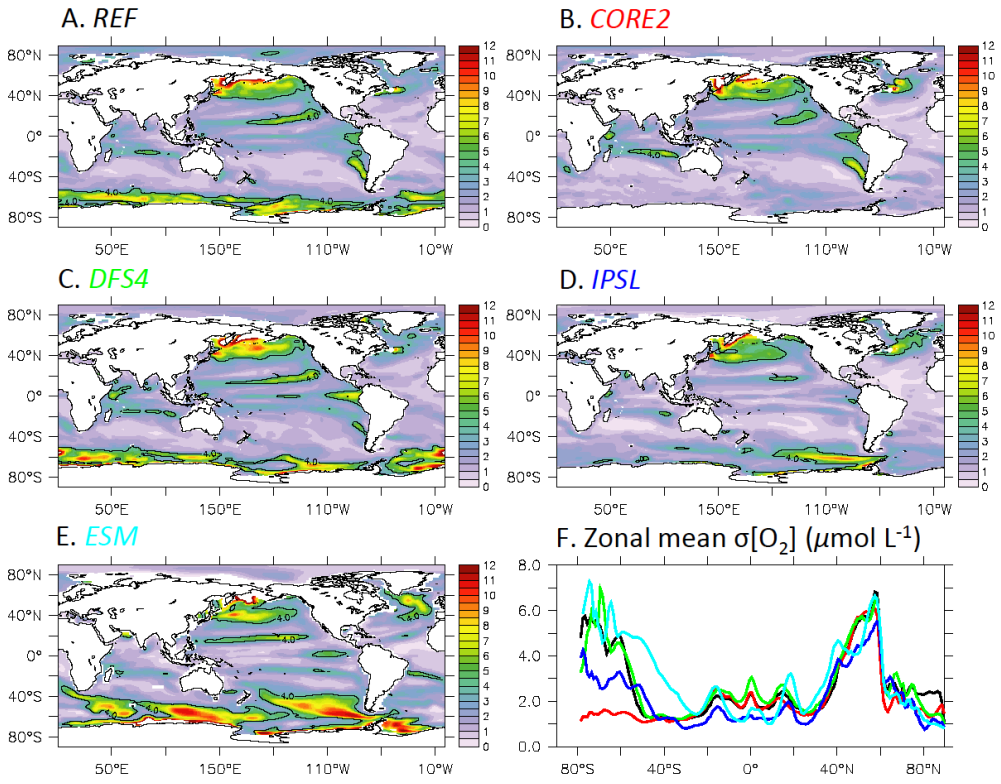

Figure 3.8: Interannual variability (σ) in annual mean [O_2] (μmol L^{-1}) at 300 m depth between 1958 – 2005 for a range of forced PlankTOM10-NEMOv3.1 hindcast experiments (*REF* = black [**A**], *CORE2* = red [**B**], *DFS4* = green [**C**], *IPSL* = blue [**D**]) and the coupled IPSL-CM5A-LR "historical" CMIP5 experiment (*ESM* = turquoise [**E**]). [O_2] contours are overlain in black for σ[O_2] = 4 μmol L^{-1}. Zonal mean interannual variability in [O_2] at 300 m for all model experiments is presented in Panel **F.**

imposed σ_θ. Specifically, reduced interannual variability in near-surface air temperature in *CORE2* and *IPSL* can be related to lower σ[O_2] relative to *REF*, which exhibits elevated σ_θ and, therefore, σ[O_2] poleward of 60°S. This modulation of tropical O_2 variability by windspeed and extratropical (subpolar) O_2 variability by surface heat flux has been reproduced by other forced ocean models investigating variability in North Atlantic O_2 fluxes (Friedrich et al., 2006).

3.4.2.2 Historical changes

Historical changes in upper thermocline [O_2] (μmol L^{-1}) at 300 m depth between 1960 – 1965 and 2000 – 2005 for hindcast model experiments are presented in Figure 3.10, relative to baseline changes in *REF* ($\Delta[O_2]_{EXP-REF}$). Atmospheric forcing perturbation experiments generally simulate [O_2] increases relative to *REF*, suggesting that the CLIO bulk formulation used for the baseline experiment produces a larger deoxygenation signal over

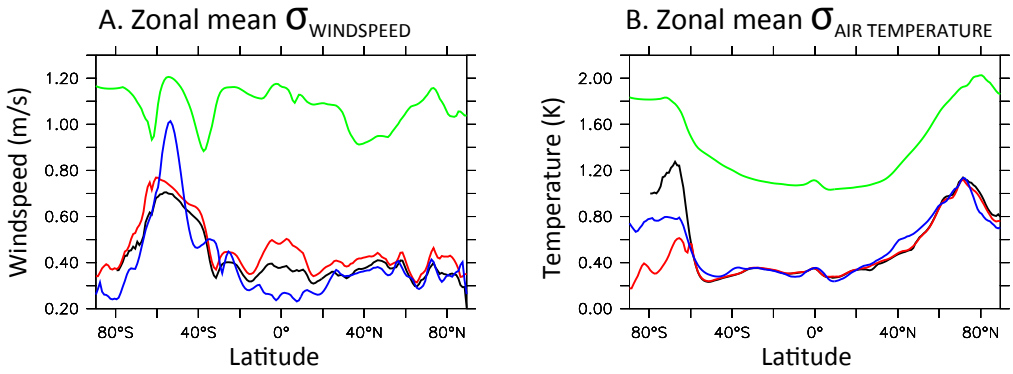

Figure 3.9: Interannual variability (σ) in de-trended zonal mean (**A**) windspeed ($\mathrm{m\,s^{-1}}$) and (**B**) near-surface air temperature (θ; K) for NCEP/NCAR reanalysis (black), COREv2-IAF (red) and DFS4.3 (green) products, and IPSL-CM5A-LR derived atmospheric fields (blue). Forcing data are provided as daily mean values for all products, and bicubically interpolated onto a common regular ($1^\circ \times 1^\circ$) grid so as to reduce sampling biases. Windspeed is calculated offline from U_{10} and V_{10} wind components. Following Swart et al. (2014) windspeed is plotted as a measure of momentum flux rather than wind stress since the latter has a strong dependency on the choice of drag co-efficient.

the historical period than those which employ a *CORE* formulation, however significant spatial heterogeneities exist between forcing products (Fig. 3.10A – 3.10C). The *CORE2* integration exhibits a reduced $\Delta[\mathrm{O_2}]_{EXP-REF}$ of $< \sim 20\,\mu\mathrm{mol\,L^{-1}}$ (Fig. 3.10A) consistent with the shared provenance of this forcing product and *REF* in NCEP/NCAR reanalysis data (Table 3.2). The largest differences in $\Delta[\mathrm{O_2}]_{EXP-REF}$ between atmospheric forcing experiments are found in the tropics (20°S – 20°N), with the zonal mean change in historical $[\mathrm{O_2}]$ relative to *REF* ranging from $-10\,\mu\mathrm{mol\,L^{-1}}$ (*CORE2*) to $+40\,\mu\mathrm{mol\,L^{-1}}$ (*DFS4* and *IPSL*). This considerable inter-forcing product spread ($\sim 50\,\mu\mathrm{mol\,L^{-1}}$) in simulated $[\mathrm{O_2}]$ change within the tropical thermocline reinforces the notion of model uncertainty in reproducing consistent trends in low-latitude $\mathrm{O_2}$ (Keeling et al., 2010; Cocco et al., 2013), and highlights the central role of imposed atmospheric forcing in determining the sign of simulated trends. Additionally, an elevated zonal mean $\Delta[\mathrm{O_2}]_{EXP-REF}$ signal (~ 20 – $60\,\mu\mathrm{mol\,L^{-1}}$; Fig. 3.10D) is found in all hindcast experiments south of 60°S, suggesting uncertainties in imposed forcings for the Southern Ocean, particularly with regard to the *REF* NCEP/NCAR forcing. Indeed, NCEP/NCAR reanalysis data has known biases in its representation of westerly winds over the Southern Ocean which have been attributed elsewhere to spurious trends in simulated biogeochemical variables for the historical period (e.g. Laufkötter et al., 2013). Overall, in this study the largest $\Delta[\mathrm{O_2}]_{EXP-REF}$ values

are found within the tropics and at mid- to high latitudes, suggesting that uncertainties in atmospheric forcing are largest in these regions.

3.5 Discussion and summary

To date, much research has focused on understanding the impact of biogeochemical (Tagliabue et al., 2011; Oschlies et al., 2008; Matear and Lenton, 2014) and physical (Bopp et al., 2013; Cocco et al., 2013) processes in OBGCMs on simulated future climate-driven perturbation to the global oxygen inventory. This work, rather, aims to better constrain the implications of the interrelated physical-biogeochemical drivers for $[O_2]$ dynamics over the historical period, towards reconciling the well-documented (*cf.* Keeling et al., 2010; Stramma et al., 2012a) discrepancies between model-simulated and observed $[O_2]$ changes. To this end, state-of-the-art OBGCM ocean-only experiments conducted in this study reveal that the sign and magnitude of $[O_2]$ change over the last $\sim$ 50 years depend critically on parameter choices made regarding ocean carbon cycle feedbacks and prescribed air-sea fluxes of heat, water and momentum.

Specifically, across the range of PlankTOM10-NEMO3.1 experiments analysed herein, differences in historical zonal mean thermocline $[O_2]$ change of more than $\pm$ 20 μmol L^{-1} are found to be associated with the inclusion of physical-biogeochemical modifications. Given that the observed signal of zonal mean deoxygenation between $\sim$ 1970 and $\sim$ 1992 (100 – 3000 m depth) reaches a maxima of $\sim$ 12 μmol L^{-1} within mid- to high-latitude regions of water renewal (see Chapter 2; Fig. 2.3), the appropriate representation in OBGCMs of processes described in this work could provide significant potential for improved model-data agreement in terms of the sign and magnitude of simulated $[O_2]$ change. However, a quantitative appraisal of model-data agreement, in terms of absolute trends in hindcast variables (*sensu* Chapter 2; Chapter 4), is beyond the scope of this analysis. Such an assessment would require a series of computationally expensive ($>$ 1000 year) spin-up integrations to remove non-equilibrium artefacts, since persistent drifts in the $[O_2]$ fields of ESMs have the potential to dominate any externally-forced historical response (Gupta et al., 2013). Instead, for a comprehensive evaluation of steady-state PlankTOM5 and PlankTOM10 model skill in terms of reproducing observed global-scale bulk properties (including surface $[O_2]$, [DIC] and chlorophyll) please refer to the recent

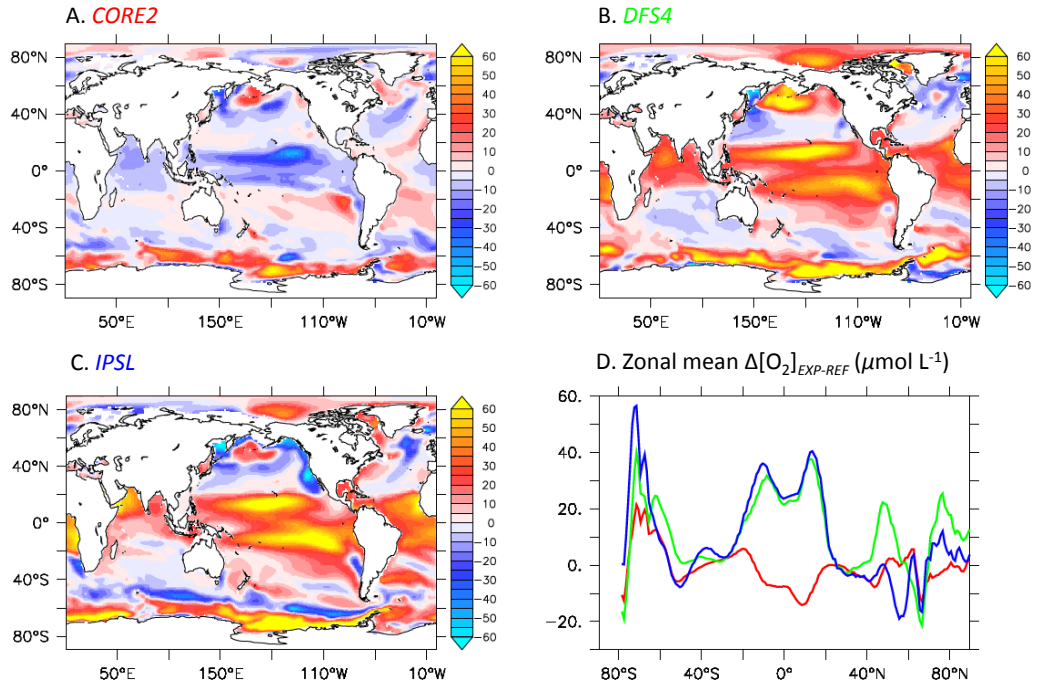

Figure 3.10: Change in upper thermocline $[O_2]$ (μmol L^{-1}) at 300 m depth between 1960 – 1965 and 2000 – 2005 from historical (**A**) *CORE2*, (**B**) *DFS4* and (**C**) *IPSL* model experiments (*EXP*), expressed relative to *REF* ($\Delta[O_2]_{EXP-REF}$; blue colours indicate historical deoxygenation relative to *REF*). (**D**) Changes presented as depth averaged, zonal mean $\Delta[O_2]$ relative to *REF* (*CORE2* = red; *DFS4* = green; *IPSL* = blue).

ocean biogeochemistry model inter-comparison of Kwiatkowski et al. (2014). Nonetheless, using a sensitivity study approach, this work indicates that the largest magnitude of uncertainty in $[O_2]$ is entrained into hindcast experiments due to choices made regarding stoichiometric effects in organic carbon fixation (Sect. 3.4.1.2) and imposed atmospheric forcing (Sect. 3.4.2.2).

In this analysis, explicit representation of observationally-based ocean acidification impacts on photosynthetic carbon drawdown yields major changes to the spatiotemporal distribution of OBGCM simulated POC export and, consequently, subsurface O_2 utilisation. Notably, historical POC export changes associated with the inclusion of a pCO_2-sensitive C:N ratio are similar in magnitude but differ in sign to the absolute historical changes predicted by current fixed stoichiometry models as a result of secular ocean warming. For example, Laufkötter et al. (2013) report zonal mean POC export decreases at 100 m of $\sim$ 0.5 mol C m^{-2} y^{-1} for much of the extrapolar ocean between 1960 and 2006 in hindcast simulations of the CCSM3-BEC model. Comparatively, the inclusion of a pCO_2-sensitive C:N ratio in this study yields global increases in POC export of $>$ 0.3 mol C m^{-2} y^{-1},

suggesting that stoichiometric effects could act to compensate a significant component of the "direct" climate-driven reduction in export production. Thus, as highlighted by Tagliabue et al. (2011), the inclusion of stoichiometric plasticity in the next generation of ESMs could alter the classical view that historical (Laufkötter et al., 2013) and future (Steinacher et al., 2010; Bopp et al., 2013) anthropogenic forcing drives a simulated reduction in global marine production, the observational basis for which remains contested (e.g. Boyce et al., 2010; Rykaczewski and Dunne, 2011). Equally, Laufkötter et al. (2013) report increases in POC export of up to 0.6 mol C m^{-2} y^{-1} in subpolar (light-limited) regimes, associated with historical density stratification increases in their hindcast model (*cf.* Bopp et al., 2001). In this case, the inclusion of ocean acidification effects on organic carbon drawdown could act to amplify secular increases in POC export change associated with ocean warming, with subpolar export production increasing by up to $\sim$ 0.5 mol C m^{-2} y^{-1} in *STO10* relative to the reference experiment.

A strengthened "soft tissue" pump associated with the inclusion of pCO_2-sensitive C:N ratio also drives major changes to simulated remineralisation within the ocean interior, as evidenced by stronger gradients in [DIC] and [O_2] relative to the reference configuration. Coeval subsurface [O_2] decreases and a reduction to the global inventory of O_2 are consistent with model projections which include pCO_2-sensitive C:N ratios in carbon fixation (e.g. Oschlies et al., 2008; Tagliabue et al., 2011). However, counter to these model experiments, the spatial pattern of [O_2] decrease associated with carbon overconsumption in this study follows the absolute fingerprint of (observed) ventilation-driven deoxygenation (see Chapter 2). As such, the most pronounced O_2 depletion occurs at mid- to high latitudes, rather than focused within the tropical OMZs. This result does not, therefore, support the suggestion (e.g. Keeling et al., 2010; Ciais et al., 2014) that inclusion of a pCO_2-sensitive C:N ratio in carbon fixation would invoke a net deoxygenation of the tropical thermocline for the historical period, in agreement with recent hindcast (Stramma et al., 2012a) and prognostic (Matear and Lenton, 2014) ESM experiments which include variable stoichiometry. Rather, stoichiometric effects in response to historical ocean acidification are shown here to bring about elevated oxygen depletion in mid- to high-latitude regions of water renewal, thus providing a biogeochemical amplifier for (chiefly) physically driven simulated [O_2] changes (e.g. Bopp et al., 2013). Accordingly, the inclusion of this process

in the next generation of ESMs could act to reduce the discrepancy between observed (Helm et al., 2011) and more muted ESM simulated historical deoxygenation trends. Specifically, Helm et al. (2011) report an area mean observed [O_2] decrease of 0.9 μmol L^{-1} between $\sim$ 1970 and $\sim$ 1992 (100 – 1000 m), compared to a global decrease of 0.7 μmol L^{-1} as simulated by the CMIP5 HadGEM2-ES ESM (see Chapter 2) over the same depth-time interval. Stoichiometric effects alone account for a model simulated historical [O_2] decrease of 0.2 μmol L^{-1} between 100 – 1000 m when compared to the reference configuration in this study, such that this process could provide an important mechanism for bringing ESM trends within the uncertainty bounds of the observed changes (see Fig. 2.3). Additionally, consistent with prognostic model studies, the inclusion of a pCO_2-sensitive C:N ratio produces an increase in the simulated volume of low-O_2 waters. Further expansion of suboxic and hypoxic water bodies in response to anthropogenic forcing has important implications for the global marine nitrogen cycle, with a coeval increase in denitrification rates (34 %; 0 – 2000 m) associated with the elevated consumption of nitrate ($NO_3{}^{2-}$) in microbial decomposition of organic material under suboxic conditions (e.g. Gruber, 2008). Although, consistent with a smaller imposed pCO_2 forcing, the magnitude of suboxic volume increase simulated for the historical period (2 % for 2013) is smaller than that projected for 2100 in variable stoichiometry models (36 – 50 % [Tagliabue et al., 2011; Oschlies et al., 2008]).

As noted by Matear and McNeill (2009), however, caution is required when extrapolating the results of mesocosm experiments carried out with one natural plankton assemblage (Riebesell et al., 2007) to the global scale for all phytoplankton taxa and biogeographical provinces. To this end, a review of experimental evidence carried out by Hutchins et al. (2009) highlights that, despite good agreement within unialgal cultures towards elevated C:N ratios in response to acidification, reported stoichiometric changes within CO_2 manipulation experiments carried out on natural plankton communities are much more variable. Differences between results are attributed in part to changing experimental practice, such as "batch-mode" versus continuous culture incubation methods. However, a number of external biological factors are also invoked to explain the inconsistent response of natural assemblages to elevated pCO_2, including differing zooplankton grazing rates or community composition between oceanographic regimes. For instance, Thingstad et al. (2008)

demonstrate for the Arctic pelagic ecosystem that elemental stoichiometry changes within phytoplankton biomass depend critically on the nature of growth-limiting factors within the heterotrophic community.

Comparatively, biogeochemical experiments which account for pCO$_2$-driven perturbation to biogeonic calcification rates are shown here to have only a negligible impact on [O$_2$] dynamics for the historical period. However, as highlighted by Ridgwell et al. (2009), unresolved questions regarding the observed "form and sensitivity" of ocean acidification impacts on calcification introduce significant uncertainties into the parameterisations adopted in global models such as PlankTOM10. Moreover, the impact of ocean acidification on the "PIC:POC rain ratio" must be considered alongside other external influences on the biological pump, particularly changes in export production in response to ocean warming (Steinacher et al., 2010; Bopp et al., 2013). For instance, model simulated historical (Laufkötter et al., 2013) and future (Steinacher et al., 2010; Bopp et al., 2013) reductions in overall export production associated with increased density stratification may act to moderate the impact of any acidification driven reductions in CaCO$_3$ production on EXP$_{CaCO_3}$/EXP$_{POC}$. Although, whilst this study suggests that interactive pCO$_2$-calcification effects may be less important for biogeochemical cycles over the historical period, these processes may remain relevant on centennial (Heinze, 2004) and millennial (Hofmann and Schellnhuber, 2009) timescales.

Imposed atmospheric forcing is also shown in this study to play a major role in modulating both interannual variability and historical changes in subsurface [O$_2$] as simulated by the hindcast PlankTOM10-NEMO3.1 model. Particularly, in agreement with forced ocean model results of Friedrich et al. (2006) for the North Atlantic, simulated interannual variability in O$_2$ is shown here to be primarily controlled by heat fluxes (σ_θ) in extratropical (mainly subpolar) regions and wind stress (σ_{wspd}) in the tropics. In terms of historical changes, the largest inter-forcing data differences in simulated [O$_2$] also occur at mid- to high latitudes and within the tropics. Large uncertainties between prescribed meteorological datasets in these regions propagate into simulated thermocline [O$_2$], consistent with a recent inter-comparison of surface reanalysis data, which attributes elevated multiproduct inconsistency in the tropics and extratropics chiefly to wind stress and heat flux uncertainties, respectively (Chaudhuri et al., 2013). The important role of

tropical zonal wind stress in controlling variations in model simulated low-O_2 water bodies has been demonstrated in recent work carried out the UVic EMIC (Ridder and England, 2014) and GFDL Generalised Ocean Layer Model (GOLD; Deutsch et al., 2014), providing further motivation for the provision of appropriate wind forcing to ocean-only models investigating O_2 dynamics.

Overall, an important outcome of this study is the demonstration that using different atmospheric forcing products to provide surface fluxes of heat, water and momentum to an ocean model can produce markedly different interannual variability and historical changes in simulated [O_2] fields, particularly within the tropics. The sensitivity of ocean biogeochemical variables to imposed atmospheric boundary conditions is supported by other recent model studies which analyse historical ocean carbon cycle changes under different meteorological forcings (Swart et al., 2014; Ishi et al., 2014). One significant implication of this work, therefore, is that whilst all atmospheric forcing products used here provide surface fluxes which are *a priori* representative of observed changes in meteorological variables (aside from *IPSL*), data choices still place major constraints on simulated changes in ocean properties. As such, further work is required to better understand the biases in atmospheric forcing datasets provided to the ocean modelling community, both in terms of comparing meteorological fields (e.g. Chauduri et al., 2013) and assessing how uncertainties in these prescribed forcings (and bulk formulae) impact upon the evolution of hindcast variables.

Towards this objective, the Coordinated Ocean-ice Reference Experiments (COREs) project proposes a standard protocol for running hindcast ocean-ice models, emphasising the need for models to be integrated using different atmospheric forcings in order to "assess implications on the ocean and sea ice climate of various atmospheric reanalysis or observational products" (Griffies et al., 2009). However, the majority of recent physical (e.g. Dansbasoglu et al., 2014) and biogeochemical (e.g. Kwiatkowski et al, 2014) multi-model hindcast studies remain focused on investigating the implications of a common atmospheric forcing for a range of ocean models. As argued here, this approach lends credence to the misconception that all data products provide an equally appropriate representation of historical changes in observed air-sea fluxes. Thus, a multifaceted approach is required in order to better evaluate surface meteorological data products, involving both multi-model

inter-comparison under a common atmospheric forcing (e.g. COREv2-IAF; Danabasoglu et al., 2014) and ensembles of different atmospheric forcing experiments using a common ocean model (e.g. Mathiot et al., 2008).

Chapter 4

Fingerprints of Ocean Deoxygenation in the North Sea

This chapter is presented as a 'scoping report' which has contributed to a collaborative research project between the Tyndall Centre for Climate Change Research and the Centre for Environment, Fisheries and Aquaculture Science (CEFAS): Fingerprints of Ocean Deoxygenation in the North Sea (FODINS).

4.1 Introduction

Coastal and shelf seas are a vital component of the marine ecosystem, accounting for up to 30 % of total ocean primary production (Longhurst et al., 1995; Gattuso et al., 1998; Walsh, 1991) and providing ~ 90 % of global fish catches (Pauly et al., 2002). To this end, coastal and shelf seas have been identified as an important repository of provisioning (e.g. fisheries), regulating (e.g. carbon sequestration), supporting (e.g. marine habitats) and cultural (e.g. recreation) ecosystem services (Millennium Ecosystem Assessment, 2005; Hoegh-Guldberg et al., 2014). These regions are also useful "natural laboratories" for examining anthropogenic perturbation to marine systems, owing to the dominant influence of external forcings from atmospheric, oceanic and terrestrial sources on trends and variability of ecologically relevant variables in marginal seas (Holt et al., 2010; Zhang et al., 2010). [O_2] is a useful metric for interrogating the competing roles of external and internal processes in driving physical and biogeochemical change (e.g. Andrews et al., 2013; Chapter 2; Sect. 1.3) and is also an important indicator of Ecological Quality in shelf seas (Painting et al., 2005).

Oxygen depletion occurs in subsurface water masses where the rate of organic carbon remineralisation exceeds that at which oxygen is re-supplied through ventilation and biological production processes (Peña et al., 2010). Low [O_2] conditions, or hypoxia, can occur naturally on a variety of spatiotemporal scales (Kemp et al., 2009), ranging from episodic or seasonal events within fjords or inland seas through to the large ($> 100{,}000\,\mathrm{km}^2$), permanent OMZs of Eastern Boundary Upwelling Systems (Fig. 4.1). In near-shore regimes eutrophication-driven hypoxic areas have developed in response to elevated nutrient and organic carbon loadings from anthropogenic sources (Rabalais et al., 2009; Rabalais et al., 2010). There is strong evidence that these "dead zones" have expanded significantly since the 1960s in response to elevated coastal eutrophication, such that over 400 hypoxic systems now affect an area of more than $245{,}000\,\mathrm{km}^2$ (Diaz and Rosenberg, 2008). Whilst reported historical [O_2] decreases are largest in the coastal zone (Gilbert et al., 2010), secular declines in [O_2] have also been recorded in the open ocean over the last 50 years (Keeling et al., 2010). Open ocean deoxygenation has been attributed to historical anthropogenic global ocean warming via increased density stratification and reduced O_2 solubility at higher temperatures (Helm et al., 2011; Andrews et al., 2013).

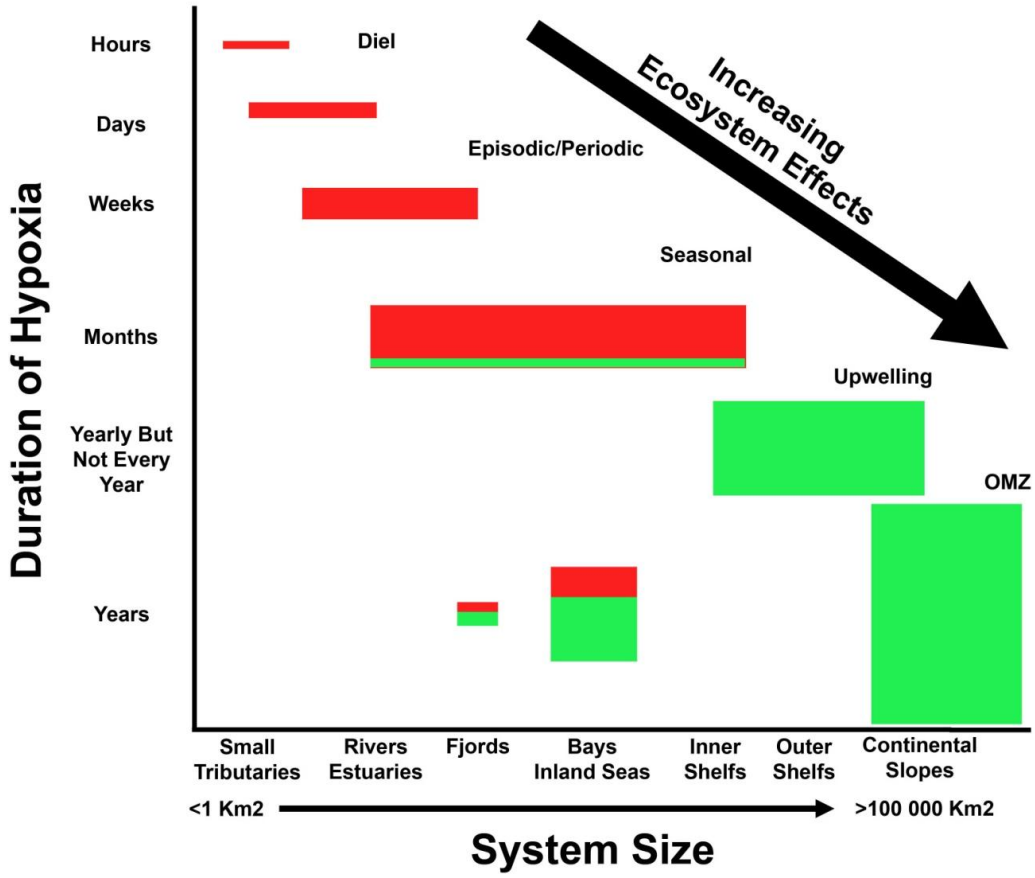

Figure 4.1: Summary of spatiotemporal variability in hypoxic systems from Rabalais et al. (2010). Green and red colours indicate the relative roles of (direct) natural and anthropogenic influences on hypoxia in each environment, respectively. However, indirect drivers of oxygen depletion such as climate change may also influence hypoxia.

Hypoxic waters (typically defined as $[O_2] < \sim 60\,\mu\text{mol}\,\text{kg}^{-1}$) [Gray et al., 2002]) occupy $\sim 5\,\%$ of the modern ocean by volume (Deutsch et al., 2011) and represent a threshold below which negative behavioural or physiological responses are elicited in marine organisms (Rabalais et al., 2010). However, responses to low-O_2 conditions vary considerably between taxa, such that the conventional hypoxic boundary of $\sim 60\,\mu\text{mol}\,\text{kg}^{-1}$ exceeds the empirical sub-lethal and lethal limit for 50 % of marine benthic organisms (Vaquer-Sunyer and Duarte, 2008). As such, when appraising $[O_2]$ depletion in this analysis, thresholds for negative ecological impacts of hypoxia are considered to range from 125–190 $\mu\text{mol}\,\text{L}^{-1}$, in accordance with Ecological Quality objectives set by the Oslo and Paris Commission (OSPAR) for coastal and offshore waters of England and Wales (Painting et al., 2005).

This study focuses on $[O_2]$ changes in the North Sea; a semi-enclosed basin on

the north-west European continental shelf with an open northern boundary to the North Atlantic Ocean. In the North Sea a general cyclonic circulation is dominated by southward propagation of warm, saline inflow from the North Atlantic (e.g. Winther and Johannessen, 2006) however other water masses, particularly low salinity Skaggerak water derived from Baltic outflow, also contribute to the region's hydrography. The North Sea is relatively shallow, with two thirds of the basin less than 100 m in depth (see model bathymetry in Sect. 4.2.2). As a result, much of the southern North Sea is well mixed year round due to a strong tidal influence. However, deeper central and northern areas stratify thermally in the summer months as air temperatures rise. Figure 4.2 highlights areas of permanent stratification, predominantly the Norwegian Trench region in the northeast, where low salinity Baltic outflow drives year-round haline stratification and isolation of denser bottom waters. Stratified regions of the North Sea provide conditions conducive to seasonal [O_2] depletion in bottom waters (Weston et al., 2008). Significant export of organic material driven by a spring bloom is accompanied by limited ventilation of the interior due to the development of a stable pycnocline and weak horizontal advection, allowing for biological oxygen utilisation to persist (Kemp et al., 2009).

There is a general lack of published work addressing the potential for hypoxia in bottom waters of the North Sea, with the majority of studies focusing on the coastal zone (Colijn et al., 2002). Recently, however, measured bottom water O_2 concentrations have declined to minima of 162 μmol L^{-1} and 203 μmol L^{-1} prior to the cessation of summer stratification at two moorings in the central North Sea (Greenwood et al., 2010). Moreover, Weston et al. (2008) report minimum [O_2] of 64.7 μmol L^{-1} within the Oyster Grounds region of the seasonally stratified North Sea following an exceptionally warm summer. Results from a hydrographic survey in August 2010 provide further support for substantial seasonal O_2 depletion ([O_2] $\leq$ 200 μmol L^{-1}) in bottom waters of the stratified North Sea (Queste et al., 2012). Significantly, observed summer oxygen concentrations of less than 200 μmol L^{-1} could indicate that Ecological Quality objectives set by OSPAR to avoid negative ecological impacts of low-O_2 conditions ([O_2] $>$ 125–190 μmol L^{-1}) are not being met in some offshore regions of the North Sea. These studies highlight the importance of coupled climate-ocean processes, particularly stratification and direct solubility effects, in determining the propensity for oxygen depletion in the North Sea.

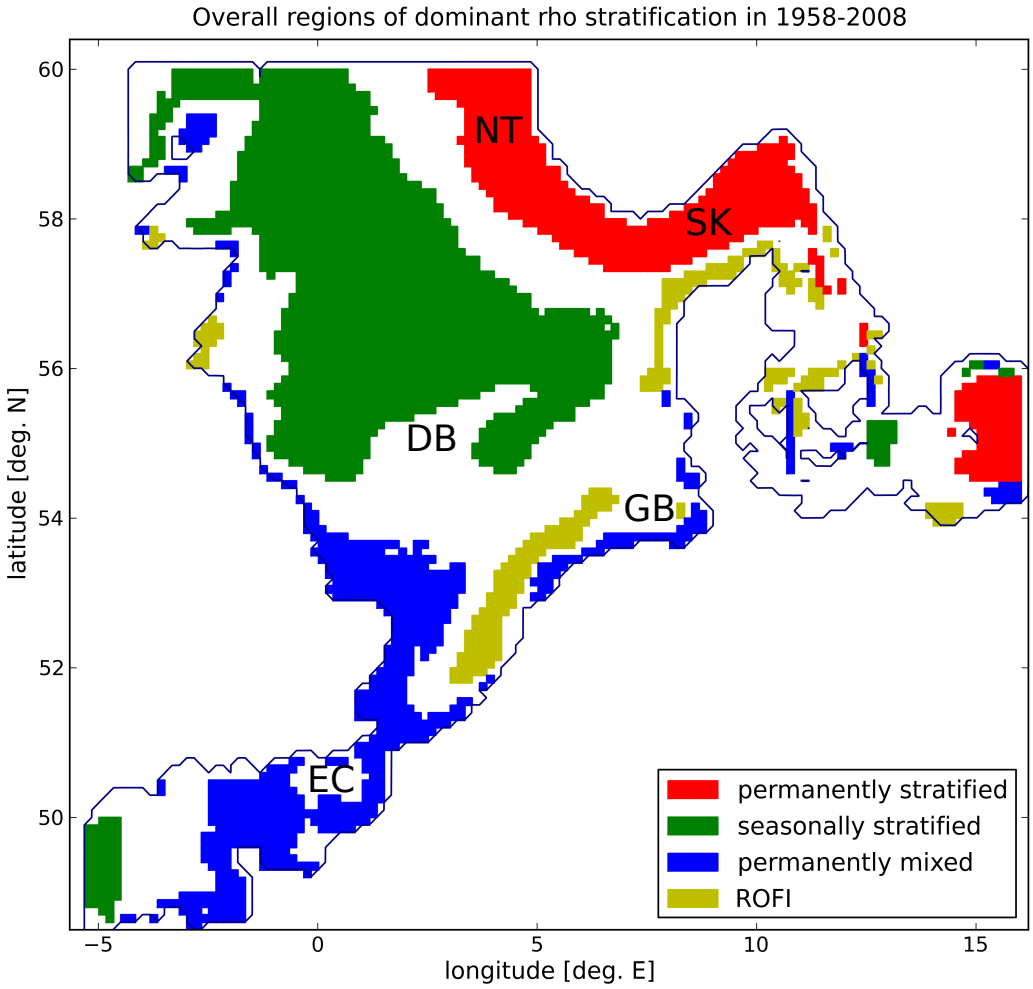

Figure 4.2: Dominant hydrodynamic regimes in the North Sea (time median) as simulated by the hindcast GETM-ERSEM simulation used in this study (adapted from van Leeuwen et al. [2014]; Sect. 4.2.2). White shading indicates that the dominant regime is present for $< 50\,\%$ of model years; highlighting transitional areas with variable hydrodynamic characteristics. ROFI = Regions of Fresh Water Influence. The locations of important regions are also highlighted (EC = English Channel, GB = German Bight, DB = Dogger Bank, SK = Skagerrak, NT = Norwegian Trench).

UK Climate Projections (Lowe et al., 2009) and forced simulations using the Proudman Oceanographic Laboratory Coastal Ocean Modelling System (POLCOMS; Holt et al., 2010) suggest that for an SRES A1B emissions scenario, the North Sea will experience future increases in the duration and intensity of stratification, conceivably increasing seasonal oxygen utilisation and leading to further bottom oxygen depletion (Keeling et al., 2010).

Coastal time series records (MacKenzie and Schiedek, 2007) and satellite remote sensing observations (Good et al., 2007) show considerable sea surface temperature (SST) warming in the North Sea since the 1980s, at three times the rate of the global mean trend.

This is supported by a recent analysis of Large Marine Ecosystems (LMEs) using U.K Met Office Hadley Centre SST (HadSST2) data that found the most rapid SST warming ($> 1°C$) for the period 1982–2006 occurred within the marginal European seas, when compared to other LMEs globally (Belkin, 2009; Fig. 4.3). Superimposed upon this rapid warming trend, time series measurements also indicate that summer North Sea SSTs have risen 2–5 times faster than those in other seasons (MacKenzie and Schidek, 2007), with implications for seasonal pycnocline development. To this end, Holt et al. (2012) demonstrate using a hindcast simulation of the POLCOMS regional model that surface warming trends in the seasonally stratified North Sea exceed those at depth, suggesting an increase in the strength of stratification over the historical period. However, these simulated changes are not validated with observations due to the lack of seasonally resolved temperature data in the analysis. Coeval with rapid surface warming, historical records derived from the International Council for the Exploration of the Sea (ICES) database show significant decreases in summer bottom water [O_2] of the stratified North Sea from 1990 onwards (Queste et al., 2012). However, the contribution of historical warming (via solubility and stratification) relative to internal changes driven predominantly by the North Atlantic Oscillation (NAO; Sharples et al., 2006) is yet to be determined.

The aim of this study is to use an integrative approach, bringing together information from historical data (Sect. 4.2.1) and a hindcast regional ocean biogeochemistry model (Sect. 4.2.2), to assess the detectability of trends in North Sea [O_2] and temperature relative to natural internal variability.

4.2 Methods

4.2.1 Data

In this study we use a collation of historical temperature, salinity and [O_2] data from the ICES oceanographic database for the North Sea, as presented by Queste et al. (2012). CTD and bottle data containing [O_2], pressure, temperature and salinity for the period 1959–2006 were processed to retain only summer values (June–September) and binned into ICES regular grid squares following Berx and Hughes (2009). Consistent with Queste et al. (2012) a mean value for the bottom third of the water column is taken, which provides

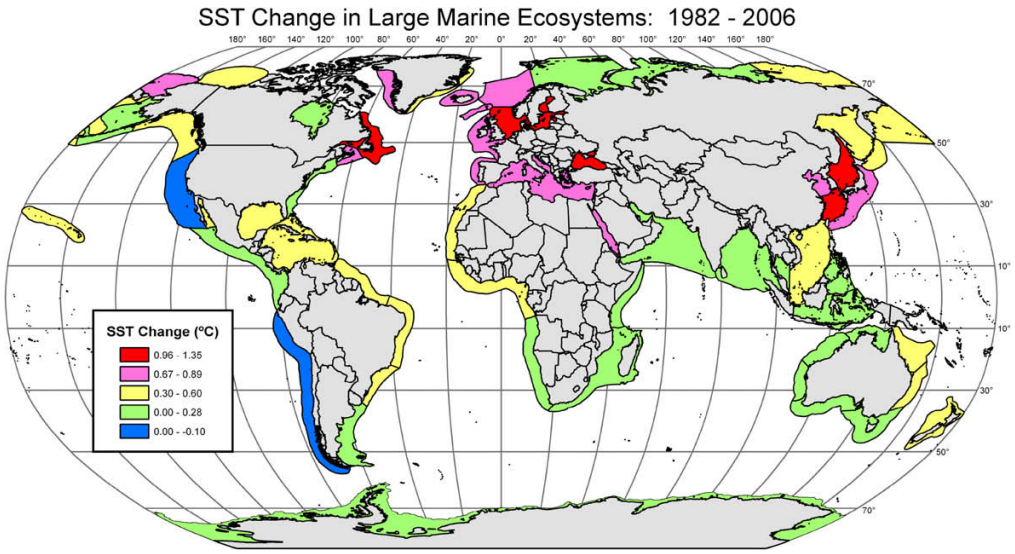

Figure 4.3: Net SST change (°C) from HadSST2 data (1982 - 2006) for a range of Large Marine Ecosystems. Reproduced with permission from Belkin (2009).

an estimate of the Bottom Mixed Layer (BML) in the summer stratified North Sea whilst also allowing measurements taken within the well-mixed southern North Sea to be retained. Data has been filtered to remove those grid boxes where summer values include fewer than 5 data points ($n < 5$), with additional masking of data to omit grid cells not sampled by the GETM-ERSEM model (see Section 4.2.2). As part of this analysis, data has also been processed to generate a regularly gridded netCDF product from which to derive a testable pattern of historical temperature and [O_2] change ('fingerprint'). Salinity fields are also included in the model validation (Sect. 4.3.1 and Sect. 4.3.2) due to the central role of active tracers in controlling model hydrography and ventilation processes. However, trends in summer BML salinity are not considered since this work focuses on historical trends in properties that are strongly constrained by the annual cycle of surface forcing rather than the slower ocean - shelf exchange processes (e.g. Holt et al., 2010).

4.2.2 North Sea ecosystem model

A 50-year (1959–2006) hindcast run of the physical - biogeochemical model GETM-ERSEM, applied to the North Sea region (van Leeuwen et al., 2013; `http://www.nioz.nl/northsea_model`), is used in this study to provide a model [O_2] response pattern along with temperature and salinity fields. The full North Sea GETM-ERSEM model

domain and bathymetry is presented in Figure 4.4. GETM-ERSEM comprises the General Estuarine Transport Model (GETM; Stips et al., 2004; Burchard and Bolding, 2002; `http://www.getm.eu`) coupled to the European Regional Seas Ecosystem Model (ERSEM; Baretta et al., 1995; Vichi et al., 2004; Blackford et al., 2004), as summarised in Figure 4.5. GETM is a fully baroclinic 3-D hydrodynamic model, which uses the General Ocean Turbulence Model (GOTM; `http://www.gotm.net`) for representation of vertical turbulence structure. The ERSEM model component has been developed from ERSEM III and the Biogeochemical Flux Model (BFM; `http://www.bfm.cmcc.it`) and describes the dynamics of pelagic and benthic biogeochemical fluxes in temperate seas. ERSEM explicitly simulates the biogeochemical cycles of carbon and oxygen along with the macronutrients nitrogen, phosphorous and silicon, and includes a functional group representation of phytoplankton (diatoms, flagellates, picophytoplankton and dinoflagellates), zooplankton (carnivorous and omnivorous mesozooplankton, microzooplankton and heterotrophic nanoflagellates) and benthos (epibenthos, deposit feeders, filter feeders, meiobenthos and benthic predators).

In this study, model fields are taken from a hindcast simulation of the GETM-ERSEM North Sea model configuration, with a spatial resolution of 6 nautical miles and 26 general coordinate vertical layers (van Leeuwen et al., 2013). Atmospheric forcing for the hindcast experiment is provided by ECMWF ERA40 6-hourly meteorological data, with model output being written on a daily basis. Climatological temperature and salinity data are used as open boundary conditions into the model domain. Fluvial inputs (fresh water, phosphate, silicate, ammonia and nitrate) are also included from 152 rivers discharging into the Greater North Sea area. The hindcast experiment was initialised from a previous multi-decadal GETM-ERSEM simulation in order to achieve quasi-steady state conditions for the benthic system. Further details of the GETM-ERSEM hindcast simulation can be found in van Leeuwen et al. (2013) and van Leeuwen et al. (2014). Monthly mean model fields have been processed in this analysis using Climate Data Operators (CDO) to retain only summer values (June–September) from each year, averaging model output for the bottom third of the water column for each grid cell (representing the BML). GETM-ERSEM data has also been interpolated from its native grid onto the regular ICES grid and masked to emulate the pattern of missing values found in the observations (Sect. 4.2.1) in order to provide a

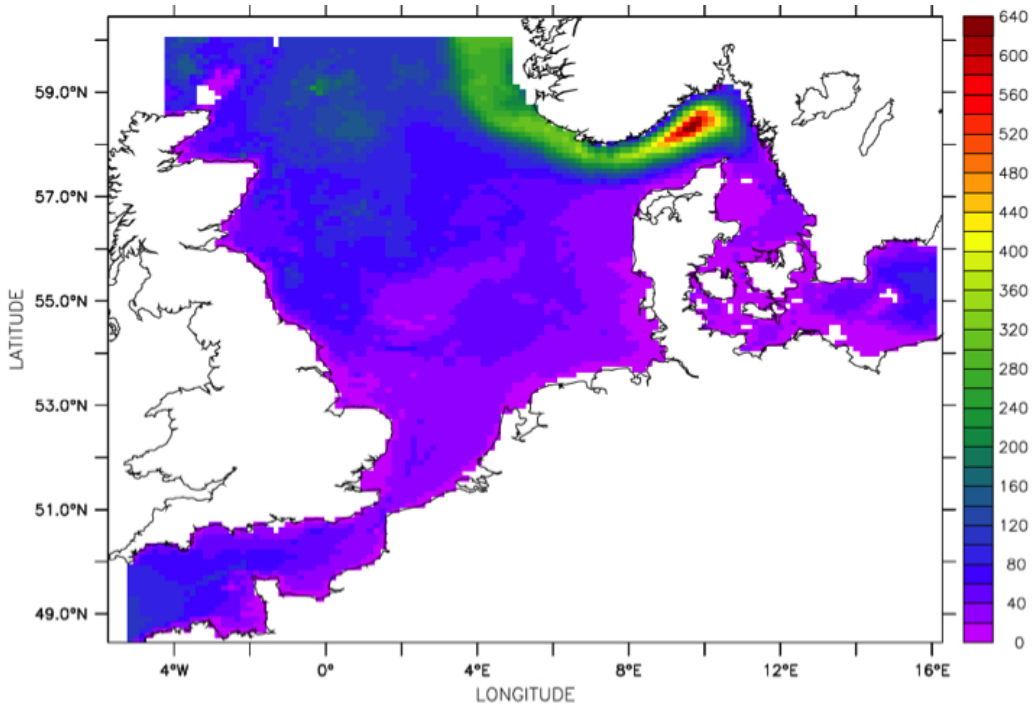

Figure 4.4: Full domain and bathymetry (metres depth) of the GETM-ERSEM hydrodynamic-biogeochemical model, as applied to the North Sea region.

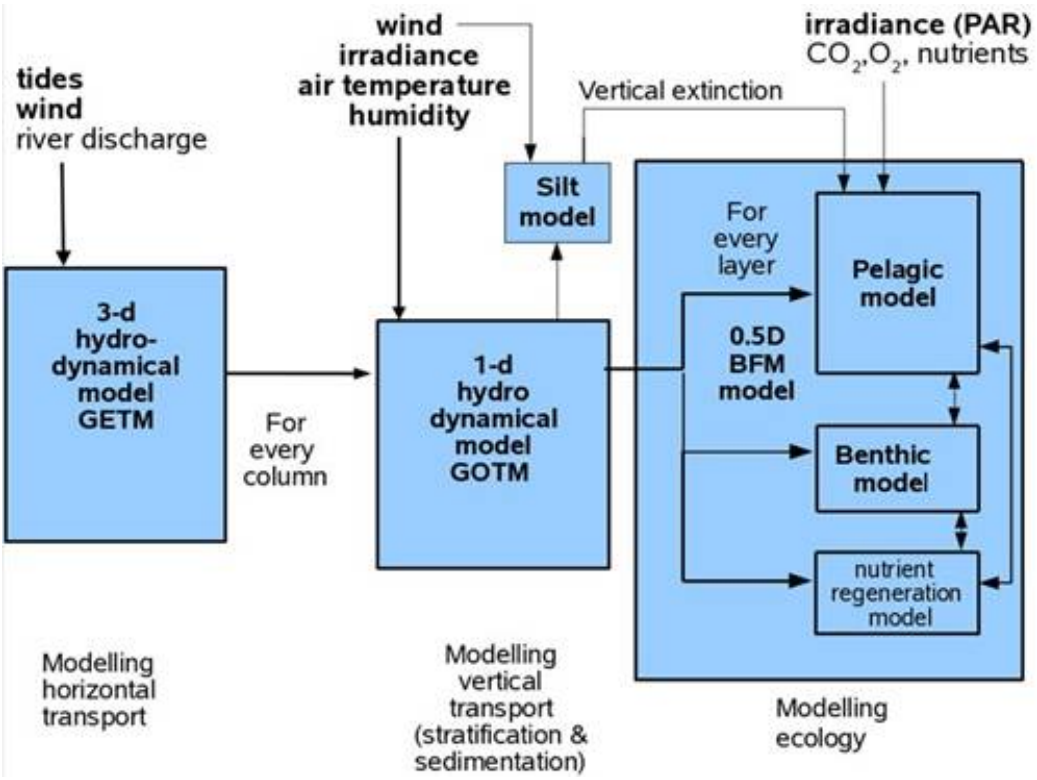

Figure 4.5: Schematic representation of the GETM-ERSEM model and its constituent physical and biological components and forcings (NIOZ, 2012).

consistent spatiotemporal domain for model-data comparison.

4.3 Results

4.3.1 Model-data comparison

Table 4.1 summarises the bias (model minus observations) and Root Mean Squared Error (RMSE) statistics resulting from comparison of gridded ICES data with the GETM-ERSEM model hindcast for the full North Sea domain using summer BML ocean properties for the period 1959–2006. Generally, the model displays some skill at simulating the bulk properties of observed summer BML temperature and salinity, with mean biases of 0.3°C and -0.2 psu respectively. However, summer BML [O_2] is considerably underestimated by the GETM-ERSEM model experiment, yielding a significant negative bias of $-36.6\,\mu\mathrm{mol\,L^{-1}}$ and an elevated RMSE value.

The spatial distributions of observed and simulated variables and their associated error metrics are shown in Figure 4.6 in order to better constrain the spatial pattern of model-data agreement. Simulated summer BML temperatures exhibit a small overall warm bias (Table 4.1). This bias is predominantly driven by model overestimation of the northward propagating elevated bottom temperatures in the shallow southern North Sea, with a contribution from an anomalously warm BML in the Skagerrak (Fig. 4.6A–Fig. 4.6D). Comparatively, model simulated bottom temperatures are generally in good agreement with the observations in central and northern regions, which are of most importance when assessing seasonal oxygen depletion in the stratified North Sea. The spatial structure of summer BML salinity is also generally well simulated by the GETM-ERSEM hindcast (Fig. 4.6E–Fig. 4.6H). A small overall negative salinity bias can be attributed chiefly to

Variable	Mean (observed)	Mean model bias (model minus observations)	RMSE
Temperature (°C)	11.8	0.3	1.8
Salinity (psu)	34.3	-0.2	1.0
[O_2] ($\mu\mathrm{mol\,L^{-1}}$)	249.9	-36.6	54.3

Table 4.1: Validation of GETM-ERSEM model hindcast for the period 1959–2006 over the full North Sea domain, using gridded ICES historical data (summer BML temperature, salinity and oxygen).

the overestimation of salinity minima in the coastal southern North Sea and Skagerrak region. Similar model errors have been reported in other studies (e.g. POLCOMS-ERSEM; Artioli et al. 2012) and are likely to be caused by deficiencies in the parameterisation of fluvial discharge and Baltic outflow in regional models. In the central and northern North Sea, RMSE is uniformly low, and the model is able to capture the important southward propagating tongue of saline (~ 35 psu) bottom water derived from the North Atlantic. However the spatial extent of this feature is overestimated in the central North Sea.

Comparatively, hindcast GETM-ERSEM [O_2] fields are dominated by an anomalously low oxygen signal ($< 200\,\mu\text{mol}\,\text{L}^{-1}$) emanating from the Skagerrak region (Fig. 4.6I–Fig. 4.6L). This feature yields a significant negative [O_2] bias and large RMSE values in the Skagerrak, Norwegian Trench and shallow southern North Sea. Whilst generally lower summer BML [O_2] values are observed in the stratified North Sea, this feature is significantly overestimated by the model and likely to be an artifact of imposed open boundary conditions which influence the inflow of Baltic water and will have an important impact on model simulated hydrography in the eastern North Sea. However, the model reproduces a [O_2] gradient of $\sim 60\,\mu\text{mol}\,\text{L}^{-1}$ between the central stratified North Sea and more oxygenated regions to the northwest as an emergent property. Moreover, RMSE values are, relatively, lower in regions of interest for historical [O_2] depletion events in the central North Sea, such as north of Dogger Bank (north of $\sim 55°$N) where the model simulates less hypoxic summer BML waters.

4.3.2 Interannual variability

Interannual variability in BML temperature, salinity and [O_2] is investigated in this analysis by calculating the temporal standard deviation (σ) of annually binned summer ICES data and contemporaneous masked model fields. Observed and model simulated zonal and meridional mean standard deviations calculated for the period 1959–2006 are presented in Figure 4.7. The impact of applying a low-pass filter in order to isolate interannual variability from long-term trends on patterns of observed variability was found to be small (results not shown). As a result, unfiltered data are used here to compare observed and model simulated variability at all scales. However, linearly de-trended model fields are plotted in Figure 4.8 to investigate model representation of interannual variability since

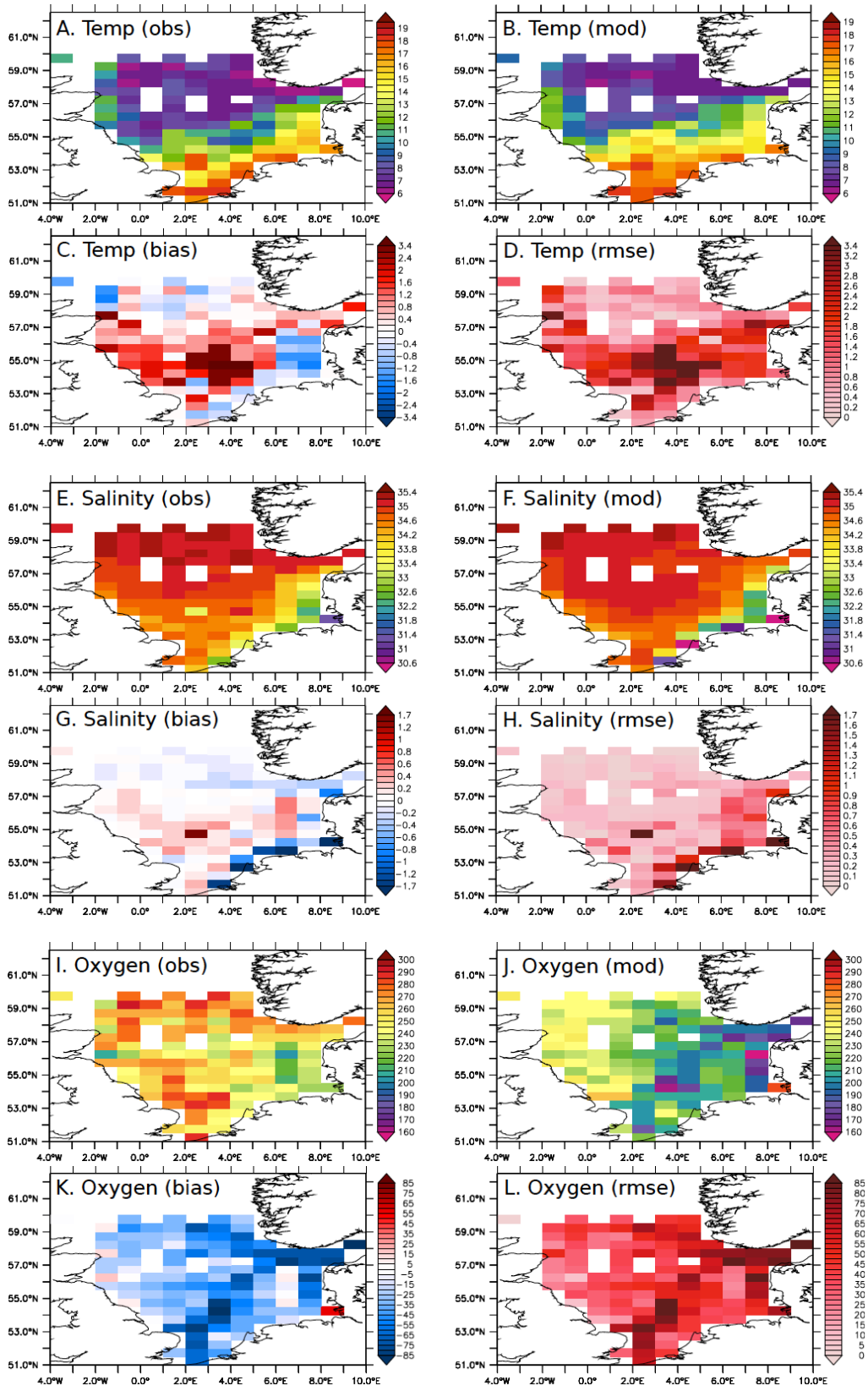

Figure 4.6: Comparison of observed and model simulated summer (June–Sept) BML temperature (**A**-**D**; °C), salinity (**E**–**H**; psu) and $[O_2]$ (**I**–**L**; μmol L^{-1}) for the period 1959–2006.

linear trends can be more appropriately fitted to spatiotemporally complete unmasked model fields.

Patterns of interannual variability are generally similar between observations and model data, with the meridional and zonal mean structure of variability being reproduced by GETM-ERSEM (Fig. 4.7). For example, both observed and model simulated summer BML temperatures display elevated interannual variability between 52–55°N (Fig. 4.7A), and reach their zonal maxima at $\sim$8°E (Fig. 4.7B; spatial correlation [r^2] = 0.36). Observed spatial patterns of variability in summer BML salinity are also well represented by the GETM-ERSEM simulation (spatial correlation [r^2] = 0.48). Particularly, elevated interannual variability is observed and simulated in the south-eastern North Sea for summer BML salinity where GETM-ERSEM captures the meridional mean peak in variability of $\sim$0.5 psu at 8–9°E. Comparatively, the observed pattern of interannual variability in summer BML [O_2] is captured less successfully by the model simulation, with an overall spatial correlation (r^2) of 0.16. However, the observed zonal mean structure of interannual variability is reproduced to some extent, with the model simulating increased variability in the central North Sea and reaching a maxima between 54–55°N. The model does not capture the observed meridional mean structure of summer BML [O_2] variability (a model error that contributes significantly to the low overall spatial correlation).

Importantly, however, whilst the GETM-ERSEM hindcast exhibits reasonable qualitative agreement in terms of the zonal and meridional patterns of interannual variability, the magnitude of variability is consistently underestimated by the GETM-ERSEM hindcast for all variables. This suggests that model information regarding the spatial structure, rather than absolute magnitude, of variability may be of more use when investigating externally driven changes in North Sea BML properties (Fig. 4.8). However, elevated noise within sampled observations could also contribute to this discrepancy, when compared to smoother "true" monthly mean fields provided by the model.

Figure 4.8 shows the simulated spatial pattern of interannual variability derived from linearly de-trended summer BML temperature, salinity and [O_2] fields. Consistent with meridional and zonal mean patterns, simulated BML temperature variability reaches a maximum in the southern and eastern North Sea (Fig. 4.8A). This elevated interannual variability can be related to strongly variable frontal positions, particularly in the German

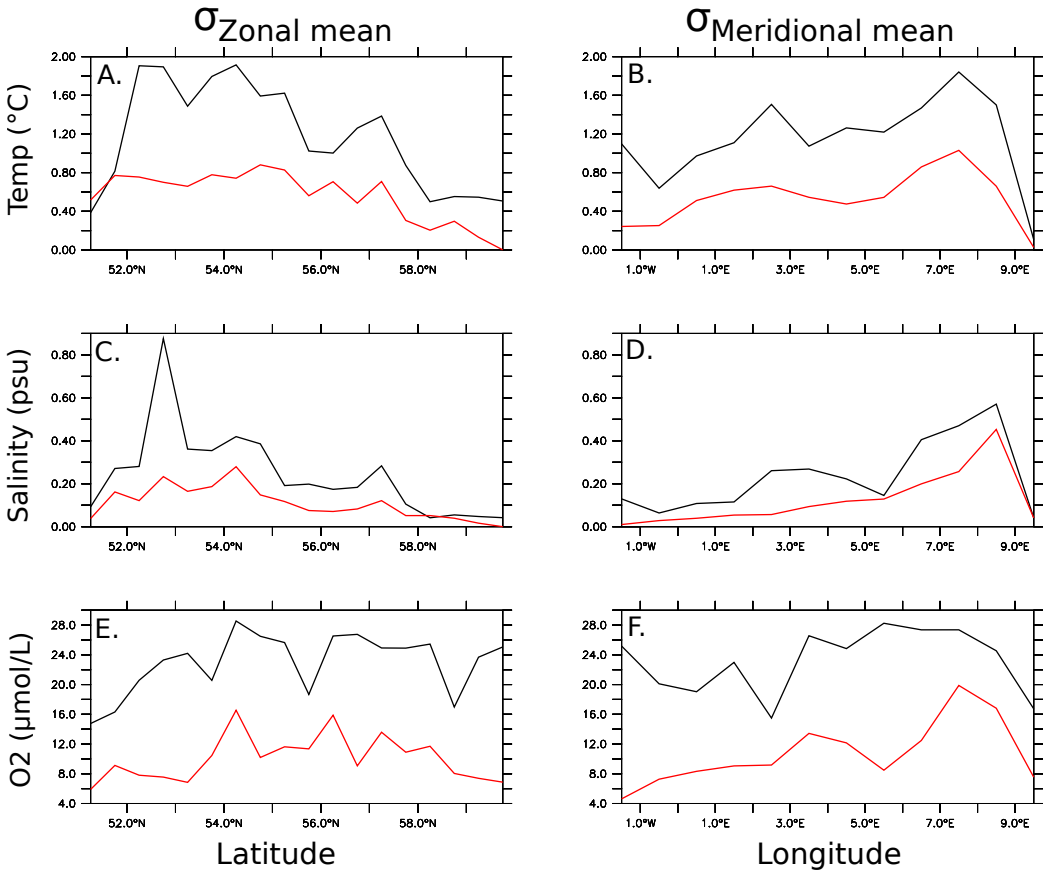

Figure 4.7: Interannual variability (σ) in observed (black) and model simulated (red) summer BML temperature (**A**–**B**; °C), salinity (**C**–**D**; psu) and [O_2] (**E**–**F**; μmol L^{-1}) for the period 1959–2006.

Bight where there is a strong riverine influence and relatively weaker tides (e.g. Holt et al., 2012). As highlighted by van Leeuwen et al. (2014) this region is an important transition zone between model simulated hydrodynamic regimes, characterised as exhibiting both periodic seasonal stratification and dominant fresh water influence (ROFI) over the course of the hindcast (Fig. 4.2). Similarly, modelled interannual variability in BML salinity is largest in the south-eastern North Sea, however this variability intensifies within the permanently mixed coastal zone (Fig. 4.8B). Considerable interannual variability in this region is likely to be coupled to variability of riverine fluxes driven by precipitation patterns within the German Bight. The structure of simulated interannual variability in bottom [O_2] is, comparatively, more complex (Fig. 4.8C). Consistent with temperature and salinity patterns, BML [O_2] variability reaches its maximum extent in the southern and eastern North Sea. However, elevated interannual variability in summer BML [O_2] is also simulated in the north-eastern North Sea, along the boundary between the central North Sea and Norwegian trench region. This variability coincides with an important transition

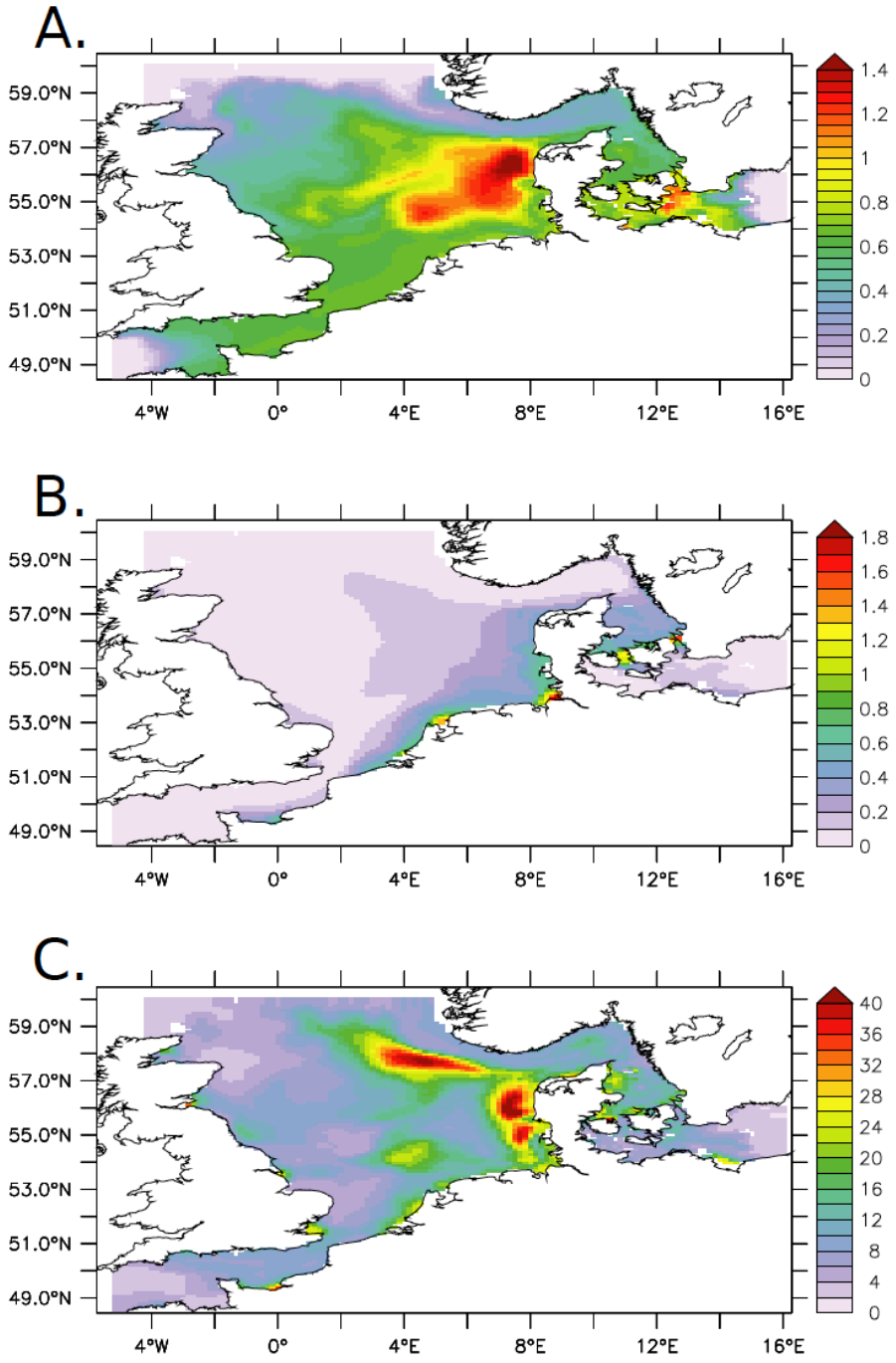

Figure 4.8: Interannual variability (σ) in linearly de-trended GETM-ERSEM simulated summer BML temperature (**A**; °C), salinity (**B**; psu) and $[O_2]$ (**C**; μmol L^{-1}).

zone between hydrodynamic regimes: displaying both permanent haline stratification due to saline Baltic outflow (as in the Norwegian trench) and seasonal thermal stratification (dominant in the central North Sea) over the historical period (Fig. 4.2; van Leeuwen et al., 2014). Historical transitions between hydrodynamic regimes are therefore found to be the dominant driver of simulated variability in summer BML [O_2] and temperature on interannual timescales.

4.3.3 Linear trends

Linear trends in modelled and observed summer BML temperature and [O_2] for the period 1959–2006 are shown in Figure 4.9. Observed trends in summer BML temperature (Fig. 4.9A) show good qualitative agreement with sub-sampled model simulated trends (Fig. 4.9B), however modelled trends are consistently smaller than observed. Simulated and observed temperature trends are dominated by warming, with the largest positive temperature signals ($> 0.1\,^{\circ}\mathrm{C\,yr^{-1}}$) within the well-mixed southern and eastern North Sea. A smaller, but more uniform, observed warming trend is also reproduced by the model in the northern North Sea, however data coverage is more limited in this region. GETM-ERSEM simulates an erroneous cooling trend within the Norwegian Trench, however this feature has been found to be an artifact of masking model data with observational coverage (results not shown). The model is able to reproduce observed cooling trends in the English Channel and in the central North Sea (north of Dogger Bank).

GETM-ERSEM hindcast trends in summer BML [O_2] (Fig. 4.9C) are also generally consistent with ICES data (Fig. 4.9D). In agreement with observations, simulated [O_2] trends are predominantly negative in the summer stratified central and eastern North Sea. However, as highlighted in historical temperature trends, model-data discrepancies are evident both in terms of sign and magnitude. For example, within the Norwegian trench and Skagerrak region GETM-ERSEM simulates positive trends in summer BML [O_2] counter to observed deoxygenation. Also, considerable [O_2] increases within English Channel waters are not reproduced by the model. Consistent with BML temperature trends, the magnitude of linear trends in summer BML [O_2] are generally underestimated by the model, with an observed area mean linear trend of $-0.62\,\mu\mathrm{mol\,L^{-1}\,yr^{-1}}$ compared to a simulated trend of $-0.35\,\mu\mathrm{mol\,L^{-1}\,yr^{-1}}$.

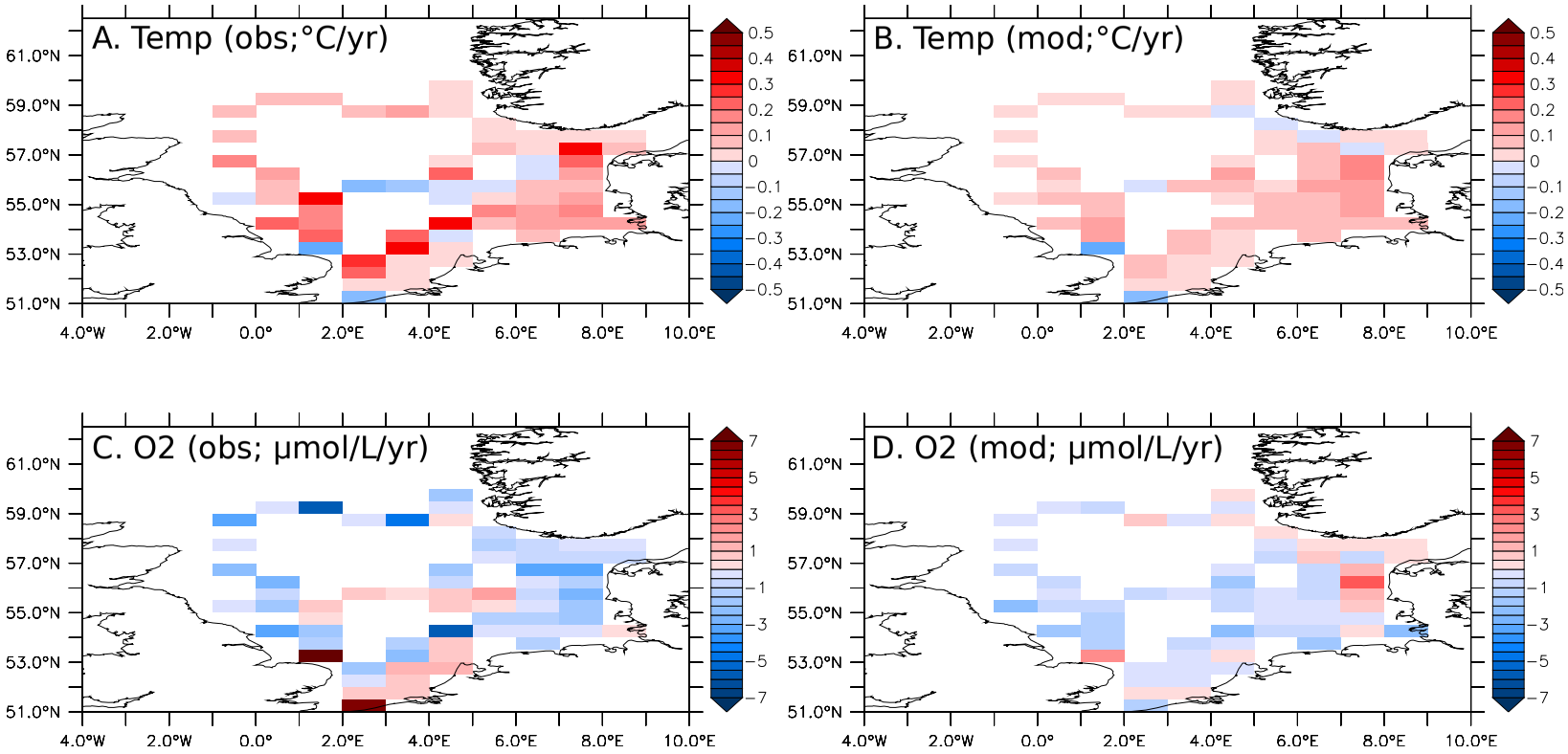

Figure 4.9: Linear trends in summer BML temperature (observed [**A**] and simulated [**B**]; $^{\circ}\mathrm{C\,yr^{-1}}$) and [$O_2$] (observed [**C**] and simulated [**D**]; $\mu\mathrm{mol\,L^{-1}\,yr^{-1}}$) for the period 1959–2006. Observations have been filtered to remove trends fitted to fewer than 4 data points. GETM-ERSEM model fields are sampled as observations.

4.3.4 Signal-to-noise ratio

By combining linear trends (Sect. 4.3.3) with estimates of interannual variability (Sect. 4.3.2) and model error (Sect. 4.3.1) it is now possible to calculate a 'signal-to-noise' ratio (SNR), which quantifies the detectability of externally forced changes in summer BML temperature and [O_2] relative to natural internal variability and model uncertainty. SNR is calculated at the 90 % confidence level using the formulation of Holt et al. (2012), following Hawkins and Sutton (2009):

$$SNR = \frac{LT}{1.65\sqrt{(\sigma^2 + E^2)}} \tag{4.1}$$

where, for unmasked model fields, L is the simulated linear trend, T is time (years), σ^2 is variance in summer BML values, and E is model error (taken as the RMSE between ICES data and model fields, with missing values in-filled using equal weighting nearest neighbour interpolation). This calculation assumes that model error (E) and internal variability (σ^2) are Gaussian and independent. Additionally, a 'potential SNR' is calculated which assumes zero model error ($NoErr$; $E = 0$) following Hawkins and Sutton (2011). This idealised signal-to-noise-ratio will establish the impact of model uncertainty relative to internal variability on the detectability of climate signals in BML variables.

The signal-to-noise ratio in simulated summer BML temperature (Fig. 4.10A) is generally largest (SNR > 0.5) in the central and eastern North Sea coeval with significant linear warming trends and more muted interannual variability (Fig. 4.8A). Comparatively, despite large warming trends in the south-eastern North Sea, signal-to-noise ratios in this region are ~ 0.5 owing to the combined impact of elevated model RMSE (Fig. 4.6D) and internal noise associated with variable frontal positions. Figure 4.10C shows 'potential SNR' in summer BML temperature. This metric demonstrates that, particularly in the south-eastern North Sea, statistically significant (SNR > 1) increases in model detectability of BML temperature change can be invoked as model uncertainty is reduced.

Equally, model skill plays a major role in determining the detectability of climate signals in simulated summer BML [O_2] (Fig. 4.10B and Fig. 4.10D). Signal-to-noise ratios in summer BML [O_2] are generally low (SNR < 0.2) for much of the North Sea domain (Fig. 4.10B). However, this deficiency can be mainly attributed to model uncertainty and elevated RMSE. Since, when compared to the traditional signal-to-noise ratio (Fig. 4.10B),

major improvements in trend detectability are yielded under the idealised 'potential SNR' formulation (Fig. 4.10D). In this case, statistically significant (SNR < -1) decreases in [O_2] can be detected in the central North Sea, with SNR generally between -0.5 and -1 across much of the model domain. Moreover, consistent with analysis of interannual variability (Fig. 4.8C), elevated noise along the transitional zones between hydrographic regimes (e.g. at the margin of the Norwegian Trench and in the German Bight) preclude positive detection results (SNR < 0.2) despite larger deoxygenation trends.

4.4 Discussion and conclusions

Bringing together historical observations and results from a hindcast 3-D physical biogeochemical model (GETM-ERSEM) this study presents a unique perspective on trends and variability in North Sea summer BML [O_2] and temperature over the last ~ 50 years. A central result is that both model simulated and observed summer BML [O_2] fields exhibit historical decreases across much of the summer stratified central North Sea, coeval with a spatially coherent BML warming trend (Fig. 4.9). This supports recent reports of elevated summer oxygen depletion associated with strong thermal stratification in the central North Sea (e.g. Greenwood et al., 2010; Weston et al., 2008) and prognostic modelling work predicting future increases in the risk of North Sea hypoxia as a result of climate-driven intensification of seasonal pycnocline development and solubility effects (Meire et al., 2013). A recent meta-analysis carried out by Gilbert et al. (2010) suggests that, globally, the coastal ocean is an important locus for deoxygenation, with depth-averaged (0–300 m) mean linear trends for the period 1976–2000 of $-0.35\,\mu\text{mol}\,\text{L}^{-1}\,\text{yr}^{-1}$ (0–30 km from coast) and $-0.19\,\mu\text{mol}\,\text{L}^{-1}\,\text{yr}^{-1}$ (30–100 km from coast). To put these global estimates into context, Table 4.2 presents a summary of linear trends and interannual variability in North Sea summer BML [O_2] and temperature derived from historical ICES data and GETM-ERSEM fields. Additional results are also reported from a prognostic simulation of the Geophysical Fluid Dynamics Laboratory (GFDL) ESM2.1 global Earth System Model (GFDL-ESM2.1 [Frölicher, Pers. Comm.]; model configuration and experimental design as described in Cocco et al. [2013] and Jones et al. [2013]; $\sim 1^\circ$ resolution) sampled for the North Sea region.

Observed area mean summer BML deoxygenation trends presented in this analysis

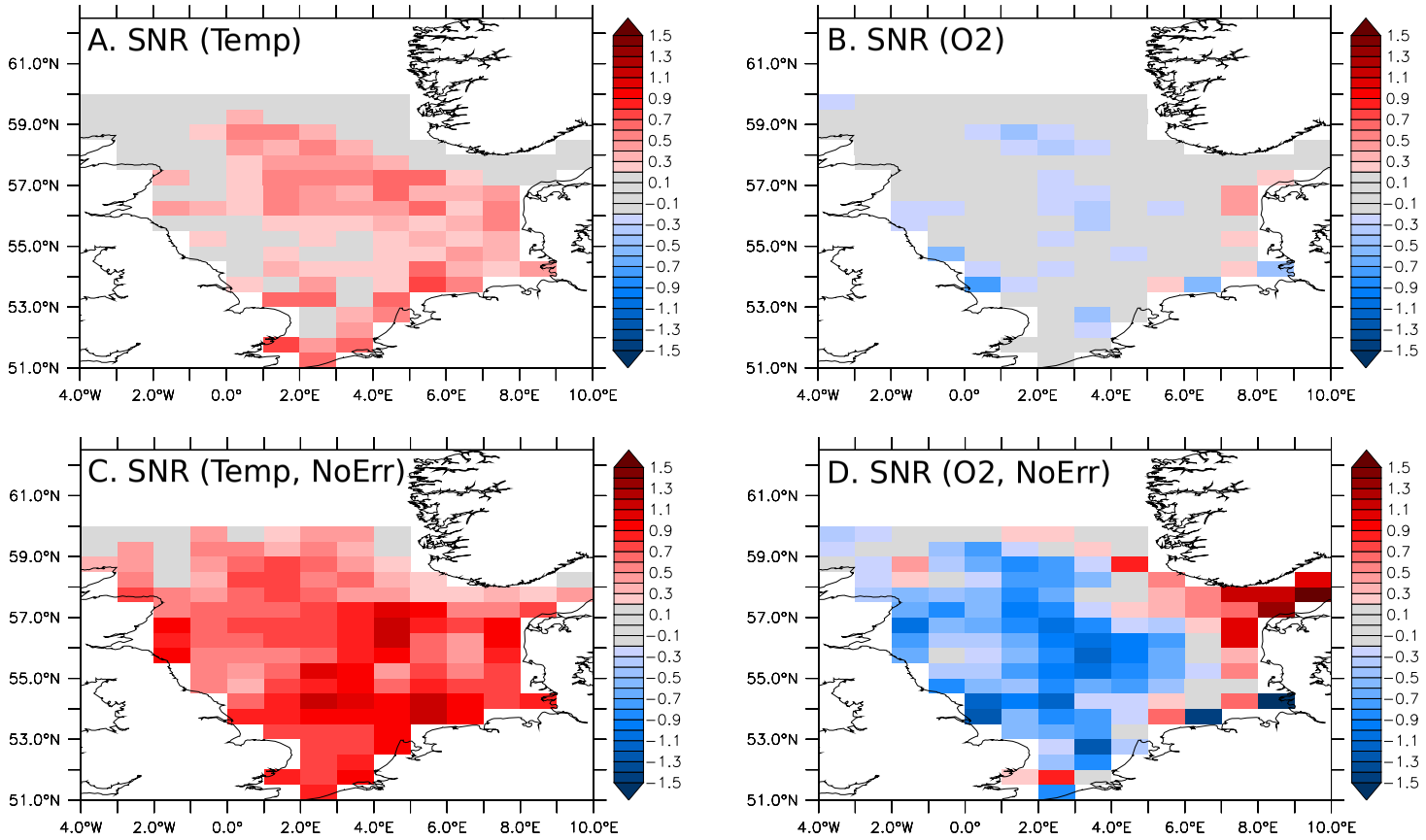

Figure 4.10: Signal-to-noise ratio (SNR) calculated for model simulated summer BML temperature (**A**) and [O_2] (**B**) and 'potential SNR' calculated for model simulated summer BML temperature (**C**) and [O_2] (**D**) assuming no model error ($E = 0$; $NoErr$). Grey shading highlights where SNR < 0.2. A negative SNR (blue) indicates where simulated linear trends are negative.

Table 4.2: Comparison of observed (OBS) and model simulated (GETM-ERSEM [GETM] and GFDL-ESM2.1 [GFDL]) area mean linear trends and interannual variability in North Sea summer BML [O_2] (μmol L^{-1}) and temperature (T; °C).

	Linear trend (1959–2006)			Interannual variability (σ; 1959–2006)			Projected change by 2080–2099 [3]		
	T	[O_2]	[O_2]/T [1]	T	[O_2]	[O_2]/T [1]	T	[O_2]	[O_2]/T [1]
OBS	0.083	−0.62	−7.4	1.23	23.75	19.4			
GETM	0.046	−0.35	−7.6	0.58	11.02	18.9			
GFDL [2]				0.63	5.56	8.8	1.34	−5.26	−3.9

[1] Ratio of area mean linear trends and interannual variability in [O_2] relative to temperature.

[2] Bottom values extracted from monthly mean 3-D data following the approach of Cheung et al. (2013) and Jones et al. (2013). Global model fields are remapped onto the regular ICES grid for the North Sea domain and processed to retain only summer mean values.

[3] GFDL-ESM2.1 configuration is forced with prescribed CO_2 emissions for the historical period (1870–2000) and follows an IPCC SRES A2 emissions scenario until 2100 (see Cocco et al. [2013] and Jones et al. [2013] for further details). Absolute changes in area mean temperature and [O_2] are calculated relative to a 1990–2009 baseline.

($-0.62\,\mu\text{mol}\,\text{L}^{-1}\,\text{yr}^{-1}$) exceed global mean estimates of Gilbert et al. (2010) by a factor of between ~ 2 and 3 (Table 4.2). As such, summer BML trends in stratified shelf regimes like the North Sea could be important in the early detection of anthropogenically driven hypoxia (Zhang et al., 2010). Comparatively, as shown in Section 4.3.3, trends in both summer BML [O_2] and temperature are considerably underestimated by the GETM-ERSEM hindcast. However, model simulated [O_2] trends are in good agreement with the estimates of Gilbert et al. (2010) for the coastal zone ($-0.35\,\mu\text{mol}\,\text{L}^{-1}\,\text{yr}^{-1}$). GETM-ERSEM is also able to reproduce the observed ratio of linear trends in [O_2] to temperature for the period 1959–2006 ($\approx -7.5\,\mu\text{mol}\,\text{L}^{-1}\,^{\circ}\text{C}^{-1}$). Similarly, whilst GETM-ERSEM exhibits more muted interannual variability, the ratio of model simulated variability in [O_2] to temperature is consistent with observations ($\approx 19\,\mu\text{mol}\,\text{L}^{-1}\,^{\circ}\text{C}^{-1}$). Taken together, these results suggest that GETM-ERSEM is able to simulate physically realistic patterns of change in summer BML [O_2] as a function of temperature, despite underestimating the absolute magnitude. A systematic underestimation of historical trends and variability in near-bottom temperature has been reported elsewhere by studies that apply 3-D regional models to the northwest European continental shelf (e.g. POLCOMS; Holt et al. 2012), however the cause of this model deficiency is uncertain. Although, reduced interannual variability in BML properties as simulated by GETM-ERSEM can likely be attributed in part to imposed climatological boundary conditions at spatial model edges, which remove an important source of internal variability associated with ocean-shelf exchange processes.

In comparison, the global GFDL-ESM2.1 Earth System Model (ESM) simulates no historical linear trend in North Sea summer bottom [O_2] or temperature for the period 1959–2006 (Table 4.2). Under a SRES A2 emissions scenario GFDL-ESM2.1 projects an area mean decline in summer North Sea bottom [O_2] of $\sim 5\,\mu\text{mol}\,\text{L}^{-1}$ between 1990–2009 and 2080–2099, corresponding to a $\sim 2\,\%$ decrease. This reduction falls at the lower end of ESM simulated decreases in global oxygen inventory for 2100 relative to the 1990s (2–4 % [Cocco et al. 2013]; 1.5–4 % [Ciais et al., 2014; Bopp et al., 2013]) suggesting that, contrary to larger observed trends, future BML [O_2] changes in the North Sea will be consistent in magnitude with global deoxygenation in the open ocean. However, poor model-data agreement for the historical period (Table 4.2), related to the limited capacity of coarsely resolved ESMs to represent shelf sea processes (e.g. Holt et al., 2009; Holt

et al., 2014), reduces the efficacy of global models in projecting future North Sea climate impacts. Indeed, this result is opposed by prognostic experiments carried out using the GOTM-ERSEM-BFM 1-D hydrodynamical-biogeochemistry model which simulates much larger climate-driven bottom [O_2] decreases (5–9 % by 2100) at three sites in the stratified North Sea for a more moderate emissions pathway (SRES A1B; van der Molen et al., 2012).

Similarly, forced experiments conducted with a 1-D ecosystem model calibrated for the central North Sea project summer BML [O_2] decreases of up to 11.5 % by the end of the century under a SRES A1B emissions scenario (Meire et al., 2013). These 1-D model integrations suggest that future climate forcings will drive a significant reduction in the oxygen inventory of the North Sea as a result of enhanced stratification and solubility effects, leading to an increased risk of seasonal hypoxia (Meire et al., 2013). However, historical ICES data and GETM-ERSEM regional model fields analysed in this study indicate that long term secular decreases in summer BML [O_2] are already occurring. Moreover, GETM-ERSEM simulates a 13 % increase in the number of grid cells where summer BML water [O_2] is less than 190 μmol L^{-1} between 1960–1965 and 2000–2005, suggesting that Ecological Quality objectives set by OSPAR to mediate the negative impacts of hypoxia in coastal and offshore regions of the North Sea (Painting et al., 2005; see Section 4.1) are not being met.

Whilst this work has identified a unique fingerprint of change in North Sea BML properties, attribution of historical trends to external climate forcing requires an understanding of climate variability on multiyear timescales. As a result, this study also investigates the detectability of GETM-ERSEM simulated trends relative to model estimates of natural internal variability and model uncertainty (Sect. 4.3.4). Signal-to-noise ratios for summer BML temperature remain less than unity across much of the central North Sea, consistent with an analysis of the POLCOMS regional model which reported similar values (SNR < 1) for annual BML temperature trends (Holt et al., 2012). Comparatively, Holt et al. (2012) found statistically significant historical trends in POLCOMS simulated SSTs across much of the North Sea domain, likely owing to the stronger warming signal at the surface which is tightly coupled to the imposed atmospheric forcing, therefore limiting the confounding influence of model error. Indeed, using a potential SNR approach (which assumes that

model error can be reduced to zero [Hawkins and Sutton, 2011]) it has also been possible here to better quantify the impact of 'structural error' (e.g. Hegerl and Zwiers, 2011; Sect. 2.5) in ocean models on the detectability of climate signals. Notably, by applying a 'perfect model' assumption, trends in both summer BML temperature and $[O_2]$ are robustly detected at the 90 % confidence level across much of the summer stratified central and eastern North Sea. This result suggests that structural error is a key factor limiting the ability of models to detect emergent climate signals in the North Sea, and highlights the potential gains of improving resolution and representation of shelf processes in both regional models (e.g. NEMO-ERSEM; Edwards et al., 2012) and the current generation of global ESMs (for instance, via dynamical downscaling methods [Holt et al., 2014] or by using a distorted spatial grid [Gröger et al., 2013]). Particularly, the large increase in detectability yielded by applying a 'perfect model' assumption to simulated $[O_2]$ changes emphasises the need for better parameterisation of the coupled physical and biogeochemical processes which control oxygen dynamics and hypoxia in ocean models (e.g. Peña et al., 2010; Keeling et al., 2010).

Results presented here also highlight the potential utility of BML $[O_2]$ and temperature as tracers for historical and future alteration to hydrographic conditions in the North Sea, which provide the dominant physical constraints on marine ecosystems and fisheries. Particularly, regions of elevated interannual variability in BML temperature and $[O_2]$ have been shown to correspond with important transition zones between dominant hydrodynamic regimes (Sect. 4.3.2). Moreover, the spatial distributions of summer BML properties, taken together, effectively demarcate boundaries between summer stratified, permanently stratified, well mixed, and fluvially influenced regions of the Greater North Sea (Fig. 4.6). To this end, the capacity of regional models and observational programs to identify shifts in hydrodynamic characteristics on the northwest European continental shelf using BML properties could play an important role in future marine spatial planning (van Leeuwen et al., 2014). Particularly, the Marine Strategy Framework Directive (MSFD), adopted by the European Union in 2008, includes a qualitative descriptor for reaching Good Environmental Status by 2020 which requires that 'Permanent alteration of hydrographical conditions does not adversely affect marine ecosystems' (Cardoso et al., 2010). As such, an integrative approach combining historical data and hindcast model results, as presented here, could

provide important reference conditions and targets for Good Environmental Status to be used as steps towards implementation of the MSFD (Borja et al., 2010).

Chapter 5

General Conclusion and Outlook

5.1 Précis of key results

The overall motivation for work presented in this thesis has been to further the understanding of secular changes in oceanic oxygen as a fingerprint of anthropogenic climate change in the ocean. In pursuit of this goal, a range of statistical and numerical methods have been developed to better elucidate the drivers and detectability of observed changes in $[O_2]$. These include regression-based optimal fingerprinting methods (Chapter 2) and hindcast 3-D ecosystem models initialised at global (Chapter 3) and regional (Chapter 4) scales. Using this multi-faceted approach it has been possible to build a coherent picture of the changing spatiotemporal distribution of O_2 over the historical period by synthesising observations and model output. The major research outcomes of this thesis are as follows, in accordance with the initial research objectives set out in Section 1.5.1 (*italicised*):

1. *Evaluate the performance of recent ESM simulations in reproducing observed historical changes and variability in oceanic oxygen.* Chapter 2 presents a model-data comparison of climatological and recent changes in subsurface $[O_2]$ using a compilation of historical $[O_2]$ data to evaluate output from two CMIP5 ESMs (MPI-ESM-LR, HadGEM2-ES). Both models are shown to reproduce the climatological distribution of $[O_2]$ within the ocean interior in terms of meridional structure, but either underestimate (HadGEM2-ES) or overestimate (MPI-ESM-LR) the extent of established low-O_2 waters, in agreement with recent CMIP5 model inter-comparisons (Gnanadesikan et al., 2013; Bopp et al., 2013). The fidelity of ESM simulated and observed historical changes in subsurface $[O_2]$ (between $\sim$ 1970 and $\sim$ 1992) was assessed using formal optimal fingerprinting methods (Sect. 2.4.2), which complement more descriptive comparisons (Sect. 2.4.1) by providing a rigorous, quantitative test of model performance accounting for the role of internal variability (Hegerl and Zwiers, 2011). Regression coefficients (β) obtained from the application of detection and attribution (D&A) methods in this analysis indicate that significant correlations exist between simulated and observed space-time patterns of historical $[O_2]$ change (100 – 3000 m depth), although CMIP5 ESMs consistently underestimate the magnitude of change by a factor of $\sim 2 - 4$. A standard (*cf.* Allen and Tett, 1999) consistency check (F-test) on the residuals of the Total Least Squares regression was used alongside β values in order to diagnose possible inconsistencies between

ESM response patterns and observations for a given number (k) of retained EOFs of internal variability. F-test p-values fall within the 0.05 – 0.95 range for all optimal detection experiments on global and ocean basin scales (excluding the Atlantic basin, for which the test marginally fails) demonstrating the capacity of ESMs to estimate forced and unforced variability in [O_2] for the historical period. Consistent with standard D&A practise (e.g. Hegerl et al., 2010) internal variability in observed [O_2] was characterised by sampling long ($\sim$ 1000 year) pre-industrial control integrations of ESMs. The residual consistency test was here used to guide the analysis towards a reduced dimension space in which internal variability is well simulated by models. ESM simulated internal variability was also generally shown to fall within the range of observed variance derived from sampling detrended long-term [O_2] time series data at Ocean Station Papa and within the Oyashio Current region (Table 2.2).

2. *Quantify the detectability of observed changes in open ocean [O_2] at global and ocean basin scales relative to natural internal variability.* In Chapter 2, formal D&A techniques were applied in a single fingerprint optimal detection analysis testing the null hypothesis that observed ($\sim$ 1970 to $\sim$ 1992) changes in subsurface [O_2] are indistinguishable from climate noise. Model fingerprints were taken from historical ensembles of two CMIP5 ESMs including "ALL" external forcings (anthropogenic + natural [Taylor et al., 2012]), sampled as pseudo-observations according to the spatiotemporal coverage of historical measurements. Positive detection results ($\beta > 0$) in response to "ALL" external forcings were found at the 90 % confidence level for global depth-averaged (1-D) and depth-resolved (2-D) zonal mean [O_2] changes. The results of this optimal regression analysis indicate that an externally forced "fingerprint" is already detected within the observational record of (mainly) decreasing subsurface [O_2], and that this signal is statistically distinct from climate variability as characterised by unforced ESMs. Additionally, the global 2-D detection experiment revealed 5 – 95 % uncertainty bounds on β scaling factors which were consistent with 1, passing the so-called "attribution test" of consistency in observed and model-simulated signal amplitudes (Hasselmann, 1997). The D&A analysis was also extended to ocean basin scales, wherein 2-D zonal mean [O_2] changes for the Pacific basin were detected in response to external forcing (90 % confidence level)

whereas those within the Atlantic basin were indistinguishable from internal noise.

3. *Investigate the impact of imposed atmospheric forcing on the spatiotemporal distribution of oceanic oxygen over the last ∼50 years in a hindcast ocean biogeochemistry model.* The role of imposed meteorological boundary conditions as an exogenous driver of historical changes and variability in model simulated O_2 was assessed in Chapter 3. A series of hindcast PlankTOM10-NEMO3.1 sensitivity experiments were initialised under different atmospheric forcings and bulk formulae. This analysis confirmed the results of previous hindcast model studies (e.g. Friedrich et al., 2006) which found tropical and extratropical variability in subsurface O_2 to be modulated by imposed wind stress and heat flux, respectively. However, the presented results also demonstrate, for the first time, that choices made regarding interannually varying atmospheric forcing products derived from observations (COREv2-IAF, DFS4.3, NCEP/NCAR) and numerical models (IPSL-CM5A-LR) place major constraints on simulated changes and variability in passive tracers for the historical period. Particularly, experiments carried out using forcing data based on "second generation" ERA-40 ECMWF reanalysis data (Uppala et al., 2005) were shown to generate more exogenous variability in O_2, and alter the sign and magnitude of historical changes, when compared to the baseline NCEP/NCAR reanalysis run. A spatially inconsistent hindcast model response to different atmospheric forcing products, which provide *a priori* equally representative historical air-sea fluxes, presents an interesting problem to ocean modellers. Namely, provision should be made within community efforts to standardise experimental protocols for ocean-ice hindcast model experimental (e.g. COREs; Griffies et al., 2009) to better constrain biases in different atmospheric forcing products. Moreover, this chapter suggests that caution is required when interpreting historical changes in ocean biogeochemistry variables using output derived from multiple OBGCMs under different atmospheric forcings (e.g. Henson et al., 2010), since competing errors associated with forcing biases and model error are difficult to disentangle.

4. *Investigate the impact of biogeochemical parameterisations of ocean carbon cycle feedbacks on the spatiotemporal distribution of oceanic oxygen in a hindcast ocean biogeochemistry model.* Chapter 3 investigated the implications of pCO_2-sensitive

(1) C:N ratios in photosynthetic carbon fixation and (2) calcification rates on hindcast [O_2] in the PlankTOM10-NEMO3.1 ocean biogeochemistry model. Using observationally based parameterisations it was shown that the inclusion of stoichiometric C:N effects in carbon drawdown yield major changes to the spatiotemporal distribution of subsurface [O_2] via enhanced carbon export production which promotes remineralisation of POC within the ocean interior. Notably, counter to prognostic model studies which include a variable C:N ratio (Tagliabue et al., 2011; Oschlies et al., 2008), stoichiometric diversity is shown to produce elevated historical deoxygenation throughout the water column at mid- to high latitudes, rather than within established OMZs. Indeed, carbon overconsumption within the tropical euphotic zone was found to drive [O_2] increases (≤ 300 m depth) due to elevated production in response to CO_2 fertilisation, with implications for model-data consistency in the tropical OMZs (see Section 5.2.2 for further discussion). Comparatively, the impact of ocean acidification on biogenic calcification rates was shown to have only a negligible impact on [O_2] dynamics for the historical period, despite yielding reductions in the ratio of $CaCO_3$ to POC export and coeval decreases in POC sinking speeds as mineral ballast fluxes weakened.

5. *Examine fingerprints of secular ocean deoxygenation in the coastal ocean, with a focus on summer stratified shelf sea regimes.* Historical trends and variability in summer Bottom Mixed Layer (BML) [O_2] and temperature for the summer stratified North Sea domain were investigated in Chapter 4 using an integrative approach which synthesised historical measurements and output from the hindcast GETM-ERSEM regional model. Negative linear trends were reported in observed and masked model simulated summer BML [O_2] across much of the summer stratified North Sea hydrodynamic regime, alongside spatially coherent summer BML warming. However, observed trends in summer BML [O_2] for the historical period (1959 – 2006; $-0.62\,\mu\text{mol}\,\text{L}^{-1}$) are underestimated by a factor of ~ 2 by the GETM-ERSEM model ($-0.35\,\mu\text{mol}\,\text{L}^{-1}$). Observed area mean North Sea deoxygenation trends are shown in this chapter to exceed global estimates provided by Gilbert et al. (2010) (0.09 – 0.35 $\mu\text{mol}\,\text{L}^{-1}$) suggesting that summer stratified shelf sea areas could be especially sensitive to warming-driven ocean deoxygenation. The analysis was

extended to examine signal-to-noise ratios (SNR) of simulated changes in summer BML $[O_2]$ and temperature, quantifying the detectability of historical trends relative to estimates of model error and internal variability provided by GETM-ERSEM. SNR is shown to be largest (~ 0.5) for summer BML temperature and $[O_2]$ (~ 0.2) within areas of the central stratified North Sea, consistent with other recent studies (e.g. Holt et al., 2012), however the detectability of this signal is reduced by high model error and internal variability associated with variable frontal regions along the margins of different hydrodynamic regimes. Finally, a 'potential SNR' formulation is used to interrogate the role of model error in masking the detectability of simulated trends. Using this 'perfect model' assumption, statistically significant signals in summer BML $[O_2]$ and temperature emerge across areas of the summer stratified central and eastern North Sea at the 90 % confidence level.

5.2 Synthesis and future work

5.2.1 Detecting changes in ocean variables

This thesis constitutes the first formal D&A assessment of changes in ocean biogeochemistry in response to external forcing, conducted using established optimal fingerprinting methods. Chapter 2 reveals that a fingerprint of secular ocean deoxygenation in response to external forcing is detectable within the historical record of subsurface $[O_2]$ at the 90 % confidence level, for the global ocean and Pacific basin individually. The results of this analysis, taken together with observed warming-driven perturbation to known physical drivers of oxygen depletion (*cf.* Rhein et al., 2013), led the IPCC to conclude in WG1 of AR5 that there is "*medium confidence* that the observed global pattern of decrease in oxygen dissolved in the oceans from the 1960s to the 1990s can be attributed in part to human influences" (Bindoff et al., 2013). However, the IPCC confidence level ascribed to attribution of changes in oceanic oxygen to human influence is, relatively, lower than for physical properties such as upper ocean temperature (*high confidence*) and (sub-)surface salinity (*high confidence*). The higher degree of certainty in D&A of physical ocean variables is evidenced by the significance threshold at which observed changes have been detected above internal variability – with historical changes in upper ocean temperature (0

– 700 m) and salinity (0 – 250 m) now being detectable at the 99 % (Glecker et al., 2012) and 95 % (Pierce et al., 2012) confidence level, respectively.

A number of possible extensions to the optimal fingerprinting work carried out in this thesis could provide greater confidence in the detection of long-term changes in oceanic oxygen. Firstly, in accordance the IPCC Good Practise Guide on Detection and Attribution (Hegerl et al., 2010), once an identifiable signal is *detected* within the observational record of a climate variable its *attribution* to a combination of causal factors requires that other possible forcing combinations can be ruled out. As such, whilst Chapter 2 provides a statistically robust demonstration that changes in subsurface [O_2] are *detected* in response to all external forcings, in order to attribute these changes to, for instance, anthropogenic influence, other external factors such as changes in solar output and volcanism must first be discounted. The ability to conduct such a multi-fingerprint D&A assessment depends critically upon the availability output from targeted ESM historical integrations which include anthropogenic ("*historicalANT*") or natural ("*historicalNAT*") climate forcing factors only. However, under CMIP5, specialised D&A ensembles comprise part of the lower priority "Tier 2" of requested model experiments (Taylor et al., 2012), with the availability of output being further reduced by the limited subset of ESMs reporting ocean biogeochemical variables. Accordingly, for the ESMs selected in Chapter 2 based on their ability to adequately reproduce observed changes in oceanic oxygen (MPI-ESM-LR and HadGEM2-ES), single-forcing experiments with sufficient ensemble members to minimise signal error (*cf.* Allen and Stott, 2003) were not available at the time of writing. As such, it was not possible to further decompose the detectable external signal of observed [O_2] change into contributions from anthropogenic (greenhouse gases and aerosols) and natural (solar and volcanic) external forcings. However, preliminary results from the implementation of a multi-pattern D&A analysis making use of *historicalNat* experiments reported for the GFDL-ESM2M model (Dunne et al., 2013) indicate that observed [O_2] decreases cannot be explained by natural external forcings alone ($\beta = 0$; results not shown). This finding is consistent with the physical understanding of volcanic forcing effects on oceanic oxygen, with Frölicher et al. (2009) demonstrating that the climate impact of explosive volcanism on [O_2] is generally limited to the upper ~ 500 m on interannual timescales.

Alongside consideration of external natural factors, robust D&A of changes in a climate sensitive variable also requires that estimates of natural internal variability be characterised appropriately. In Chapter 2, long pre-industrial control ESM integrations are sampled as pseudo-observations in order to provide an estimate of internal variability in $[O_2]$, consistent with established optimal fingerprinting practise (e.g. IDAG, 2005). This approach is based on the underlying rationale in D&A assessment that climate noise is not easily estimated from observations on large spatial and temporal scales, and that unforced climate models provide a pure expression of variability in the internal system. Using this method, the detection analysis is optimised by projecting all data onto the k leading eigenvectors calculated from an estimate of the inverse of the covariance matrix of internal variability. The choice of k is determined using a standard "consistency check" (Allen and Tett, 1999) whereby model simulated variability on the scales retained in the analysis is compared against the residuals of the regression using an F-test. However, this test is relatively weak (e.g. Allen et al., 2006; Terray et al., 2012) and does not take into account the shape of the residuals, only their amplitude. Moreover, as highlighted by Ribes et al. (2013), the relatively arbitrary choice to truncate at k EOFs introduces a degree of uncertainty into detection results, with regression coefficients (β) being somewhat sensitive to the retained dimension space (as shown in Figure 2.9). However, as demonstrated in a recent analysis of global mean temperature changes conducted by Imbers et al. (2014), D&A results generally hold independent of the chosen characterisation of internal variability. Nonetheless, the authors recommend that a wider range of statistical tests are used in D&A studies to improve confidence in detection results, for instance, via comparison with long-term time series data, as undertaken in Chapter 2 (Table 2.2).

Moreover, despite the established attribution of changes in the physical ocean system to human influence (*cf.* Bindoff et al., 2013), a number of uncertainties remain regarding the detectability of changes in the physical factors which control the spatiotemporal distribution of passive tracers like $[O_2]$. Particularly, whilst qualitative links have been made between historical changes in upper ocean stratification and deoxygenation (e.g. Figure 2.6; Rhein et al., 2013; Capotondi et al., 2012), the signal of upper ocean density change and, indeed, its impact on biogeochemical processes remains debated (e.g. Dave and Lozier, 2013; Dave, 2014). This deficiency could be addressed using an optimal fingerprinting method, making

use of recently available co-located historical temperature and salinity observations (e.g. MIMOC [Schmidtko et al., 2013]) and the wealth of active tracer output made available from CMIP5 ESMs (Taylor et al., 2012) in order to better constrain the detectability of long-term ventilation changes as a driver of historical deoxygenation. Such an analysis would build on recent work utilising multivariate signal vectors to detect climate change in the ocean wherein combined temperature-salinity model fingerprints are shown to yield greater signal strengths within historical observations (Pierce et al., 2012; Santer et al., 1995). Additionally, as highlighted by atmospheric forcing experiments conducted in Chapter 3 (Sect. 3.4.2), surface wind stress places major constraints on historical changes in thermocline [O_2] via its direct influence on large-scale patterns of ocean circulation and air-sea fluxes of energy. However, major uncertainties remain regarding the relative roles of stratification and wind forcing in driving historical and future changes in ventilation at mid- to high latitudes (e.g., Le Quéré et al., 2007; Böning et al., 2008). Thus, the application of D&A approaches to historical changes in near surface wind speeds could provide further process-level understanding of historical changes in subsurface ocean biogeochemistry, whilst also affording an opportunity for the validation of observed and model simulated atmospheric state variables, as called for in Chapter 3.

A major limiting step in the statistical attribution of changes in biogeochemical properties to climate change is the availability of sustained observations with sufficient spatiotemporal coverage to adequately characterise trends and variability on multiyear timescales (*cf.* Henson, 2014; Dunstone, 2014). This deficiency is particularly relevant to the evaluation of historical changes in O_2, where pronounced variability on interannual to decadal timescales associated with internal ocean-atmosphere feedbacks can act to mask any secular changes (e.g. Sect. 1.3.2; Frölicher et al., 2009; Deutsch et al., 2005). As such, concerted efforts are required to improve observational capabilities at all scales, from the addition of dissolved O_2 sensors to the global array of ARGO profiling floats (*ARGO-oxygen* program [Gruber et al., 2010]) through to continued support for established fixed-point time series stations (Send et al., 2009). Not only this, but the growing scientific focus on warming-driven changes to biogeochemical variables also necessitates further application of temperature-dependent functions in observational descriptions of oceanic oxygen status (Hofmann and Brewer, 2014). Importantly, as noted by Séférian et al. (2014), D&A techniques can be

used to identify regions of the global ocean where secular changes in ocean variables are likely to be most detectable relative to internal noise, thus informing decisions as to where to target future *in situ* observations. For instance, in the case of open ocean [O_2], the most detectable deoxygenation signal is shown to emerge from the envelope of internal variability in high-latitude regions of water renewal (Chapter 2). As such, this work provides further impetus for the development of co-ordinated marine biogeochemistry observational networks in the Arctic and Southern Ocean (e.g. Southern Ocean Carbon and Climate Observations and Modelling project [SOCCOM; Sarmiento et al., 2014]) in order to better constrain anthropogenic perturbation to the oceanic oxygen inventory. Additionally, the results of Chapter 4 indicate that summer BML [O_2] changes within the central and eastern stratified North Sea could provide a detectable signal of deoxygenation within the coastal zone, warranting further observations of sufficient temporal resolution to detect seasonal [O_2] patterns.

The application of fingerprinting methods to assess the detectability of external signals at regional scales (Stott et al., 2010; Zwiers and Zhang, 2003) and on observed climate change impacts (Rosenzweig and Neofotis, 2013) is a growing area of interest, currently restricted by limited regional model-data capacity and the confounding influences of elevated internal variability and poorly understood (non-climate) drivers (Hegerl and Zwiers, 2011; Hegerl and Stott, 2014). However, as shown in Chapter 4, good observational coverage coupled with regional model fields that reproduce aspects of observed trends and variability suggest that summer BML [O_2] changes in the North Sea may provide a useful case study for regional D&A. Such an analysis would, however, necessitate a coupled ocean-atmosphere model for the North Sea region able to reproduce shelf sea processes, an application for which global models are not currently fit for task (Sect. 4.4; Holt et al., 2009; Holt et al., 2014). Another interesting avenue would be to explore the detectability of changes in the intensity and frequency of extreme hypoxic events, which have been recorded in recent years for the North Sea (e.g. Weston et al., 2008) and are projected to increase in number under future climate forcing (Meire et al., 2013). A statistical framework is currently under development for climate event attribution (Attribution of Climate Related Events group [Stott et al. 2013]), with recent studies successfully applying optimal fingerprinting methods to detect changes temperature and precipitation extremes

(Bindoff et al., 2013).

Nonetheless, work presented in Chapter 2 demonstrates that the capacity already exists, using current model-data resources and fingerprinting methods, to detect statistically significant changes in $[O_2]$ at the global scale in response to external forcing, motivating further efforts to better quantify forced changes in ocean biogeochemistry. To this end, recent work carried out under an optimal detection framework (Séférian et al., 2014) and using a Time of Emergence (ToE) SNR approach (Keller et al., 2014b; Mora et al., 2013) suggests that anthropogenic influences on the surface ocean carbon cycle are already detected above internal variability.

5.2.2 Model-data agreement

D&A methods applied to CMIP5 ESMs in Chapter 2 and trend estimates calculated for the GETM-ERSEM regional model in Chapter 4 show that ocean biogeochemistry models at both global and regional scales systematically underestimate observed deoxygenation over the last ~ 50 years. As discussed in Section 3.1, the inadequate representation of various physical and biogeochemical processes in current models has been widely posited in the literature as a likely source of error, motivating the PlankTOM10-NEMO3.1 sensitivity study presented in Chapter 3. Of particular importance to the simulation of historical changes in $[O_2]$ are possible carbon cycle feedbacks associated with ocean acidification (*cf.* Matear and Lenton, 2014), particularly the impact of a pCO_2-sensitive C:N ratio in the photosynthetic fixation of organic carbon. To this end, the inclusion of stoichiometric effects in the PlankTOM10-NEMO3.1 ocean biogeochemistry model was shown in Section 3.4.1 to amplify historical zonal mean $[O_2]$ decreases by up to $10\,\mu\text{mol}\,\text{L}^{-1}$ between the 1950s and 2000s due to the enhanced export flux of organic carbon to the ocean interior. Therefore, if the historical impact of a pCO_2-sensitive C:N ratio were to be incorporated into historical deoxygenation estimates provided by the fixed stoichiometry ESM (Chapter 2) the model underestimation of observed $[O_2]$ decreases would reduce markedly. This supposition, however, assumes equivalent behaviour between CMIP5 ESM biogeochemistry sub-models and PlankTOM10 in terms of the stoichiometric response to elevated pCO_2 – an assumption which may be appropriate given that current model parameterisations are based on the inclusion of a simple observationally-derived

"CO_2 sensitivity" factor (Riebesell et al., 2007; Oschlies et al., 2008; Tagliabue et al., 2011). Accordingly, the results of this thesis suggest that accounting for stoichiometric effects within the next generation of IPCC-class ESMs could yield improvements in terms of reproducing observed historical deoxygenation at mid- to high latitudes.

However, in agreement with the EMIC sensitivity study of Stramma et al. (2012a), inclusion of stoichiometric effects did not produce a net deoxygenation of the tropical thermocline, which is required to reconcile ESMs (Cocco et al., 2013; Bopp et al., 2013) with observations (Stramma et al., 2008). In the light of persistent and irresolute tropical [O_2] biases within current ESMs one intriguing possibility is that coupled model responses may be mechanistically correct but out of phase with observed multidecadal patterns of internal variability over the historical period. This assertion is based on two lines of evidence brought to the fore by recent model-data analyses. First, Deutsch et al. (2014) reconstruct variations in the extent of North Pacific anoxia using a geochemical proxy for integrated denitrification rates (δ^{15}N) obtained from sediment core data extended back to $\sim$ 1850. This sedimentary δ^{15}N record for the eastern tropical North Pacific indicates that, consistent with recent observations (Stramma et al., 2008), the North Pacific OMZ has expanded since $\sim$ 1990, however this expansion was preceded by a longer term contraction throughout much of the 20^{th} century – such that the current spatial extent of the North Pacific OMZ is not without precedent over the last $\sim$ 150 years. Deutsch et al. (2014) show using climate model data and reanalysis products that, in agreement with Ridder and England (2014) and results presented in Chapter 3, the spatial extent of low-O_2 water over the historical period is modulated by the strength of equatorial trade winds. Specifically, weakening low-latitude wind stress causes a reduction in the wind-driven upwelling of nutrient rich waters such that biological activity and associated oxygen consumption rates decrease, causing a net oxygenation within eastern boundary shadow zones. Thus, the recent expansion of OMZ waters in the equatorial North Pacific (since $\sim$ 1990) can be explained by the pronounced strengthening of trade winds over the same period. However, as reported by England et al. (2014), recent intensification of easterly surface wind stress over the tropical Pacific is not well captured by recent coupled climate models, since this feature is a manifestation of a strongly negative Interdecadal Pacific Oscillation and coupled models do not reproduce the phasing of natural internal variability. Indeed, some

CMIP5 models predict a small weakening of eastern trade winds over the last 20 years, such that coeval OMZ contraction as simulated by many ESMs could be explained by an erroneous periodicity of wind forcing rather than lacking model processes. As such, future ESM studies should focus on initialised decadal hindcasts (Meehl and Teng, 2012) and data assimilation methods (e.g. Guemas et al., 2013) in order to investigate absolute changes in $[O_2]$ over the last 20 years, making use of the range of atmospheric data products presented in Chapter 3. However, the timescales over which wind-driven forcing associated with trade wind dynamics will dominate tropical OMZ extent relative to the impact of solubility and ventilation effects associated with historical and future ocean warming remains uncertain.

Finally, whilst further process-level understanding of the spatiotemporal distribution of oceanic oxygen will improve model-data agreement, the robust statistical treatment of remaining model error, particularly within D&A studies (Hegerl and Zwiers, 2011), remains important. In Chapter 2, as discussed in Section 5.1, a standard residual consistency F-test (Allen and Tett, 1999) is employed which checks for adequate model-data agreement and identifies possible structural errors. However, a possible extension to this method would be to apply an Error in Variables (EIV) optimal detection technique (Huntingford et al., 2006), which explicitly accounts for inter-model error as an additional uncertainty in the optimal detection regression. Moreover, Hannart et al. (2014) extend this methodology to formalise an "easily implementable" statistical inference procedure based on the likelihood maximisation approach of EIV. Nonetheless, 'perfect model' assumptions, which explicitly disregard structural model error, are commonplace in optimal fingerprinting (TLS; Allen and Stott, 2003) and signal-to-noise studies, and remain central to policy relevant D&A assessments and hypothesis testing. Moreover, as shown in Chapter 4, perfect model assumptions can also inform model development needs. Specifically, using a 'potential SNR' formulation (Hawkins and Sutton, 2009) for summer BML temperature and $[O_2]$ alongside a traditional SNR it was possible to identify areas of the greater North Sea where model error, as opposed to internal variability, precludes detectable changes in simulated properties.

5.3 Wider perspectives

This thesis contributes to a growing body of scientific evidence highlighting the current (Rhein et al., 2013; Bindoff et al., 2013) and projected future (Ciais et al., 2013) extent of ocean oxygen depletion driven by secular warming. Anthropogenic perturbation to the oxygen inventory of the global ocean poses a major risk to marine communities due to the increased exposure of aerobic organisms to hypoxic conditions (Vaquer-Sunyer & Duarte 2008) and associated habitat restriction (e.g. Stramma et al., 2012b). Of particular significance for marine ecosystems is the shoaling and expansion of established OMZs (Gilly et al., 2013), which will cause decreases in biodiversity (Gooday et al., 2010) and abundance losses for [O_2]-sensitive groups such as mesopelagic and epipelagic fishes, amongst many other taxa (*cf.* Pörtner et al., 2014). As a result, the IPCC caution in Working Group 2 of AR5 that ocean deoxygenation associated with climate warming is very likely to increase the vulnerability of fisheries and aquaculture – particularly within eastern boundary upwelling zones and semi-enclosed seas (Hoegh-Guldberg et al., 2014). This statement is supported by model studies which find the combined effects of ocean deoxygenation, ocean warming and acidification to drive reductions in the body size (Cheung et al., 2013) and catch potential (Cheung et al., 2011) of exploited demersal fish and invertebrates. Indeed, the potential for synergistic effects between multiple ocean stressors, or the so-called "triple whammy" of deoxygenation, warming and acidification (Gruber, 2011), has further implications for the vulnerability of marine ecosystems to global change (e.g. Brewer and Pelzer, 2009) such that these effects such should not be considered in isolation (Doney, 2010). To this end, ecosystem-based adaption in fisheries management is required to improve the resilience of species and habitats to future climate change and safeguard coastal livelihoods, food resources and other valuable marine ecosystem services (Ruckelshaus et al., 2013). For instance, Micheli et al. (2012) show, for the Baja California region, that the establishment of marine protected areas has increased local resilience within benthic invertebrate communities to mass mortality events caused by episodic hypoxia.

Aside from climate impacts and adaptation, further understanding of oceanic oxygen is also useful in informing the debate around climate change mitigation. Firstly, as discussed elsewhere (e.g. Section 1.2.1), observed and on-going expansion of low-O_2 waters is likely

to affect the biogeochemical cycles of redox-sensitive elements, potentially increasing the role of the ocean as a net source of climatically important gases like N_2O and CH_4 to the atmosphere (e.g. Bakker et al., 2014). In the Gaian sense (Lovelock, 1979), this process constitutes a potential "positive feedback" within the Earth System, whereby warming-driven ocean deoxygenation increases the marine production of greenhouse gases, promoting further warming. However, the form, magnitude and sensitivity of this effect to persistent O_2 depletion remain uncertain. Additionally, recent evaluations of different climate geoengineering proposals have included an assessment of the associated impact on ocean oxygen dynamics as a "side affect" of Carbon Dioxide Reduction (CDR) based methods within the marine realm. For instance, Keller et al. (2014a) show, using idealised EMIC experiments which include artificial ocean upwelling and iron fertilization climate engineering, that subsurface ocean deoxygenation intensifies under both experiments, with enhanced suboxia in eastern boundary systems and for the Southern Ocean, respectively. Indeed, as argued by Bauman et al. (2014), the net benefits of proposed enhanced upwelling as a geoengineering option must be balanced carefully against the associated long-term impact of enhanced productivity, acidification and deoxygenation on marine ecosystems. Finally, Cao et al. (2014) show, using prognostic model experiments, that continued uncertainties around equilibrium climate sensitivity (1.5°C – 4.5°C [*high confidence*; IPCC, 2013]) have a major impact on projected ocean deoxygenation due its tight coupling to ocean temperature. As a result, for the year 2500, each degree of increase in climate sensitivity causes a further 5 % simulated reduction in global mean $[O_2]$. Thus, the detection of forced responses in climate sensitive tracers like oceanic oxygen, as presented in this thesis, can enable observationalists and modellers to better characterise fundamental properties of the climate system and their implications for future warming.

Overall, this thesis has contributed to improve our quantitative understanding of the interactions between climate change and oceanic oxygen. The results, taken together, support the potential utility of oceanic ocean as a bellwether indicator of "dangerous anthropogenic interference with the climate system" (*cf.* UNFCC, 1992), owing to its sensitivity to external forcing on decadal to centennial timescales, and the deleterious implications for marine ecosystems and coastal communities of continued ocean deoxygenation. However, many uncertainties remain – particularly regarding the competing roles of buoyancy forcing and

regional wind dynamics in modulating [O_2] changes, and the confounding influence of (under-sampled) long-period variability in detecting climate signals. Thus, as highlighted by Keeling et al. (2010), a "critical first step" in our understanding of oxygen dynamics in a warming world is the development of models at regional and global scales with the capacity to reproduce observed trends and variability. Accordingly, of the many further research directions that could be explored, it is suggested here that continued efforts to improve model-data agreement in O_2 at the process level are required, drawing upon the growing availability of high-quality observations and high-complexity ESMs. Using this approach it will be possible to garner a mechanistic understanding of observed changes in oceanic oxygen towards improved predictions of future change.

References

Allen, M. R. and Stott, P. A.: Estimating signal amplitudes in optimal fingerprinting, Part I: Theory, Clim. Dynam., 21, 477–491, 2003.

Allen, M. R. and Tett, S. F. B.: Checking for model consistency in optimal ngerprinting, Clim. Dynam., 15, 419–434, 1999.

Andreev, A. G., and Baturina, V. I.: Impacts of tides and atmospheric forcing variability on dissolved oxygen in the subarctic North Pacific, J. Geophys. Res., 111, C07S10, doi:10.1029/2005JC003103, 2006.

Andrews, O. D., Bindoff, N. L., Halloran, P. R., Ilyina, T., and Le Quéré, C.: Detecting an external influence on recent changes in oceanic oxygen using an optimal fingerprinting method, Biogeosciences, 10, 1799-1813, doi:10.5194/bg-10-1799-2013, 2013.

Antonov, J. I., Locarnini, R. A., Boyer, T. P., Mishonov, A. V., and Garcia, H. E.: World Ocean Atlas 2005, Vol. 2: Salinity, edited by: Levitus, S.,. NOAA Atlas NESDIS 62, US Government Printing Office, Washington, DC, 182 pp., 2006.

Armstrong, R. A., Lee, C., Hedges, J. I., Honjo, S., and Wakeham, S. G.: A new, mechanistic model for organic carbon uxes in the ocean: based on the quantitative association of POC with ballast minerals, Deep-Sea Res. II, 49, 219–236, 2002.

Artioli, Y., Blackford, J. C., Butenschon, M., Holt, J. T., Wakelin, S. L., Thomas, H., Borges, A. V., and Allen, J. I.: The carbonate system in the North Sea: Sensitivity and model validation, J. Mar. Syst., 102–104, 1–13, 2012.

Bakker, D. C. E., Bange, H. W., Borges, A. V., Delille, B., Gruber, N., Johannessen, T., Löscher, C., Naqvi, S. W. A., Omar, A. M., Santana-Casiano, J. M., and Upstill-Goddard, R. C.: Air-sea interactions of natural long-lived greenhouse gases (CO_2, N_2O, CH_4) in a changing climate, in: Ocean-Atmosphere Interactions of Gases

and Particles, edited by: Liss, P. S. and Johnson, M. T., Springer, Berlin, 113–169, 2014a.

Bakker, D. C. E., Pfeil, B., Smith, K., Hankin, S., Olsen, A., Alin, S. R., Cosca, C., Harasawa, S., Kozyr, A., Nojiri, Y., O'Brien, K. M., Schuster, U., Telszewski, M., Tilbrook, B., Wada, C., Akl, J., Barbero, L., Bates, N. R., Boutin, J., Bozec, Y., Cai, W.-J., Castle, R. D., Chavez, F. P., Chen, L., Chierici, M., Currie, K., de Baar, H. J. W., Evans, W., Feely, R. A., Fransson, A., Gao, Z., Hales, B., Hardman-Mountford, N. J., Hoppema, M., Huang, W.-J., Hunt, C. W., Huss, B., Ichikawa, T., Johannessen, T., Jones, E. M., Jones, S. D., Jutterström, S., Kitidis, V., Körtzinger, A., Landschützer, P., Lauvset, S. K., Lefèvre, N., Manke, A. B., Mathis, J. T., Merlivat, L., Metzl, N., Murata, A., Newberger, T., Omar, A. M., Ono, T., Park, G.-H., Paterson, K., Pierrot, D., Ríos, A. F., Sabine, C. L., Saito, S., Salisbury, J., Sarma, V. V. S. S., Schlitzer, R., Sieger, R., Skjelvan, I., Steinhoff, T., Sullivan, K. F., Sun, H., Sutton, A. J., Suzuki, T., Sweeney, C., Takahashi, T., Tjiputra, J., Tsurushima, N., van Heuven, S. M. A. C., Vandemark, D., Vlahos, P., Wallace, D. W. R., Wanninkhof, R., and Watson, A. J.: An update to the Surface Ocean CO_2 Atlas (SOCAT version 2), Earth Syst. Sci. Data, 6, 69-90, doi:10.5194/essd-6-69-2014, 2014b.

Banks, H. T. and Bindoff, N. L.: Comparison of Observed Temperature and Salinity Changes in the Indo-Pacific with Results from the Coupled Climate Model HadCM3: Processes and Mechanisms, J. Climate, 16, 156–166, 2003.

Banks, H. T. and Wood, R. A.: Where to look for anthropogenic climate change in the ocean, J. Climate, 15, 879–891, 2002.

Baretta, J., Ebenhoh, W., and Ruardij, P.: The European Regional Seas Ecosystem Model, a complex marine ecosystem model, J. Sea Res., 33, 233–246, 1995.

Barnett, T. P., Pierce, D. W., AchutaRao, K. M., Gleckler, P. J., Santer, B. D., Gregory, J. M., and Washington, W. M.: Penetration of Human-Induced Warming into the World's Oceans, Science, 309, 284–287, doi:10.1126/science.1112418, 2005.

Bauman, S.J., Costa, M. T., Fong, M. B., House, B. M., Perez, E. M., Tan, M. H., Thornton, A. E., and Franks, P. J. S.: Augmenting the biological pump: The shortcomings of geoengineered upwelling, Oceanography 27, 17–23, http://dx.doi.org/10.5670/oceanog.2014.79,

2014.

Beaulieu, C., Henson, S. A., Sarmiento, J. L., Dunne, J. P., Doney, S. C., Rykaczewski, R. R., and Bopp, L.: Factors challenging our ability to detect long-term trends in ocean chlorophyll, Biogeosciences, 10, 2711-2724, doi:10.5194/bg-10-2711-2013, 2013.

Belkin, I. M.: Rapid warming of large marine ecosystems, Prog. Oceanogr., 81, 207–213, doi:10.1016/j.pocean.2009.04.011, 2009.

Bellerby, R. G. J., Schulz, K. G., Riebesell, U., Neill, C., Nondal, G., Heegaard, E., Johannessen, T., and Brown, K. R.: Marine ecosystem community carbon and nutrient uptake stoichiometry under varying ocean acidification during the PeECE III experiment, Biogeosciences, 5, 1517-1527, doi:10.5194/bg-5-1517-2008, 2008.

Berx, B., and Hughes, S. L.: Climatology of Surface and Near-bed Temperature and Salinity on the North-West European Continental Shelf for 1971-2000, Cont. Shelf Res., 29, 2286-2292, doi:10.1016/j.csr.2009.09.006, 2009.

Bianchi, D., Dunne, J. P., Sarmiento, J. L., and Galbraith, E. D.: Data-based estimates of suboxia, denitrication, and N_2O production in the ocean and their sensitivities to dissolved O_2, Global Biogeochem. Cy., 26, GB2009, doi:201210.1029/2011GB004209, 2012.

Bindoff, N.L. and Wunsch, C.: Comparison of Synoptic and Climatologically Mapped Sections in the South Pacific Ocean, J. Climate, 5, 631–645, 1992.

Bindoff, N., Willebrand, J., Artale, V., Cazenave, A., Gregory, J., Gulev, S., Hanawa, K., Le Quéré, C., Levitus, S., Norjiri, Y., Shum, C., Talley, L., and Unnikrishnan, A.: Observations: oceanic climate change and sea level, in: Climate Change 2007: The Physical Science Basis, Contribution of Working Group I to the Fourth Assessment Report of the Intergovernmental Panel on Climate Change, edited by: Solomon, S., Qin, D., Manning, M., Chen, Z., Marquis, M., Averyt, K. B., Tignor, M., and Miller, H. L., Tech. Rep., Intergovernmental Panel on Climate Change, Cambridge University Press, Cambridge, United Kingdom and New York, NY, USA, 2007.

Bindoff, N.L., Stott, P.A., AchutaRao, K. M., Allen, M. R., Gillett, N., Gutzler, D., Hansingo, K., Hegerl, G., Hu, Y., Jain, S., Mokhov, I. I., Overland, J., Perlwitz, J., Sebbari, R., and Zhang, X.: Detection and attribution of climate change: From

global to regional, in: Climate Change 2013: The Physical Science Basis. Contribution of Working Group I to the Fifth Assessment Report of the Intergovernmental Panel on Climate Change, edited by: Stocker, T. F., Qin, D., Plattner, G.- K., Tignor, M., Allen, S. K., Boschung, J., Nauels, A., Xia, Y., Bex, V., and Midgley, P. M., Cambridge University Press, Cambridge, UK and New York, NY, USA, 2013.

Blackford, J. C., Allen, J. I., and Gilbert, F. J.: Ecosystem dynamics at six contrasting sites: a generic modelling study, J. Marine Syst., 52, 191–215, 2004.

Bograd, S. J., Castro, C. G., Di Lorenzo, E., Palacios, D. M., Bailey, H., Gilly, W., and Chavez, F. P.: Oxygen declines and shoaling of the hypoxic boundary in the California Current, Geophys. Res. Lett., 35, L12607, doi:10.1029/2008GL034185, 2008.

Böning, C. W., Dispert, A., Visbeck, M., Rintoul, S. R., and Schwarzkopf, F. U.: The response of the Antarctic Circumpolar Current to recent climate change, Nat. Geosci., 1, 864–869, doi:10.1038/ngeo362, 2008.

Bopp, L., Monfray, P., Aumont, O., Dufresne, J. L., Le Treut, H., Madec, G., Terray, L., and Orr, J. C.: Potential impact of climate change on marine export production, Global Biogeochem. Cy., 15, 81–99, 2001.

Bopp, L., Le Quéré, C., Heimann, M., Manning, A. C., and Monfray, P.: Climate-induced oceanic oxygen uxes: Implications for the contemporary budget, Glob. Biogeochem. Cy., 16, 1022, doi:10.1029/2001GB001445, 2002.

Bopp, L., Resplandy, L., Orr, J. C., Doney, S. C., Dunne, J. P., Gehlen, M., Halloran, P., Heinze, C., Ilyina, T., Séférian, R., Tjiputra, J., and Vichi, M.: Multiple stressors of ocean ecosystems in the 21^{st} century: projections with CMIP5 models, Biogeosciences, 10, 6225-6245, doi:10.5194/bg-10-6225-2013, 2013.

Borja, A., Elliott, M., Carstensen, J., Heiskanen, A. S., van de Bund, W.: Marine management – Towards an integrated implementation of the European Marine Strategy Framework and the Water Framework Directives, Mar. Pollut. Bull., 60, 2175–2186, 2010.

Boyce, D. G., Lewis, M. R., and Worm, B.: Global phytoplankton decline over the past century, Nature, 466, 591–596, doi:10.1038/nature09268, 2010.

Boyer, T. P., Antonov, J. I., Baranova, O. K., Garcia, H. E., Johnson, D. R., Locarnini, R.

A., Mishonov, A. V., O'Brien, T. D., Seidov, D., Smolyar, I. V., and Zweng, M. M.: World Ocean Database 2009, edited by: Levitus, S., NOAA Atlas NESDIS 66, US Gov. Printing Ofce, Washington, DC, 216 pp., DVDs, 2009.

Brandt, P., Hormann, V., Körtzinger, A., Visbeck, M., Krahmann, G., and Stramma, L.: Changes in the Ventilation of the Oxygen Minimum Zone of the Tropical North Atlantic, J. Phys. Oceanogr., 40, 1784–1801, doi:http://dx.doi.org/10.1175/2010JPO4301.1, 2010.

Brennan, C. E., Matear, R. J., and Keller, K.: Measuring oxygen concentrations to improve the detection capabilities of an ocean circulation observation array, J. Geophys. Res., 113, C01019, doi:10.1029/2007JC004113, 2008.

Brewer, P. G., and Hofmann, A. F.: A plea for temperature in descriptions of the oceanic oxygen status, Oceanography, 27, 160-167, 2014.

Brewer, P. G. and Peltzer, E. T.: Limits to marine life, Science, 324, 347–348, 2009.

Brodeau, L., Barnier, B., Penduff, T., Treguier, A.-M., and Gulev, S.: An ERA 40 based atmospheric forcing for global ocean circulation models, Ocean Modell., 31, 88–104, 2010.

Buitenhuis, E. T., van der Wal, P., and de Baar, H.: Blooms of *Emiliania huxleyi* are sinks of atmospheric carbon dioxide: A field and mesocosm study derived simulation, Global Biogeochem. Cy., 15, 577–587, doi:10.1029/2000GB001292, 2001.

Buitenhuis, E. T., Rivkin, R. B., Sailley, S., and Le Quéré, C.: Biogeochemical fluxes through microzooplankton, Global Biogeochem. Cy., 24, GB4015, doi:10.1029/2009GB003601, 2010.

Buitenhuis, E. T., Hashioka, T., and Le Quéré, C.: Combined constraints on global ocean primary production using observations and models, Global Biogeochem. Cy., 27, 847–858, doi:10.1002/gbc.20074, 2013.

Burchard, H. and Bolding, K.: GETM – A general estuarine transport model, Scientific documentation (Technical report No. EUR 20253 EN), European Commission, 2002.

Capotondi, A., Alexander, M. A., Bond, N. A., Curchitser, E. N., and Scott, J. D.: Enhanced upper ocean stratication with climate change in the CMIP3 models, J. Geophys. Res.-Oceans, 117, C04031, doi:10.1029/2011JC007409, 2012.

Cao, L., Wang, S., Zheng, M., and Zhang, H.: Sensitivity of ocean acidification and oxygen to the uncertainty in climate change. Environ. Res, Lett., 9, 064005, doi:10.1088/1748-9326/9/6/064005, 2014.

Cardoso, A., Cochrane, S., Doemer, H., Ferreira, J., Galgani, F., Hagebro, C., Hanke, G., Hoepffner, N., Keizer, P., Law, R., Olenin, S., Piet, G., Rice, J., Rogers, S., Swartenbroux, F., Tasker, M., and Van de Bund, W.: Scientic Support to the European Commission on the Marine Strategy Framework Directive, 24336, Publications Ofce of the European Union, Luxembourg, 2010.

Carrillo, C. J., Smith, R. C., and Karl, D. M.: Processes regulating oxygen and carbon dioxide in surface waters west of the Antarctic Peninsula, Mar. Chem., 84, 161–179, 2004.

Chan, F., Barth, J. A., Lubchenco, J., Kirincich, A., Weeks, H., Peterson, W. T., and Menge, B. A.: Emergence of anoxia in the California Current large marine ecosystem, Science, 319, 920, 2008.

Charette, M. A., Smith W. H. F.: The volume of Earth's ocean, Oceanography, 23, 112 – 114, 2010.

Chaudhuri, A. H., Ponte, R. M., Forget, G., and Heimbach, P: A comparison of atmospheric reanalysis surface products over the ocean and implications for uncertainties in air–sea boundary forcing, J. Clim, 26, 153–170. doi:http://dx.doi.org/10.1175/JCLI-D-12-00090.1, 2013.

Cheung, W. W. L., Dunne, J., Sarmiento, J., and Pauly, D.: Integrating eco-physiology and plankton dynamics into projected changes in maximum fisheries catch potential under climate change in the northeast Atlantic, ICES J. Mar. Sci., 68, 1008–1018, 2011.

Cheung, W. W. L., Sarmiento, J. L., Dunne, J., Frölicher, T. L., Lam, V. W. Y., Palomares, M. L. D., Watson, R. and Pauly, D.: Shrinking of fishes exacerbates impacts of global ocean changes on marine ecosystems, Nature Clim. Change, 3, 254-258, doi:10.1038/nclimate1691, 2013.

Cheng, W., Chiang, J., and Zhang, D.: Atlantic Meridional Overturning Circulation (AMOC) in CMIP5 models: RCP and Historical Simulations, J. Climate, 26, 7187–7197, doi:10.1175/JCLID-12-00496.1, 2013.

Church, J., White, N., Konikow, L., Domingues, C., Cogley, J., Rignot, E., Gregory, J., van den Broeke, M., Monaghan, A., and Velicogna, I.: Revisiting the Earth's sea-level and energy budgets from 1961 to 2008, Geophys. Res. Lett., 38, L18601, doi:10.1029/2011GL048794, 2011.

Ciais, P., Sabine, C., Bala, G., Bopp, L., Brovkin, V., Canadell, J., Chhabra, A., DeFries, R., Galloway, J., Heimann, M., Jones, C., Le Quéré, C., Myneni, R. B., Piao, S., and Thornton, P.: Carbon and Other Biogeochemical Cycles, in Climate Change 2013: The Physical Science Basis. Contribution of Working Group I to the Fifth Assessment Report of the Intergovernmental Panel on Climate Change, edited by: T. F. Stocker, Qin, D., Plattner, G.-K., Tignor, M., Allen, S. K., Boschung, J., Nauels, A., Xia, Y., Bex, V., and Midgley, P. M., Cambridge University Press, Cambridge, United Kingdom and New York, NY, USA, 2013.

Cocco, V., Joos, F., Steinacher, M., Frölicher, T. L., Bopp, L., Dunne, J., Gehlen, M., Heinze, C., Orr, J., Oschlies, A., Schneider, B., Segschneider, J., and Tjiputra, J.: Oxygen and indicators of stress for marine life in multi-model global warming projections, Biogeosciences, 10, 1849-1868, doi:10.5194/bg-10-1849-2013, 2013.

Codispoti, L. A.: Interesting times for marine N_2O, Science, 327, 1339–1340, 2010.

Codispoti, L. A. and Christensen, J. P.: Nitrication, Denitrication and nitrous oxide cycling in the eastern tropical South Pacic Ocean, Mar. Chem., 16, 277–300, 1985.

Colijn, F., Hesse, K., Ladwig, N., and Tillman, U.: Effects of the large-scale uncontrolled fertilisation process along the continental coastal North Sea, Hydrobiologia, 484, 133–148, doi:10.1023/A:1021361206529, 2002.

Collins, W. J., Bellouin, N., Doutriaux-Boucher, M., Gedney, N., Halloran, P., Hinton, T., Hughes, J., Jones, C. D., Joshi, M., Liddicoat, S., Martin, G., O'Connor, F., Rae, J., Senior, C., Sitch, S., Totterdell, I., Wiltshire, A., and Woodward, S.: Development and evaluation of an Earth-System model – HadGEM2, Geosci. Model Dev., 4, 1051–1075, doi:10.5194/gmd-4-1051-2011, 2011.

Cummins, P. F., and Masson, D.: Wind-driven variability of dissolved oxygen below the mixed layer at Station P, K. Geophys. Res., 117, C08015, doi:10.1029/2011JC007847, 2012.

Crutzen, P. J.: Geology of mankind, Nature, 415, 23, 2002.

Crutzen, P. J. and Stoermer, E. F.: The “Anthropocene”, Global Change Newsletter, 41, 17–18, 2000.

Curry, R.: HydroBase3, http://www.whoi.edu/science/PO/hydrobase/, 2008.

da Cunha, L. C. and Buitenhuis, E. T.: Riverine influence on the tropical Atlantic Ocean biogeochemistry, Biogeosciences, 10, 6357-6373, doi:10.5194/bg-10-6357-2013, 2013.

Dave, A. C.: Correction to “Examining the global record of interannual variability in stratification and marine productivity in the low- and mid-latitude ocean”, J. Geophys. Res. Oceans, 119, 2121-2128, doi:10.1002/2013JC009823, 2014.

Dave, A. C., and Lozier, M. S.: Examining the global record of interannual variability in stratification and marine productivity in the low-latitude and mid-latitude ocean, J. Geophys. Res. Oceans, 118, 3114-3127, doi:10.1002/jgrc.20224, 2013.

Danabasoglu, G., Yeager, S. G., Bailey, D., Behrens, E., Bentsen, M., Bi, D., Biastoch, A., Böning, C., Bozec, A., Canuto, V. M., Cassou, C., Chassignet, E., Coward, A. C., Danilov, S., Diansky, N., Drange, H., Farneti, R., Fernandez, E., Fogli, P. G., Forget, G., Fujii, Y., Griffies, S. M., Gusev, A., Heimbach, P., Howard, A., Jung, T., Kelley, M., Large,W. G., Leboissetier, A., Lu, J., Madec, G., Marsland, S. J., Masina, S., Navarra, A., George Nurser, A. J., Pirani, A., y Mélia, D. S., Samuels, B. L., Scheinert, M., Sidorenko, D., Treguier, A.-M., Tsujino, H., Uotila, P., Valcke, S., Voldoire, A., and Wang, Q.: North Atlantic simulations in coordinated ocean-ice reference experiments phase II (CORE-II), Part I: Mean states, Ocean Model., 73, 76–107, doi:10.1016/j.ocemod.2013.10.005, 2014.

Deser, C., Phillips, A. Bourdette, V., and Teng, H.: Uncertainty in climate change projections: the role of internal variability, Clim. Dynam., 38, 527–546, doi:10.1007/s00382-010-0977-x, 2012.

Deutsch, C., Emerson, S., and Thompson, L.: Fingerprints of climate change in North Pacic oxygen, Geophys. Res. Lett., 32, L16604, doi:10.1029/2005GL023190, 2005.

Deutsch, C., Emerson, S., and Thompson, L.: Physical-biological interactions in North Pacific oxygen variability, J. Geophys. Res., 111, C09S90, doi:10.1029/2005JC003179, 2006.

Deutsch, C., Brix, H., Ito, T., Frenzel, H., and Thompson, L.: Climate-forced variability of ocean hypoxia, Science, 333, 336–339, 2011.

Deutsch, C., Berelson, W., Thunell, R., Weber, T., Tems, C., McManus, J., Crusius, J., Ito, T., Baumgartner, T., Ferreira, V., Mey, J., and van Geen, A.: Centennial changes in North Pacific anoxia linked to tropical trade winds, Science, 345, 665, 10.1126/science.1252332, 2014.

Diaz, R. J. and Rosenberg, R.: Spreading dead zones and consequences for marine ecosystems, Science, 321, 926–929, doi:10.1126/science.1156401, 2008.

Doney, S. C.: The growing human footprint on coastal and open ocean biogeochemistry, Science, 328, 1512–1516, 2010.

Doney, S. C., Fabry, V. J., Feely, R. A., and Kleypas, J. A.: Ocean acidication: the other CO_2 problem, Ann. Rev. Mar. Sci., 1, 169–192, doi:10.1146/annurev.marine.010908.163834, 2009.

Doney, S. C., Ruckelshaus, M., Duffy, J. E., Barry, J. P., Chan, F., English, C. A., Galindo, H. M., Grebmeier, J. M., Hollowed, A. B., Knowlton, N., Polovina. J., Rabalais, N. N., Sydeman, W. J., and Talley, L. D.: Climate change impacts on marine ecosystems, Annu. Rev. Mar. Sci., 4, 4.1–4.27, doi:10.1146/annurev-marine-041911-111611, 2012.

Doney, S.C., Bopp, L., and Long, M. C.: Historical and future trends in ocean climate and biogeochemistry, Oceanography, 2, 108–119, http://dx.doi.org/10.5670/oceanog.2014.14, 2014.

Downes, S. M., Bindoff, N. L., and Rintoul, S. R.: Changes in the Subduction of Southern Ocean Water Masses at the End of the Twenty-First Century in Eight IPCC Models, J. Climate, 23, 6526–6541, doi: http://dx.doi.org/10.1175/2010JCLI3620.1, 2010.

Dunne, J. P., John, J., Shevliakova, E., Stouff er, R., Krasting, J., Malyshev, S., Milly, P., Sentman, L., Adcroft, A., Cooke, W., Dunne, K., Griffies, S., Hallberg, R., Harrison, M., Levy, H., Wittenberg, A., Phillips, P. and Zadeh, N.: GFDL's ESM2 global coupled climate-carbon Earth System Models Part II: carbon system formulation and baseline simulation characteristics, J. Climate, doi:10.1175/JCLI-D-12-00150.1, 2013.

Dunstone, N. J.: A perspective on sustained marine observations for climate modeling and

predictions, Phil. Trans. R. Soc. A., 372, 20130340, doi: 10.1098/rsta.2013.0340, 2014.

Durack, P. J. and Wijffels, S. E.: Fifty-Year Trends in Global Ocean Salinities and Their Relationship to Broad-Scale Warming, J. Climate, 23, 4342–4362, doi:10.1175/2010JCLI3377.1, 2010.

Durack, P. J., Wijffels, S. E., and Matear, R. J.: Ocean Salinities Reveal Strong Global Water Cycle Intensification During 1950 to 2000, Science, 336, 455–458, doi:10.1126/science.1212222, 2012.

Duteil, O. and Oschlies, A.: Sensitivity of simulated extent and future evolution of marine suboxia to mixing intensity, Geophys. Res. Lett., 38, L06607, doi:10.1029/2011GL046877, 2011.

Duteil, O., Koeve, W., Oschlies, A., Bianchi, D., Galbraith, E., Kriest, I., and Matear, R.: A novel estimate of ocean oxygen utilisation points to a reduced rate of respiration in the ocean interior, Biogeosciences, 10, 7723-7738, doi:10.5194/bg-10-7723-2013, 2013.

Duteil, O., Schwarzkopf, F. U., Böning, C. W., and Oschlies, A.: Major role of the equatorial current system in setting oxygen levels the eastern tropical Atlantic Ocean: A high-resolution model study, Geophys. Res. Lett., 41, 2033 – 2040, doi:10.1002/2013GL058888, 2014.

Edwards, K. P., Barciela, R., and Butenschön, M.: Validation of the NEMO-ERSEM operational ecosystem model for the North West European Continental Shelf, Ocean Sci., 8, 983-1000, doi:10.5194/os-8-983-2012, 2012.

Emerson, S., Watanabe, Y., Ono, T., and Mecking, S.: Temporal trends in apparent oxygen utilization in the upper pycnocline of the North Pacic: 1980–2000, J. Oceanogr., 60, 139–147, 2004.

England, M. H., McGregor, S., Spence, P., Meehl, G. A., Timmermann, A., Cai, W., Gupta, A. S., McPhaden, M. J., Purich, A., and Santoso, A.: Recent intensification of wind-driven circulation in the Pacific and the ongoing warming hiatus, Nature Clim. Change, 4, 222–227, doi:10.1038/nclimate2106, 2014.

Enright, C., Buitenhuis, E. T., and Le Quéré, C.: Description of the PlankTOM10 equations, available at: `http://lgmacweb.env.uea.ac.uk/green_ocean/`

model/TOM10Appendix_v4.pdf, (last access: 23rd April 2014), 2014.

Falkowski, P. G., Algeo, T., Codispoti, L., Deutsch, C., Emerson, S., Hales, B., Huey, R. B., Jenkins,W. J., Kump, L. R., Levin, L. A., Lyons, T. W., Nelson, N. B., Schofield, O., Summons, R., Talley, L. D., Thomas, E., Whitney, F., and Pilcherm C. B.: Ocean deoxygenation: past, present, and future, Eos Trans. AGU, 92, 409–411, 2011.

Flynn, K. J.: Ecological modelling in a sea of variable stoichiometry: Dysfunctionality and the legacy of Redfield and Monod, Prog. Oceanog., 84, 52–65, 2010.

Frame, C. H. and Casciotti, K. L.: Biogeochemical controls and isotopic signatures of nitrous oxide production by a marine ammonia-oxidizing bacterium, Biogeosciences, 7, 2695–2709, doi:10.5194/bg-7-2695-2010, 2010.

Freing, A., Wallace, D. W. R., and Bange, H. W.: Global oceanic production of nitrous oxide (N_2O), Philos. T. R. Soc. B, 367, 1245–1255, doi:10.1098/rstb.2011.0360, 2012.

Friedrich, T., Oschlies, A., and Eden, C.: Role of wind stress and heat fluxes in interannual-to-decadal variability of air-sea CO_2 and O_2 fluxes in the North Atlantic, Geophys. Res. Lett., 33, L21S04, doi:10.1029/2006GL026538, 2006.

Frölicher, T. L., Joos, F., Plattner, G.-K., Steinacher, M., and Doney, S. C.: Natural variability and anthropogenic trends in oceanic oxygen in a coupled carbon-climate model ensemble, Global Biogeochem. Cy., 23, GB1003, doi:10.1029/2008GB003316, 2009.

Garcia, H. E. and Gordon, L. I.: Oxygen solubility in seawater – better fitting equations, Limnol. Oceanogr., 37, 1307–1312, 1992.

Garcia, H. E., Boyer, T. P., Levitus, S., Locarnini, R. A., and Antonov, J.: On the variability of dissolved oxygen and apparent oxygen utilization content for the upper world ocean: 1955 to 1998, Geophys. Res. Lett., 32, L09604, doi:10.1029/2004GL022286, 2005.

Garcia, H. E., Locarnini, R. A., Boyer, T. P., and Antonov, J. I.: World Ocean Atlas 2005, Volume 3: Dissolved Oxygen, Apparent Oxygen Utilization, and Oxygen Saturation, in: World Ocean Atlas 2005, edited by: Levitus, S., NOAA Atlas NESDIS 62, US Government Printing Office, Washington, DC, pp. 342, 2006a.

Garcia, H. E., Locarnini, R. A., Boyer, T. P., and Antonov, J. I.: World Ocean Atlas

2005, Volume 4: Nutrients (phosphate, nitrate, silicate), in: World Ocean Atlas 2005, edited by Levitus, S., NOAA Atlas NESDIS 64, US Government Printing Office,Washington, DC, pp. 396, 2006b.

Gaspar, P., Grégoris, Y., and Lefevre, J.-M.: A simple eddy kinetic energy model for simulations of the oceanic vertical mixing tests at station papa and long–term upper ocean study site, J. Geophys. Res., 95, 16179–16193, 1990.

Gattuso, J.-P., Frankignoulle, M., and Wollast, R.: Carbon and carbonate metabolism in coastal aquatic ecosystems, Annu. Rev. of Ecol. Syst., 29, 405–434, 1998.

Gent, P. and McWilliams, J.: Isopycnal mixing in ocean circulation models, J. of Phys. Oceanog., 20, 1–6, 1990.

Gilbert, D., Rabalais, N. N., Díaz, R. J., and Zhang, J.: Evidence for greater oxygen decline rates in the coastal ocean than in the open ocean, Biogeosciences, 7, 2283–2296, doi:10.5194/bg-7-2283-2010, 2010.

Gilly, W. F., Beman, J. M., Litvin, S. Y., and Robison, B. H.: Oceanographic and biological effects of shoaling of the oxygen minimum zone, Ann. Rev. Mar. Sci., 5, 393–420, doi:10.1146/annurev-marine-120710-100849, 2013.

Giorgetta, M. A., Jungclaus, J., Reick, C. H., Legutke, S., Bader, J., Böttinger, M., Brovkin, V., Crueger, T., Esch, M., Fieg, K., Glushak, K., Gayler, V., Haak, H., Hollweg, H.-D., Ilyina, T., Kinne, S., Kornblueh, L., Matei, D., Mauritsen, T., Mikolajewicz, U., Mueller, W., Notz, D., Pithan, F., Raddatz, T., Rast, S., Redler, R., Roeckner, E., Schmidt, H., Schnur, R., Segschneider, J., Six, K. D., Stockhause, M., Timmreck, C., Wegner, J., Widmann, H., Wieners, K.-H., Claussen, M., Marotzke, J., and Stevens, B.: Climate and carbon cycle changes from 1850 to 2100 in MPI-ESM simulations for the coupled model intercomparison project phase 5, J. Adv. Model. Earth Syst., 5, 572–597, doi:10.1002/jame.20038, 2013.

Gleckler, P. J., Santer, B. D., Domingues, C. M., Pierce, D. W., Barnett, T. P., Church, J. A., Taylor, K. E., AchutaRao, K. M., Boyer, T. P., Ishii, M., and Caldwell, P. M.: Human-induced global ocean warming on multidecadal timescales, Nature Clim. Change, 2, 524–529, doi:10.1038/nclimate1553, 2012.

Gnanadesikan, A., Russell, J. L., and Zeng, F.: How does ocean ventilation change under global warming?, Ocean Sci., 3, 43–53, doi:10.5194/os-3-43-2007, 2007.

Gnanadesikan, A., Dunne, J. P., and John, J.: Understanding why the volume of suboxic waters does not increase over centuries of global warming in an Earth System Model, Biogeosciences, 9, 1159–1172, doi:10.5194/bg-9-1159-2012, 2012.

Gnanadesikan, A., Bianchi, D., and Pradal, M. A.: Critical role for mesoscale eddy diffusion in supplying oxygen to hypoxic ocean waters, Geophys. Res. Lett., 40, 5194–5198, doi:10.1002/Grl.50998, 2013.

Good, S. A., Corlett, G. K., Remedios, J. J., Noyes, E. J., and Llewellyn-Jones, D. T.: The Global Trend in Sea Surface Temperature from 20 Years of Advanced Very High Resolution Radiometer Data, J. Climate, 20, 1255-1264, 2007.

Gooday, A. J., Bett, B. J., Escobar, E., Ingole, B., Levin, L. A., Neira, C., Raman, A. V., and Sellanes, J.: Habitat heterogeneity and its relationship to biodiversity in oxygen minimum zones, Mar. Ecol., 31, 125–147, 2010.

Goosse, H., Deleersnijder, E., Fichefet, T., and England, M.: Sensitivity of a global coupled ocean-sea ice model to the parameterization of vertical mixing, J. Geophys. Res., 104, 13681–13695, 1999.

Gordon, A. and Huber, B.: Southern ocean mixed layer, J. Geophys. Res.-Oceans, 95, 11655–11672, 1990.

Grantham, B. A., Chan, F., Nielsen, K. J., Fox, D. S., Barth, J. A., Huyer, A., Lubchenco, J., and Menge, B. A.: Upwelling driven near shore hypoxia signals ecosystem and oceanographic changes in the northeast Pacific, Nature, 429, 749–754, doi:10.1038/nature02605, 2004.

Gray, J. S., Wu, R. S. S., and Or, Y. Y.: Effects of hypoxia and organic enrichment on the coastal marine environment, Mar. Ecol.-Prog. Ser., 238, 249–279, 2002.

Greenwood, N., Parker, E. R., Fernand, L., Sivyer, D. B., Weston, K., Painting, S. J., Kröger, S., Forster, R. M., Lees, H. E., Mills, D. K., and Laane, R. W. P. M.: Detection of low bottom water oxygen concentrations in the North Sea; implications for monitoring and assessment of ecosystem health, Biogeosciences, 7, 1357-1373, doi:10.5194/bg-7-1357-2010, 2010.

Griffies, S., Biastoch, A., Boening, C., Bryan, F., Danabasoglu, G., Chassignet, E. P., England, M. H., Gerdes, R., Haak, H., Hallberg, R. W., Hazeleger, W., Jungclaus, J., Large, W. G., Madec, G., Pirani, A., Samuels, B. L., Scheinert, M., Sen Gupta,

A., Severijns, C. A., Simmons, H. L., Treguier, A. M., Winton, M., Yeager, S., and Yin, J.: Coordinated ocean-ice reference experiments (COREs), Ocean Model., 26, 1–46, 2009.

Gröger, M., Maier-Reimer, E., Mikolajewicz, U., Moll, A., and Sein, D.: NW European shelf under climate warming: implications for open ocean – shelf exchange, primary production, and carbon absorption, Biogeosciences, 10, 3767-3792, doi:10.5194/bg-10-3767-2013, 2013.

Gruber, N.: The marine nitrogen cycle: overview and challenges, in: Nitrogen in the Marine Environment, edited by: Capone, D. G., Bronk, D. A., Mulholland, M. R., and Carpenter, E. J., Elsevier, Amsterdam, 1–50, 2008.

Gruber, N.: Carbon cycle: Fickle trends in the ocean, Nature, 458, 155–156, 2009.

Gruber, N.: Warming up, turning sour, losing breath: ocean biogeochemistry under global change, Phil. Trans. R. Soc. A, 369, 1980–1996, doi:10.1098/rsta.2011.0003, 2011.

Gruber, N., Doney, S. C., Emerson, S. R., Gilbert, D., Kobayashi, T., Körtzinger, A., Johnson, G. C., Johnson, K. S., Riser, S. C., and Ulloa, O.: Adding oxygen to Argo: Developing a global in-situ observatory for ocean deoxygenation and biogeochemistry, in: Proceedings of the "OceanObs09: Sustained Ocean Observations and Information for Society" Conference (Vol. 2), Venice, Italy, 21–25 September 2009, 1–10, 2010.

Guemas, V., Doblas-Reyes, F. J., Andreu-Burillo, I., and Asif, M.: Retrospective prediction of the global warming slowdown in the past decade, Nature Clim. Change, 3, 649–653, doi:10.1038/nclimate1863, 2013.

Hannart, A., Ribes, A. and Naveau, P.: Optimal fingerprinting under multiple sources of uncertainty, Geophys. Res. Lett., 41, 1261–1268, doi:10.1002/2013GL058653, 2014.

Hansen, J., Russell, G., Lacis, A., Fung, I., Rind, D., and Stone, P.: Climate response times: dependence on climate sensitivity and ocean mixing, Science, 229, 857–859, 1985.

Hartmann, D. L., Klein Tank, A. M. G., Rusticucci, M., Alexander, L. V., Brönnimann, S., Charabi, Y., Dentener, F. J., Dlugokencky, E. J., Easterling, D. R., Kaplan, A., Soden, B. J., Thorne, P. W., Wild, M., and Zhai, P. M.: Observations: Atmosphere

and Surface. in: Climate Change 2013: The Physical Science Basis. Contribution of Working Group I to the Fifth Assessment Report of the Intergovernmental Panel on Climate Change, edited by: Stocker, T. F., Qin, D., Plattner, G.-K., Tignor, M., Allen, S. K., Boschung, J., Nauels, A., Xia, Y., Bex, V., and Midgley, P. M., Cambridge University Press, Cambridge, UK and New York, NY, USA, 2013.

Hasselmann, K.: Stochastic climate models. 1. Theory, Tellus, 28, 473–485, 1976.

Hasselmann, K.: Multi-pattern ngerprint method for detection and attribution of climate change, Clim. Dynam., 13, 601–612, 1997.

Hawkins, E. and Sutton, R. T.: The potential to narrow uncertainties in regional climate predictions, B. Am. Meteorol. Soc., 90, 1095–1107, doi:10.1175/2009BAMS2607.1171, 2009.

Hawkins, E. and Sutton, R. T.: The potential to narrow uncertainty in projections of regional precipitation change, Clim. Dynam., 37, 407–418, doi:10.1007/s00382-010-0810-6, 2011.

Hegerl, G. C., and Stott.: P. A.: From Past to Future Warming, Science, 343, 844–845, doi:10.1126/science.1249368, 2014.

Hegerl, G. C. and Zwiers, F.: Use of models in detection and attribution of climate change, WIREs Clim. Change, 2, 570–591, doi:10.1002/wcc.121, 2011.

Hegerl, G.C., von Storch, H., Hasselmann, K., Santer, B. D., Cubasch, U., and Jones, P. D.: Detecting Greenhouse Gas induced Climate Change with an Optimal Fingerprint Method, J. Climate, 9, 2281 – 2306, 1996.

Hegerl, G. C., Karl, T. R., Allen, M., Bindoff, N. L., Gillett, N., Karoly, D., Zhang, X. B., and Zwiers, F.: Climate change detection and attribution: Beyond mean temperature signals, J. Clim., 19, 5058–5077, doi:10.1175/JCLI3900.1, 2006.

Hegerl, G. C., Zwiers, F. W., Braconnot, P., Gillett, N. P., Luo, Y., Marengo Orsini, J. A., Nicholls, N., Penner, J. E., and Stott, P. A.: Understanding and Attributing Climate Change., in: Climate Change 2007: The Physical Science Basis, Contribution of Working Group I to the Fourth Assessment Report of the Intergovernmental Panel on Climate Change, edited by: Solomon, S., Qin, D., Manning, M., Chen, Z., Marquis, M., Averyt, K. B., Tignor, M., and Miller, H. L., Cambridge Univ. Press, Cambridge and New York, 2007.

Hegerl, G. C., Hoegh-Guldberg, O., Casassa, G., Hoerling, M. P., Kovats, R. S., Parmesan, C., Pierce, D.W., and Stott, P. A.: Good practice guidance paper on detection and attribution related to anthropogenic climate change, in: Meeting report of the Intergovernmental Panel on Climate Change Expert Meeting on Detection and Attribution Related to Anthropogenic Climate Change, 14–16 September 2009, IPCC Working Group I Technical Support Unit, University of Bern, Bern, Switzerland, 1–8, 2010.

Heinze, C.: Simulating oceanic $CaCO_3$ export production in the greenhouse, Geophys. Res. Lett., 13, L16308, doi:10.1029/2004GL020613, 2004.

Helm, K.P.: Decadal ocean water-mass changes: Global observations and interpretation, Ph.D. thesis, University of Tasmania, Australia, 2008.

Helm, K. P., Bindoff, N. L., and Church, J. A.: Changes in the global hydrological-cycle inferred from ocean salinity, Geophys. Res. Lett., 37, L18701, doi:10.1029/2010GL044222, 2010.

Helm, K. P., Bindoff, N. L., and Church, J. A.: Observed decreases in oxygen content of the global ocean, Geophys. Res. Lett., 38, L23602, doi:10.1029/2011GL049513, 2011.

Henson, S., A.: Slow sciences: the value of long ocean biogeochemistry records, Phil. Trans. R. Soc. A., 372, 20130334, doi: 10.1098/rsta.2013.0334, 2014.

Henson, S. A., Sarmiento, J. L., Dunne, J. P., Bopp, L., Lima, I., Doney, S. C., John, J., and Beaulieu, C.: Detection of anthropogenic climate change in satellite records of ocean chlorophyll and productivity, Biogeosciences, 7, 621-640, doi:10.5194/bg-7-621-2010, 2010.

Hirst, A. C., O'Farrell, S. P., and Gordon, H. B.: Comparison of a Coupled Ocean-Atmosphere Model with and without Oceanic Eddy-Induced Advection. Part I: Ocean Spinup and Control Integrations, J. Climate, 13, 139–163, 2000.

Hoegh-Guldberg, O., Cai, R., Poloczanska, E. S., Brewer, P. G., Sundby, S., Hilmi, K., Fabry, V. J., and Jung, S.: The Ocean, in Climate Change 2014: Impacts, Adaptation, and Vulnerability. Part B: Regional Aspects. Contribution of Working Group II to the Fifth Assessment Report of the Intergovernmental Panel on Climate Change, edited by: Barros, V.R., Field, C. B., Dokken, D. J., Mastrandrea, M. D.,

Mach, K. J., Bilir, T. E., Chatterjee, M., Ebi, K. L., Estrada, Y. O., Genova, R. C., Girma, B., Kissel, E. S., Levy, A. N., MacCracken, S., Mastrandrea, P. R., and White, L. L., Cambridge University Press, Cambridge, United Kingdom and New York, NY, USA, 2014.

Hofmann, M. and Schellnhuber, H. J.: Ocean acidication affects marine carbon and triggers extended marine oxygen holes, Proc. Natl. Acad. Sci., 106, 3017–3022, doi:10.1073/pnas.0813384106, 2009.

Holt, J., Harel, J., Proctor, R., Michel, S., Ashworth, M., Batstone, C., Allen, J. I., Holmes, R., Smyth, T. J., Haines, K., Bretherton, D., and Smith, G.: Modelling the global coastal ocean, Phil. Trans. R. Soc. A, 367, 939–951, 2009.

Holt, J., Wakelin, S., Lowe, J., and Tinker, J.: The potential impacts of climate change on the hydrography of the Northwest European Continental shelf, Prog. Oceanogr., 86, 361–379, doi:10.1016/j.pocean.2010.1005.1003, 2010.

Holt, J., Hughes, S., Hopkins, J., Wakelin, S. L., Holliday, N. P., Dye, S., Gonzalez-Pola, C., Hjöllo, S. S., Mork, K. A., Nolan, G., Proctor, R., Read, J., Shammon, T., Sherwin, T., Smyth, T., Tattersall, G., Ward, B. and Wiltshire, K. H.: Multi-decadal variability and trends in the temperature of the northwest European continental shelf: A model-data synthesis, Prog. Oceanogr., 106 , 96–117, doi: 10.1016/j.pocean.2012.08.001, 2012.

Holt, J., Schrum, C., Cannaby, H., Daewel, U., Allen, I., Artioli, Y., Bopp, L., Butenschon, M., Fach, B. A., Harle, J., Pushpadas, D., Salihoglu, B., and Wakelin, S.: Physical processes mediating climate change impacts on regional sea ecosystems, Biogeosciences Discuss., 11, 1909–1975, doi:10.5194/bgd-11-1909-2014, 2014.

Huntingford, C., Stott, P. A., Allen, M. R., and Lambert, F. H.: Incorporating model uncertainty into attribution of observed temperature change, Geophys. Res. Lett., 33, L05710, doi:10.1029/2005GL024831, 2006.

Hurrell, J. W., Kushnir, Y., Ottersen, G., and Visbeck, M.: An overview of the North Atlantic Oscillation, The North Atlantic Oscillation: Climatic signicance and environmental impact, edited by: Hurrell, J. W., Kushnir, Y., Ottersen, G., and Visbeck, M., American Geophysical Union, Geoph. Monog. Series, 134, 1–35, 2003.

Hutchins, D. A., Mulholland, M. R., and Fu, F.: Nutrient cycles and marine microbes in a CO_2-enriched ocean, Oceanography, 22, 128–145, 2009.

IDAG (The International Ad Hoc Detection and Attribution Group): Detecting and Attributing External Inuences on the Climate System: A Review of Recent Advances, J. Climate, 18, 1291–1314, 2005.

Ilyina, T., Six, K. D., Segschneider, J., Maier-Reimer, E., Li, H., and Nunez-Riboni, I.: The global ocean biogeochemistry model HAMOCC: Model architecture and performance as component of the MPI-Earth System Model in different CMIP5 experimental realizations, doi:10.1002/jame.20017, 2013.

Imbers, J., Lopez, A., Huntingford, C., and Allen, M.: Sensitivity of Climate Change Detection and Attribution to the Characterization of Internal Climate Variability, J. Climate, 27, 3477–3491, 2014.

IPCC: Summary for Policymakers, in: Climate Change 2013: The Physical Science Basis. Contribution of Working Group I to the Fifth Assessment Report of the Intergovernmental Panel on Climate Change, edited by: Stocker, T. F., Qin, D., Plattner, G.-K., Tignor M., Allen, S. K., Boschung, J., Nauels, A., Xia, Y., Bex, V., and Midgley, P. M., Cambridge University Press, Cambridge, United Kingdom and New York, NY, USA, 2013.

Ishii, M., Feely, R. A., Rodgers, K. B., Park, G.-H., Wanninkhof, R., Sasano, D., Sugimoto, H., Cosca, C. E., Nakaoka, S., Telszewski, M., Nojiri, Y., Mikaloff Fletcher, S. E., Niwa, Y., Patra, P. K., Valsala, V., Nakano, H., Lima, I., Doney, S. C., Buitenhuis, E. T., Aumont, O., Dunne, J. P., Lenton, A., and Takahashi, T.: Air–sea CO_2 flux in the Pacific Ocean for the period 1990–2009, Biogeosciences, 11, 709-734, doi:10.5194/bg-11-709-2014, 2014.

Ito, T and Deutsch, C.: A conceptual model for the temporal spectrum of oceanic oxygen variability, Geophys. Res. Lett., 37, L03601, doi:10.1029/2009GL041595, 2010.

Ito, T., Follows, M., and Boyle, E.: Is AOU a good measure of respiration in the oceans?, Geophys. Res. Lett., 31, L17305, doi:10.1029/2004GL020900, 2004. Jochum, M., Deser, C., Philips, A.: Tropical Atmospheric Variability Forced by Oceanic Internal Variability, J. Climate, 20, 765–771, doi:10.1175/JCLI4044.1, 2007.

Johnson, G. C. and Gruber, N.: Decadal water mass variations along 20°W in the Northeastern Atlantic Ocean, Prog. Oceanogr., 73, 277–295, 2007.

Johnson, K. S., Berelson, W. M., Boss, E. S., Chase, Z. C., Claustre, H., Emerson, S. R., Gruber, N., Kortzinger, A., Perry, M. J., and Riser, S. C.: Observing biogeochemical cycles at global scales with profiling floats and gliders. Prospects for a global array, Oceanography, 22, 216–225, 2009.

Jones, C. D., Hughes, J. K., Bellouin, N., Hardiman, S. C., Jones, G. S., Knight, J., Liddicoat, S., O'Connor, F. M., Andres, R. J., Bell, C., Boo, K.-O., Bozzo, A., Butchart, N., Cadule, P., Corbin, K. D., Doutriaux-Boucher, M., Friedlingstein, P., Gornall, J., Gray, L., Halloran, P. R., Hurtt, G., Ingram, W. J., Lamarque, J.-F., Law, R. M., Meinshausen, M., Osprey, S., Palin, E. J., Parsons Chini, L., Raddatz, T., Sanderson, M. G., Sellar, A. A., Schurer, A., Valdes, P., Wood, N., Woodward, S., Yoshioka, M., and Zerroukat, M.: The HadGEM2-ES implementation of CMIP5 centennial simulations, Geosci. Model Dev., 4, 543–570, doi:10.5194/gmd-4-543-2011, 2011.

Jones, E., Zemlyak, F., and Stewart, P.: Operating manual for the Bedford Institute of Oceanography automated dissolved oxygen titration system, Can. Tech. Rep. Hydrogr. Ocean Sci., 138, 51 pp., 1992.

Jones, M. C., Dye, S. R., Fernandes, J. A., Frölicher, T. L., Pinnegar, J. K., Warren, R., and Cheung W. W. L.: Predicting the Impact of Climate Change on Threatened Species in UK Waters, PLoS ONE, 8, e54216, doi:10.1371/journal.pone.0054216, 2013.

Joos, F., Plattner, G.-K., Stocker, T. F., Körtzinger, A., and Wallace, D. W. R.: 2003. Trends in marine dissolved oxygen: implications for ocean circulation changes and carbon budget, Eos Trans. AGU, 84, 197–204, doi:10.1029/2003EO$_2$10001, 2003.

Jungclaus, J. H., Fischer, N., Haak, H., Lohmann, K., Marotzke, J., Matei, D., Mikolajewicz, U., Notz, D., and von Storch, J.: Characteristics of the ocean simulations in MPIOM, the ocean component of the MPI-Earth system model, J. Adv. Model. Earth Syst., 5, 422–446, doi:10.1002/jame.20023, 2013.

Kalnay, E., Kanamitsu, M., Kistler, R., Collins, W., Deaven, D., Gandin, L., Iredell, M., Saha, S., White, G.,Woollen, J., Zhu, Y., Chelliah, M., Ebisuzaki, W., Higgins, W., Janowiak, J., Mo, K. C., Ropelewski, C., Wang, J., Leetmaa, A., Reynolds, R.,

Jenne, R., and Joseph, D.: The NCEP/NCAR 40-year reanalysis project, B. Am. Meteorol. Soc., 77, 437–471, 1996.

Karstensen, J., Stramma, L., and Visbeck, M.: Oxygen minimum zones in the eastern tropical Atlantic and Pacic oceans, Progr. Oceanogr., 77, 331–350, 2008.

Keeling, C. D., and Whorf, T. P.: Atmospheric CO_2 records from sites in the SIO air sampling network, In Trends: A Compendium of Data on Global Change. Carbon Dioxide Information Analysis Center, Oak Ridge National Laboratory, U.S. Department of Energy, Oak Ridge, Tenn., USA, 2005.

Keeling, R. and Garcia, H.: The change in oceanic O_2 inventory associated with recent global warming, P. Natl. Acad. Sci. USA, 99, 7848–7853, 2002.

Keeling, R. F. and Manning, A. C.: Studies of Recent Changes in Atmospheric O_2 Content. in: Treatise on Geochemistry, 2nd Edition, 5, edited by: Holland, H.D. and Turekian, K.K., Elsevier, Oxford, 2013.

Keeling, R. F., Körtzinger, A., and Gruber, N.: Ocean deoxygenation in a warming world, Ann. Rev. Mar. Sci., 2, 199–229, doi:10.1146/annurev.marine.010908.163855, 2010.

Keller, D. P., Feng, E. Y., and Oschlies, A: Potential climate engineering effectiveness and side effects during a high carbon dioxide emission scenario. Nat. Commun., 5, 3304, http://dx.doi.org/10.1038/ncomms4304, 2014a.

Keller, K. M., Joos, F., and Raible, C. C.: Time of emergence of trends in ocean biogeochemistry, Biogeosciences, 11, 3647-3659, doi:10.5194/bg-11-3647-2014, 2014b.

Kemp, W. M., Testa, J. M., Conley, D. J., Gilbert, D., and Hagy, J. D.: Temporal responses of coastal hypoxia to nutrient loading and physical controls, Biogeosciences, 6, 2985-3008, doi:10.5194/bg-6-2985-2009, 2009.

Key, R. M., Kozyr, K. A., Sabine, C. L., Lee, K., Wanninkhof, R., Bullister, J. L., Feely, R. A., Millero, F. J., Mordy, C., and Peng, J.-H.: A global ocean carbon climatology: Results from Global Data Analysis Project (GLODAP). Global Biogeochem. Cy., 18, GB4031, doi:10.1029/2004GB002247, 2004.

Khatiwala, S., Tanhua, T., Mikaloff Fletcher, S., Gerber, M., Doney, S. C., Graven, H. D., Gruber, N., McKinley, G. A., Murata, A., Ríos, A. F., and Sabine, C. L.: Global ocean storage of anthropogenic carbon, Biogeosciences, 10, 2169-2191,

doi:10.5194/bg-10-2169-2013, 2013.

Körtzinger, A., Schimanski, J., and Send, U.: High quality oxygen measurements from profiling floats: a promising new technique, J. Atmos. Ocean. Tech., 22, 302–308, 2005.

Kwiatkowski, L., Yool, A., Allen, J. I., Anderson, T. R., Barciela, R., Buitenhuis, E. T., Butenschön, M., Enright, C., Halloran, P. R., Le Quéré, C., de Mora, L., Racault, M.-F., Sinha, B., Totterdell, I. J., and Cox, P. M.: iMarNet: an ocean biogeochemistry model inter-comparison project within a common physical ocean modelling framework, Biogeosciences Discuss., 11, 10537-10569, doi:10.5194/bgd-11-10537-2014, 2014.

Kwon, E. Y., Deutsch, C., Xie, S.-P., and Schmidtko, S.: The North Pacific oxygenation rate over the past half-century, J. Climate, submitted, 2014.

Large, W. G. and Yeager, S. G.: Diurnal to decadal global forcing for ocean and sea-ice models: the datasets and flux climatologies, Tech. Rep. TN-460+STR, National Center for Atmospheric Research, Boulder, Colorado, 2004.

Large, W. G. and Yeager, S. G.: The global climatology of an interanually varying air-sea flux dataset, Clim. Dynam., 33, 341–364, 2009.

Laufkötter, C., Vogt, M., and Gruber, N.: Long-term trends in ocean plankton production and particle export between 1960–2006, Biogeosciences, 10, 7373-7393, doi:10.5194/bg 10-7373-2013, 2013.

Le Quéré, C., Rödenbeck, C., Buitenhuis, E. T., Conway, T. J., Langenfelds, R., Gomez, A., Labuschagne, C., Ramonet, M., Nakazawa, T., Metzl, N., Gillett, N., and Heimann, M.: Saturation of the Southern Ocean CO_2 sink due to recent climate change, Science, 316, 1735–1738, 2007.

Le Quéré, C., Takahashi, T., Buitenhuis, E. T., Rödenbeck, C., and Sutherland, S. C.: Impact of climate change and variability on the global oceanic sink of CO_2, Global Biogeochem. Cy., 24, GB4007, doi:10.1016/0012-821X(72)90242-7, 2010.

Le Quéré, C., Buitenhuis, E. T., Moriarty, R., Aumont, O., Bopp, L., Chollet, S., Enright, C., Franklin, D. J., Geider, R. J., Harrison, S. P., Hirst, A., Larsen, S., Legendre, L., Platt, T., Prentice, I. C., Rivkin, R. B., Sathyendranath, S., Stephens, N., Vogt, M., Sailley, S., and Vallina, S. M.: Role of zooplankton dynamics for ecosystem –

climate interactions, Glob. Change Biol., submitted, 2014a.

Le Quéré, C., Peters, G. P., Andres, R. J., Andrew, R. M., Boden, T. A., Ciais, P., Friedlingstein, P., Houghton, R. A., Marland, G., Moriarty, R., Sitch, S., Tans, P., Arneth, A., Arvanitis, A., Bakker, D. C. E., Bopp, L., Canadell, J. G., Chini, L. P., Doney, S. C., Harper, A., Harris, I., House, J. I., Jain, A. K., Jones, S. D., Kato, E., Keeling, R. F., Klein Goldewijk, K., Körtzinger, A., Koven, C., Lefèvre, N., Maignan, F., Omar, A., Ono, T., Park, G.-H., Pfeil, B., Poulter, B., Raupach, M. R., Regnier, P., Rödenbeck, C., Saito, S., Schwinger, J., Segschneider, J., Stocker, B. D., Takahashi, T., Tilbrook, B., van Heuven, S., Viovy, N., Wanninkhof, R., Wiltshire, A., and Zaehle, S.: Global carbon budget 2013, Earth Syst. Sci. Data, 6, 235-263, doi:10.5194/essd-6-235-2014, 2014b.

Levitus, S., Antonov, J. I., Boyer, T. P., Locarnini, R. A., Garcia, H. E., and Mishonov, A. V.: Global ocean heat content 1955-2008 in light of recently revealed instrumentation problems, Geophys. Res. Lett., 36, L07608, doi:10.1029/2008GL037155, 2009.

Levitus, S., Antonov, J. I., Boyer, T. P., Baranova, O. K., Garcia, H. E., Locarnini, R. A., Mishonov, A. V., Reagan, J. R., Seidov, D., Yarosh, E. S., and Zweng, M. M.: World ocean heat content and thermosteric sea level change (0–2000m), 1955–2010, Geophys. Res. Lett., 39, L10603, doi:10.1029/2012GL051106, 2012.

Locarnini, R. A., Mishonov, A. V., Antonov, J. I., Boyer, T. P., and Garcia, H.E: World Ocean Atlas 2005, Vol. 1: Temperature, edited by: Levitus, S., NOAA Atlas NESDIS 61, US Government Printing Office, Washington, DC, 182 pp., 2006 Longhurst, A., Sathyendranath, S., Platt, T., and Caverhill, C.: An estimate of global primary production in the ocean from satellite radiometer data, J. Plankton Res., 17, 1245–1271, 1995.

Lovelock, J. E.: Gaia: A New Look at Life on Earth, Oxford University Press, 1979.

Lowe, J. A., Howard, T. P., Pardaens, A., Tinker, J., Holt, J., Wakelin, S., Milne, G., Leake, J., Wolf, J., Horsburgh, K., Reeder, T., Jenkins, G., Ridley, J., Dye, S., and Bradley, S.: UK Climate Projections science report: Marine and coastal projections, Met Office Hadley Centre, Exeter, UK, 99, 2009.

Luyten, J. L, Pedlosky, J., and Stommel, H. M.: The ventilated thermocline, J. Phys. Oceanogr., 13, 292–309, 1983.

Mackenzie, B. R. and Schiedek, D.: Daily ocean monitoring since the 1860s shows record warming of northern European seas, Glob. Change Biol., 13, 1335–1347, doi: 10.1111/j.1365-2486.2007.01360.x, 2007.

Madec, G.: NEMO ocean engine, Note du Pole de modélisation, Institut Pierre-Simon Laplace (IPSL), Paris, No 27, 2008.

Madec, G. and Imbard, M.: A global ocean mesh to overcome the North Pole singularity, Clim. Dynam., 12, 381–388, 1996.

Maier-Reimer, E.: Geochemical cycles in an ocean general circulation model: preindustrial tracer distributions, Global Biogeochem. Cy., 7, 645–677, 1993.

Maier-Reimer, E., I. Kriest, J. Segschneider, and Wetzel, P.: The HAMburg Ocean Carbon Cycle model HAMOCC5.1 – Technical description., Berichte zur Erdsystemforschung 14/2005, 14, Max-Planck-Institut fr Meteorologie, Hamburg, Germany, available at: `http://www.mpimet.mpg.de` (last access: 12 May 2012), 2005.

Manizza, M., Le Quéré, C., Watson, A. J., and Buitenhuis, E. T.: Ocean biogeochemical response to phytoplankton-light feedback in a global model, J. Geophys. Res.-Oceans, 113, C10010, doi:10.1029/2007JC004478, 2008.

Marsland, S. J., Haak, H., Jungclaus, J. H., Latif, M., and Röske, F. R.: The Max-Planck-Institute global ocean/sea ice model with orthogonal curvilinear coordinates, Ocean Model., 5, 91–127, 2003.

Masson, D. and Knutti, R.: Spatial-scale dependence of climate model performance in the CMIP3 ensemble, J. Climate, 24, 2680–2692, 2011.

Masson-Delmotte, V., Schulz, M., Abe-Ouchi, A., Beer, J., Ganopolski, A., Gonzlez Rouco, J. F., Jansen, E., Lambeck, K., Luterbacher, J., Naish, T., Osborn, T., Otto-Bliesner, B., Quinn, T., Ramesh, R., Rojas, M., Shao, X., and Timmermann, A.: Information from Paleoclimate Archives, in: Climate Change 2013: The Physical Science Basis, Contribution of Working Group I to the Fifth Assessment Report of the Intergovernmental Panel on Climate Change, edited by: Stocker, T. F., Qin, D., Plattner, G.-K., Tignor, M., Allen, S. K., Boschung, J., Nauels, A., Xia, Y., Bex, V., and Midgley, P. M., Cambridge University Press, Cambridge, UK and New York, NY, USA, 2013.

Matear, R. J.: Ocean carbon cycle in a changing climate: Climate change detection, in: The

Ocean Carbon Cycle and Climate, edited by Follows, M, and Oguz, T., 297-315, Springer, New York.

Matear, R. J. and Hirst, A. C.: Long-term changes in dissolved oxygen concentrations in the ocean caused by protracted global warming, Global Biogeochem. Cy., 17, 1125, doi:10.1029/2002GB001997, 2003.

Matear, R. J. and Lenton, A.: Quantifying the impact of ocean acidification on our future climate, Biogeosciences, 11, 3965-3983, doi:10.5194/bg-11-3965-2014, 2014.

Matear, R. and McNeil, B.: Enhanced biological carbon consumption in a high CO_2 ocean: a revised estimate of the atmospheric uptake efficiency, Biogeosciences Discuss., 6, 8101-8128, doi:10.5194/bgd-6-8101-2009, 2009.

Matear, R. J., Hirst, A. C., and McNeil, B. I.: Changes in dissolved oxygen in the Southern Ocean with climate change, Geochem. Geophys. Geosyst., 1, 1050, doi:10.1029/2000GC000086, 2000.

Mathiot, P., Jourdain, N. C., Barnier, B., and Gallée, H: Sensitivity of a model of the Ross Ice shelf polynya to different atmospheric forcing sets, Mercator Ocean, Quarterly Newsletter, 28, 22–30, 2008.

Mauritsen, T., Stevens, B., Roeckner, E., Crueger, T., Esch, M., Giorgetta, M. A., Haak, H., Jungclaus, J. H., Klocke, D., Matei, D., Mikolajewicz, U., Notz, D., Pincus, R., Schmidt, H., and Tomassini, L.: Tuning the climate of a global model, J. Adv. Model. Earth Syst., 4, M00A01, doi:10.1029/2012MS000154, 2012.

Mauritzen, C., Melsom, A., and Sutton, R. T.: Importance of density-compensated temperature change for deep North Atlantic Ocean heat uptake, Nat. Geosci.,5, 905–910, doi:10.1038/ngeo1639, 2012.

McKinley, G. A., Follows, M. J., Marshall, J., and Fan, S. M.: Interannual variability of air-sea O_2 fluxes and the determination of CO_2 sinks using atmospheric O_2/N2, Geophys. Res. Lett., 30, 1101, doi:10.1029/2002GL016044, 2003.

Meehl, G. A. and Teng, H. Y.: Case studies for initialized decadal hindcasts and predictions for the Pacific region, Geophys. Res. Lett., 39, L22705, doi:10.1029/2012gl053423, 2012.

Millennium Ecosystem Assessment: Ecosystems and Human Well-Being: Full Report, Island Press, Washington DC, USA, 2005.

Meire, L., Soetaert, K. E. R., and Meysman, F. J. R.: Impact of global change on coastal oxygen dynamics and risk of hypoxia, Biogeosciences, 10, 2633-2653, doi:10.5194/bg-10-2633-2013, 2013.

Micheli, F., Saenz-Arroyo, A., Greenley, A., Vazquez, L., Espinoza, A., Rossetto, M., and De Leo, G.: Evidence that marine reserves enhance resilience to climatic impacts, PLoS ONE, 7, e40832, doi:10.1371/journal.pone.0040832, 2012.

Mora, C., Frazier, A. G., Longman, R. J., Dacks, R. S., Walton, M. M., Tong, E. J., Sanchez, J. J., Kaiser, L. R., Stender, Y. O., Anderson, J. M., Ambrosino, C. M., Fernandez-Silva, I., Giuseffi, L. M., and Giambelluca, T. W.: The projected timing of climate departure from recent variability, Nature, 502, 183–187, 2013.

Morrison, J. M., Codispoti, L. A., Smith, S. L., Wishner, K., Flagg, C., Gardner, W. D., Gaurin, S., Naqvi, S. W. A., Manghnani, V., Prosperie, L., and Gundersen, J. S.: The oxygen minimum zone in the Arabian Sea during 1995, Deep-Sea Res. II, 46, 1903–1931, 1999.

Myhre, G., Shindell, D., Bréon, F.-M., Collins, W., Fuglestvedt, J., Huang, J., Koch, D., Lamarque, J.-F., Lee, D., Mendoza, B., Nakajima, T., Robock, A., Stephens, G., Takemura, T., and Zhan, H.: Anthropogenic and natural radiative forcing, in: Climate Change 2013: The Physical Science Basis. Contribution of Working Group I to the Fifth Assessment Report of the Intergovernmental Panel on Climate Change, edited by: Stocker, T. F., Qin, D., Plattner, G.- K., Tignor, M., Allen, S. K., Boschung, J., Nauels, A., Xia, Y., Bex, V., and Midgley, P. M., Cambridge University Press, Cambridge, UK and New York, NY, USA, 2013.

Naqvi, S. W. A., Bange, H. W., Farías, L., Monteiro, P. M. S., Scranton, M. I., and Zhang, J.: Marine hypoxia/anoxia as a source of CH_4 and N_2O, Biogeosciences, 7, 2159-2190, doi:10.5194/bg-7-2159-2010, 2010a.

Naqvi, S. W. A., Banse, K., Narvekar, P.V, and Postel, J. R.: Are the open-ocean oxygen minimum zones intensifying and expanding?, Eos Trans. AGU, 91, Ocean Sci. Meet. Suppl., Abstract, $BO_2$1B-02, 2010b.

NIOZ (Royal Netherlands Institute for Sea Research): ERSEM-GETM Model Details, NIOZ, Netherlands, available at: `http://www.nioz.nl/ersem-getm` (last access: 10 January 2014), 2012.

Notz, D., Haumann, F. A., Haak, H., Jungclaus, J. H., and Marotzke, J.: Arctic sea-ice evolution as modeled by Max Planck Institute for Meteorology's Earth system model, J. Adv. Model. Earth Syst., 5, 173–194, doi:10.1002/jame.20016, 2013.

Ono, T., Midorikawa, T., Watanabe, Y. W., Tadokoro, K., and Saino, T.: Temporal increases of phosphate and apparent oxygen utilization in the subsurface waters of western subarctic Pacific from 1968 to 1998, Geophys. Res. Lett., 28, 3285–3288, 2001.

Oschlies, A., Schultz, K. G., Riebesell, U., and Schmittner, A.: Simulated 21^{st} century's increase in oceanic suboxia by CO_2-enhanced biotic carbon export, Global. Biogeochem. Cy., 22, GB4008, doi:10.1029/2007GB003147, 2008.

Painting, S. J., Devlin, M. J., Rogers, S. I., Mills, D. K., Parker, E. R., and Rees, H. L.: Assessing the suitability of OSPAR EcoQOs for eutrophication vs ICES criteria for England and Wales, Mar. Pollut. Bull., 50, 1569–1584, doi:10.1016/j.marpolbul.2005.06.042, 2005.

Palmer, J. R and Totterdell, I. J.: Production and export in a global ocean ecosystem model, Deep-Sea Res. Pt. I, 48, 1169–1198, 2001.

Palmer, M. D., Good, S. A., Haines, K., Rayner, N. A., and Stott, P. A.: A new perspective on warming of the global oceans, Geophys. Res. Lett., 36, L20709, doi:10.1029/2009GL039491, 2009.

Paulmier, A. and Ruiz-Pino, D.: Oxygen minimum zones (OMZs) in the modern ocean, Prog. Oceanogr., 80, 113–128, 2009.

Pauly, D., Christensen, V., Guenette, S., Pitcher, T. J., Rashid, T. U., Walters, C. J., Watson, R., and Zeller, D.: Towards sustainability in world sheries, Nature, 418, 689–695, 2002.

Peña, M. A., Katsev, S., Oguz, T., and Gilbert, D.: Modeling dissolved oxygen dynamics and hypoxia, Biogeosciences, 7, 933-957, doi:10.5194/bg-7-933-2010, 2010.

Pierce, D. W., Barnett, T. P., AchutaRao, K. M., Gleckler, P. J., Gregory, J. M. and Washington, W. M.: Anthropogenic warming of the oceans: observations and model results, J. Climate, 19, 1873–1900, doi:http://dx.doi.org/10.1175/JCLI3723.1, 2006.

Pierce, D. W., Barnett, T. P. and Gleckler, P. J.: Ocean Circulations, Heat Budgets, and Future Commitment to Climate Change, Ann. Rev. Environ. Res., 36, 27 – 43, doi:265 10.1146/annurev-environ-022610-112928, 2011.

Pierce, D. W., Gleckler, P. J., Parnett, T. P., Santer, B. D., and Durack, P. J.: The fingerprint of human-induced changes in the ocean's salinity and temperature fields, Geophys. Res. Lett, 39, L21704, doi:10.1029/2012GL053389, 2012.

Plattner, G.-K., Joos, F., Stocker, T. F., and Marchal, O.: Feedback mechanisms and sensitivities of ocean carbon uptake under global warming, Tellus B, 53, 564–592, 2001.

Plattner, G., Joos, F., and Stocker, T.: Revision of the global carbon budget due to changing air-sea oxygen uxes, Global Biogeochem. Cy., 16, 1096–1108, doi:10.1029/2001GB001746, 2002.

Ploug, H., Iversen, M. H., Koski, M., and Buitenhuis, E. T.: Production, oxygen respiration rates, and sinking velocity of copepod fecal pellets: Direct measurements of ballasting by opal and calcite, Limnol. Oceanogr., 53, 469–476, 2008.

Pörtner H. O., Karl, D., Boyd, P. W., Cheung, W. W. L., Lluch-Cota, S. E., Nojiri, Y., Schmidt, D. N., and Zavialov, P.: Ocean Systems, in Impacts, Adaptation and Vulnerability, Volume II: Contribution of Working Group II to the Fifth Assessment Report of the Intergovernmental Panel on Climate Change, edited by: Barros, V.R., Field, C. B., Dokken, D. J., Mastrandrea, M. D., Mach, K. J., Bilir, T. E., Chatterjee, M., Ebi, K. L., Estrada, Y. O., Genova, R. C., Girma, B., Kissel, E. S., Levy, A. N., MacCracken, S., Mastrandrea, P. R., and White, L. L., Cambridge University Press, Cambridge, United Kingdom and New York, NY, USA, 2014

Purkey, S. G. and Johnson, G. C.: Warming of global abyssal and deep Southern Ocean waters between the 1990s and 2000s: contributions to global heat and sea level rise budgets, J. Climate, 23, 6336–6351, 2010.

Queste, B. Y., Fernand, L., Jickells, T. D., and Heywood, K. J.: Spatial extent and historical context of North Sea oxygen depletion in August 2010, Biogeochemistry, 1-16, doi:10.1007/s10533-012-9729-9, 2012.

Rabalais, N. N., Turner, R. E., Díaz, R. J., and Justic, D.: Global change and eutrophication of coastal waters, ICES J. Mar. Sci., 66, 1528–1537, 2009.

Rabalais, N. N., Díaz, R. J., Levin, L. A., Turner, R. E., Gilbert, D., and Zhang, J.: Dynamics and distribution of natural and human-caused hypoxia, Biogeosciences, 7, 585-619, doi:10.5194/bg-7-585-2010, 2010.

Redfield, A. C., Ketchum, B. H., and Richards, F. A.: The influence of organisms on the composition of sea-water, in: The sea, edited by: Hill, M. N., New York, Wiley, 2, 26–77, 1963.

Resplandy, L., Lévy, M., Bopp, L., Echevin, V., Pous, S., Sarma, V. V. S. S., and Kumar, D.: Controlling factors of the oxygen balance in the Arabian Sea's OMZ, Biogeosciences, 9, 5095-5109, doi:10.5194/bg-9-5095-2012, 2012.

Ribes, A., Terray, L., and Planton, S.: Application of regularised optimal fingerprinting to attribution. Part I: method, properties and idealised analysis, Clim. Dynam., doi:10.1007/s00382-013-1735-7, 2013.

Ridgwell, A., Schmidt, D. N., Turley, C., Brownlee, C., Maldonado, M. T., Tortell, P., and Young, J. R.: From laboratory manipulations to Earth system models: scaling calcification impacts of ocean acidification, Biogeosciences, 6, 2611-2623, doi:10.5194/bg-6-2611-2009, 2009.

Riebesell, U., Schulz, K. G., Bellerby, R. G. J., Botros, M., Fritsche, P., Meyerhöfer, M., Neil, C., Nondal, G., Oschies, A., Wohlers, J., and Zollner, E.: Enhanced biological carbon consumption in high CO_2 ocean, Nature, 450, 545–548, 2007.

Rhein, M., Rintoul, S. R., Aoki, S., Campos, E., Chambers, D., Feely, R. A., Gulev, S., Johnson, G. C., Josey, S. A., Kostianoy, A. , Mauritzen, C., Roemmich, D., Talley, L. D., and Wang, F.: Observations: Ocean. in: Climate Change 2013: The Physical Science Basis. Contribution of Working Group I to the Fifth Assessment Report of the Intergovernmental Panel on Climate Change, edited by: Stocker, T. F., Qin, D., Plattner, G.-K., Tignor, M., Allen, S. K., Boschung, J., Nauels, A., Xia, Y., Bex, V., and Midgley, P. M., Cambridge University Press, Cambridge, 2013.

Ridder, N. N., and England, M. H.: Sensitivity of ocean oxygenation to variations in tropical zonal wind stress magnitude, Global Biogeochem. Cycles, 28, doi:10.1002/2013GB004708, 2014.

Rödenbeck, C., Le Quéré, C., Heimann, M., and Keeling, R. F.: Interannual variability in oceanic biogeochemical processes inferred by inversion of atmospheric O_2/N2 and CO_2 data, Tellus B – Chem. Phys. Meteorol., 60, 685–705, 2008.

Rosenzweig, C., and Neofotis, P.: Detection and attribution of anthropogenic climate change impacts. WIREs Clim. Change, 4, 121-150, doi:10.1002/wcc.209, 2014.

Roeckner, E., Brokopf, R., Esch, M., Giorgetta, M., Hagemann, S., Kornblueh, L., Manzini, E., Schlese, U., and Schulzweida, U.: Sensitivity of simulated climate to horizontal and vertical resolution in the ECHAM5 atmosphere model, J. Climate, 19, 3771–3791, 2006.

Ruckelshaus, M., S.C. Doney, H.M. Galindo, J.P. Barry, F. Chan, J.E. Duffy, C.A. English, S.D. Gaines, J.M. Grebmeier, and A.B. Hollowed: Securing ocean benefits for society in the face of climate change. Mar. Policy 40:154–159, http://dx.doi.org/10.1016/j.marpol.2013.01.009, 2013.

Rykaczewski, R. R. and Dunne, J. P.: A measured look at ocean chlorophyll trends, Nature, 472, E5–E6, doi:10.1038/nature09952, 2011.

Santer, B. D., Mikolajewicz, U., Bruggemann, W., Cubasch, U., Hasselmann, K., Hock, H., Maier-Reimer, E., and Wigley, T. M. L.: Ocean variability and its inuence on the detectability of greenhouse warming signals, J. Geophys. Res., 100(C6), 10693–10725, 1995.

Sarmiento, J. L., Hughes, T. M. C., Stouffer, R. J., and Manabe, S.: Simulated response of the ocean carbon cycle to anthropogenic climate warming, Nature, 393, 245–249, 1998.

Sarmiento, J. L., A. K. Morrison, T. L. Frölicher.: Observing and understanding the Southern Ocean: A paradigm shift, Physics today, submitted, 2014.

Schmittner, A., Oschlies, A., Matthews, H. D., and Galbraith, E. D.: Future changes in climate, ocean circulation, ecosystems, and biogeochemical cycling simulated for a business as-usual CO_2 emission scenario until year 4000 AD, Global Biogeochem. Cy., GB1013, doi:10.1029/2007GB002953, 2008.

Schmidtko, S., Johnson, G. C., and Lyman, J. M.: MIMOC: A global monthly isoopycnal upper ocean climatology with mixed layers, J. Geophys. Res. Oceans, 118 1658-1672, goi:10.1002/jgrc.20122, 2013.

Séférian R., Bopp, L., Gehlen, M., Orr, J., Éthé, C., Cadule, P., Aumont, O., Salas-y-Mélia, D., Voldoire, A., and Madec, G.: Skill Assessment of Three Earth System Models with Common Marine Biogeochemistry, Clim. Dynam., 40, 9–10, doi:10.1007/s00382-012-1362-8, 2013.

Séférian, R., Ribes, A., and Bopp L.: Detecting the anthropogenic influences on recent

changes in ocean carbon uptake, Geophys. Res. Lett., 41, doi:10.1002/2014GL061223, 2014.

Send, U., Weller, R. A., Wallace, D., Chavez, F., Lampitt, R. L., Dickey, T., Honda, M., Nittis, K., Lukas, R., McPhaden, M., and Feely, R.: OceanSITES, in: Proceedings of OceanObs'09: Sustained Ocean Observations and Information for Society (Vol. 2), Venice, Italy, 21–25 September 2009, edited by: Hall, J., Harrison, D. E., and Stammer, D., ESA Publication WPP-306, doi:10.5270/OceanObs09.cwp.79, 2010.

Shaffer, G., Olsen, S. M., and Pedersen, J. O. P.: Long-term ocean oxygen depletion in response to carbon dioxide emissions from fossil fuels, Nat. Geosci., 2, 105–109, 2009.

Sharples, J., Ross, O., Scott, B., Greenstreet, S., and Fraser, H.: Inter-annual variability in the timing of stratification and the spring bloom in the North-western North Sea, Cont. Shelf Res., 26, 733–751, 2006.

Six, K. D. and Maier-Reimer, E.: Effects of plankton dynamics on seasonal carbon uxes in an ocean general circulation model, Global Biogeochem. Cy., 10, 559–583, 1996.

Steinacher, M., Joos, F., Frölicher, T. L., Bopp, L., Cadule, P., Cocco, V., Doney, S. C., Gehlen, M., Lindsay, K., Moore, J. K., Schneider, B., and Segschneider, J.: Projected 21^{st} century decrease in marine productivity: a multi-model analysis, Biogeosciences, 7, 979-1005, doi:10.5194/bg-7-979-2010, 2010.

Stendardo, I., and Gruber, N.: Oxygen trends over ve decades in the North Atlantic, J. Geophys. Res., 117, C11004, doi:10.1029/2012jc007909, 2012.

Stevens B., Crueger, T., Esch, M., Giorgetta, M., Mauritsen, T., Rast, S., Schmidt, H., Bader, J., Block, K., Brokopf, R., Fast, I., Kinne, S., Kornblueh, L., Lohmann, U., Pincus, R., Reichler, T., Salzmann, M., and Roeckner, E.: The Atmospheric Component of the MPI-M Earth System Model: ECHAM6, J. Adv. Model. Earth Syst., 5, 1–27, doi:10.1002/jame.20015, 2013.

Stips, A., Bolding, K., Pohlmann, T., and Burchard, H.: Simulating the temporal and spatial dynamics of the North Sea using the new model GETM (General Estuarine Transport Model), Ocean Dyn., 54, 266–283, 2004.

Stocker, T. F.: The ocean as a component of the climate system. in: Ocean Circulation and Climate: A 21^{st} Century Perspective, 2nd Edition, 103, International Geophysics

Series, edited by: Siedler, G., Griffies, S. M., Gould J., and Church, J. A., 2nd Edition, Academic Press, Oxford, UK, 2013.

Stone, D. A., Allen, M. R., Stott, P. A., Pall, P., Min, S.-K., Nozawa, T., and Yukimoto, S.: The Detection and Attribution of Human Influence on Climate, Ann. Rev. Environ. Res., 34, 1- 16, doi:10.1146/annurev.environ.040308.101032, 2009.

Stott, P. A., Allen, M. R., and Jones, G. S.: Estimating signal amplitudes in optimal fingerprinting. Part II: application to general circulation models, Clim. Dynam., 21, 493–500, doi: 10.1007/s00382-003-0314-8, 2003a.

Stott, P. A., Jones, G. S., and Mitchell, J. F. B.: Do models underestimate the solar contribution to recent climate change?, J. Climate, 16, 2079 – 4093, 2003b.

Stott, P. A., Sutton, R. T., and Smith, D. M.: Detection and attribution of Atlantic salinity changes, Geophys. Res. Lett., 35, L21702, doi:10.1029/2008GL035874, 2008.

Stott, P. A., Gillett, N. P., Hegerl, G. C., Karoly, D. J., Stone, D. A., Zhang, X., and Zwiers, F.: Detection and attribution of climate change: a regional perspective, WIREs Clim. Change, 1, 192–211, doi: 10.1002/wcc.34, 2010.

Stott, P. A., Allen, M., Christidis, N., Dole, R. M., Hoerling, M., Huntingford, C., Pall, P., Perlwitz, J., and Stone, D. Attribution of weather and climate-related events. in: Climate Science for Serving Society: Research, Modeling and Prediction Priorities, edited by Asrar, G. R. and Hurrell, J. W, 307–337, Springer, Dordrecht, 2013.

Stramma, L., Johnson, G. C., Sprintall, J., and Mohrholz, V.: Expanding oxygen-minimum zones in the tropical oceans, Science, 320, 655–658, 2008.

Stramma, L., Johnson, G. C., Firing, E., and Schmidtko, S.: Eastern Pacic oxygen minimum zones: Supply paths and multidecadal changes, J. Geophys. Res., 115, C09011, doi:10.1029/2009JC005976, 2010.

Stramma, L., Oschlies, A., and Schmidtko, S.: Mismatch between observed and modeled trends in dissolved upper-ocean oxygen over the last 50 yr, Biogeosciences, 9, 4045-4057, doi:10.5194/bg-9-4045-2012, 2012a.

Stramma, L., Prince, E. D., Schmidtko, S., Luo, J., Hoolihan, J. P., Visbeck, M., Wallace, D. R.W., Brandt, P., and Körtzinger, A.: Expansion of oxygen minimum zones may reduce available habitat for tropical pelagic shes, Nature Clim. Change, 2, 33–37, doi:10.1038/nclimate1304, 2012b.

Suntharalingam, P., Sarmiento, J. L., and Toggweiler, J. R.: Global significance of nitrous-oxide production and transport from oceanic low-oxygen zones: A modeling study, Glob. Biogeochem. Cy., 14, 1353–1370, 2000.

Suntharalingam, P., Buitenhuis, E., Le Quéré, C., Dentener, F., Nevison, C., and Butler, J.: Quantifying the Impact of Anthropogenic Nitrogen Deposition on Oceanic Nitrous Oxide, Geophys. Res. Lett., 39, L07605, doi:10.1029/2011GL050778, 2012.

Swanson, K. L., Sugihara, G., and Tsonis, A. A.: Long-term natural variability and 20th century climate change, Proc. Natl. Acad. Sci., 106, 16111–16123, doi:10.1073/pnas.0908699106, 2009.

Swart, N. C., Fyfe, J. C., Saenko, O. A., and Eby, M.: Wind driven changes in the ocean carbon sink, Biogeosciences Discuss., 11, 8023-8048, doi:10.5194/bgd-11-8023-2014, 2014.

Sydeman, W. J., Thompson, S. A., Field, J. C., Peterson, W. T., Tanasichuk, R. W., Freeland, H. J., Bograd, S. J., and Rykaczewski, R. R.: Does positioning of the North Pacific Current affect downstream ecosystem productivity?, Geophys. Res. Lett., 38, L12606, doi:10.1029/2011GL047212, 2011.

Tagliabue, A., Bopp, L., and Gehlen, M.: The response of marine carbon and nutrient cycles to ocean acidification: Large uncertainties related to phytoplankton physiological assumptions, Global Biogeochem. Cy., 25, GB3017, doi:10.1029/2010GB003929, 2011.

Taylor, K. E., Stouffer, R. J., and Meehl, G. A.: L A Summary of the CMIP5 Experiment Design, available at: `http://www-pcmdi.llnl.gov/` (last access: 12 May 2012), 2009.

Taylor, K. E., Stouffer, R. J., and Meehl, G. A.: An overview of CMIP5 and the Experiment Design, Bull. Amer. Meteor. Soc., 93, 485–498, doi:10.1175/BAMS-D-11-00094.1, 2012.

Terray, L., Corre, S. Cravatte, T. Delcroix, Reverdin, G., and Ribes, A.: Nearsurface salinity as Nature's rain gauge to detect human influence on the tropical water cycle, J. Clim., 25, 958–977, doi:10.1175/JCLI-D-10-05025.1, 2012.

The HadGEM2 Development Team: Martin, G. M., Bellouin, N., Collins, W. J., Culverwell, I. D., Halloran, P. R., Hardiman, S. C., Hinton, T. J., Jones, C. D., McDonald, R. E.,

McLaren, A. J., O'Connor, F. M., Roberts, M. J., Rodriguez, J. M., Woodward, S., Best, M. J., Brooks, M. E., Brown, A. R., Butchart, N., Dearden, C., Derbyshire, S. H., Dharssi, I., Doutriaux-Boucher, M., Edwards, J. M., Falloon, P. D., Gedney, N., Gray, L. J., Hewitt, H. T., Hobson, M., Huddleston, M. R., Hughes, J., Ineson, S., Ingram, W. J., James, P. M., Johns, T. C., Johnson, C. E., Jones, A., Jones, C. P., Joshi, M. M., Keen, A. B., Liddicoat, S., Lock, A. P., Maidens, A. V., Manners, J. C., Milton, S. F., Rae, J. G. L., Ridley, J. K., Sellar, A., Senior, C. A., Totterdell, I. J., Verhoef, A., Vidale, P. L., and Wiltshire, A.: The HadGEM2 family of Met Office Unified Model Climate configurations, Geosci. Model Dev. Discuss., 4, 765–841, doi:10.5194/gmdd-4-765-2011, 2011.

Thingstad, T. F., Bellerby, R. G. J., Bratbak, G., Borsheim, K. Y., Egge, J. K., Heldal, M., Larsen, A., Neill, C., Nejstgaard, J., Norland, S., Sandaa, R. A., Skjoldal, E. F., Tanaka, T., Thyrhaug, R., and Topper, B.: Counterintuitive carbon-to-nutrient coupling in an Arctic pelagic ecosystem, Nature, 455, 387–390, doi:10.1038/Nature07235, 2008.

Timmermann, R., Goosse, H., Madec, G., Fichefet, T., Ethe, C., and Duliere, V.: On the representation of high latitude processes in the ORCA-LIM global coupled sea ice–ocean model, Ocean Model., 8, 175–201, doi:10.1016/j.ocemod.2003.12.009, 2005.

Trenberth, K. and Hurrell, J.: Decadal atmosphere-ocean variations in the Pacic, Clim. Dynam., 9, 303–319, 1994.

Uppala, S., Kallberg, P., Simmons, A. J., Andrae, U., Bechtold, V. D. C., Fiorino, M., Gibson, J. K., Haseler, J., Hernandez, A., Kelly, G. A., Li, X., Onogi, K., Saarinen, S., Sokka, N., Allan, R. P., Andersson, E., Arpe, K., Balmaseda, M. A., Beljaars, A. C. M., van de Berg, L., Bidlot, J., Bormann, N., Caires, S., Chevallier, F., Dethof, A., Dragosavac, M., Fisher, M., Fuentes, M., Hagemann, S., Holm, E., Hoskins, B. J., Isaksen, L., Janssen, P. A. E. M., Jenne, R., McNally, A. P., Mahfouf, J. F., Morcrette, J. J., Rayner, N. A., Saunders, R. W., Simon, P., Sterl, A., Trenberth, K. E., Untch, A., Vasiljevic, D., Viterbo, P., and Woollen, J.: The ERA-40 re-analysis, Q. J. R. Meteorol. Soc., 131, 2961–3012, 2005.

United Nations Framework Convention on Climate Change (UNFCC): United Nations,

New York, 25 pp., 1992.

van der Molen, J., Aldridge, J. N., Coughlan, C., Parker, E. R., Stephens, D., and Ruardij, P.: Modelling marine ecosystem response to climate change and trawling in the North Sea, Biogeochemistry, 1–24, doi:10.1007/s10533-012-9763-7, 2012.

van Leeuwen, S. M., van der Molen, J., Ruardij, P., Fernand, L., and Jickells, T.: Modelling the contribution of deep chlorophyll maxima to annual primary production in the North Sea, Biogeochemistry, 1–16, doi:10.1007/s10533-012-9704-5, 2013.

van Leeuwen, S. M., Tett, P., Mills, D. K., and van der Molen, J.: Stratified areas in the North Sea: long-term variability and implications for marine spatial planning, Biogeochemistry, in preparation, 2014.

Vaquer-Sunyer, R. and Duarte, C. M.: Thresholds of hypoxia for marine biodiversity, P. Natl. Acad. Sci. USA, 105, 15452–15457, doi:10.1073/pnas.0803833105, 2008.

Vichi, M., Ruardij, P., and Baretta, J. W.: Link or sink: a modelling interpretation of the open Baltic biogeochemistry, Biogeosciences, 1, 79-100, doi:10.5194/bg-1-79-2004, 2004.

Vogt, M., Vallina, S. M., Buitenhuis, E. T., Bopp, L., and Le Quéré, C.: Simulating dimethylsulphide seasonality with the Dynamic Green Ocean Model PlankTOM5, J. Geophys. Res., 115, C06021, doi:10.1029/2009JC005529, 2010.

Von Storch, H. and Zwiers, F. W.: Statistical Analysis in Climate Research, Cambridge University Press, Cambridge, 1999.

Walsh, J. J.: Importance of continental margins in the marine biogeochemical cycling of carbon and nitrogen, Nature, 350, 53–55, 1991.

Weiss, R. F.: The solubility of nitrogen, oxygen and argon in water and sea water, Deep-Sea Res., 17, 721–735, 1970.

Weston, K., Fernand, L., Nicholls, J., Marca-Bell, A., Mills, D., Sivyer, D., and Trimmer, M.: Sedimentary and water column processes in the Oyster Grounds: A potentially hypoxic region of the North Sea, Mar. Environ. Res., 65, 235–249, doi:10.1016/j.marenvres.2007.11.002, 2008.

Whitney, F. A., Freeland, H. J., and Robert, M.: Persistently declining oxygen levels in the interior waters of the eastern subarctic Pacic, Prog. Oceanogr., 75, 179–199, 2007.

Whitney, F. A., Bograd, S. J., and Ono, T.: Nutrient enrichment of the subarctic Pacific

Ocean pycnocline, Geophys. Res. Lett., 40, 2200 – 2205, doi:10.1002/grl.50439, 2013.

Williams, J. H. T., Totterdell, I. J., Halloran, P. R., and Valdes, P. J.: Numerical simulations of oceanic oxygen cycling in the FAMOUS Earth-System model: FAMOUS-ES, version 1.0, Geosci. Model Dev., 7, 1419-1431, doi:10.5194/gmd-7-1419-2014, 2014.

Winkler, L. W.: Determination of dissolved oxygen in water, Berlin Deut. Chem. Ges., 21, 2843–2854, 1888.

Winther, N. G. and Johannessen, J. A.: North Sea circulation: Atlantic inflow and its destination, J. Geophys. Res.-Oceans, 111, C12018, doi:10.1029/2005JC003310, 2006.

Wong, G. T. F. and Li, K.-Y.: Winkler's method overestimates dissolved oxygen in seawater: Iodate interference and its oceanographic implications, Mar. Chem., 115, 86–91, doi:10.1016/j.marchem.2009.06.008, 2009.

Wyrtki, K.: The oxygen minima in relation to ocean circulation, Deep-Sea Res., 9, 11–23, 1962.

Yool, A., Popova, E. E., Coward, A. C., Bernie, D., and Anderson, T. R.: Climate change and ocean acidification impacts on lower trophic levels and the export of organic carbon to the deep ocean, Biogeosciences, 10, 5831–5854, doi:10.5194/bg-10-5831-2013, 2013.

Zhang, J., Gilbert, D., Gooday, A. J., Levin, L., Naqvi, S. W. A., Middelburg, J. J., Scranton, M., Ekau, W., Pea, A., Dewitte, B., Oguz, T., Monteiro, P. M. S., Urban, E., Rabalais, N. N., Ittekkot, V., Kemp, W. M., Ulloa, O., Elmgren, R., Escobar-Briones, E., and Van der Plas, A. K.: Natural and human-induced hypoxia and consequences for coastal areas: synthesis and future development, Biogeosciences, 7, 1443–1467, doi:10.5194/bg-7-1443-2010, 2010.

Zhang, Y.-C., Rossow, W. B., Lacis, A. A., Oinas, V., and Mishchenko, M. I.: Calculation of radiative fluxes from the surface to top-of-atmosphere based on ISCCP and other global datasets: Refinements of the radiative transfer model and the input data, J. Geophys. Res., 109, D19105, doi:10.1029/2003JD004457, 2004.

Zondervan, I., Zeebe, R. E., Rost, B., and Riebesell, U.: Decreasing marine biogenic

calcification: A negative feedback on rising atmospheric pCO_2, Global Biogeochem. Cy., 15, 507–516, 2001.

Zwiers, F. W., and Zhang, X.: Toward regional scale climate change detection, J. Clim., 16, 793 – 797, 2003.